Evaluating Support Conditions for Precast Concrete Inlay Panels using Finite Element Analysis

by

Dahlia Katerina Malek

A thesis
presented to the University Of Waterloo
in fulfilment of the
thesis requirement for the degree of
Master of Applied Science
in
Civil Engineering

Waterloo, Ontario, Canada, 2019

Author's Declaration

I hereby declare that I am the sole author of this thesis. This is a true copy of the thesis, including any required final revisions, as accepted by my examiners.

I understand that my thesis may be made electronically available to the public.

Abstract

Precast concrete inlay panels (PCIPs) are a unique application of precast concrete pavement used for overnight rehabilitations of high-traffic volume asphalt highways exhibiting structural rutting issues. The pavement is rehabilitated by partially milling the existing asphalt, preparing the panel support layer, placing the panels, and grouting. Proper panel support is essential for successful, long-lasting performance of the PCIPs. For this reason, three different types of support conditions (referred to as asphalt-supported, grade-supported, and grout-supported) were constructed in a trial installation of the PCIPs to compare performance of the three alternatives. The panels rest directly on top of the asphalt in the asphalt-supported condition, and the panels are supported by a cement-treated bedding material or by a rapid-setting grout in the grade-supported and grout-supported conditions, respectively. Earth Pressure Cells (EPCs) and thermistors were installed in the PCIP trial construction at the top of the base layer to measure pressure and temperature in this location.

The hypothesis of this research is that the performance of the PCIPs will be affected by the type of support condition, the properties of the support layer and the existing asphalt. The performance of the PCIPs was evaluated by analysis of the field data and by finite element analysis (FEA).

The field data was analyzed to identify seasonal trends, trends over time, and to compare the three types of support conditions. The pavement base layer is subjected to larger magnitude compressive pressures in the winter and smaller magnitude upwards pressures in the summer. Furthermore, in the second winter, the average pressure increased by 0.9 kPa and the average temperature was 1°C cooler relative to the first winter; a t-test indicated that these differences were statistically significant. These changes could potentially be a result of some deterioration in the pavement, but this is not conclusive. Statistical analyses were also performed to compare the pressures collected from two different EPC pairs that corresponded to the same support condition. Results of the t-test indicated that there were statistically significant differences in the average pressure for the same support condition, and this was the case for all three types of support conditions. This indicated that the pressure differences were not a result of the type of support condition, but were caused by other factors. Therefore, conclusions about the relative performance of the support conditions cannot be drawn from the data at this time. It is recommended to continue monitoring and evaluating the field data.

A finite element model of the PCIPs was developed using Abaqus software. The model consisted of three panels on a base and subbase, all modelled as continuum elements, on a dense-liquid foundation. Dowel bars for load transfer were modelled as embedded beam elements, and frictional contact properties were defined at the pavement layer interfaces. Two variations of the model were developed: one model did not have a support layer (the "AS" model) and one model included a support layer (the "GR" model). The AS model represents the asphalt-supported condition, and the GR model represents the grade- and grout-supported conditions. The model was verified with theoretical solutions and the mesh, number of panels, and extents of the base/subbase were chosen through verification tests. The model was calibrated and validated using field test data.

Parametric studies were completed to evaluate the performance of the pavement for a range of conditions. The parameters considered were low and high interface friction between the panel and underlying layer, a support modulus of 4,000, 12,000, or 20,000 MPa, a support thickness of 12, 18, or 24 mm, and a base modulus of 1,000, 8,000, and 15,000 MPa. The maximum tensile stress in the panel and the base layers were evaluated as measures of the pavement performance. The loading combinations evaluated were a +10°C temperature gradient, a -10°C temperature gradient, a +10°C gradient with axle loading, and a -10°C gradient with axle loading.

For each combination of parameters, the minimum tensile stresses in the panel and base was obtained from the finite element analysis (FEA). The trends in the stresses were analyzed and synthesized to produce practical recommendations for the optimal support condition, support modulus and thickness that would minimize panel and base stresses for the parameters and loading studied. It is recommended to reduce the bonding at the interface and to use the grade-supported condition for the most optimal performance. The presence of a thin support layer in between the panel and base was beneficial in reducing stresses in the base layer. Furthermore, two flow charts were developed as decision-making tools for selecting the most optimal conditions for PCIP, given information about the existing base stiffness or for a pre-selected support condition.

In conclusion, the FEA demonstrated that the research hypothesis was correct; the properties of the support, base, and type of support condition had an impact on the pavement performance. The recommendations of this research can be used to make choices in the design or construction of the PCIP that will minimize stresses and make this pavement more durable and long-lasting.

Acknowledgements

I would like to express a warm thanks to the many people that have helped me throughout this process. I would not have accomplished this and had as much fun along the way without all of you.

First and foremost, thank you to my supervisor, Dr. Susan Tighe, for all her support and guidance on this research and for being such an encouraging mentor over the past few years.

I would also like to thank Dr. Daniel Pickel who has always made the time to answer my questions and who has provided me with valuable expertise.

Thank you to Bev Seibel and all the members of CPATT who have always provided a friendly and helpful community, and a special thanks to Victoria Speller, Michelle Liu, and Donghui Lu for always listening, being supportive, and for helping me with site trips.

A big thank you to all my family and friends, who have helped me to reach this point and who have been infinitely understanding and encouraging every step of the way.

The partners sponsoring this research project are The Centre for Pavement and Transportation Technology (CPATT), Norman W. McLeod Chair, The University of Waterloo, The Ministry of Transportation Ontario (MTO), The Cement Association of Canada (CAC), and The Natural Sciences and Engineering Research Council of Canada (NSERC) Collaborative Research and Development Program.

Table of Contents

List of Figures

List of Tables

List of Abbreviations

AADT	annual average daily traffic
AS	asphalt-supported
ATB	asphalt-treated base
CTB	cement-treated base
CTBM	cement-treated bedding material
DL	dense-liquid
EPC	earth pressure cell
ES	elastic solid
FEA	finite element analysis
FEM	finite element model
FWD	falling weight deflectometer
GR	grade- and grout-supported (generally refers to both of these support conditions)
GradeS	grade-supported
GroutS	grout-supported
HMA	hot mix asphalt
IWP	inner wheel path
LCB	lean concrete base
MTO	Ministry of Transportation of Ontario
OWP	outer wheel path
PCIP	precast concrete inlay panel
PCP	precast concrete pavement
RSG	rapid setting grout

CHAPTER 1 Introduction

1.1 Background

In Canada, the primary mode of transportation for passengers and goods is by road. Highways are relied upon for the movement of freight and people, and highway pavements sustain heavy truck loading and high volumes of passenger traffic. There are two main challenges associated with maintaining pavement under these traffic conditions. The first is that pavements exposed to high truck traffic volumes deteriorate at a faster rate and require more frequent pavement maintenance and rehabilitation to maintain adequate levels of service. The second obstacle is that lane closures on high-volume highways must be short because they have a significant user impact. Construction-related lane closures cause increased traffic congestion, delay, and safety risks for roadway users and workers (Abdelmohsen & El-Rayes, 2016; Tayabji, Ye, & Buch, 2013a). To minimize these impacts, highway construction lane closures are typically restricted to off-peak hours between 10 p.m. and 6 a.m. with full reinstatement of the traffic lanes after this period.

High volumes of passenger and freight traffic are especially prevalent on some of the 400-series highways in the province of Ontario, Canada, which are among the busiest highways in North America. Near the City of Toronto, the annual average daily traffic (AADT) is as high as 416,000 ("Ontario Provincial Highways Traffic Volumes On Demand," 2016).

On some sections of Highway 400, north of Toronto, the asphalt pavement has exhibited structural rutting issues. Structural rutting is caused by deformations originating in the lower layers of the pavement structure that results in rutting of the surface layer (White, Haddock, Hand, & Fang, 2002). A full-depth reconstruction would address the deep-seated rutting issue; however, this strategy cannot be completed within an overnight construction period. Instead, the rutted pavement was rehabilitated by milling and replacing the asphalt with a new layer of hot mix asphalt. The mill-and-replace strategy had an expected service life of 10 to 15 years; however, rutting reoccurred after only 3 to 4 years following the rehabilitation (Pickel, 2018).

The Ministry of Transportation of Ontario (MTO) is the agency responsible for managing highways in the province of Ontario. To address the rutting issue on Highway 400, the MTO sought rapid rehabilitation techniques that would minimize traffic disruption and provide long-term

durability to minimize future rehabilitation work. The MTO chose to use precast concrete pavement (PCP), having successfully used PCP for past rehabilitation projects.

PCP is constructed from concrete panels that are prefabricated, transported to site after curing, and installed. PCP can be used for new constructions or for repairs to existing pavement. Common applications of PCP include the rehabilitation of high-traffic volume highways, highway ramps, intersections, and bus pads, all of which all experience heavy traffic loads and/or short construction periods (Tayabji & Brink, 2015).

PCP has a few main advantages over conventional pavements such as asphalt-concrete or cast-in-place concrete pavements. The precast panels are fabricated in a controlled environment which results in higher quality and durability pavement than cast-in-place. Prefabrication eliminates concrete curing from the activities that must be performed on site, which allows the precast panels to be transported to site and installed overnight. In contrast, cast-in-place concrete is poured on site and typically requires 2 to 4 days to achieve sufficient strength to support traffic loads (Delatte, 2014). Furthermore, pavement made from Portland Cement Concrete is stiffer and distributes loads over a greater area than asphalt pavement, which makes it more durable under heavy truck loads (Delatte, 2014). It is expected that PCP will reduce the stresses that are transferred to the lower pavement layers where the structural rutting originates.

Precast concrete inlay panels (PCIP) are a novel application of PCP developed to address the deep-seated rutting issue on Highway 400. PCIPs are precast panels that are inlaid into the existing asphalt pavement after milling the rutted asphalt. The PCIP rehabilitation strategy is expected to provide a longer service life and require less frequent rehabilitation than the asphalt milling-and-replacement treatment and will minimize construction time to reduce the disruption to highway users.

1.2 Precast Concrete Inlay Panels Trial Installation

In 2016, a trial section of PCIP was constructed in the province of Ontario, Canada, in the Town of Bradford West Gwillimbury, which is located approximately 50 km north of the City of Toronto. The 100-metre long trial section was installed on Highway 400, between Highway 89 and Simcoe County Road 88, in the third (rightmost) lane of the highway (Figure 1-1).

Figure 1-1. Precast concrete inlay panels installation in-service on Highway 400

The rehabilitation using PCIP was performed in four main steps: partial-depth milling of the existing asphalt, preparation of a support condition for the panels, inlaying the panels into the traffic lane, and grouting (Figure 1-2).

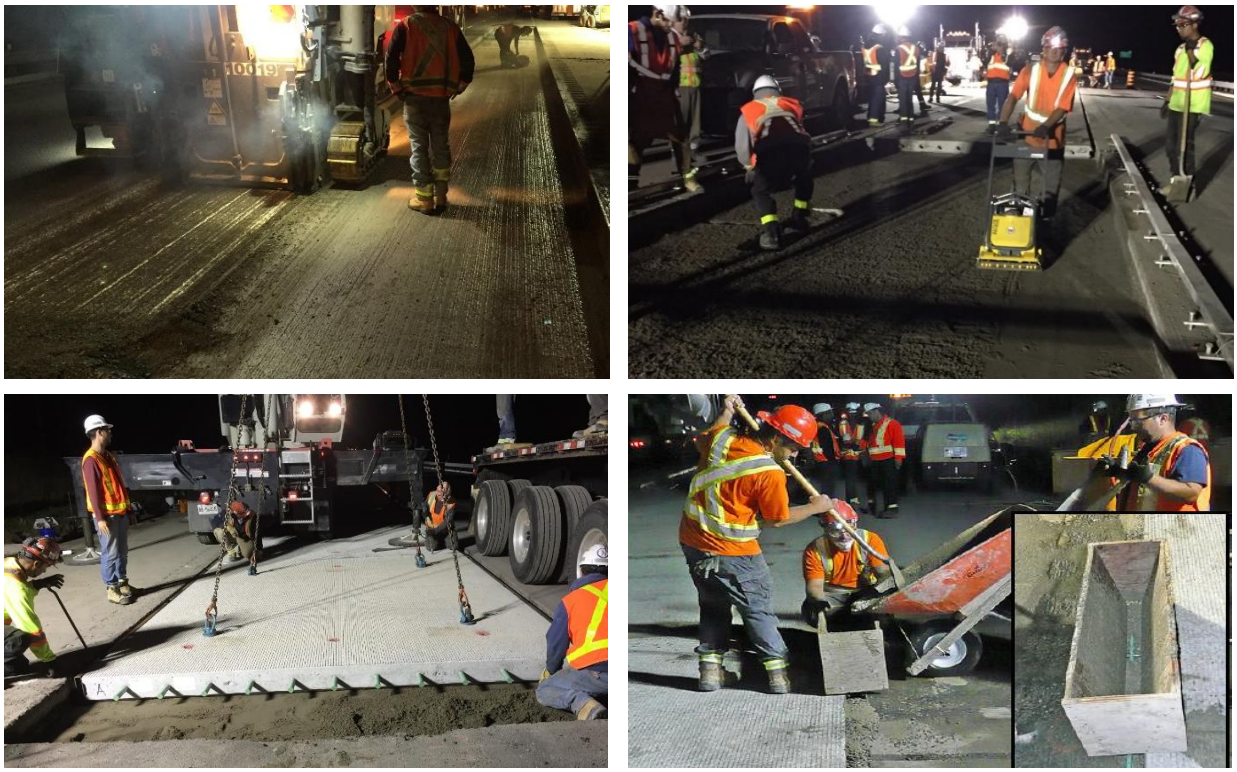

Figure 1-2. Rehabilitation process using PCIP: asphalt milling (top left), preparation of support (top right), placing panels (bottom left), grouting (bottom right)

The final pavement structure consists of the untouched subgrade, granular subbase and base layers, a layer of existing asphalt that remains after milling, the support condition, and finally the precast concrete panel.

1.3 Panel Support

Proper panel support is one of the essential components to achieve successful, long-lasting performance of PCP (Tayabji et al., 2013a). Since the bottom surface of the panels will not precisely match the field-prepared surface that they are placed upon, such as the milled asphalt, small voids remain underneath the panels. The support layer is installed between the panels and the underlying layer to provide stable, uniform support to the panels.

Voids underneath the panels resulting from non-uniform support can lead to early stress development in the panels, premature cracking, and joint faulting (Merritt, McCullough, Burns, & Schindler, 2000; Tayabji, Ye, & Buch, 2012). These distresses significantly reduce the service life of the pavement and can ultimately lead to premature failure of the pavement. Distresses such as cracking and settlement have been observed repeatedly in PCP systems that did not have adequately constructed support systems (Tayabji et al., 2012). A well-constructed support layer also contributes to joint load transfer, reduces erosion of the subbase and prevents pumping of materials under the slab, improves drainage, insulates subgrade soils from frost penetration, and controls shrinkage or swelling of the subgrade soils (Bing Sii, 2014; Tutumluer, Xiao, & Wilde, 2015).

Three different types of panel support conditions were developed and constructed in the PCIP trial installation; they are referred to as asphalt-supported, grade-supported, and grout-supported. The 100-m long section contains three segments that each made use of a different support condition. Twenty-three panels were installed in total in which eight consecutive panels were installed with the asphalt-supported condition, followed by seven grade-supported panels, and seven grout-supported panels.

For the asphalt-supported condition, the panels were placed directly on top of the asphalt that was milled to a tolerance of ±3 mm. Bedding grout was then pumped underneath to fill any remaining voids between the asphalt and panel. For the grade-supported panels, the existing asphalt was

milled, then a cement-treated base material (CTBM) was placed, levelled, and compacted. The panels were placed on the CTBM, and any voids were again filled with bedding grout. For the grout-supported panels, the panels were placed directly on the milled asphalt, then raised to the proper position using levelling inserts cast into the bottom of the panels. A rapid-setting grout (RSG) was pumped underneath the panels for support (Figure 1-3) (Pickel, Tighe, Lee, & Fung, 2018).

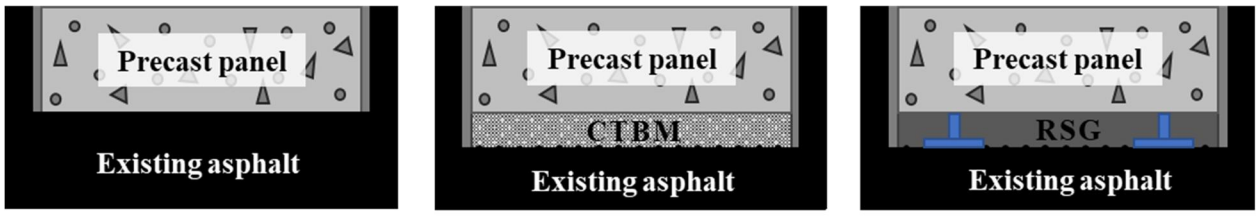

Figure 1-3. Support condition alternatives (asphalt-supported, grade-supported, and grout-supported, from left to right)

The PCIP rehabilitation strategy is unique because the existing asphalt is left in place, and the base, subbase, and subgrade layers are not modified. This reduces the rehabilitation time, which is extremely valuable in an overnight application. It is also hypothesized that the asphalt layer will be beneficial in providing a strong, stable layer which can either serve as the panel support (in the asphalt-supported condition) or can serve as the underlying support material (in the grout-supported and grade-supported conditions).

1.4 Problem Statement

This research focuses on evaluating the performance of the PCIPs, which is a type of precast concrete pavement. PCP has many advantages in pavement construction and rehabilitation applications; however, there is a lack of understanding and familiarity with PCP and a shortage of long-term performance information that deters more widespread use of this technology (Tayabji, Buch, & Kohler, 2009; Tayabji et al., 2013a). Monitoring and evaluating performance of PCP systems can help to fill these knowledge gaps and generate greater acceptance of PCP in industry.

PCP offers many benefits over the use of conventional pavement materials, including rapid construction that reduces traffic impacts, controlled fabrication conditions, and high durability pavement. However, the advantages of PCP are weighed against its disadvantages, which include

higher initial construction and installation cost, lower production rate, and lack of familiarity by contractors and transportation agencies (Merritt et al., 2000). Improvements to PCP's design efficiency, ease of construction, production rate, long-term durability, or cost reductions would increase the appeal of this technology.

Performance monitoring and evaluation of in-service PCPs can provide information to better understand and improve PCP performance. Performance information can be used to identify successes and deficiencies, which provides the experience to optimize the design, construction, and installation practices. Performance information will lead to a better understanding of PCP systems, and performance data can be used to calibrate design specifications for various types of PCP systems (Tayabji et al., 2013a).

The performance of the PCIPs cannot be easily predicted for two main reasons. First, the performance of PCP in general is not well understood because their use has been infrequent and performance data is limited. More frequent use of PCP only began in the early 2000's when there had been sufficient technological advancements to make PCP a more feasible and cost-effective option for some projects (Tayabji, Ye, & Buch, 2013b). Presently, long-term performance information is limited because there are few in-service installations of PCP that are older than 15 years, which falls short of their expected service life of 20+ years for repairs and 40+ years for new construction, and performance data has not been well documented in the past (Tayabji et al., 2013a). As of yet, there is not a thorough understanding of the behaviour of all the components of PCP systems, and experience-based design specifications are not well-developed (Tayabji et al., 2013a). Secondly, PCIP is a novel application of precast concrete pavement and it has unique features that have not yet been investigated. Rehabilitation using PCIP is unique in that the existing asphalt is only partially-milled and the remaining asphalt provides a base for the panels. Furthermore, there are three types of support conditions that were constructed in the PCIP trial section. Therefore, the effect of the existing pavement structure and the relative performance of the three support conditions are unique aspects that must be considered. Performance monitoring and evaluation is a critical step to gain an understanding of PCIP behaviour and its feasibility as a rehabilitation strategy.

Performance evaluation can be completed by various methods, including collecting and analyzing field data and by finite element analysis (FEA). FEA is a powerful tool for evaluating pavement performance. Abaqus is a general-purpose finite element software that has been successfully used in the past to perform rigid pavement analyses (ARA Inc., 2003). Among its many capabilities, Abaqus can be used to model pavement joints and load transfer mechanisms, bonding, friction and separation of interfaces, environmental effects such as thermal and moisture gradients, and traffic loading. FEA can be used to evaluate the effects of varying site conditions, design and construction changes, and different loads to analyze pavement behavior across a wide range and combination of these factors.

1.5 Research Hypothesis and Objectives

The successful performance of PCP is largely influenced by the provision of proper panel support. The hypothesis of this research is that the performance of the PCIPs will be affected by the type of support condition constructed, the properties of the support layer, and the properties of the existing asphalt.

The focus of this research is on evaluating the performance of the PCIPs using FEA to evaluate the effect of the type of support condition, the material properties and thickness of the support layer, and the properties of the base layer. Specific objectives of this research are as follows:

1. Develop a finite-element model that is representative of the PCIPs and that is reasonably accurate and fast.
2. Determine the optimal type of support condition, of the three alternatives constructed in the PCIP trial installation, to minimize pavement stresses under various loading conditions.
3. Determine the optimal support layer thickness and stiffness for the support layer to minimize pavement stresses.

1.6 Research Methodology

The research methodology is summarized by Figure 1-4. Each of these steps is described in more detail in the following chapters of this thesis.

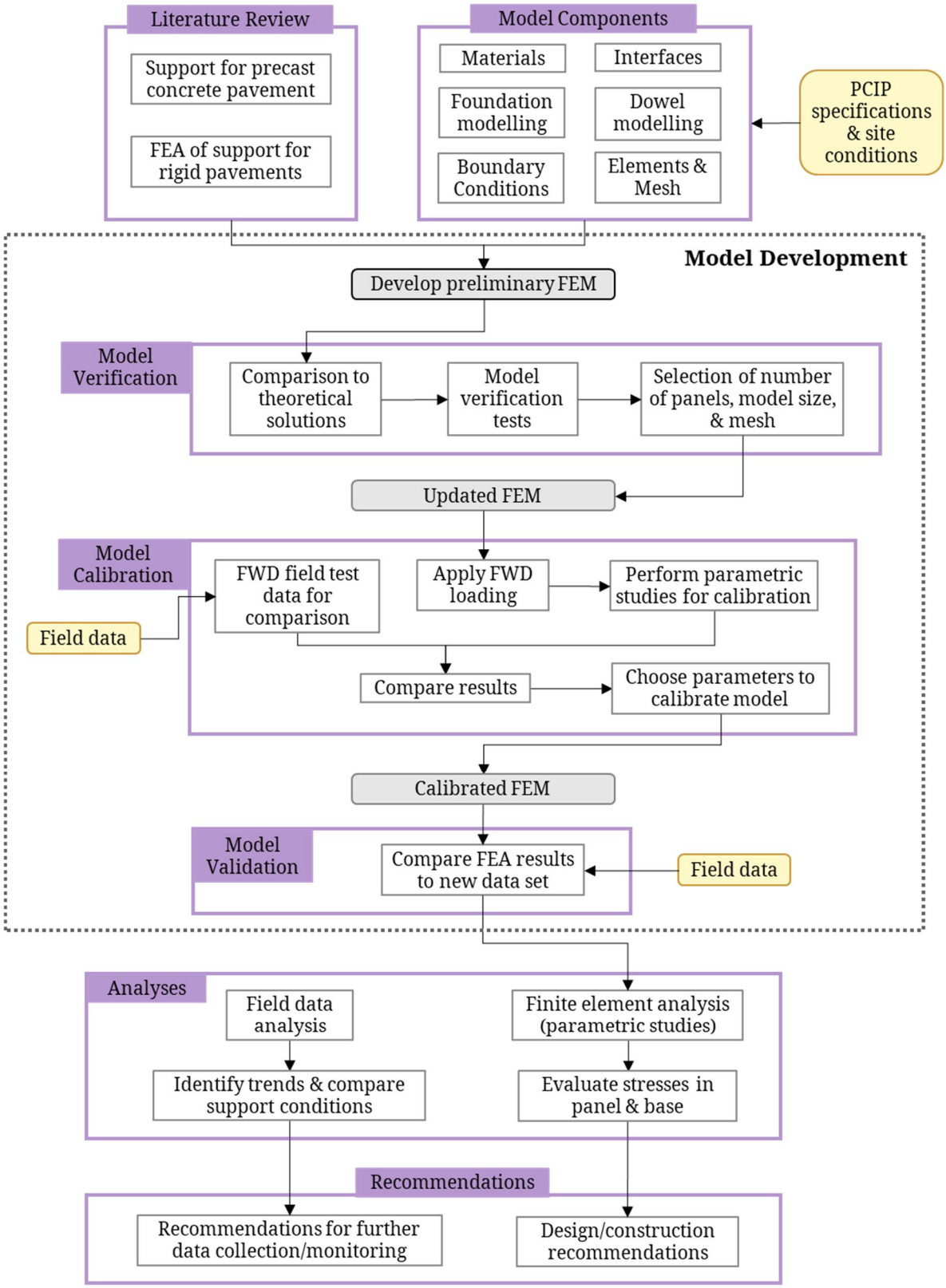

Figure 1-4. Research methodology flow chart

1.7 Thesis Organization

The contents of each chapter in this thesis are summarized as follows:

Chapter 1: Introduces the use of PCIPs as a rapid rehabilitation strategy for high-volume highway pavements and describes the motivation for the performance evaluation of the PCIPs by FEA. This section also provides an overview of the research hypothesis, objectives, and methodology.

Chapter 2: Outlines the literature on the topics of support for PCP and previous finite element analyses of rigid pavement.

Chapter 3: Describes the site conditions of the PCIP trial installation and the components of the finite element model (FEM).

Chapter 4: Presents the model development process, including verification, calibration, and validation of the FEM.

Chapter 5: Presents the analysis of field data, which included analyzing pressure and temperature measurements to gain insight into PCIP performance.

Chapter 6: Contains the results of the FEA analysis, in which parametric studies were completed to evaluate the effect of the support on the pavement performance.

Chapter 7: Summarizes the conclusions of this research, focusing on the significance of the FEA results as it pertains to design and construction recommendations for the PCIP. Recommendations for further improvements to field data collection, the FEM development, and FEA are also outlined.

CHAPTER 2 Literature Review

A literature review was conducted to establish the unique features of the precast concrete inlay panels (PCIPs), from a design and modelling perspective, that have not been thoroughly investigated in previous research. The literature review includes typical practices for constructing support for precast concrete pavement (PCP) and previous studies that evaluated the support for rigid pavements using FEA.

2.1 Support for Precast Concrete Pavements

This section describes the typical method for constructing the base and support for PCP and discusses past PCP projects, to provide context as to how PCIPs differs from typical PCP installations.

2.1.1 Panel Support and Base

Since precast concrete panels are installed after they have been cured, the bottom of the panel will not conform to the underlying surface. While the base layer provides support for the precast panels, an additional support layer, which is also referred to as the "interlayer", is required to fill voids that remain between the prepared base and the panel (Tayabji et al., 2013a). The support layer is typically a flowable, void-filling material that will provide uniform support to the panels. Types of commonly-used support layers include a cemented grout pumped underneath the panel, a flowable grout placed and screeded before placing the panels, or polyurethane foam injected underneath the panels (Tayabji et al., 2013a).

For PCP rehabilitation applications, the base can be constructed from the existing material or new material. An existing granular base can be left in place and reworked, graded, or compacted, if necessary. If the granular base is inadequate a partial layer can be removed and a support layer can be prepared to meet the required grade (Tayabji et al., 2013a). The support layer can be a thin layer of cemented granular or cemented sand, a fast-setting cementitious grout or flowable fill, or polyurethane foam (Tayabji et al., 2013a). If there is an existing stabilized base such as a cement-treated base (CTB) or lean concrete base (LCB), this may be used in conjunction with a rapid-setting cementitious material as the support layer to achieve a level surface for panel placement

(Tayabji et al., 2013a). If the existing base cannot provide adequate support, then a new dense-graded granular base or LCB can be constructed (Tayabji et al., 2013a). Cement-treated or asphalt-treated bases are also viable alternatives, but require more construction effort and time that may render them infeasible in overnight construction applications (Tayabji et al., 2013a).

2.1.2 Asphalt Rehabilitation using Precast Concrete Pavement

PCP can be constructed as continuous applications, for new constructions, or intermittently, for repairs to existing pavement (Tayabji et al., 2013b). PCP can be used to repair concrete pavements and for rehabilitations to existing concrete or asphalt pavements. Common applications of PCP include the rehabilitation of high-traffic volume highways, highway ramps, intersections, and bus pads (Tayabji & Brink, 2015).

Previous projects have been undertaken to rehabilitate hot mix asphalt (HMA) pavements using PCP, however the purpose and installation processes differ from that of PCIP. One project undertaken in Connecticut used PCP to rehabilitate rutted HMA bus pads (Figure 2-1). The existing HMA was completely removed, the existing base was regraded and compacted, and a rapid-setting grout was pumped underneath the panels to provide a support layer.

Figure 2-1. Connecticut HMA bus pad rehabilitation (Tayabji & Tyson, 2017)

There were some issues with the base preparation and panel installation; however the PCP installation was largely successful with the newly-rehabilitated bus pads being used at 4 a.m. at the start of the daily bus operations (Tayabji & Tyson, 2017).

A second project in Texas involved rehabilitating an HMA intersection experiencing heavy rutting using PCP. The existing HMA was removed, the subgrade was cement-treated, and a new HMA layer was placed as a base for the panels (Tayabji & Tyson, 2017). The goal of installing all the panels within one weekend was not achieved; however, the project was considered to be successful in demonstrating the use of PCP for pavement rehabilitation (Tayabji & Tyson, 2017).

2.2 Finite Element Modelling Studies

Past studies investigating the support for rigid pavement structures using FEA have often studied either the effect of different types of base materials or the effect of varying degrees of bonding at the slab-to-base interface; this research is described in this section.

2.2.1 Effect of Base Type

Masad, Taha, and Muhunthan (1996) investigated the effect of the base modulus on the maximum and minimum slab stresses using Abaqus. The base modulus had a minimal effect on the tensile stresses under a uniform temperature change in temperature, when the friction factor was held constant, which led to the conclusion that base materials affect the slab stresses due to the texture of the material not its stiffness.

Davids (2000) used EverFE software to evaluate the effect of base layer stiffness on panel stresses and dowel shear stresses. The study considered three typical base materials, an asphalt-treated base (ATB), CTB, and granular base, with elastic moduli of 200 MPa, 3500 MPa, and 7000 MPa, respectively. The base had a fixed thickness of 150 mm with linear, elastic material properties. The study evaluated the effect of the base type on critical stresses in the panel due to a temperature gradient combined with wheel loading, considering one load case for the positive gradient and one for the negative gradient. Increased base stiffness reduced the critical panel stresses under combined loading. The stress reduction was substantial when using the ATB in comparison to granular and less significant for the CTB compared to the ATB. Under temperature loading alone, increased base stiffness increased the critical panel stresses.

Zhang and Gao (2016) evaluated the effect of the base stiffness and base thickness on the stresses at the bottom of the panel, bottom of the base, and panel-to-base interface shear stress using a three-dimensional layered model. The base stiffness ranged from 1,500 MPa to 20,000 MPa with thicknesses of 150 mm, 200 mm, and 250 mm. Only one loading case was considered, a positive temperature gradient with an axle centred longitudinally and positioned towards the panel edge. For the bottom of slab stresses, the stress increased with an increase in base modulus for high friction but remained approximately the same with low friction. For the bottom of base stresses, the stress increased with an increase in the base modulus or a decrease in base thickness. The interface shear stress showed little change for variations in the base modulus and thickness.

Wu, Liang, and Adhikari (2014) investigated the effect of including an asphalt isolating layer in between a panel and gravel base under a moving load using Abaqus. The effect of changes in the isolating layer thickness, modulus, and slab-asphalt friction on the critical panel stresses and deflections were investigated. These parameters ranged from 0 to 30 mm, 800 to 2000 MPa, and 0 to 3.0 for the isolating layer thickness, modulus, and friction factor, respectively. While one parameter was varied, the other parameters were held at a constant value. The critical panel deflections and maximum stresses increased as the isolating layer thickness increased and decreased slightly as the isolating layer modulus increased. The final recommendation was to use a thinner isolating layer that is thick enough to provide waterproofing.

2.2.2 Effect of Panel-Base Friction

In the pavement structure, there is some degree of bonding at the interfaces between different layers of the pavement structure. Of particular interest is the bonding at the interface of the concrete slab and underlying base material because this influences the stresses in the concrete slab. The slab and base may be unbonded, partially bonded, or fully bonded. In practice, the assumption of a perfectly unbonded or fully-bonded interface is unrealistic.

Two-dimensional modelling constrains the nodes such that no separation can occur between pavement layers and only unbonded or bonded states can be represented (Kuo, Hall, & Darter, 1995). Three-dimensional finite element modelling provides the capability to model varying degrees of bonding at the slab-base interface and separation of the slab and base (Kuo et al., 1995). Separation of the slab and base has been modelled in EverFE software using a frictionless nodal

contact method (Davids, 2000, 2001). Using Abaqus software, Kuo, Hall, and Darter (1995) recommended the use of interface elements in combination with vertical and horizontal bonding properties that permit modelling of fully unbonded, fully bonded, and intermediate levels of bonding. Using ANSYS software, S. R. Maitra, Reddy, and Ramachandra (2009) used contact elements with normal and tangential stiffness properties to model the slab-base interface with smooth and rough bonding. Priddy et al. (2015), Kim and Hjelmstad (2003), and Northmore and Tighe (2016) used Abaqus' surface-to-surface contact interaction to model frictional contact between the slab and base. Hammons (1998) used Abaqus to compare two methods of modelling interface contact, either using "INTER" interface elements or using the surface-to-surface contact interaction approach and concluded that the contact interaction approach was easier to use and slightly more accurate.

Many studies consider only one level of bonding, such as frictionless contact or partially-bonded contact with an assumed coefficient of friction (Davids, 2000, 2001; Kim & Hjelmstad, 2003; Priddy et al., 2015). Researchers have also investigated the effects that varying degrees of bonding have on pavement responses through experimental testing, field evaluations, and FEA.

For conventional concrete pavements constructed on a granular base or a lean concrete base, a separation membrane or bond-breaker is often applied to create a smooth surface between the concrete slab and the underlying material to avoid issues such as reflective cracking, pumping, and voids under the slab (S. R. Maitra et al., 2009; Wu et al., 2014). Common bond-breaking methods include a sprayed-on asphaltic emulsion, a wax-based curing compound, or polyethylene layers. Tarr et al. (1999) evaluated the effect of five different interface treatments on the bonding between a concrete slab and lean concrete base. The bond-breaking materials influence the level of bonding between the slab and the base and can have a significant influence on the stresses in the pavement system. Even with bond-breaking materials, the shear friction can be large enough that the slab-base acts as a partially bonded interface which can reduce tensile stresses at the bottom of the concrete (Tarr et al., 1999). In some cases, the interface shear friction may be significant enough that the pavement structure acts more as a monolithic system than a multi-layered system (Tarr et al., 1999). The results of Tarr's study demonstrate that, in practice, partial bonding can significantly reduce pavement stresses and deflections in comparison to lower bonding at the interface.

The effect of varying degrees of bonding on the slab stresses has been investigated through FEA of rigid pavements. S. R. Maitra, Reddy, and Ramachandra (2009) used ANSYS software to evaluate the effect of the slab-base interface friction on panel stresses and deflections under various combinations of axle loading, positive and negative temperature gradients, and uniform temperature changes. The study evaluated the effects of a smooth versus rough interface between the concrete panels and dry lean concrete base. The tensile stresses in the panel were reduced with the smooth interface since there was less restraint, although the panel deflections and loss of support under the panel was greater. Under axle loading alone, a rougher interface contributed stiffness to the panel, reducing the panel tensile stresses and deflections.

Masad, Taha, and Muhunthan (1996) investigated the effect of slab-base friction on the critical slab stresses for positive and negative temperature gradients and uniform temperature changes using Abaqus. Changes in the friction factor from values of 1 to 3 had a negligible impact on the curling stresses. The degree of bonding corresponding to these friction factors was not specified. For slab curling stresses, the negative temperature gradient induced larger critical stresses than the positive temperature gradient of the same magnitude. Under a uniform temperature change, the tensile stresses increased with an increasing friction factor from 1 to 3, caused by greater restraint at the slab-base interface.

Davids et al. (2003) evaluated the effect of varying slab-base shear stiffness on the maximum panel stresses, by considering three levels of shear stiffness. The lowest shear stiffness is expected to correspond to a pavement with a bond-breaker at the interface, whereas the highest corresponds to a hot mix asphalt base. Under a positive and negative thermal gradient, the maximum stress in the centre panel increased with increasing slab-base shear stiffness.

Zhang and Gao (2016) evaluated the effect of slab-base interface friction on the stresses at the bottom of the panel, bottom of the base, and panel-base interface shear stress under a combined axle and positive temperature gradient load. The slab-base interface friction was varied from a low friction bond slip state to a completely bonded state. The stresses at the bottom of the slab, bottom of the base, and interface shear stress increased with increasing friction.

Wu, Liang, and Adhikari (2014) investigated the effects of introducing an asphalt isolating layer in between the panel and a gravel base. The effect of changes in contact friction between the slab

and asphalt isolating layer on the critical panel stresses was studied, and it was found that the critical deflections and maximum stresses decreased as the panel-asphalt friction increased.

2.3 Research Gaps

Rehabilitation using PCIPs is unique because the existing asphalt pavement is used as a base for the pavement and the underlying subbase and subgrade layers are not improved or otherwise modified during the rehabilitation; this reduces the rehabilitation time. In the previous projects using PCP for asphalt pavement rehabilitation, the existing asphalt was entirely removed, or the base/subbase/subgrade layers were modified. Another unique aspect of PCIP, is that three different support conditions (asphalt-supported, grade-supported, and grout-supported) were constructed in the trial installation. A bedding grout, cement-treated base material or rapid-setting grout was installed underneath the panels, between the concrete slab and underlying asphalt, to fill voids and provide uniform, level support. These three alternatives were constructed so that the performance of the PCIP with each of these different support conditions could be monitored and evaluated over time.

The unique features of PCIP lead to aspects of research that have not been largely investigated in previous FEA studies of rigid pavements. In the finite element model of the PCIP for the asphalt-supported case, a support layer is not explicitly modelled and the slab-base contact is modelled similarly to previous studies. In the model for the grade- and grout-supported conditions, the support layer is explicitly modelled. Therefore, the slab-base contact must consider the slab-support and support-base interaction rather than the slab-base interaction. Based on the literature review, the effect of the support for PCP has not been studied frequently by FEA of the pavement. There is limited research that has evaluated the effect of an additional layer (the support layer) separating the slab and base and the effect that it has on pavement responses. While the effect of the base type has been investigated previously, the effect of the base type when this support layer is present in the pavement structure has not been researched.

Therefore, the main research question is: How are the stresses in the slab and base affected by the inclusion of a support layer? Furthermore, how are the stresses affected by the support modulus and thickness and by the base type and friction condition (with and without a support layer)?

CHAPTER 3 Finite Element Model Components

This chapter describes the construction specifications for precast concrete inlay panels (PCIPs) and the finite element model (FEM) and each of its components in detail.

3.1 PCIP Specifications and Site Conditions

3.1.1 Panel Specifications

The FEM was based on the construction specifications for the PCIPs. Figure 3-1 shows a typical panel.

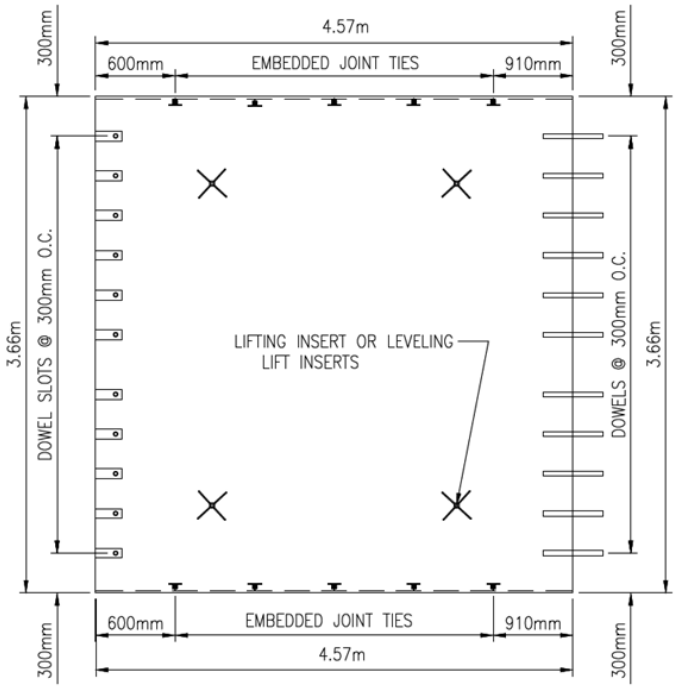

Figure 3-1. Typical precast concrete inlay panel specifications

Each panel is 3.66 m wide by 4.57 m long and 0.205 m thick. The panels contain two mats of steel reinforcement, composed of 15M bars (diameter 15.875 mm) at 300 mm spacing. The reinforcement allows for handling and transportation of the panels. There are 11 dowels cast into one transverse edge of the panel to provide load transfer. The dowels are 355 mm long, with a 38 mm diameter, located at mid-height of the panel and spaced at 300 mm centre to centre. The dowels are located asymmetrically with a group of five dowels and a group of six dowels as shown in

Figure 3-1. On the other transverse edge of the panel, there are inverted dovetail slots cut out from the bottom of the panel that cover the exposed dowels of the preceding panel, when the panels are placed consecutively. The dowel slots are 135 mm high, 200 mm long, and 63 mm wide at the base and 75 mm wide at the top of the slot.

3.1.2 Existing site conditions

Site investigations were performed at the trial site prior to the PCIP rehabilitation, which provided some information about the existing site conditions in the location of the PCIP installation.

Ground penetrating radar was used to ascertain the thickness of the existing asphalt. After the PCIP rehabilitation, the thickness of the remaining asphalt ranged from 139 to 195 mm, with an average thickness of 175 mm. Boreholes and cores were taken to determine the type and thickness of the base, subbase, and subgrade layers. The subgrade contained sand, sandy silt, and clayey silt soil. The average thickness of the combined base and subbase layers was approximately 600 mm.

3.2 Model Components

3.2.1 Model Overview

The FEM consists of 3 consecutive concrete panels, on top of the support, base, and subbase layers each modelled as elastic solid continuums, on top of a dense-liquid foundation representing the subgrade. In the PCIP construction, the base is the asphalt layer and the subbase is granular material. The base and subbase are generally referred to as the "sublayers" in this thesis. Two variations of the model were created; the asphalt-supported condition is represented by the "AS" model and the grade- and grout-supported conditions are represented by the "GR" model (Figure 3-2).

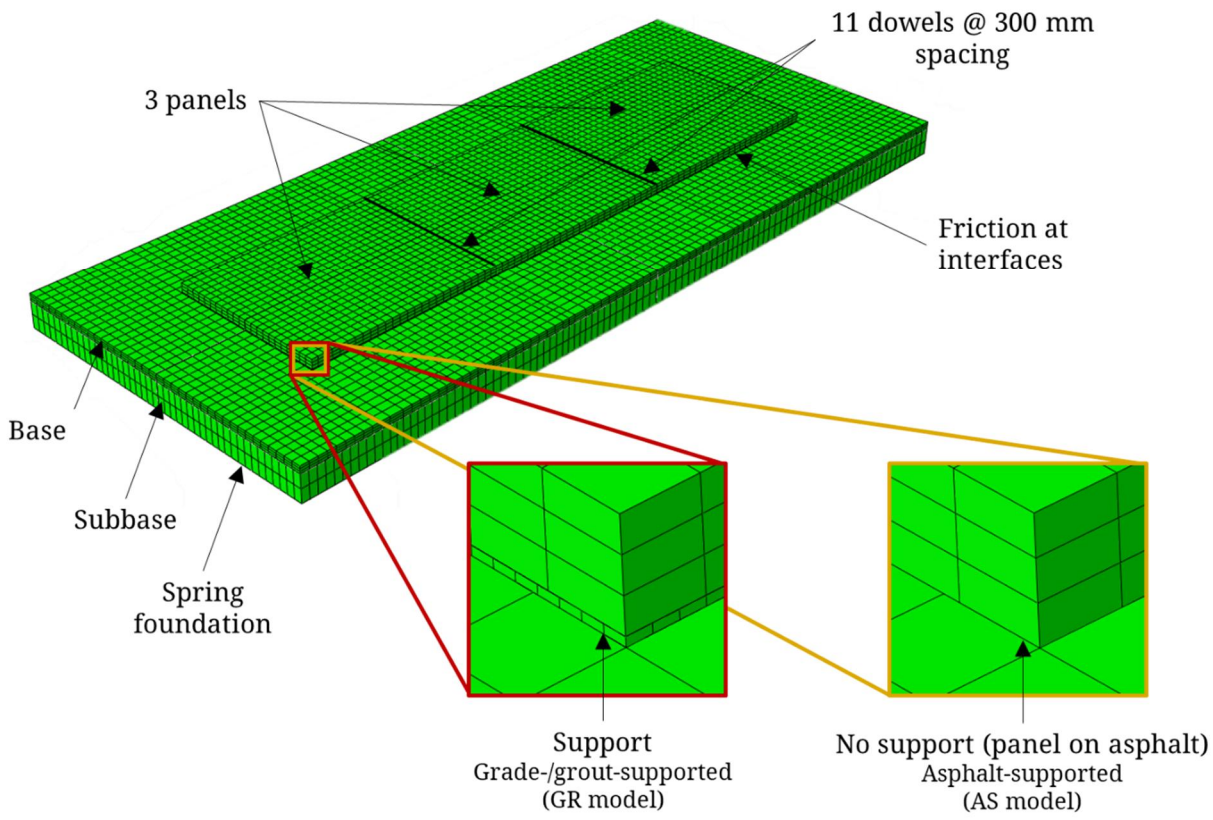

Figure 3-2. Finite element model of PCIP pavement structure

For the asphalt-supported condition, a support layer was not explicitly included in the AS model because the panels are placed directly on top of the prepared base, with a small amount of bedding grout used to fill any voids at the panel-to-base interface. For the grade- and grout-supported conditions, the support is provided by cement-treated bedding material (CTBM) and rapid-setting grout (RSG), respectively, which were modelled as a layer with a specified thickness and material properties. A generic support material was included in the GR model which can represent the CTBM, RSG, or any other similar support material. Contact properties were defined at the interfaces between pavement layers to define the frictional interaction between the materials.

The sublayers were extended 2 m in length and width beyond the panel edges. The number of panels modelled and the extent of the sublayers was chosen to reduce computation time while maintaining sufficiently accurate results. This selection process is described in Section 4.1.4.3.

Boundary conditions were applied at the sides of the sublayers to restrain movement in the lateral direction and at the edges to restrain movement in the longitudinal direction. Movement of the panels in the lateral direction was also restrained.

The inverted dovetail slots were not modelled for simplicity. The dowels were modelled as beam elements embedded directly into the concrete panel instead. The transverse joint width was assumed to be 15 mm. The reinforcement was also excluded from the model for simplicity.

Each component of the model is explained in further detail in the following sections.

3.2.2 Geometry

The model geometry was chosen to match the actual specifications and site conditions of the PCIP trial construction as closely as possible. The dimensions of each of the model components are summarized in Table 3-1.

Table 3-1. PCIP model dimensions

Component	Width (m)	Length (m)	Thickness (m)
Panel	3.66	4.57	0.205
Support	3.66	13.74	0.012 to 0.024[†]
Base (asphalt)	7.66	17.74	0.151 to 0.163 (GR model) [†‡] 0.175 (AS model)
Subbase (granular)	7.66	17.74	0.600

[†]Varies in parametric studies

[‡]Thickness adjusted for the presence of the support layer, ranging from 12 to 24 mm

The panel dimensions are based on the PCIP fabrication specifications. The base and subbase thicknesses are the average thicknesses of the asphalt and granular layers based on the site investigation. The recommended support thickness for precast concrete panels is 12.5 to 25 mm (Tayabji et al., 2013a).

3.2.3 Materials

All of the pavement materials (concrete, base, subbase, and steel) were assumed to be linear elastic, homogenous, and isotropic. This is a common idealization used for static pavement analyses (Davids, 2001; Kuo, 1994; Swati Roy Maitra, Reddy, & Ramachandra, 2009; Northmore & Tighe, 2016; Priddy et al., 2015). It is assumed that the pavement is not distressed and that the soils can be approximated by idealized linear behaviour. For the standard 80-kN equivalent single axle load (ESAL) used in pavement design and analysis, the induced stresses in the pavement are not likely to exceed the elastic range (Mallela & George, 1994). In the case that the actual pavement behaviour does pass into the nonlinear region, a linear elastic approximation may overestimate the pavement strength.

The material properties of each component of the pavement structure are summarized in Table 3-2.

Table 3-2. Finite element model material properties

Component	Elastic Modulus (MPa)	Poisson's ratio (-)	Density (kg/m^3)
Concrete	34,109	0.15	2,400
Support	4,000 to 20,000†	0.15	2,300
Base (asphalt)	1,000 to 15,000†	0.35	2,300
Subbase (granular)	100	0.35	2,300
Steel (dowels)	200,000	0.27	7,850

†Varies in parametric studies

The average 28-day compressive strength of the concrete used in PCIP fabrication was 52 MPa. The modulus of elasticity of concrete is 34,109 MPa calculated by Equation 1 (American Concrete Institute, 2005):

$$E_c = 4.75 {f'_c}^{0.5} \quad (1)$$

where: E_c is the modulus of elasticity of concrete (GPa), and
f'_c is the compressive strength of concrete (MPa).

The moduli of the support and base layers were varied for parametric studies, which are presented in detail in Section 6.2. The range of modulus values is based on typical values found in literature (Hajek, Smith, Rao, & Darter, 2008; Huang, 2004; Pavement ME Deign User Group, 2014; Tayabji et al., 2013a).

Typical values were selected for the concrete density and the Poisson's ratio for the materials. The same density was chosen for the support, base, and subbase so that the self-weight of the model would remain the same while the combined thickness of these layers remained constant. This may over-estimate some of the material densities, but this eliminated the influence of self-weight on the results.

The modulus of subgrade reaction was 29 MPa/m based on the previous site investigation. This was the average k-value; however, the estimated k-value ranged from approximately 24 to 33 MPa/m.

3.2.4 Foundation and Base Layers

The dense-liquid (DL) foundation, also called a Winkler foundation, and the elastic solid (ES) foundation are two commonly used subgrade models for rigid pavement systems. Neither of these subgrade models is a perfect representation of the behaviour of real soils which lies somewhere in between the behaviour predicted by the two models (Khazanovich, 1994). The DL model represents the subgrade as vertical springs without any shear interaction between the springs; the subgrade deflections are localized underneath the loaded area and do not affect the deflections of neighbouring nodes (ARA Inc., 2003). The ES model exhibits a higher degree of shear interaction than what exists in real soils and predicts infinite stresses under the edges and corners of a slab resting on an ES foundation (ARA Inc., 2003). The ES model requires more computation time because it significantly increases the number of elements in the model. The ES model is characterized by two parameters, the elastic modulus and Poisson's ratio, and the DL model is characterized by one parameter, the modulus of subgrade reaction, which is also called the k-value (ARA Inc., 2003).

To reduce computation time of the FEM, the subgrade was modelled as a dense-liquid foundation. The foundation was modelled in Abaqus using the 'elastic foundation' option from the Interactions module. The applied k-value was 29 MPa/m.

The pavement base layers can either be modelled as elastic solid continuum elements or they can be incorporated into the model by increasing the k-value of the foundation, which is referred to as "bumping the k-value". This method considers the base layer to contribute to the stiffness of the underlying subgrade, rather than as a material that lends support to the top concrete layer. The theoretical basis of this method has been questioned and the composite k-value found using this method is often very high (Ioannides, Khazanovich, & Becque, 1992; Khazanovich, 1994). It is recommended to model stiff bases as a continuum rather than the alternative method, particularly to accurately determine panel and dowel stresses (Davids, 2000). Modelling the base layers as a continuum also allows the responses through the depth of these sub-surface layers to be determined. Therefore, the support, base, and subbase layers were modelled as elastic solid continuums, all resting on the Winkler foundation. This is a typical finite-element representation of a rigid pavement structure (Davids, 2001; Kim & Hjelmstad, 2003; Kuo et al., 1995; S. R. Maitra et al., 2009; Priddy et al., 2015).

3.2.5 Interfaces

The interfaces between different layers of the pavement structure were modelled using Abaqus' 'surface-to-surface' contact option. The two surfaces in contact were defined; the master surface was the larger of the two surfaces, or the stiffer surface, or the surface with the coarser mesh, and the other surface was the slave surface ("Abaqus Analysis User's Guide (6.14)," 2014). Contact was defined using the classical isotropic Coulomb friction model by creating a friction interaction property in Abaqus that comprises tangential and normal behaviour.

Various options were available for the tangential friction formulation, including 'penalty', 'rough', and 'frictionless'. The 'penalty' option is used to simulate partial bonding of the surfaces. A friction coefficient (μ) was defined which regulates the degree of bonding between the two layers. The critical interface shear stress is related to the contact pressure of the surfaces by the friction coefficient as defined by Equation 2 ("Abaqus Analysis User's Guide (6.14)," 2014).

$$\tau_{crit} = \mu p \quad (2)$$

where: τ_{crit} is the critical interface shear stress (Pa),
p is the contact pressure (Pa), and
μ is the friction coefficient $(unitless)$.

While the interface shear stress is less than the critical magnitude, τ_{crit}, it is said that the surfaces are 'sticking'.

To represent fully bonded layers, the tangential friction formulation can be defined as 'rough' rather than 'penalty'. A friction coefficient is not required, and it is equivalent to specifying an infinite friction coefficient that prevents any relative slip between the two surfaces in contact ("Abaqus Analysis User's Guide (6.14)," 2014).

To simulate unbonded layers, the tangential friction formulation can be defined as 'frictionless'. This is equivalent to specifying a friction coefficient equal to zero; the contacting surfaces slide freely without friction ("Abaqus Analysis User's Guide (6.14)," 2014).

The normal behaviour is specified by the pressure-overclosure relationship, which is the relationship between the contact pressure and overclosure distance of the contacting surfaces. A 'hard' pressure-overclosure relationship was assigned in combination with 'rough' tangential behaviour, and a 'linear' relationship (Northmore, 2014) was assigned in combination with the 'penalty' and 'frictionless' tangential behaviours. The 'hard' pressure-overclosure relationship transmits any contact pressure when the surfaces are in contact, and if the surfaces separate then the contact pressure is set to zero ("Abaqus Analysis User's Guide (6.14)," 2014). The softened 'linear' contact relationship was used because it improves convergence for contact problems that involve a thin or lower stiffness layer, such as the support and subbase layers ("Abaqus Analysis User's Guide (6.14)," 2014). With linear contact, the surfaces transmit pressure when in contact, where the slope of the pressure-overclosure relationship is equal to a specified stiffness ("Abaqus Analysis User's Guide (6.14)," 2014). For contact with the support layer a stiffness of 5000 MPa/m was used, and for contact with the subbase layer a stiffness of 500 MPa/m was used. These stiffnesses were selected because they provided similar results to those using the 'hard' contact option, but convergence was more readily achieved.

The normal behaviour also includes an option to 'allow separation after contact'; this was enabled for the 'penalty' and 'frictionless' formulations and disabled for the 'rough' formulation. The constraint enforcement method was set as 'default' which is the 'Penalty method' ("Abaqus Analysis User's Guide (6.14)," 2014).

The contact between different pavement layers has been successfully modelled in the past using this frictional contact method (Hammons, 1998; Kim & Hjelmstad, 2003; Kuo et al., 1995; Northmore & Tighe, 2016; Priddy et al., 2015).

Frictional contact properties were assigned at the panel-to-base interface for the AS model and at the panel-to-support and support-to-base interfaces for the GR model. To consider the effects of different degrees of bonding at the interfaces, the friction properties were modelled using either the 'penalty' behaviour with a friction coefficient of 0.5 to represent a low level of bonding or using the 'rough' behaviour to represent a high level of bonding. Contact was also defined at the base-to-subbase interface for both the AS and GR models, using a friction coefficient of 0.5. Selection of the friction coefficient was based on previous research (Kuo, 1994; Priddy et al., 2015), and it closely approximated the behaviour of the 'frictionless' condition indicating a low degree of bonding.

3.2.6 Boundary conditions

Under symmetrical loading, symmetry was used to reduce the number of elements in the model by modelling only half or a quarter of the full three-panel model. In these cases, symmetry boundary conditions were applied at the lines of symmetry along the x-axis and y-axis (Figure 3-3).

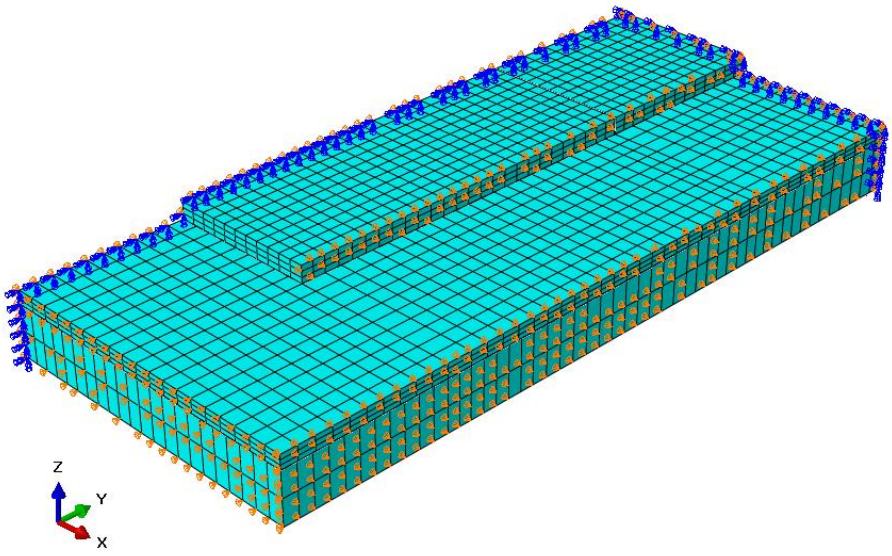

Figure 3-3. Boundary conditions applied to finite-element quarter model with symmetry

Vertical rollers were applied to the sublayers (base and subbase) that prevented lateral translation of the longitudinal edges and longitudinal translation of the transverse edges. The boundaries of the sublayers were extended beyond the panels such that the roller boundary conditions had a negligible effect on the responses of the loaded panel and the portion of the sublayer directly underneath. It was concluded that extending the sublayers 2 m in length and width beyond the panels was sufficient for results accuracy. The selection of the sublayer extents and results are discussed in more detail in Section 4.1.4.3.

The longitudinal edges of the panels are bordered by the adjacent lane of asphalt pavement, and the longitudinal concrete-asphalt joint is filled with grout. Therefore, the longitudinal edges of the panels and the support layer were assigned boundary conditions that prevent lateral movement.

Panels are placed consecutively in a lane and are connected at the joints by dowel bars. Three consecutive panels were included in the FEM without any boundary conditions applied to the edges of the end panels. A study was performed to evaluate which boundary conditions on the panel edges of the three-panel model would most closely approximate a model with additional panels (i.e. a five-panel model). Leaving the edges of the end panels free from any restraints most closely matched the five-panel model. The selection of the end panel boundary conditions and results are discussed in more detail in Section 4.1.4.2.

3.2.7 Dowels

Various methods of modelling dowels for load transfer in rigid pavements have been used in research. The dowels can be modelled as three-dimensional continuum elements with contact interfaces between the dowel and surrounding material, or the dowels can be modelled by embedded beam elements (Kim & Hjelmstad, 2003).

The first method using continuum elements (Figure 3-4) provides more detailed strain and stress distributions in the dowels and the surrounding area, which is beneficial for studies focusing on the behaviour of the dowels and surrounding concrete. However, this method requires a finer mesh for the dowels and for the slab near the doweled area; this drastically increases the computation time especially for multi-panel models and when performing parametric studies (Kim & Hjelmstad, 2003).

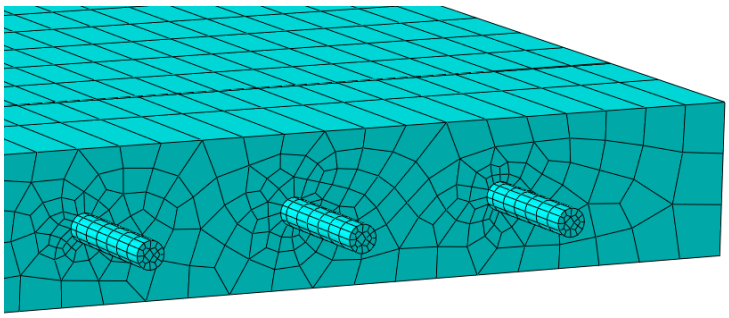

Figure 3-4. Dowels modelled as continuum elements

The embedded element formulation (Figure 3-5) saves computation time by eliminating the need to align the fine dowel mesh with a fine panel mesh near the doweled area. The dowel is modelled by three-noded quadratic beam elements (Davids & Turkiyyah, 1997).

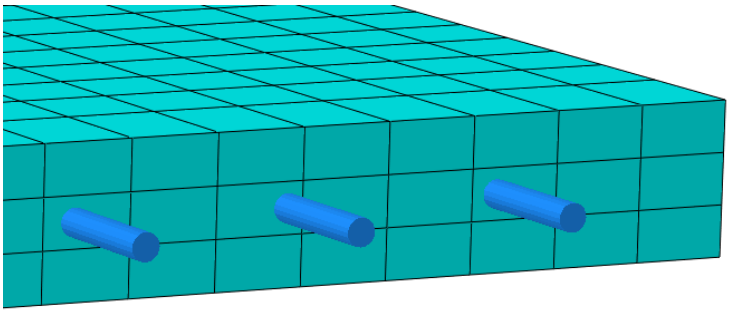

Figure 3-5. Dowels modelled as embedded beam elements

Using Abaqus, Kim and Hjelmstad (2003) and Uddin et al. (1995) modelled the dowels as beam elements that were directly embedded in a continuum of solid elements.

For this research, both methods were compared and these results are discussed in Section 4.1.3.3. Based on this comparison, the embedded dowel approach yielded results that were sufficiently accurate and greatly reduced the computation time. Therefore, the embedded dowel approach was selected.

The embedded element formulation is achieved using the 'embedded region' option in Abaqus which allows a set of beam elements, such as the dowel bars, to be embedded in another set of solid host elements, such as the panels. The host elements constrain the translational degrees of freedom of the nodes of the embedded elements ("Abaqus Analysis User's Guide (6.14)," 2014).

3.2.8 Element Types & Mesh

The panel was meshed using C3D20R elements, which are three-dimensional 20-noded quadratic brick elements using reduced integration. The elements have 3 translation degrees of freedom per node. Second-order (quadratic) elements were chosen because they are more accurate and are more effective in bending problems than first-order (linear) elements ("Abaqus Analysis User's Guide (6.14)," 2014). Convergence studies for element types used in 3D pavement modelling have confirmed that the responses of quadratic C3D20R elements are better than those of linear C3D8R elements (Hammons, 1998; Kuo et al., 1995). The use of quadratic elements can cause convergence difficulties with contact problems, however second-order elements work well with the contact interactions definition if a 'surface-to-surface' contact formulation is used ("Abaqus Analysis User's Guide (6.14)," 2014).

The mesh size influences both the accuracy of results and computation time of the models. The mesh aspect ratio $(2a/h)$ is the ratio of the maximum dimension to the minimum characteristic dimension of the element. (Kuo et al., 1995) recommended that a mesh with an aspect ratio of less than 2.0 near the loaded area will provide accurate responses. The aspect ratio can be increased further away from the loaded area where the responses are not as critical, and aspect ratios up to 4.5:1 are often used (Davids, 2000, 2001; Saleh, Steven, & Alabaster, 2003).

The model was meshed with rectangular elements with a side length of approximately 175 mm, 48 mm, 200 mm, and 180 mm for the panel, support, base, and subbase layers respectively. The slave surfaces were chosen to have finer meshes than their master surfaces to avoid non-convergent solutions and inaccurate stress results ("Abaqus Analysis User's Guide (6.14)," 2014). The panel and base layer were meshed with three elements each through their thickness, the support layer with one element, and the subbase layer with two elements (Figure 3-6). Using more than one element through the layer thickness improves accuracy of the stresses through the thickness (Davids, 2001; Mallela & George, 1994).

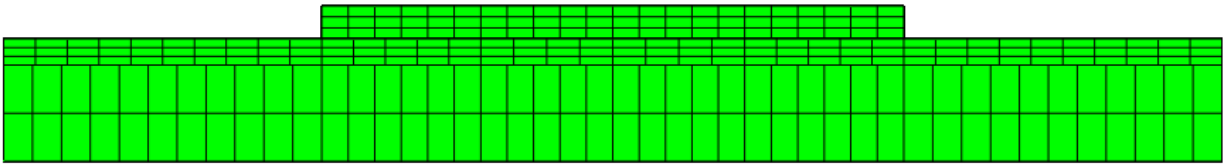

Figure 3-6. Cross-sectional view of finite element mesh

The maximum aspect ratio of the elements was 4:1, and the maximum aspect ratio of the panel elements was 2.2:1. The selection of the mesh size and verification for the accuracy of results is described in detail in Section 4.1.4.1.

3.3 Loads

3.3.1 Self-weight

Self-weight was applied to each layer of the pavement structure by assigning a 'gravity' load in Abaqus in conjunction with the respective material densities for each component that are summarized in Table 3-2.

The densities of the support, base, and subbase were identical and the combined thickness of these layers was the same for all models to ensure that the combined self-weight would be constant for easy comparison between models. Therefore, the base layer is thinner in the GR models than the AS model to account for the thickness of the support layer. If the support thickness was increased, then the base thickness was decreased by the same magnitude to keep the combined thickness constant.

3.3.2 Traffic

Wheel loads were applied as a uniform pressure over a rectangular area. This assumption for pressure distribution and loaded area is adequate for rigid pavements since the tire pressure distribution does not have a significant effect on the responses (Channakeshava, Barzegar, & Voyiadjis, 1993).

The axle loading was a standard 80-kN (18 kip) axle equivalent single axle load (ESAL) used in pavement design (Huang, 2004). The tire area was modelled as a square 0.25 m by 0.25 m load, which corresponds to a tire pressure of 640 kPa (Cho, McCullough, & Weissmann, 1996; Saleh et al., 2003). The axles are applied as static loads.

3.3.3 Temperature Gradient

Temperature gradients through the thickness of the concrete cause panel curling (Delatte, 2014). Under a temperature gradient, the concrete expands on the warmer face of the panel and contracts on the cooler face of the panel. Under a positive temperature gradient the top of the panel is warmer than the bottom causing the centre of the panel to curl upwards, and under a negative gradient the top of the panel is cooler than the bottom side causing the panel edges to curl upwards (Figure 3-7). The temperature gradients applied to the FEM were 10°C and -10°C, which corresponds to a magnitude of 0.49°C/cm. The magnitudes of the temperature gradient were selected based on temperature readings collected from the PCIP trial section. The maximum temperature gradient had a magnitude of 12°C, but a 10°C gradient occurred more frequently.

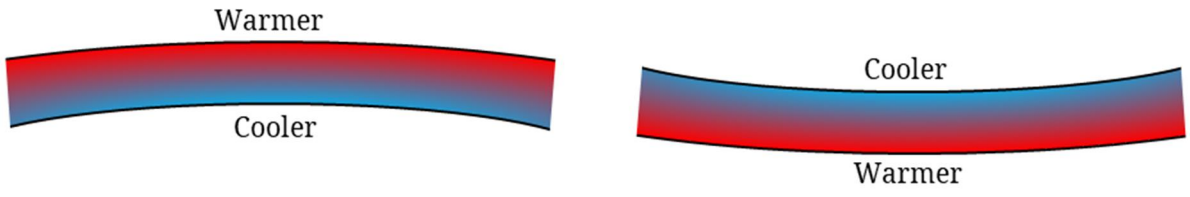

Figure 3-7. Panel curling under positive temperature gradient (left) and under a negative temperature gradient (right)

Panel curling is restrained by the support underneath the panels and is counteracted by the self-weight of the slabs and possibly by axle loading, depending on the wheel positions (Merritt et al., 2000). The panel self-weight induces tensile stresses in the unsupported areas of the deformed

panel; the stresses develop at the bottom centre or top edges of the panel under a positive or negative gradient, respectively (Merritt et al., 2000).

3.3.4 Combined Loading

The pavement responses were investigated under a combination of temperature gradients, self-weight, and axle loading, since combined loading can produce more critical responses than any of these loads alone. Panel distresses are exacerbated when there is a temperature gradient that reduces the support under the axle-loaded area and under the influence of the panel's self-weight (Merritt et al., 2000). Repeated, heavy axle loads cause fatigue damage to the panels and cracking eventually occurs in the locations of high tensile stress (ARA Inc., 2004).

The axle locations inducing maximum tensile stresses are where the wheels are positioned on areas with reduced support (Figure 3-8).

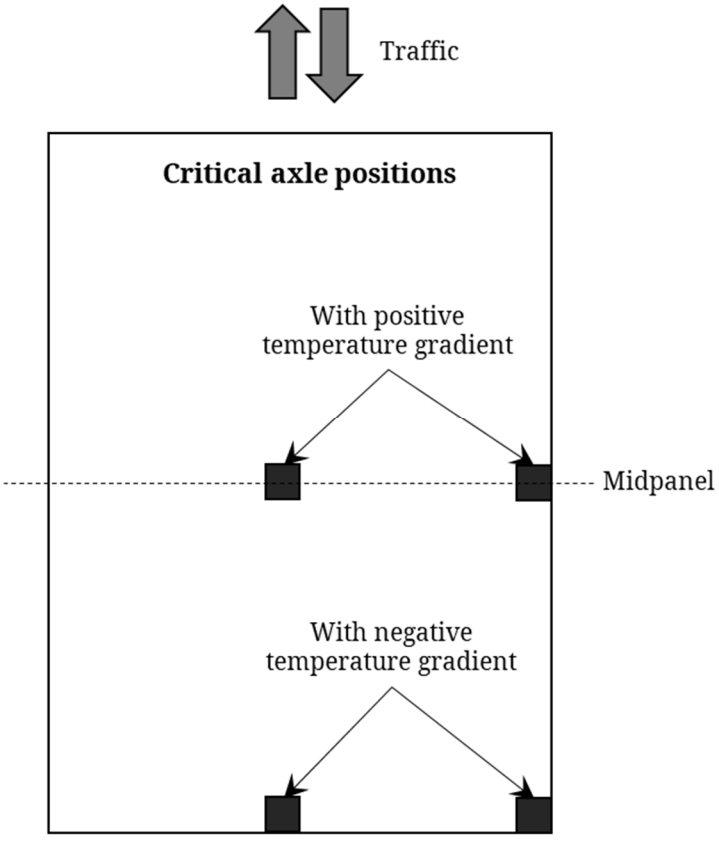

Figure 3-8. Critical axle locations for traffic loading combined with temperature gradient

Combined with a positive temperature gradient, when the panel curls upwards, the critical axle position is at midpanel with the axle shifted transversely to the panel edge. Combined with a negative temperature gradient, when the panel curls downwards, the critical axle position is at the joint and shifted transversely to the panel corner (ARA Inc., 2003; Davids, 2000; S. R. Maitra et al., 2009; Merritt et al., 2000).

3.3.5 Falling Weight Deflectometer Load Testing

The Falling Weight Deflectometer (FWD) test is a non-destructive method used to evaluate the structural capacity of pavement structures. It is used to estimate the in-situ characteristics of the pavement materials, and for rigid pavement, to determine load transfer efficiency of the joints and predict the presence of voids under the pavement (Chan & Lane, 2005). The test is performed by dropping an impulse load on the pavement and measuring the deflection response at various radial locations from the centre of the applied load (Chan & Lane, 2005).

FWD testing was performed two weeks after the PCIP construction, in October 2016, and again one year after construction, in September 2017. The test was performed for three load levels, with target loads of 40 kN, 55 kN, and 70 kN. Each panel was tested in four locations – the inner wheel path (IWP) and outer wheel path (OWP) on the approach and leave side of the panel. The IWP and OWP are 0.78 m and 2.92 m from the inner edge of the panel, respectively. The load was applied at 15 cm from the joint, and the deflections were measured at distances of -30 cm, 0 cm, and 30 cm from the centre of the load (Figure 3-9) (Chan & Lane, 2005).

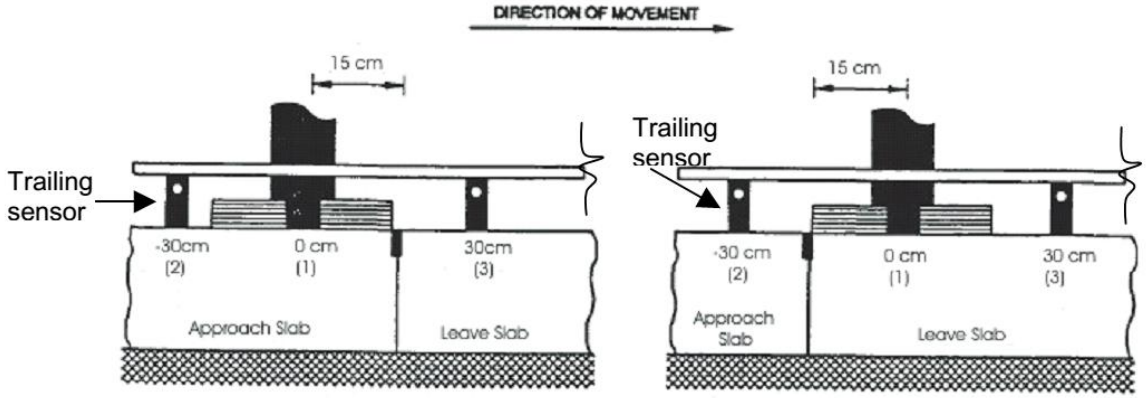

Figure 3-9. FWD testing (Chan & Lane, 2005)

In 2017, the same testing was performed, and in addition, full deflection basins were measured for four of the panels for the FWD load applied at the centre of the panel. For the deflection basin, the deflections were measured at radial distances of 0, 20, 30, 45, 60, 90, 120 and 150 cm from the centre of the load.

The FWD load is a short impulse load, typically with a 25 millisecond duration. The time-dependent load was modelled by the function in Figure 3-10. This load pulse approximates the load-time history recorded during the field test. The same pulse applies for all three load levels.

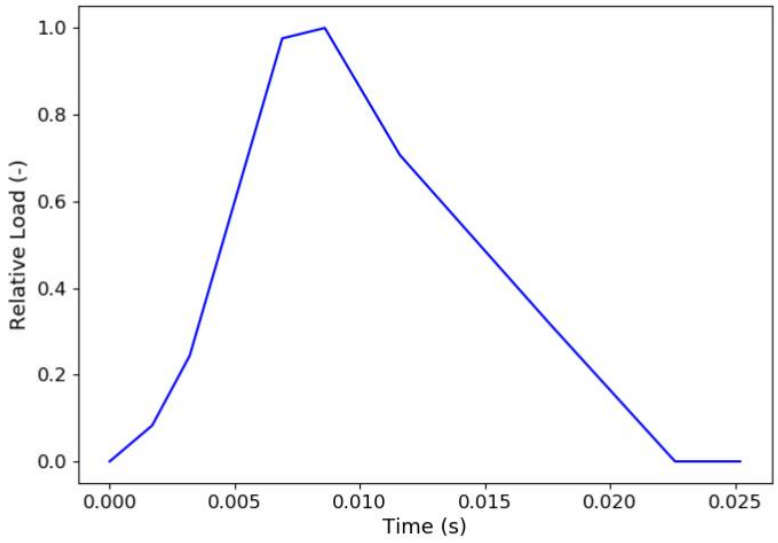

Figure 3-10. FWD load pulse

The FWD impulse load was applied using a 'Dynamic, Implicit' type of step in Abaqus with a duration of 25 ms. In the field test, the measured deflection corresponds to the maximum deflection recorded at the sensor. The peak load occurs at approximately 8.6 ms, and the peak deflection 0 cm to 30 cm away from the applied load occurs at approximately 12.5 ms, which is halfway through the time step.

The measured FWD deflections were compared to theoretical deflections obtained from the FEA to calibrate the model, as described in Section 4.2.

CHAPTER 4 Finite Element Model Development

This chapter describes the model verification, calibration, and validation processes which are part of the model development phase. These steps in the model development were performed after conducting research about the different model components and before completing the final analyses.

4.1 Model Verification

4.1.1 Verification Methodology

The finite element model (FEM) of the PCIP was developed through many iterations of models, starting from a single-panel model on a dense-liquid foundation to the final multi-panel, multi-layered model. Model verification was performed throughout the model development phase. The model responses were compared with theoretical solutions, and verification tests were performed to make choices about certain modelling aspects, including the number of panels, sublayer extents, and mesh size. The model verification process is summarized in Figure 4-1.

This section first describes the theoretical solutions for pavement responses, followed by the comparisons to theoretical solutions and the verification tests.

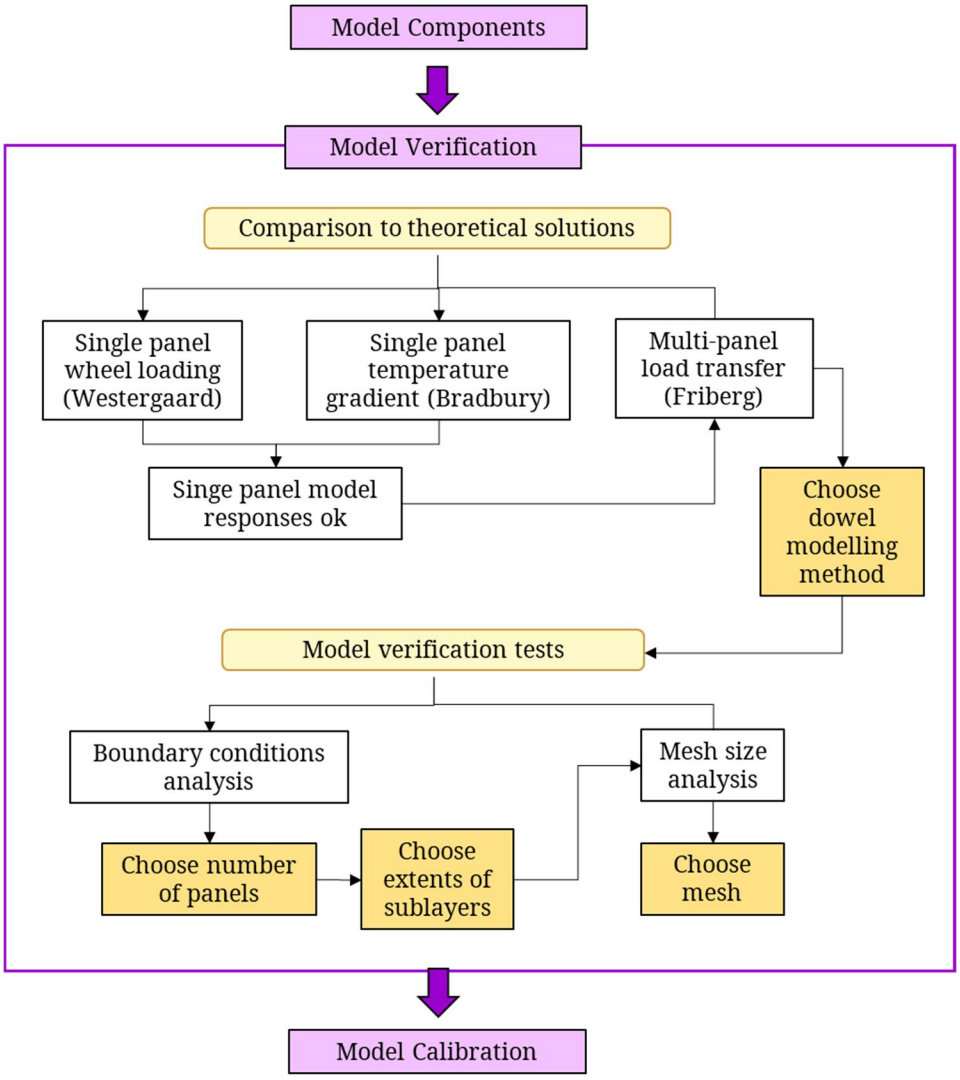

Figure 4-1. Verification Methodology

4.1.2 Theoretical Solutions

4.1.2.1 Westergaard Theory

Westergaard (1926, 1948) developed theoretical solutions for the maximum stress and deflection response of a slab-on-grade subjected to an interior, edge, or corner load. Only the interior and edge loading cases were used for comparison because these responses most accurately match with predictions from FEA (Khazanovich, 1994). The maximum stress in the panel for interior loading and edge loading predicted by Westergaard theory are given by Equation 3 and Equation 4, respectively (Ioannides, Thompson, & Barenberg, 1985).

$$\sigma_i = \frac{3P(1+\mu)}{2\pi h^2}\left[ln\left(\frac{2l}{a_i}\right) + 0.5 - \gamma + \frac{\pi}{32}\left(\frac{a_i}{l}\right)^2\right] \quad (3)$$

$$\sigma_e = \frac{3P(1+\mu)}{\pi(3+\mu)h^2}\left[\ln\left(\frac{Eh^3}{100ka_e{}^4}\right) + 1.84 - \frac{4}{3}\mu + \frac{1}{2}(1-\mu) + 1.18(1+2\mu)\left(\frac{a_e}{l}\right)\right] \quad (4)$$

where: σ_i is the maximum bending stress due to interior loading (Pa),

σ_e is the maximum bending stress due to edge loading under a circular load (Pa),

P is the total applied load (N),

μ is the slab Poisson's ratio $(unitless)$,

k is the modulus of subgrade reaction (Pa/m),

π is the mathematical constant approximately equal to 3.142 $(unitless)$,

h is the slab thickness (m),

l is the radius of relative stiffness (m), given by Equation 5,

γ is Euler's constant which is equal to 0.577 $(unitless)$,

a_i is the radius of the circular-loaded area with the same diameter as the side length of the square-loaded area in the finite element model (m), and

a_e is the radius of the circular-loaded area that yields the same area for the circular area as the square area in the finite element model (m).

Ioannides (1984) performed studies to compare FEA results using a square-loaded area with theoretical solutions using different choices of radius for the circular-loaded area. Similarly, the radius of the circular area for this study was selected to produce the closest match between the FEA results and the theoretical responses.

The radius of relative stiffness is calculated by Equation 5 (Delatte, 2014):

$$l = \sqrt[4]{\frac{Eh^3}{12(1-\mu^2)k}} \quad (5)$$

where: l is the radius of relative stiffness (m),
E is the modulus of elasticity (Pa), and
the other parameters were described previously.

The maximum deflection responses of the panel under interior loading and edge loading predicted by Westergaard theory are given by Equation 6 and Equation 7, respectively (Ioannides et al., 1985).

$$\delta_i = \frac{P}{8kl^2}\left[1 + \frac{1}{2\pi}\left(ln\frac{a_i}{2l} + \gamma - \frac{5}{4}\right)\left(\frac{a_i}{l}\right)^2\right] \tag{6}$$

$$\delta_e = \frac{P\sqrt{2 + 1.2\mu}}{\sqrt{Eh^3k}}\left[1 - (0.76 + 0.4\mu)\left(\frac{a_e}{l}\right)\right] \tag{7}$$

where: δ_i is the maximum deflection due to interior loading (m),
δ_e is the maximum deflection due to edge loading for a circular loaded area (m),
and the other parameters were described previously.

Westergaard's theory assumes a single infinite slab on a semi-infinite foundation, a single load, and no slab curling or warping (Ioannides et al., 1985). The Westergaard solutions should approximate the finite element responses of a model that meets these assumptions. There are additional recommendations for the mesh size, size of the loaded area, and slab size limitations. The ratio of the mesh dimension to the slab thickness $(2a/h)$ should be less than 0.8 to for 98% accuracy (Kuo et al., 1995). The ideal ratio of side length of the loaded area to the radius of relative stiffness (c/l) is 0.2 to achieve good comparison between the Westergaard solutions and the FEA results; as the load size increases, the Westergaard solutions diverge (Ioannides et al., 1985). The ratio of the radius of relative stiffness to the slab length (l/L) should be greater than 3.5 and 5.0 for convergence of the interior loading stresses and edge loading stresses, respectively, and greater than 8.0 for convergence of the deflections with Westergaard theory (Ioannides et al., 1985).

4.1.2.2 Bradbury Theory

Bradbury (1938) developed equations to estimate the curling stresses developed in a concrete panel due to a temperature gradient through the panel thickness. The edge and interior curling stresses are calculated using Equation 8, and Equations 9 and 10, respectively.

$$\sigma = \frac{CE\alpha_t \Delta T}{2} \tag{8}$$

where: σ is the slab edge curling stress (Pa), which is σ_x or σ_y when C is C_x or C_y, respectively,
C is a coefficient which is a function slab length and the radius of relative stiffness, determined using Figure 4-2 ($unitless$),
E is the modulus of elasticity of concrete (Pa),
α_t is the thermal coefficient of concrete which was 1x10-5 $\left(\frac{1}{℃}\right)$, and
ΔT is the temperature differential between the top and bottom of the slab ($°C$).

$$\sigma_x = \frac{E\alpha_t \Delta T}{2}\left[\frac{C_\mathrm{x} + \mu C_\mathrm{y}}{1-\mu^2}\right] \tag{9}$$

where: σ_x is the slab interior curling stress (Pa),
C_x is the coefficient in the direction of the calculated stress, determined using Figure 4-2 ($unitless$),
C_y is the coefficient in the direction perpendicular to C_x, determined using Figure 4-2 ($unitless$), and
μ is the Poisson ratio of concrete which was 0.15.

The slab interior curling stress in the perpendicular direction can be calculated by switching the coefficients C_x and C_y in Equation 9 to obtain the following equation:

$$\sigma_y = \frac{E\alpha_t \Delta T}{2}\left[\frac{C_\mathrm{y} + \mu C_x}{1-\mu^2}\right] \tag{10}$$

Figure 4-2 is used to determine the coefficients for the slab curling stress.

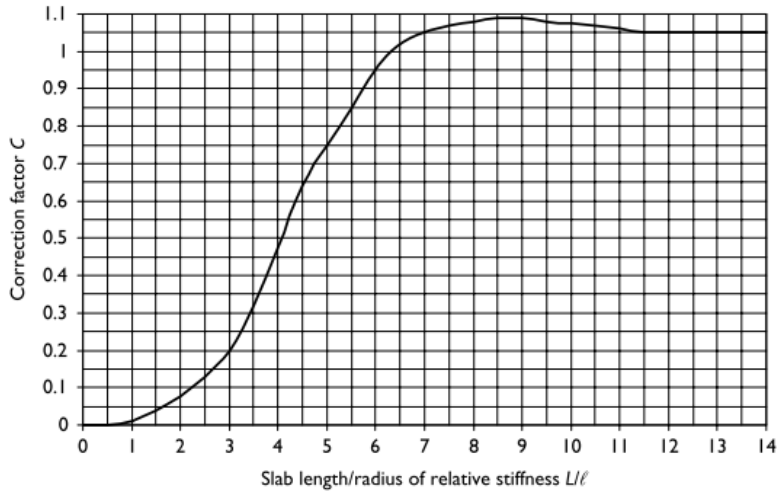

Figure 4-2. Coefficients for Westergaard-Bradbury curling stress equations (Delatte, 2014)

4.1.2.3 Timoshenko and Lessels and Friberg Theory

Timoshenko and Lessels (1925) and Friberg (1940) developed solutions for the shear force and bending moment along the length of a dowel bar for panel joint load transfer, given by Equation 11 and Equation 12, respectively.

$$V = -e^{-\beta x}[(2\beta M_o - P_t)sin\beta x + P_t cos\beta x] \quad (11)$$

$$\mathrm{M} = -\frac{e^{-\beta x}}{\beta}[P_t sin\beta x - \beta M_o(sin\beta x + cos\beta x)] \quad (12)$$

where: β is the relative stiffness of a dowel embedded in concrete ($\frac{1}{m}$),

M_o is the bending moment on the dowel at the face of the concrete ($N \cdot m$), and

P_t is the load transferred through the dowel bar .

The relative stiffness of the dowel embedded in concrete can be calculated by Equation 13.

$$\beta = \sqrt[4]{\frac{Kd}{4E_d I_d}} \quad (13)$$

where: K is the modulus of dowel support ($\frac{Pa}{m}$),

d is the diameter of the dowel (m^2),

E_d is the Young's modulus of the dowel bar (Pa), and

I_d is the moment of inertia of the dowel bar (m^4).

The bending moment at the face of the concrete is given by Equation 14.

$$M_o = \frac{-P_t z}{2} \tag{14}$$

where: z is the joint width (m), and

M_o and P_t are as previously defined.

4.1.3 Comparison to Theoretical Solutions

4.1.3.1 Slab on Winkler foundation with wheel loading

The first model created was a three-dimensional model of a single PCIP supported by a dense-liquid foundation. The model details are summarized in Table 4-1.

Table 4-1. 3D single slab PCIP model

Model Input	Value
Slab width	3.66 m
Slab length	4.57 m
Slab thickness	0.205 m
Square load side length	0.3 m
Load pressure	0.5 MPa
Modulus of subgrade reaction	135 MPa/m
Modulus of elasticity of concrete	34,109 MPa
Poisson's ratio of concrete	0.15
Element type	C3D20R
Mesh dimension	0.125
Number of elements through panel thickness	3

The k-value of 135 MPa is recommended to account for the high stiffness provided by the existing asphalt under a concrete overlay (Delatte, 2014).

A wheel load was applied, at the centre of the panel or at the edge in two separate loading scenarios, and the FEA responses were compared with Westergaard's theoretical solutions for the maximum panel stresses and deflections under interior and edge loading. The comparison of the FEA responses with the theoretical responses are summarized in Table 4-2.

Table 4-2. Comparison of panel responses with wheel loading

Model	Maximum Stress (MPa)	Percent difference from theory (%)	Maximum Deflection (mm)	Percent difference from theory (%)
Interior Loading				
Theory (Westergaard)	1.339		-0.095	
Finite Element	1.343	0.3%	-0.106	12%
Edge Loading				
Theory (Westergaard)	2.390		-0.275	
Finite Element	2.390	0.0%	-0.304	11%

The responses predicted by FEA match reasonably well with those predicted by Westergaard theory; the stress responses match very closely with the theoretical responses, and the deflection responses overpredicted the theoretical responses by up to 12%.

The cause of this discrepancy may be that the properties of the PCIP slab do not meet all the recommended criteria for the assumptions of Westergaard theory. The length-to-thickness ratio of the slab is 17.9 (considering the shorter dimension of the slab) which is close to but does not meet the recommended ratio of 20 for a thin plate (Kuo et al., 1995). The mesh consists of uniform elements with a side length of 0.125, resulting in a ratio of $2a/h$ of 0.61 that meets the recommended limit. The ratio l/L for the slab is 5.58, which meets the recommended criterion for convergence of stresses with Westergaard theory, but is less than the recommended ratio of 8.0 for convergence of deflections. The ratio of c/l is 0.38, which exceeds the ideal ratio of 0.2. Therefore, the FEA-predicted deflections are reasonable considering that not all of these requirements are satisfied. Furthermore, refining the panel mesh produces very similar responses, indicating that the mesh size used in this study is adequate.

4.1.3.2 Slab on Winkler Foundation with temperature gradient

To verify the modelling of a temperature gradient applied across the thickness of the concrete panel, FEA results were compared to the Westergaard-Bradbury theoretical equations that predict the curling stress in a panel on a Winkler foundation subjected to a temperature gradient.

A thermal gradient was applied to the panel that corresponded to a temperature of 0°C and -10°C at the top and bottom of the slab, respectively, and varied linearly through the thickness of the panel. Self-weight was not included. The geometry and properties of the model were the same as described previously in Section 4.1.3.1.

The edge and interior curling stresses were calculated using Equation 8, Equation 9 and Equation 10. The radius of relative stiffness of the PCIPs is 0.656 m, and for the 3.66 m wide by 4.57 m long panel, the coefficients C_x and C_y are taken as 1.05 and 0.87, respectively, using Figure 4-2.

Table 4-3 summarizes the maximum curling stresses in the concrete panel, as predicted by Westergaard-Bradbury theory and the FEA.

Table 4-3. Comparison of maximum panel response with thermal gradient

Model	Maximum Stress, S11 (MPa)	Percent difference from theory (%)	Maximum Stress, S22 (MPa)	Percent difference from theory (%)
Interior Stress				
Theory (Bradbury)	-1.79		-2.06	
Finite Element	-1.70	-5%	-1.99	-3%
Edge Stress				
Theory (Bradbury)	-1.48		-1.79	
Finite Element	-1.43	-3%	-1.77	-1%

The stress responses predicted by the FEA match Westergaard-Bradbury theory very closely, indicating that the model and application of a temperature gradient load are adequate.

4.1.3.3 Multi-panel on Winkler foundation load transfer

To verify that the panel load transfer was modelled correctly, the FEA results for a multi-panel model were compared with theoretical solutions for shear and bending moment in the dowels, from Equation 11 and Equation 12, respectively. The dowel bars were modelled using the two methods of solid continuum elements and embedded beam elements discussed in Section 3.2.7. The dowels modelled as continuum elements are inserted into dowel hole cut-outs in the panel and at the dowel-to-panel interface either a low friction or high friction condition was applied.

The load transferred through the dowel bar, P_t, is typically assumed to be 0.45 or 0.5 times the applied load, in theory. However, since FEA responses were available, the load transferred through the central dowel could be identified from the analysis. For the dowel modelled with solid elements and low friction the shear force at the joint was approximately 7 kN; this value was used for P_t. For the other dowel modelling methods, P_t would be slightly different but the difference is not significant when comparing the results to the theoretical solution, so it was neglected. The β value was back-calculated by choosing the value that produced a close match between the theoretical solution and the FEA results for the solid dowel with low friction. By this method, the obtained β value was 19 m^{-1}, and the resulting value of K back-calculated from Equation 13 was 281 GPa/m. Among researchers, there is not a consensus on a precise value for the modulus of dowel support but the suggested range is between 81.5 GPa/m to 409 GPa/m (Huang, 2004). Therefore, the back-calculated K falls within the recommended range.

Figure 4-3 and Figure 4-4 respectively compare the shear force and bending moment in the central dowel bar from theory and FEA responses.

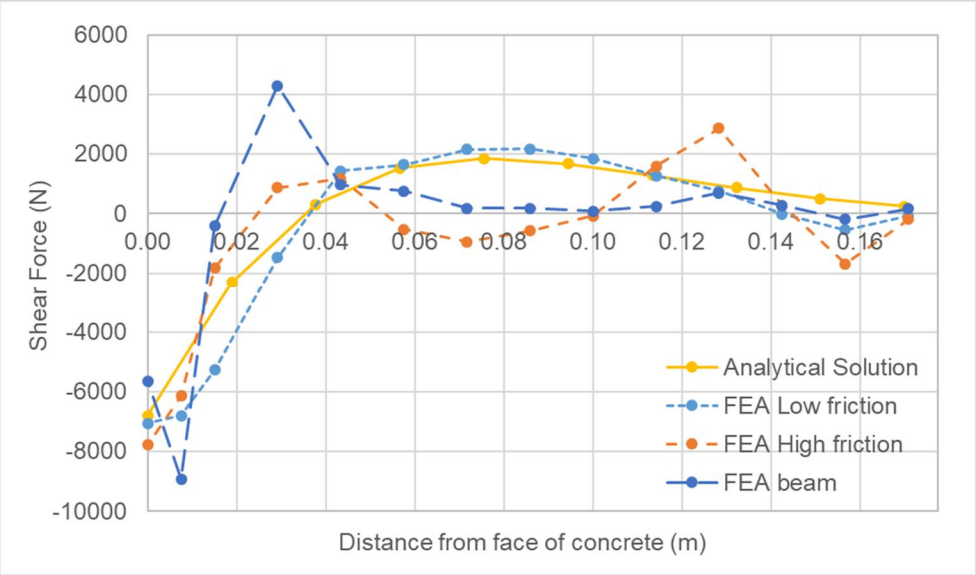

Figure 4-3. Shear force along length of central dowel bar

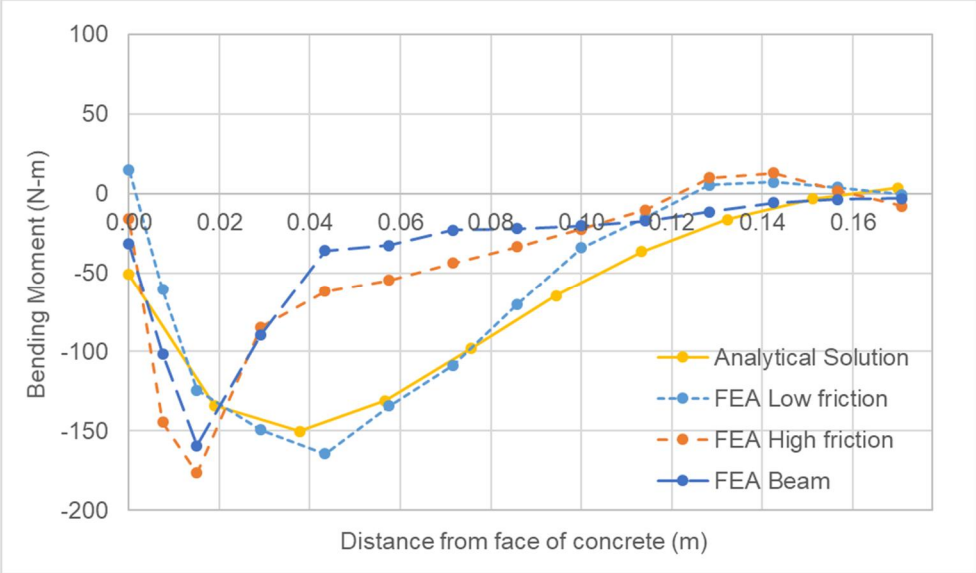

Figure 4-4. Bending moment along length of central dowel bar

The shear force and bending moment for the dowels modelled as a continuum with a low friction interface match the theoretical solutions fairly well. With high friction, the FEA results and theoretical response begins to deviate.

With higher friction, the shear force in the dowel fluctuates more than with low friction; the shear force at first increases as the distance from the face of concrete increases, then decreases. With

higher friction, the movement of the dowel bar is more restrained and this fluctuation in shear forces is likely caused because there are larger reaction forces from the concrete.

With higher friction, the maximum bending stress in the dowel is slightly larger and occurs closer to the concrete face, and the bending stresses decrease more rapidly moving away from the concrete face. This can be explained by the fact that with higher friction, the dowel will be more restrained by the surrounding concrete resulting in lower stresses where the dowel is more deeply embedded in the concrete and a sharper stress increase near the joint. With lower friction, the stresses are more distributed along the length of the dowel bar.

While the embedded beam model does not match the theoretical solutions very closely, the bending moment responses are extremely similar and the shear forces follow a similar pattern to that of the solid dowel with high friction. Using Abaqus' 'embedded region' constraint, the degrees of freedom of the beam are constrained by those of the surrounding concrete. Therefore, it is expected that the dowel beam would behave more similarly to the dowel with high friction that is more restrained by the surrounding concrete than the dowel with low friction, as observed. This provides confidence that the dowel bars modelled as embedded beam elements are behaving as expected.

The responses of the concrete panel were compared for the two different dowel modelling methods, as continuum elements with high interface friction and as embedded beam elements. The dowel forces and stresses and the panel stresses immediately surrounding the dowels differ significantly. However, the responses in the panels further from the doweled area are very similar. The minimum panel stresses and deflections in the loaded panel are compared for both dowel modelling methods in Figure 4-5 and Figure 4-6.

The responses of interest in this research are the minimum stresses in the pavement and the panel deflections which were used for calibration and validation. Detailed evaluation of the dowel behaviour and concrete immediately surrounding the dowel are not being investigated. Therefore, the embedded beam element method was used for all further analyses. This method provides high enough accuracy for the responses of interest and greatly reduces the computation time.

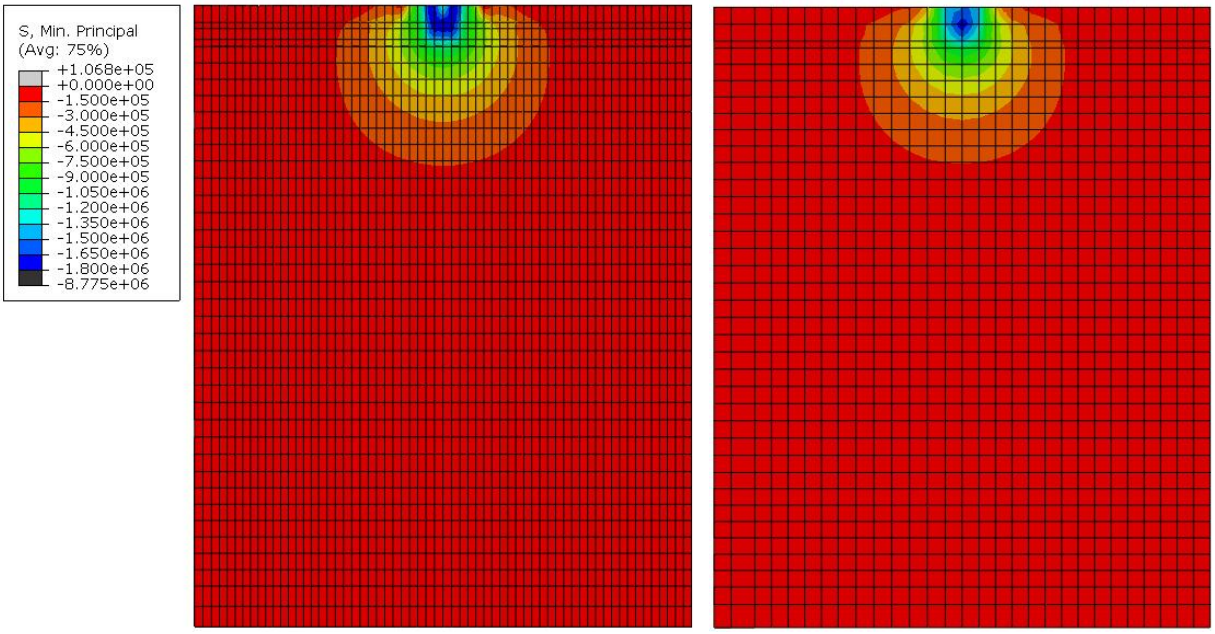

Figure 4-5. Comparison of minimum principal stresses in the loaded panel for dowels modelled as solid elements (left) and embedded beam elements (right)

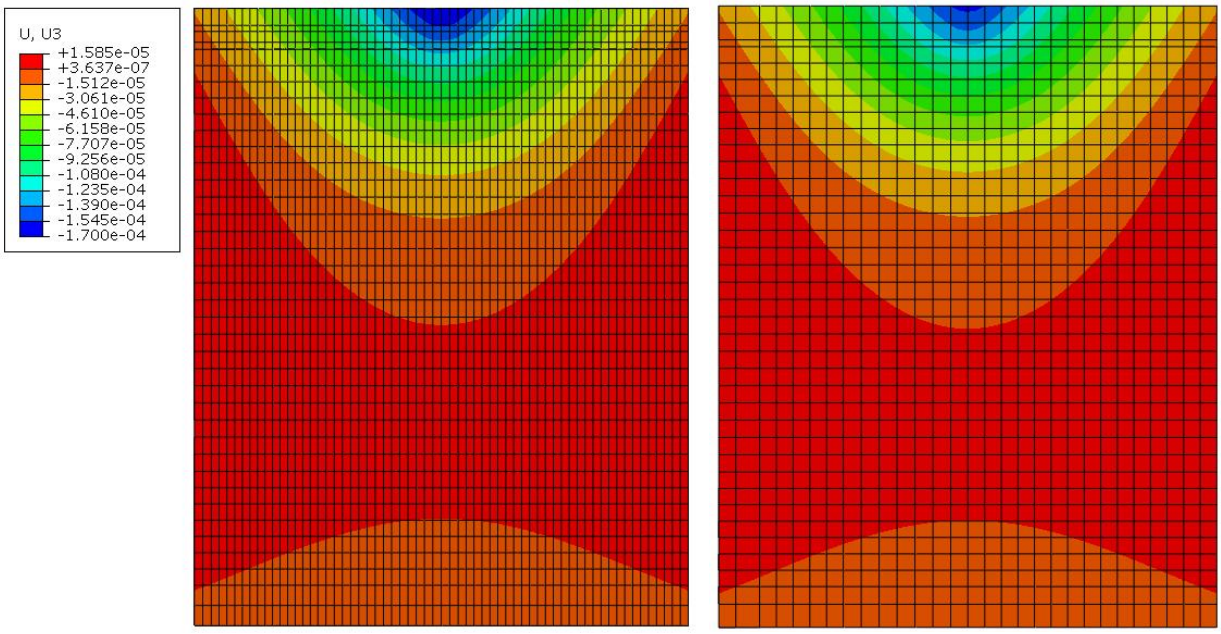

Figure 4-6. Comparison of deflections in loaded panel for dowels modelled as solid elements (left) and embedded beam elements (right)

4.1.4 Verification Tests

4.1.4.1 Mesh Verification

In meshing a finite-element model, there is a trade-off between the accuracy of the results and the computation time. A finer mesh produces more accurate analysis results, but increases the analysis run time in comparison to a coarser mesh. To establish suitable mesh sizes for the FEM, sensitivity analyses were performed to evaluate the effect of various mesh sizes on the pavement responses.

The model used for the mesh sensitivity analysis had sublayers extended beyond the panel edges to reduce the effects of the boundary conditions on the panel responses. The granular base was modelled to a depth of only 0.3 m to reduce the number of elements in the model. A temperature gradient was applied in combination with an axle applied at each joint and transversely centred to take advantage of symmetry to reduce the model size.

To study the effect of mesh size on the pavement responses, critical responses in the panel, support, base, and subbase were compared for models with a range of mesh sizes summarized in Table 4-4. A model with a very fine mesh was used as the base model to compare how closely the coarser meshes approximated the responses of the finely meshed model.

Table 4-4. Mesh sizes and run times for mesh sensitivity analysis

Model No.	Run Time (min)	Mesh size (mm)			
		Panel (A)	Support (B)	Base (C)	Subbase (D)
Base	829	60	36	85	65
1	263	75	36	125	100
2	190	100	36	150	125
3	141	125	36	175	150
4	100	125	48	175	150
5	78	125	60	175	150
6	125	150	36	200	175
7	82	150	48	200	175
8	61	150	60	200	175
9	76	175	48	200	180
10	74	175	48	225	200
11	63	200	48	250	225

The mesh sizes of the panel, support, base, and subbase are denoted by dimensions A, B, C, and D, respectively in Figure 4-7.

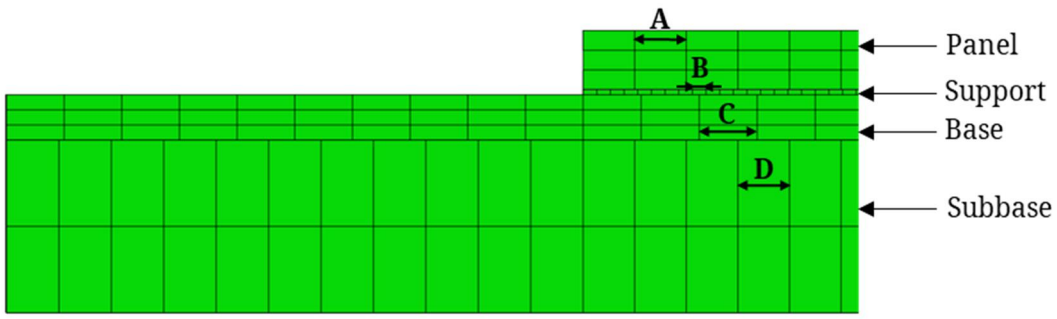

Figure 4-7. Mesh sizes of PCIP finite element model

For the base model, there were 4 elements each through the thickness of the panel and base, 3 elements through the subbase, and 1 element through the support thickness. For all other models, there were 3 elements each through the panel and base, 2 elements through the subbase, and 1 element through the support thickness. The maximum aspect ratio of any element was 5:1.

For all the mesh sizes tested, the deflections of the panel, base, and subbase at critical locations were within 1% of the deflections predicted by the finely-meshed model. For all mesh sizes, the

critical stresses in the panel and subbase layers were within 2% of the responses obtained by the base model. The support and base stresses deviated more; therefore, these responses were compared more closely to select the optimal mesh size.

First, the effect of the support mesh size was studied. The support mesh size was varied from 36 mm to 60 mm while the mesh size of the panel, base, and subbase were held constant for two different combinations. The mesh sizes and the difference in critical support stresses are summarized in Table 4-5.

Table 4-5. Comparison of support stresses for varying support mesh sizes

Model No.	Run Time (min)	Mesh size (mm)				Difference in support stresses	
		Panel (A)	Support (B)	Base (C)	Subbase (D)	Maximum Stress	Minimum Stress
3	141	125	36	175	150	2%	-5%
4	100	125	48	175	150	6%	2%
5	78	125	60	175	150	11%	8%
6	125	150	36	200	175	1%	-7%
7	82	150	48	200	175	5%	-1%
8	61	150	60	200	175	9%	3%

The difference in the maximum principal stress increased significantly as the support mesh size increased. The minimum principal stress was underestimated for the smallest mesh size and was overestimated for the largest mesh size. Taking into account the analysis run time of each model, the medium-sized support mesh of 48 mm is recommended. Some precision in the maximum stress response was compromised; however, the run time was reduced by approximately 40 minutes. The mesh size of 60 mm was rejected because it achieved a less substantial reduction in the run time with a relatively large decrease in precision.

The difference in critical stresses in the base for all mesh sizes was less than 6%, in comparison to the base model. Therefore, the results are not shown here since all the meshes are acceptable from the standpoint of precision of base stresses.

After selection of a support mesh size of 48 mm, a second study was completed to compare the effect of varying mesh sizes of the panel, base, and subbase layers, summarized in Table 4-6.

Table 4-6. Comparison of support stresses for varying mesh sizes with medium-size support mesh

Model No.	Run Time (min)	Mesh size (mm)				Difference in support stresses	
		Panel (A)	Support (B)	Base (C)	Subbase (D)	Maximum Stress	Minimum Stress
4	100	125	48	175	150	8%	0%
7	82	150	48	200	175	8%	-1%
9	76	175	48	200	180	7%	-1%
10	74	175	48	225	200	14%	6%
11	63	200	48	250	225	12%	5%

Model 4 and Model 7 are the same models used in the previous study of support mesh size. Models 10 and 11 were rejected because the precision was considerably lower than other meshes. Model 9 was selected as optimal because the responses are comparable to the more finely-meshed models and the run time was reduced by 24 minutes in comparison to Model 4.

The critical base stresses were within 6% of the base model for Model 9, which was acceptable.

The critical pavement responses using Model 9 were at least 93% accurate in comparison to the finely-meshed base model, and the run time was 76 min in comparison to 829 min for the base model. The number of elements through the thickness of the panel and base layers was varied from 3 to 2; however, this change had a negligible impact on the run time. Therefore, the selected mesh used three elements through the thickness in favour of more accurate stresses. The maximum aspect ratio of the elements was 4:1. The maximum aspect ratio of the panel elements was 2.2:1. The mesh sizes from Model 9 were used for all subsequent analyses.

4.1.4.2 Selection of Panel Edge Boundary Conditions

To adequately capture the behaviour of the in-service PCIP, three consecutive panels were modelled to include the effects of load transfer between panels. Dowel bars connect adjacent panels, and transfer load from the loaded panel to the adjacent unloaded panel causing both panels to deflect.

The responses of the three-panel model should approximate the behaviour that would result from modelling additional panels in the traffic lane. To verify this hypothesis, the responses of the three-

panel model were compared to the responses of a five-panel model, for two loading combinations. The first loading combination was a -12°C temperature gradient combined with two transversely-centred 80-kN equivalent single axle loads (ESALs), one at each joint, and the second loading combination was a 12°C temperature gradient with a transversely-centred 80-kN ESAL at midpanel. The temperature gradient was applied to all panels and the axle load was applied to the central panel only.

The three-panel model very closely approximated the five-panel model within the area of interest, which is the central panel and the underlying layers beneath the central panel. The difference in critical stresses were less than 5% within the area of interest, and the deflections in critical locations were within 1% of the five-panel model. Therefore, a three-panel model can adequately capture the pavement responses in the area of interest with 95% precision.

4.1.4.3 Selection of Sublayer Extents

Following selection of an appropriate mesh size and the number of panels, a sensitivity analysis was completed to evaluate the effect of the horizontal extents of the base and subbase on the pavement responses. Since rollers were applied to the boundaries of the sublayers to restrict their movement, the sublayer extension had to be large enough to not affect the responses of interest, the central panel and the base underneath. The objective was to limit the size of the sublayers to minimize the analysis run time, while maintaining precise results.

This study made use of the three-panel model established previously. Two loading cases were considered: a positive temperature gradient combined with axle loading or a negative temperature gradient combined with axle loading. A range of sizes for the sublayers were evaluated, extending 2 m at minimum and 10 m at maximum beyond the panel edges. The maximum and minimum principal stresses in the loaded panel, base, and subbase were compared to determine the effects of the model size.

By visual examination of the pavement responses, it was observed that the boundary conditions had a minimal effect on the responses of interest for the largest of these models with 10 m extension in width and length. Therefore, the responses of this model (Model 1) were used as the point of comparison for the models of reduced size. Table 4-7 summarizes the model sizes, run times, and

the maximum difference between the principal stresses of each model in comparison to Model 1 for the loading combination with a negative temperature gradient.

Table 4-7. Comparison of run times and critical stresses for carrying horizontal sublayer extents

Model No.	Run time (min)	Width extension (m)	Length extension (m)	Maximum percent difference in critical stresses		
				Panel	Base	Subbase
1	215	10	10	-	-	-
2	81	6	6	0%	0%	1%
3	47	4	4	0%	1%	3%
4	33	3	3	0%	1%	5%
5	31	3	2	0%	1%	6%
6	24	2	2	0%	2%	7%

A similar comparison was performed for the positive temperature gradient loading combination. The results follow a similar trend, with the percent difference increasing for smaller model sizes. Detailed results are not shown since the maximum difference in critical stresses for any of the components was 3%, which is less than the negative temperature gradient loading combination.

The critical responses of the models with smaller sublayer extents all match the responses of Model 1 fairly closely. Model 6 was selected as the most optimal in the interest of minimizing run time and because the precision of the results is within a reasonable tolerance. The stresses in critical locations and other high stress locations that were evaluated are 93% accurate or better. The deflections were also evaluated and were within 99% accuracy. Therefore, for all future studies the sublayers were extended 2 m in width and length beyond the panel edges.

4.2 Model Calibration

4.2.1 Calibration Methodology

Finite element modelling was performed to develop a pavement model that is representative of the behaviour of the installed PCIPs. However, some properties of the constructed pavement structure were unknown due to limited information from site investigations and field testing. The purpose

of model calibration was to establish reasonable model inputs for these unknown parameters to match the behaviour of the modelled PCIPs with the constructed PCIPs.

Results of the falling weight deflectometer (FWD) field tests were used for calibration. The same FWD loading that was applied in the field was replicated in the FEM and the FEA deflections were compared to the field-measured deflections. Parametric studies were performed considering a range of values for the unknown parameters to determine which values produced the closest match between the FEA and measured deflections. This approach to choosing parameters has been used by Uddin et al. (1995) to backcalculate the moduli of materials in a pavement structure.

4.2.2 FWD Field Test Data

The falling weight deflectometer testing performed in 2016, shortly after installation of the PCIP, was used to calibrate the FEM. Details of the FWD testing are described in Section 3.3.5.

The FWD tests were performed on the approach and leave end of each panel, on the inner wheel path (IWP) and outer wheel path (OWP). The measured deflections were very similar for the approach versus leave end and the IWP versus OWP loading, and the deflections were also very similar for each of the three support conditions. Therefore, the deflection measurements were not differentiated by the approach versus leave end, IWP versus OWP, or support condition. This also means that the FWD data could not be used to calibrate differences in the model relating to the support condition type.

The deflections were measured at three sensors located at a distance of -30 cm, 0 cm, and 30 cm from the load. The location at 0 cm from the load is referred to as D0, and the locations at -30 cm and 30 cm from the load are referred to as D-30 and D30, respectively.

The target load levels were 45 kN and 70 kN; however, the actual load range was approximately 43.5 to 47 kN and 73.5 to 76 kN, respectively. The loads applied to the FEM were 45 kN and 75 kN; therefore, only the field deflections measured for a load of 45 and 75 kN within a tolerance of ± 1kN were used for comparison. Even within this load range, there was a large variance in the measured deflections, with a range as high as 100 μm for deflections in the magnitude of 100 μm.

A statistical evaluation was performed to evaluate the field data. The data was grouped into four sets by the load level and sensor location, which were the D0 and D30 deflections for the 45 kN load, and the D0 and D30 deflections for the 75 kN load. A normal distribution was a good fit for each of the four data sets; the R^2 value for the probability plots was 0.92 or greater. On this basis, a likely range of deflection values was calculated by prediction intervals. A prediction interval predicts the percentage of tests that will fall within a certain range, if additional tests were performed. For instance, with additional testing it is predicted that 90% of the measured deflections would fall within the range given by the 90% prediction interval.

The 75% and 90% prediction intervals were calculated for the field data. Table 4-8 summarizes the R^2 value of the normal distribution probability plots and the prediction intervals.

Table 4-8. Range of deflections and variability in deflections for FWD field testing

			90% Prediction Interval		75% Prediction Interval	
Load (kN)	**Deflection Location**	**Normal Dist. R^2 Value**	**Maximum Deflection (mm)**	**Minimum Deflection (mm)**	**Maximum Deflection (mm)**	**Minimum Deflection (mm)**
45	D0	0.92	-73	-128	-81	-120
	D30/D-30	0.93	-61	-102	-67	-96
75	D0	0.97	-131	-215	-144	-202
	D30/D-30	0.93	-107	-172	-117	-162

There is a trade-off between the size of the prediction interval and the percentage. A high percentage prediction interval means that a larger percentage of the tests will fall within the given range; however, the range is larger. A smaller percentage prediction interval means that a smaller percentage of tests will fall within the given range; however, the range is more precise.

4.2.3 Calibration Model

The FEM used for calibration is the same model that was developed and verified previously. The mesh size, panel edge boundary conditions, and sublayer extents chosen based on the verification studies all had negligible effects on the pavement deflections in comparison to more refined models. Therefore, this FEM predicts accurate deflection responses which were compared to the field data to calibrate the model.

Self-weight and the falling-weight deflectometer load were applied to the model. The applied FWD loading is as described in Section 3.3.5. The FWD load is applied in the field by a circular plate with a 0.3 m diameter. For simplicity, the FWD load was modelled as a uniform pressure over a square area with a side length of 0.3 m, with a total load of either 45 kN or 75 kN. The theoretical deflections using the square loaded area were compared with those using a cross-shaped loaded area that more closely approximates the circular plate. The deflections responses were not sensitive to the shape of the loaded area; therefore, the square load approximation was adequate.

The subgrade was modelled as a dense-liquid (Winkler) foundation with a k-value of 29 MPa/m. The panel deflections were not very sensitive to changes in the k-value.

The model is symmetrical about the transverse joints and about the centreline of the lane. Therefore, there was no way to differentiate between the approach versus leave end of the panel or the IWP versus OWP, so the FWD load was applied in only one location on the model. Moreover, since the field-measured deflections did not vary significantly for different support conditions, the AS model, without a support layer, was used for the calibration study.

4.2.4 Parametric Studies and Results

The unknown parameters were the elastic modulus of the base and subbase materials, and the degree of bonding at the interface between the panel-to-base. To eliminate one of the unknown parameters, the elastic modulus of the subbase was chosen as 100 MPa. The base modulus is the more sensitive input since it will have greater impact on the responses. The degree of bonding is captured in the model by specifying the panel-to-base friction. Table 4-9 summarizes range of values evaluated in the parametric studies.

Table 4-9. Parametric Study for Calibration

Property	Parametric Study Values
Base Elastic modulus (MPa)	1000, 3000, 5000, 7000, 9000, 11000, 13000, 15000
Panel-to-base friction (-)	0.5, Rough

The base modulus values encompass a wide range of possible values. Two levels of bonding at the panel-to-base interface were considered. A friction coefficient of 0.5 corresponds to a low degree of bonding and the ‘rough’ friction property represents a high degree of bonding.

The calibration model produced one deflection measurement at each sensor location (D0, D-30, and D30), for each combination in the parametric studies. These deflections are summarized in Table 4-10. Those that fall within the 75% and 90% prediction intervals for the field data are highlighted in green and yellow, respectively.

Table 4-10. Finite-element FWD deflections results

Friction	Asphalt Modulus (MPa)	45 kN Load			75 kN Load		
		D0 (µm)	D30 (µm)	D-30 (µm)	D0 (µm)	D30 (µm)	D-30 (µm)
0.5	1000	-122	-133	-108	-206	-225	-184
0.5	3000	-112	-122	-101	-191	-206	-172
0.5	5000	-107	-115	-96	-181	-195	-164
0.5	7000	-102	-110	-93	-173	-186	-157
0.5	9000	-98	-105	-89	-167	-179	-152
0.5	11000	**-95**	**-102**	**-87**	-162	-173	-148
0.5	13000	**-93**	**-99**	**-85**	**-158**	**-168**	**-144**
0.5	15000	**-90**	**-96**	**-82**	**-153**	**-163**	**-141**
Rough	1000	-98	-104	-91	-167	-176	-154
Rough	3000	-78	-81	-73	-134	-138	-125
Rough	5000	-69	-71	-65	-118	-121	-111
Rough	7000	-63	-65	-59	-108	-111	-102
Rough	9000	-59	-60	-55	-101	-103	-95
Rough	11000	-55	-57	-52	-95	-98	-90
Rough	13000	-53	-54	-50	-91	-93	-86
Rough	15000	-51	-52	-48	-87	-89	-83

The FEA deflections were considered to match the measured deflections well if the D0 deflection was within the 75% prediction interval, both the D30 and D-30 deflections were within the 90% prediction interval, and at least one of the D30 or D-30 deflections was within the 75% confidence interval. This gives fairly high confidence that the deflections predicted by the FEA are deflection responses that would be observed in field testing. The FEA deflections that met these criteria are in boldface in Table 4-10. The only FEA deflection results that met these criteria for both the 45 and 75 kN loads, were the models with a friction coefficient of 0.5 and an asphalt modulus of 13,000 MPa and 15,000 MPa.

Based on this calibration, it can be established that the model properties resulting in the closest match with the PCIP field behaviour are low bonding at the interface, with an estimated friction coefficient of 0.5, and a base modulus in the approximate range of 13,000 to 15,000 MPa.

4.2.5 Limitations of Calibration

The calibration was performed to establish appropriate model inputs for the unknown properties of PCIP, such as the base modulus and the degree of bonding between the panel and base. However, there were other unknown properties of the pavement, including the modulus of the base, subbase, and support layer, thickness of the base and subbase, and k-value. The pavement layer thicknesses vary along the length of the PCIP installation, so average or typical thicknesses were assumed. The subgrade k-value was also not known precisely, but was estimated from the available field data.

There were too many unknown variables to calibrate all of these properties given the limited field data. The effect of changes in the k-value and the subbase modulus were briefly evaluated. The deflections predicted by FEA were not sensitive to changes in the k-value, therefore the k-value was justifiably excluded from the parametric study. The subbase modulus had some effect on the deflections which was less substantial than the effect of changes in the base modulus. Therefore, to reduce the parameters in the study, the subbase modulus was excluded from the study under the assumption that the base modulus would capture most of the effects of varied stiffness under the panel. Changes in the support modulus and base and subbase thicknesses were not evaluated, and may affect the deflection results. Therefore, there is some uncertainty in the accuracy of the properties selected through the calibration process in terms of how well they represent the field condition. However, the calibration that was performed provides one possible set of properties that matches the available field data.

If more properties had been considered, there would be more combinations of properties that match the measured FWD deflections which would broaden the range of possible properties. With a wider range of properties, precise properties could not be determined with certainty and the calibration would have been inconclusive. If more field testing is conducted in the future such as FWD testing or pavement cores, the calibration could be refined.

4.3 Model Validation

4.3.1 Validation Methodology

Model validation was performed to ensure that the calibrated model adequately represented the behaviour of the in-service pavement. Validation was performed by comparing the FEM with data that was different than the field data used for calibration.

There was limited field data available that could be used for validation. The available data was a different set of FWD deflections from testing performed in 2017. In these tests, full deflection basins were measured for four panels with FWD loading applied at the centre of the panel. The full deflection basin includes measurements at radial distances of 0, 20, 30, 45, 60, 90, 120 and 150 cm from the centre of the load.

Based on the previously-completed calibration of the model parameters, a friction coefficient of 0.5 was applied to the panel-to-base interface and the base modulus was varied from 13,000 MPa to 15,000 MPa.

4.3.2 Comparison to FWD field data

The FWD tests were performed on four panels. The average deflection at each sensor was calculated. Figure 4-8 compares the average deflections at each sensor location measured from field tests and the deflections predicted by FEA.

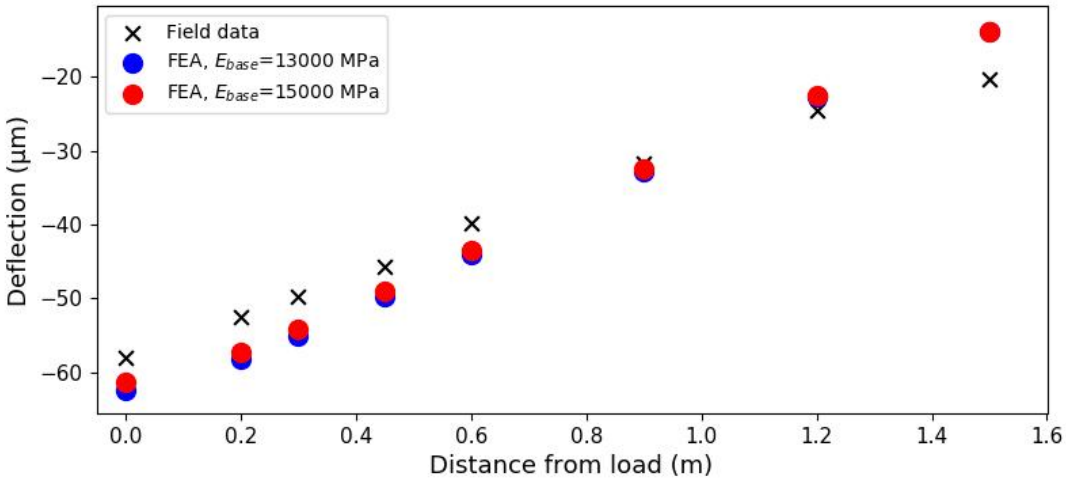

Figure 4-8. Comparison of measured deflection basin and predicted deflection basin

The model with a base modulus of 15,000 MPa matches the field deflections slightly better than that with a base modulus of 13,000 MPa. For the 15,000 MPa model, the difference between the measured deflection and predicted deflection is a maximum of 6 mm at the sensor 1.5 m from the load and is less than 5 mm at all the other sensors. The FEA over-predicts deflections at a distance of 0.9 m from the load or less and under-predicts the deflections at a distance of 1.2 m from the load or greater.

This discrepancy could be caused by offsets in the time that the deflection is recorded. In the field test, the deflection at each sensor is recorded at different times because the load pulse reaches the farther sensors later than the sensors closer to the point of load application. The load pulse is very quick, with a duration of only 25 milliseconds approximately. Based on the time-load history from the FWD field data, the maximum deflections at the sensors occurred at approximately 14 to 15 ms, depending on the sensor location. The FEM deflections were output at 12.5 ms, which is fairly close to the observed timing. However, there is some error because the output time can significantly affect the predicted FEA deflections. For example, the FEA deflection at the furthest sensor is approximately 14 mm at 12.5 ms and approximately 35 mm at 25 ms. Therefore, at the farther sensors the deflection predicted by the FEA may be slightly underestimated because of the chosen output time. Increasing the predicted deflection would bring it closer to the measured deflections. The difference is not as significant for the sensors closer to the load; at the closest sensor the predicted deflection is 61 mm at 12.5 ms and 66 mm at 25 ms.

Furthermore, the FEM is an idealized representation of the in-service panels. Some discrepancy in the results may be due to the model assumptions, such as linear elastic materials and perfect bonding between the dowels and concrete panels. This FWD testing was performed after one year of service at which time the materials and bonding may have deteriorated slightly. Therefore, some discrepancy between the measured and predicted deflections is expected. In general, the FEM predicts the deflections with 10% accuracy or better, which is a reasonable tolerance.

4.3.3 Limitations of Validation

The FEM was calibrated and validated using the FWD field test deflections. However, the FEA results of interest in this research were the pavement stresses. While the model may be well calibrated and validated for the deflections, this does not guarantee that the stress responses are

representative of the stresses for in-service PCIPs. Without strain gauges or other field data that provides information about the in-service stresses, the stress responses of the FEM could not be validated.

Earth pressure cells (EPC) were installed at the top of the base layer, which measure pressure due to panel curling and warping. The FEA responses were compared to the pressure data, and this is described in detail in Section 5.3. The results of the comparison provided some additional confidence that the FEA responses matches the field conditions reasonably well, however the responses cannot be compared with high accuracy.

CHAPTER 5 Evaluation of Field Data

5.1 Instrumentation

Instrumentation was installed during the PCIP trial installation to collect field data that might be used to compare the performance of the support conditions or to understand the conditions that the PCIP are subjected to in the field. An instrumentation cluster containing two Earth Pressure Cells (EPCs) and a thermistor was placed underneath six of the panels in the PCIP trial installation to collect data. The instrumentation cluster was placed in a milled-out portion at the top of the asphalt layer (Figure 5-1).

Figure 5-1. Instrumentation cluster installed underneath panels (Pickel, 2018)

Within each instrumentation cluster a pair of EPCs were installed; one EPC was placed under the panel edge and one EPC was placed under the midpanel. Six pairs of EPC were installed in total, with two pairs for each type of support condition. EPC 1 and 2 (Pair 1) and 3 and 4 (Pair 2) correspond to the asphalt-supported condition, EPC 5 and 6 (Pair 3) and 7 and 8 (Pair 4) were installed with the grade-supported condition, and EPC 9 and 10 (Pair 5) and 11 and 12 (Pair 6) were installed with the grout-supported condition. (Figure 5-2)

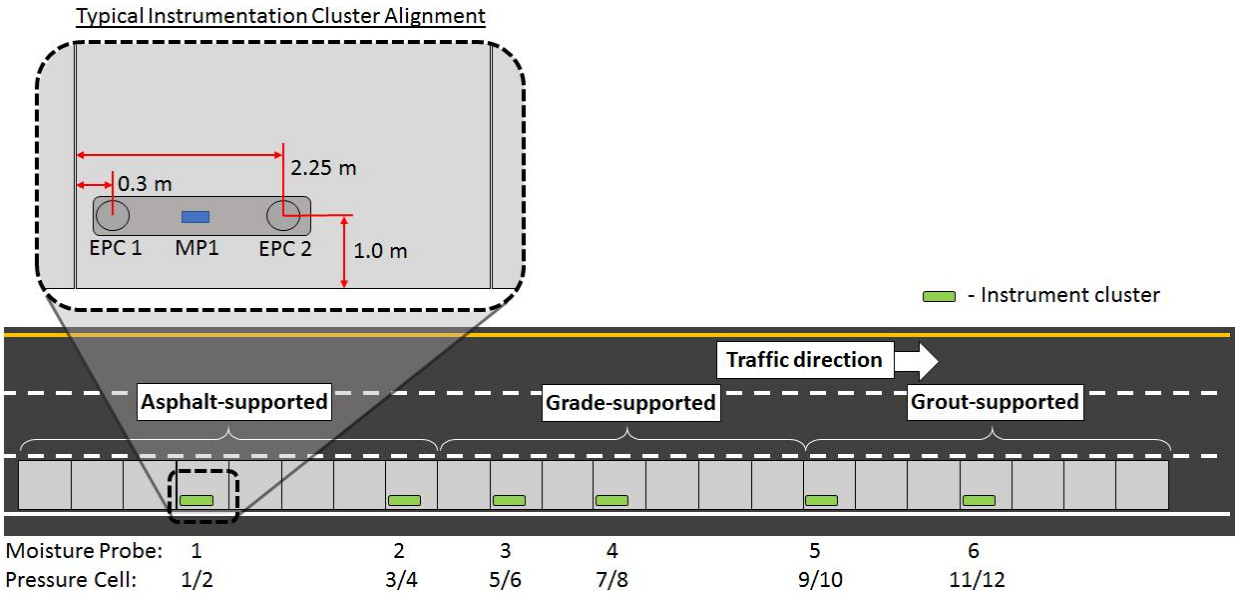

Figure 5-2. Earth Pressure Cells Instrumentation Arrangement (Pickel, 2018)

The EPC measures the pressure at the top of the base layer due to static loads, which are those caused by curling or warping of the panel. It does not record pressures to due traffic loading. The pressures were recorded at intervals of 15 minutes.

To test the EPC, a static load test was performed to measure the pressures when a gravel truck was positioned on the panels. Details of the test can be found elsewhere in (Pickel, 2018). During this load test, EPCs 6 and 11 were presumed to be malfunctioning because the pressure cells recorded zero pressure even with the test load. In the following analysis all the EPCs are considered, however it should be noted that there is a possibility of malfunctioning in some of the EPCs.

5.2 Field Data Analysis

The data collected from the Earth Pressure Cells (EPC) was evaluated to identify correlations between the collected data types and to compare the support conditions. Analyses of different aspects of this field data have also been performed in previous research, and these results can be found elsewhere (Pickel, 2018).

5.2.1 Collected Data

The data types collected were the bottom of panel temperature (measured by thermistors), ambient temperature (air temperature measured by weather stations), and the pressure measured under the panel edge and under the midpanel which are referred to as the edge pressure and centre pressure, respectively. From this data, the temperature difference was calculated as the ambient temperature minus the bottom of panel temperature. The ambient temperature was assumed as a proxy for the panel surface temperature because the pavement was not instrumented to record the surface temperature. The pressure difference was also calculated as the difference between the edge and centre pressures.

5.2.2 Trends

The data collected from the Earth Pressure Cells (EPCs) was analyzed to evaluate general trends, such as maximum pressures, temperatures, and variations over the seasons.

The pressure and bottom of panel temperature measurements collected from November 2016 through May 2018 are shown in Figure 5-3.

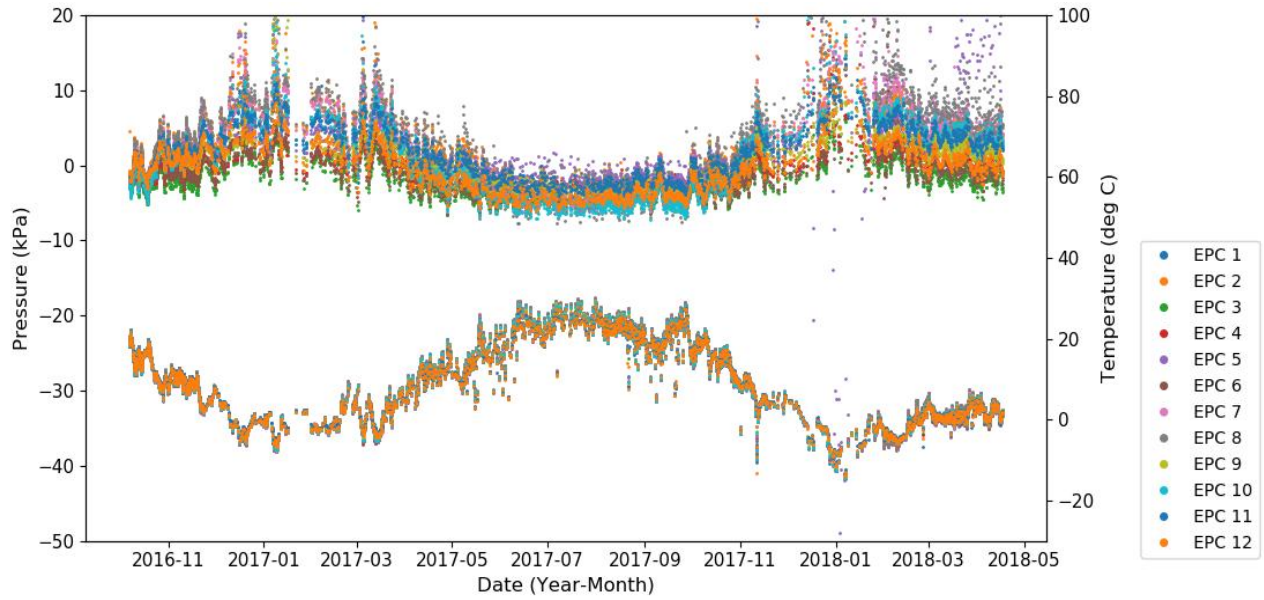

Figure 5-3. Trends in pressure and temperature over time

The collected data was divided into three main time periods, based on the seasons and general trends. By observation, the time periods were designated as the summer season from June to October, the winter season from December to April, and the transition zones from April to June and from October to December. The typical range for the average pressure and average temperature measured during each of these time periods is summarized in Table 5-1 and Table 5-2, respectively. The typical range is calculated as the mean (μ) ± three times the standard deviation (3σ).

Table 5-1. Typical range of average pressure

Time Period	Mean μ (kPa)	Standard Deviation σ (kPa)	Range (kPa)	
			μ - 3σ	μ + 3σ
Winter 1 (Dec 2016 - Apr 2017)	5.2	3.4	-5.0	15.5
Winter 2 (Dec 2017 - Apr 2018)	6.1	3.8	-5.4	17.6
Summer 1 (June 2017 - Oct 2017)	-3.0	1.3	-6.9	1.0
Transition 1 (Apr 2017 - June 2017)	-1.1	1.7	-6.2	4.0
Transition 2 (Oct 2017 - December 2017)	-0.1	2.4	-7.4	7.2

Table 5-2. Typical range of average temperature

Time Period	Mean μ (°C)	Standard Deviation σ (°C)	Range (°C)	
			μ - 3σ	μ + 3σ
Winter 1 (Dec 2016 - Apr 2017)	-0.3	3.5	-10.6	10.1
Winter 2 (Dec 2017 - Apr 2018)	-1.3	3.7	-12.3	9.7
Summer 1 (June 2017 - Oct 2017)	19.9	4.9	5.1	34.7
Transition 1 (Apr 2017 - June 2017)	12.7	4.3	-0.1	25.5
Transition 2 (Oct 2017 - December 2017)	11.2	5.9	-6.6	29.0

The pressures are generally lower during the summer season than the winter season, and there is less variance in the pressures during the summer season. In the summer season the pressures are negative more often than they are positive. This means that the asphalt layer in the PCIP installation is generally subjected to higher magnitude compressive pressures in winter, and in summer there is usually a smaller magnitude upwards pressure on the asphalt which may indicate that the panels are curling off the support.

Comparing the two winter seasons, the pressure and temperature ranges seem fairly similar, and there is greater variance in the data from the second winter. A t-test was performed using Microsoft Excel to evaluate whether the difference between the two winter seasons was statistically significant. In the t-test, the null hypothesis is that the means of the tests are equal (H_o: $\mu_1 - \mu_2 = 0$). A test result with a P-value less than 0.05 would mean that there is a low probability that the data occurred by chance and the data is likely valid; the null hypothesis would be rejected meaning that there is a statistically significant difference between the means. A test result with a P-value greater than 0.05 would mean that there is not enough evidence to suggest that there is a statistically significant difference between the means.

The P-value was approximately zero for the evaluation of pressure and temperature means between the two winter seasons, which means that there is a statistically significant difference between the means of the two data sets. Therefore, the average pressures and temperatures recorded from one winter season to the next have changed. In the second winter season, the mean pressure increased by 0.9 kPa and the average bottom of panel temperature decreased by approximately 1°C. Definitive causes of these changes cannot be made at this time; however, this could potentially be a sign that some deterioration has occurred which is causing more stresses to be transferred to the asphalt layer and which is reducing the insulating properties the pavement. Data collection and monitoring should continue over the upcoming years to evaluate changes as the PCIP installation ages.

5.2.3 Comparison of Support Conditions

For each support condition, two pairs of EPCs were installed. The pressure measurements were compared to determine if the pressures were similar within the same support condition and to evaluate how they compared to other support conditions.

The support conditions are referred to as AS, GradeS, and GroutS for the asphalt-supported, grade-supported, and grout-supported conditions, respectively.

The pressure data was compared over the winter season from December 2016 through March 2017 and over the summer season from June 2017 through September 2017.

5.2.3.1 Pressure Measurements during Winter Season

The edge and centre pressures measured during the winter season are shown in Figure 5-4 and Figure 5-5, respectively.

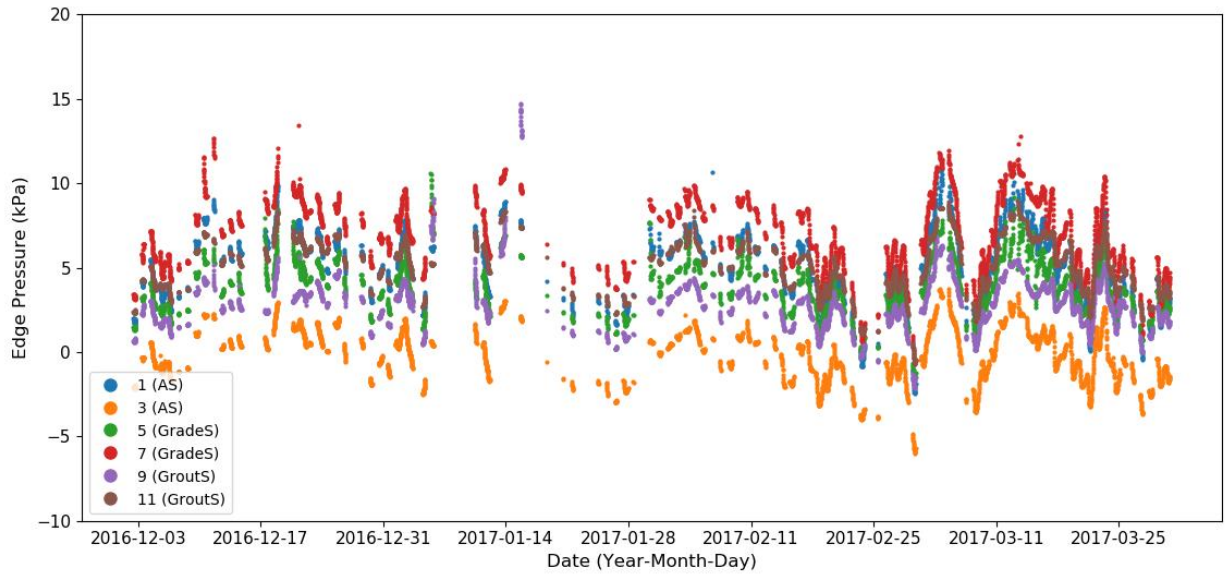

Figure 5-4. Edge pressure measurements over winter season

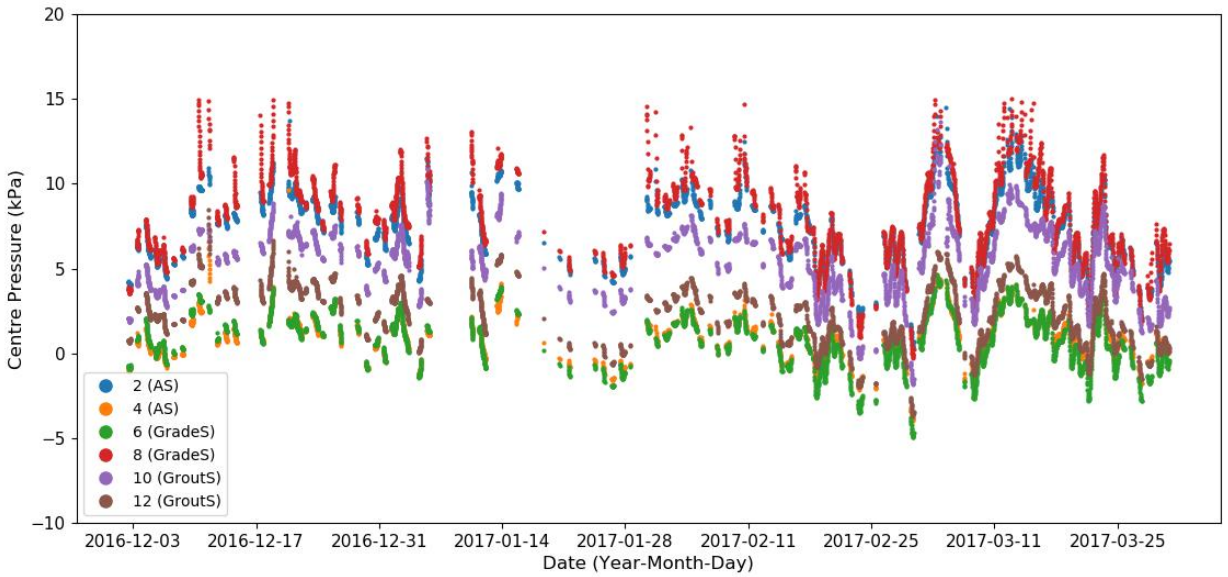

Figure 5-5. Centre pressure measurements over winter season

By observation, the edge and centre pressures recorded by the EPCs for the same support condition do not match very closely. Furthermore, data sets which belong to different support conditions

appear to match more closely than data sets that belong to the same support condition; for example this is the case with EPC 4 (AS) and EPC 6 (GradeS) which appear to be more similar than EPC 4 (AS) and 2 (AS), for the centre pressures.

To verify the visual observations, the mean of the data sets was calculated for comparison and paired t-tests were performed to determine whether the differences in the mean pressure for the same support condition were statistically significant. All the pressure data sets closely follow a normal distribution. A paired t-test was used because the EPCs are all subjected to the same environmental conditions and within the same type of support the construction conditions should be similar. The data set means and P-values for the t-tests are summarized in Table 5-3 and Table 5-4 for the edge and centre pressures, respectively.

Table 5-3. Results of statistical analysis of edge pressure data during the winter season

Data Set	Support Condition	Mean	Standard Deviation	P-value
EPC 1	AS	5.06	2.19	0.0E+00
EPC 3	AS	-0.09	1.58	
EPC 5	GradeS	3.89	1.65	0.0E+00
EPC 7	GradeS	6.91	2.33	
EPC 9	GroutS	2.92	1.69	0.0E+00
EPC 11	GroutS	5.20	1.65	

Table 5-4. Results of statistical analysis of centre pressure data during the winter season

Data Set	Support Condition	Mean	Standard Deviation	P-value
EPC 2	AS	7.39	2.17	0.0E+00
EPC 4	AS	1.02	1.33	
EPC 6	GradeS	0.82	1.53	0.0E+00
EPC 8	GradeS	8.03	2.66	
EPC 10	GroutS	5.42	2.06	0.0E+00
EPC 12	GroutS	2.43	1.75	

The P-values obtained from the t-test were all approximately zero indicating that the data did not occur by chance and that there is a statistically significant difference between the two sets of pressure data for the same support condition.

A t-test was also performed to compare the edge and centre pressures, averaged over all the EPC. The means were 2.77 and 3.01 for the average edge and centre pressures, respectively. The P-value was close to zero indicating that there is a statistically significant difference between the edge and centre pressures.

5.2.3.2 Pressure Measurements during Summer Season

The same process was performed for the pressures measured during the summer season. The edge and centre pressures measured during the summer season are shown in Figure 5-6 and Figure 5-7, respectively.

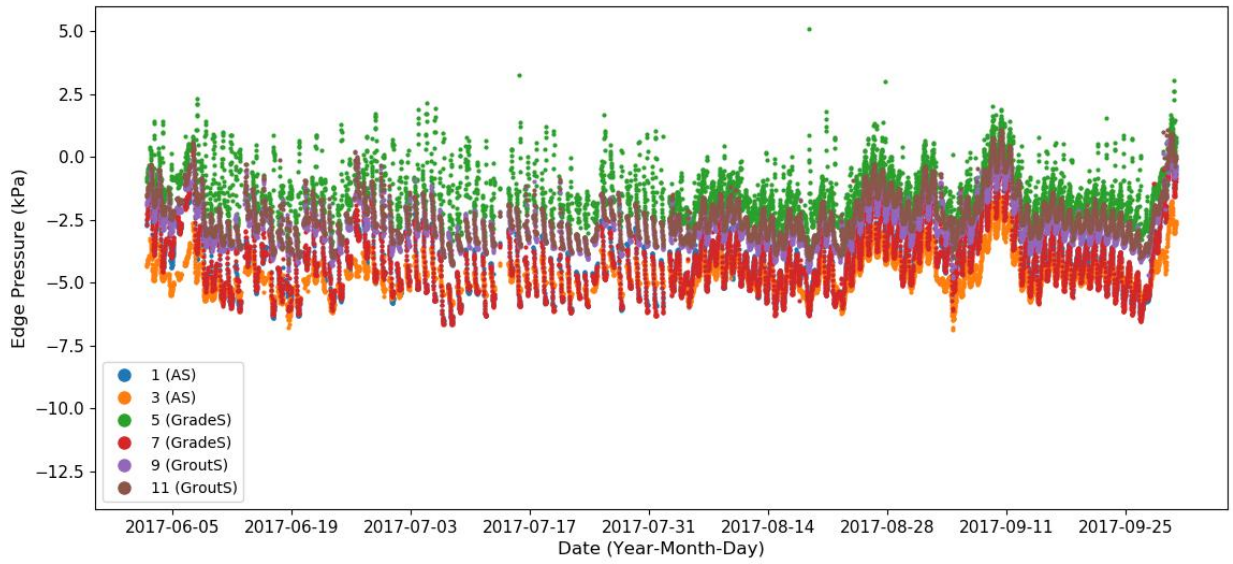

Figure 5-6. Edge pressure measurements over summer season

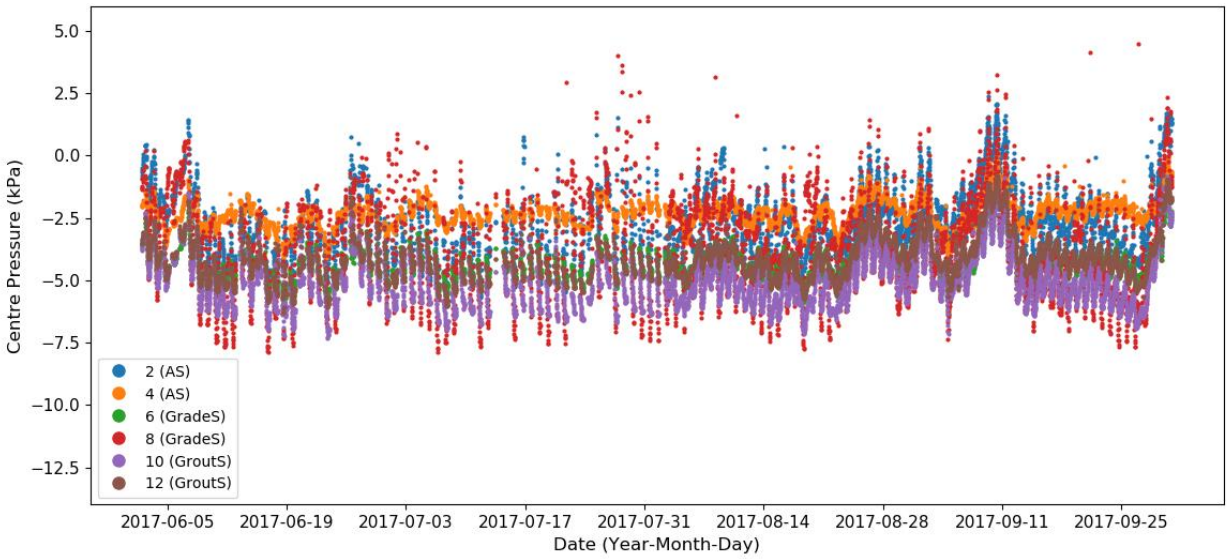

Figure 5-7. Centre pressure measurements over summer season

The means of the data sets and results of the t-tests are summarized in Table 5-5 and Table 5-6, for the edge and centre pressures, respectively.

Table 5-5. Results of statistical analysis of edge pressure data during the summer season

Data Set	Support Condition	Mean	Standard Deviation	P-value
EPC 1	AS	-4.03	1.36	0.0E+00
EPC 3	AS	-4.67	0.75	
EPC 5	GradeS	-1.38	1.02	0.0E+00
EPC 7	GradeS	-4.06	1.33	
EPC 9	GroutS	-2.66	0.90	0.0E+00
EPC 11	GroutS	-2.36	0.95	

Table 5-6. Results of statistical analysis of centre pressure data during the summer season

Data Set	Support Condition	Mean	Standard Deviation	P-value
EPC 2	AS	-2.66	1.40	1.3E-96
EPC 4	AS	-2.32	0.61	
EPC 6	GradeS	-4.25	0.77	6.2E-86
EPC 8	GradeS	-3.78	1.93	
EPC 10	GroutS	-5.05	1.11	0.0E+00
EPC 12	GroutS	-4.12	0.91	

Similarly to the results obtained for the winter season, the P-values were all approximately zero indicating that the data is valid and that there is a statistically significant difference between the two sets of pressure data for the same support condition.

The average edge and centre pressures were again compared using a t-test. The means were -3.19 and -3.69 for the edge and centre pressures averaged for all the EPC, respectively. The P-value was close to zero indicating that there is a statistically significant difference between the edge and centre pressures.

5.2.3.3 Discussion of Results

The analysis of the EPC data indicated that there is a statistically significant difference in the pressures measured by the EPC pairs within the same type of support condition. This leads to the conclusion that the variations in the pressures cannot be explained by differences in the type of support conditions. Other factors may be influencing the pressures, such as variations in the PCIP installation or EPC installation, sensitivity or calibration of the EPC, or other factors. As noted previously, some of the EPC may be malfunctioning based on the static load test results. The EPC also had to be installed very rapidly since the PCIP were installed during overnight lane closures. In a quick installation it is possible that there were inconsistencies in the installation process, in the preparation of the surface or precision in the location. Differences between the installations of the EPC pairs are likely to affect their measurements. Therefore, conclusions about the relative performance of the support conditions cannot be established from the EPC data collected to-date.

For instrumentation of future pavement sections, it would be recommended to use other instrumentation such as strain gauges which may be more accurate. The EPCs may be able to provide valuable information, however, the installation should be completed carefully and consistently to ensure that significant differences in the data are due to the factors being investigated. The collected EPC data was useful in providing general information about the seasonal variations in pressure and temperature.

There is also a statistically significant difference between the average edge pressures and average centre pressures. This is expected since curling and warping of the panels will result in uneven

pressure distributions on the underlying layers. The panel will curl off the support in some locations and the curling will increase pressure on the support in other spots.

5.3 Finite Element Analysis Comparison to Field Data

The FEA results were compared to the field-collected data by extracting the pressures at the EPC locations when a positive or negative temperature gradient was applied to the model. Both a positive and negative gradient were tested with a magnitude of 10°C.

The field data did not have a correlation between the temperature gradient and the measured pressure (Figure 5-8). With any given temperature gradient, a large range of pressures occurred and vice versa.

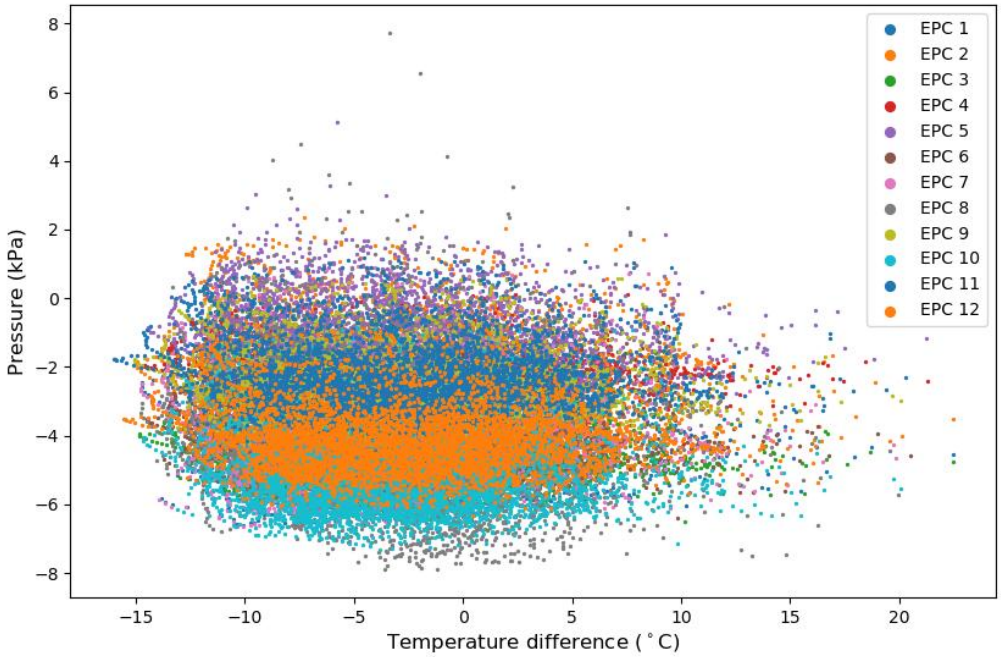

Figure 5-8. Correlation between pressure and temperature difference

Therefore, the responses of the field data and FEM cannot be directly compared; the FEA pressure are dependent on the temperature difference, but the field data is not. However, by applying a reasonable temperature gradient the FEM responses can be evaluated to determine if they fall within a reasonable range for the expected pressure.

Self-weight of the pavement structure will influence the panel curling and the resulting pressures that are measured in the field. However, the EPCs installed in the field should be calibrated so that the recorded pressure in the field is zero when there is no temperature gradient. Therefore, self-weight was applied to the FEM so that the panel curling would be realistic, but the pressure due to self-weight only was subtracted from the pressure due to self-weight and the temperature gradient to obtain the pressures that would correspond to the field measurements. The pressure due to self-weight was approximately 3 to 4 kPa.

5.3.1 Centre Pressures

The centre pressures at the top of the base layer were predicted by the FEA for a positive and negative 10°C temperature gradient, considering a low and high friction at the panel-to-base interface and base moduli ranging from 1,000 MPa to 15,000 MPa. The centre pressures predicted by FEA are summarized in Table 5-7.

Table 5-7. FEA-predicted centre pressures under temperature gradients

Temperature gradient (°C)	Friction condition	Range of pressures (kPa)
10	Low friction	1 to 3
10	High friction	0 to 1
-10	Low friction	-3 to -4
-10	High friction	-1 to 0

There was a range of pressures because the pressure varied for the different base moduli. The FEA-predicted pressures follow the expected behaviour. Under a positive temperature gradient, the centre of the panel curls upwards and the resulting pressures at the top of the base layer are positive. Under a negative temperature gradient, the centre of the panel curls downwards resulting in negative pressures at the top of the asphalt layer under the midpanel. With rough friction, curling is reduced resulting in smaller magnitude pressures under both gradients.

The centre pressures range from -4 kPa to 3 kPa, which matches closely with the average centre pressures of 3.01 and -3.69 that were calculated for the winter and summer season. The pressures predicted by the FEA are dependent on the applied temperature gradient, and do not correspond to any particular season. However, the positive and negative temperature gradients encompass a

range of exposure conditions while the winter and summer season averages also encompass the extreme exposure conditions.

5.3.2 Edge Pressures

The edge pressures predicted by the FEA under a positive and negative 10°C temperature gradient are summarized in Table 5-8.

Table 5-8. FEA-predicted edge pressures under temperature gradients

Temperature gradient (°C)	Friction condition	Range of pressures (kPa)
10	Low friction	11 to 13
10	High friction	30 to 180
-10	Low friction	3 to 5
-10	High friction	-40 to -190

The pressures predicted with high friction had very large magnitudes up to 190 kPa, which greatly exceed the range of pressures observed in the field. Therefore, the high friction condition is not a good comparison to the field data.

The edge pressures predicted by the FEM range from approximately 3 kPa to 13 kPa (under both gradients). At first glance, this does not compare well with the average edge pressures of 2.77 kPa and -3.19 kPa calculated from the field data in the winter and summer season, respectively. However, on closer inspection this occurs because the location where the pressure is measured, 30 cm away from the joint, is near a point of an inflection where the pressure transitions from a negative pressure to a positive pressure in a very short distance because of the panel curling. Therefore, these FEM responses cannot be reliably compared with the field-measured pressures because the responses are extremely sensitive to any small change in distance. Given even a small imprecision in the EPC location on site, the responses would be vastly different.

In general, the FEM responses seem reasonable. Under a positive temperature gradient the panel ends curl downwards and under a negative gradient the panel ends curl upwards off the support layer. This is reflected by the results because the pressure under a positive gradient is larger than the pressure under a negative gradient.

5.3.3 Model calibration and validation with pressure data

In general, the FEM responses in the pressure cell locations cannot be compared very precisely with the field data to further calibrate or validate the model. As mentioned, the edge pressures are extremely sensitive to the location and cannot be reliably compared with the field data. The centre pressures are very small, and there was very little variation in the FEM responses over the range of friction conditions and asphalt moduli. Therefore, these responses are not useful for calibrating the appropriate material properties or friction conditions.

These responses are also not precise enough to validate the model. However, the responses do reasonably match the magnitude of the pressures measured in the field which provides some additional confidence in the model validation.

CHAPTER 6 Finite Element Analysis

6.1 Analysis Objectives

The purpose of the finite element analysis (FEA) was to evaluate the support conditions for the precast concrete inlay panels (PCIPs). The objectives were to determine the optimal support condition, support layer thickness and stiffness (if applicable), and base layer stiffness to minimize pavement stresses.

Specifically, the analysis evaluated the effect of the degree of bonding between the panels and the underlying support, the support condition type, support modulus and thickness, and the modulus of the base layer (Figure 6-1).

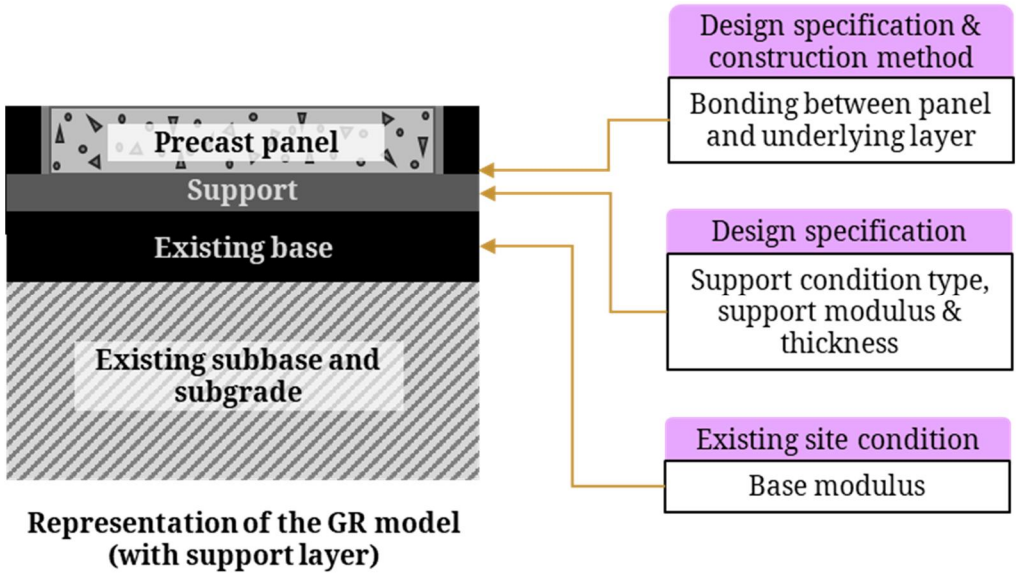

Figure 6-1. Parameters for finite element analysis

These reflect changes to the design or construction of the PCIPs or the site conditions. The type of support condition, support modulus, and support layer thickness are specified in the design phase and are subject to some variability during construction. The degree of bonding between the panels and underlying layer can be specified in design and is also influenced by the construction techniques. The base cannot be controlled for in design or construction because the PCIPs are installed on top of the existing base, but this parameter is considered to evaluate the effect of the base condition on PCIP performance.

The pavement responses of interest in the study were the minimum tensile stresses in the panel and base layers. Concrete and base materials are weaker in tension than in compression, and locations with higher tensile stresses are critical locations that may crack under repeated loading (Delatte, 2014). Tensile stresses in the panel should be minimized to reduce the potential for cracking. The tensile stresses in the base were also evaluated to establish the degree to which stresses are transferred to pavement layers below the support, to determine which conditions are most effective in reducing stresses in the lower layers.

6.2 Parametric Studies

Parametric studies were performed to evaluate the effect of the support modulus and thickness, base modulus, and friction condition on the panel and base stresses. The parametric studies were performed for the two variations of the model. The AS model represents the asphalt-supported condition and does not include a support layer, and the GR model represents the grade-/grout-supported conditions and includes a support layer.

The values evaluated in the parametric studies for the AS and GR models are summarized in Table 6-1 and Table 6-2, respectively.

Table 6-1. Parametric study values for AS Model

Property	Parametric Study Values
Panel-to-base friction condition (-)	0.5, 'Rough'
Base layer elastic modulus (MPa)	1000, 8000, 15000

Table 6-2. Parametric study values for GR Model

Property	Parametric Study Values
Panel-to-support and support-to-base friction condition (-)	0.5, 'Rough'
Base layer elastic modulus (MPa)	1000, 8000, 15000
Support layer elastic modulus (MPa)	4000, 12000, 20000
Support layer thickness (mm)	12, 18, 24

The friction coefficient of 0.5 corresponds to low friction at the interface of the panel and underlying layer, and the 'Rough' friction condition corresponds to high interface friction.

The parametric studies were performed for four different loading combinations. The combinations were a 10°C temperature gradient, a -10°C temperature gradient, a 10°C temperature gradient combined with an ESAL at midpanel and shifted towards the panel edge, and a -10°C temperature gradient combined with an ESAL at the joint and shifted towards the panel edge. The loading is described in more detail in Section 3.3.

6.3 Results

The minimum stresses in the concrete panel and base layer, for the four different loading combinations, are presented and discussed in this section.

The results of the parametric studies are presented in two ways. First, a comparison of the AS and GR models are presented with the parametric studies for the friction condition and base modulus. This is used to evaluate the effects of the GR vs. AS model, high vs. low interface friction, and various base moduli. The middle value of the support modulus, 12,000 MPa, and middle value of the support thickness, 18 mm, were used to present these results. Secondly, the results for the GR model only are presented with the parametric studies for the friction level, support modulus and support thickness. This is used to evaluate the effects of various support moduli and thickness on the stresses for the two friction levels.

The results are presented for the panel stresses first then the asphalt stresses and are separated by the loading combination. A final summary is provided to synthesize the trends observed throughout the parametric studies for all loading combinations, and recommendations are made for improvements to the design and construction of PCIP.

6.3.1 Panel Stresses

6.3.1.1 Positive Temperature Gradient

The minimum panel stresses under a positive temperature gradient for the first set of parametric studies is shown by Figure 6-2.

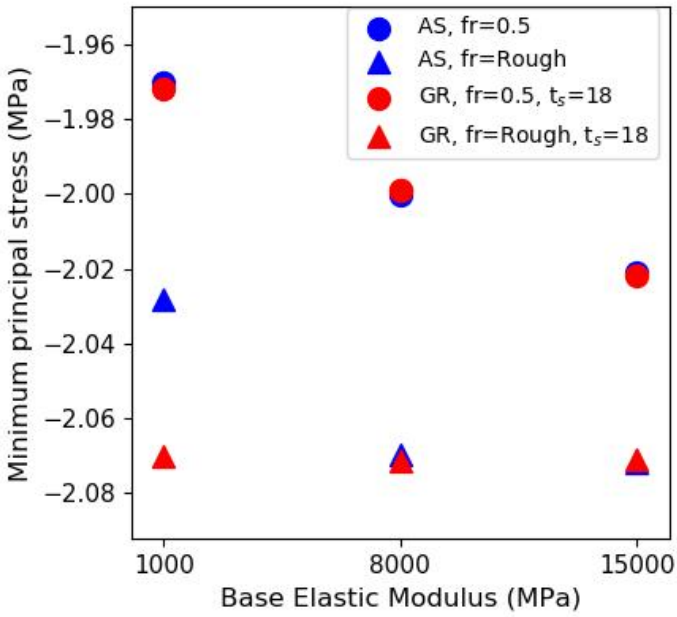

Figure 6-2. Minimum panel stresses under positive temperature gradient

The minimum panel stresses occurred at the top of the panel. For low friction, the peak stress was near the centre of the panel where there is the most panel curling. For high friction, the peak stress was on the centreline near the joint where curling of the panel edges is restrained by the strong interface bond.

The panel stresses increased with increasing friction, which is the expected behaviour. Higher interface friction restrains panel movement which induces higher stresses.

With low friction the AS and GR stresses were the same. With high friction the AS and GR stresses were the same for a higher base modulus (8,000+ MPa), but the GR stresses are slightly higher than AS when the base modulus is low (1,000 MPa).

For low friction the stresses increased as the base modulus increased. It is expected that stiffer bases increase temperature-induced curling stresses (Delatte, 2014). For high friction, as the base modulus increased, the GR stresses remained constant and the AS stresses increased from a base modulus of 1,000 to 8,000 MPa. When the base was stiff (8,000+ MPa) or when a stiff support layer was present such as in the GR model, then an increase in the base stiffness had little effect. Therefore, changes in the base stiffness may have an effect when the base stiffness is low, but

there is some threshold for the base stiffness beyond which the stresses remain constant. In any case, the effect of changes in the base modulus was fairly small (3% maximum).

The minimum panel stresses for changes in the support are shown by Figure 6-3, for a base modulus of 8,000 MPa.

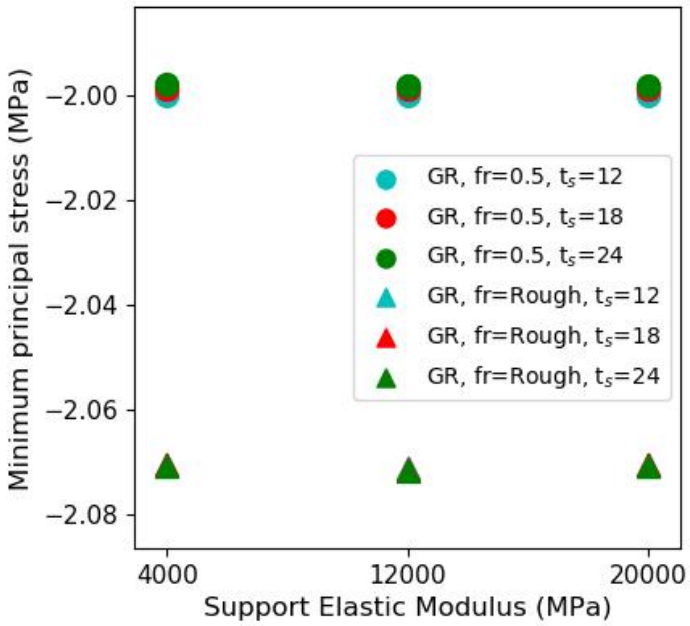

Figure 6-3. Minimum panel stresses under positive temperature gradient with changes in support properties

For low and high friction, changes in the support thickness and modulus had negligible effects on the minimum panel stresses. This trend was similar for other values of the base modulus as well.

6.3.1.2 Negative Temperature Gradient

The minimum panel stresses under a negative temperature gradient for the first set of parametric studies is shown by Figure 6-4.

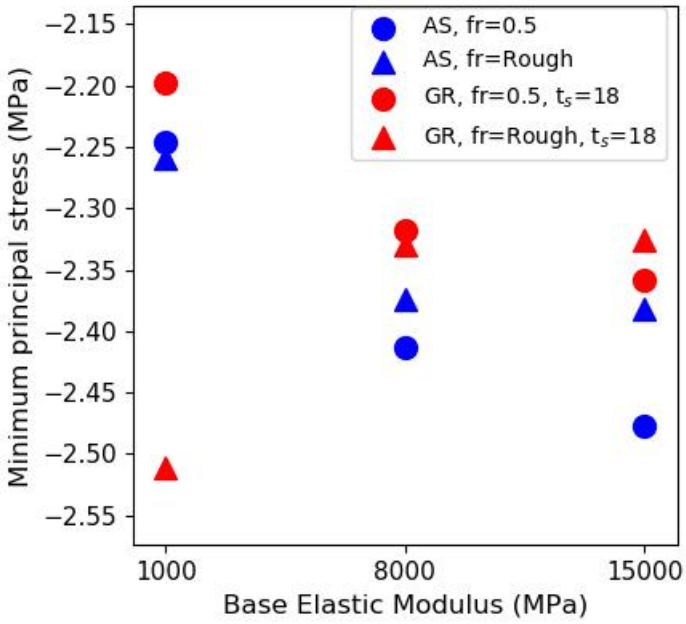

Figure 6-4. Minimum panel stresses under negative temperature gradient

The minimum panel stresses occurred at the bottom of the panel under a negative temperature gradient. For low friction, the stresses were located at the longitudinal edge at midpanel. For high friction, the critical stress locations varied. For the AS model, the peak stress was located at the longitudinal edge at midpanel for a base modulus of 1,000 MPa and near the joint for a base modulus of 8,000 MPa or greater. For the GR model with a base modulus of 1,000 MPa, the peak stress was offset approximately 70 cm from the centreline and near the joint. With a base modulus of 8,000 MPa the peak stress was located at the longitudinal edge at midpanel, and with a base modulus of 15,000 MPa the peak stress was located in the panel corner.

For a base modulus of 1,000 MPa the stresses increased with greater interface friction, and for a base modulus of 8,000 MPa or greater the stresses generally decreased with higher friction. The stresses are expected to increase with increased frictional restraint, however, it is hypothesized that for a higher base modulus the stiffer base provided more support to the panel which distributed and reduced the stresses over the panel.

For low friction, the AS stresses were higher than the GR stresses. The difference between the AS and GR stresses increased as the base modulus increased. For high friction, the GR stresses were higher than AS stresses when the base modulus was low and slightly lower than AS stresses when the base modulus was high. It is hypothesized that with a weak base the presence of the support

layer increased panel stresses because it increased the restraint to panel curling, and there is little support provided by the weak base and the thin support layer. When the base modulus was higher, its stiffness is closer to that of the support modulus, and the difference between AS and GR stresses may be smaller because the presence of a thin, strong support layer is less significant when the underlying base is also strong.

With low friction, the panel stresses increased with an increasing base modulus which is the same trend observed under the positive temperature gradient loading. For high friction, the stresses remained more constant for a base modulus of 8,000 MPa and greater, which was similar to the trend observed for the positive temperature gradient. With high friction, the AS stresses increased as the base modulus increased. This is the same behaviour as the positive gradient. It is hypothesized that a stiffer base increased panel curling, which results in increased stresses because of higher frictional restraint. With high friction, the GR stresses decreased as the base modulus increased. This is not the expected behaviour, and on closer inspection, the effect of changes in the base modulus depended on the relative stiffness of the support and base in the GR models. To understand this effect, the panel stresses for a support modulus of 4,000 MPa are also shown in Figure 6-5.

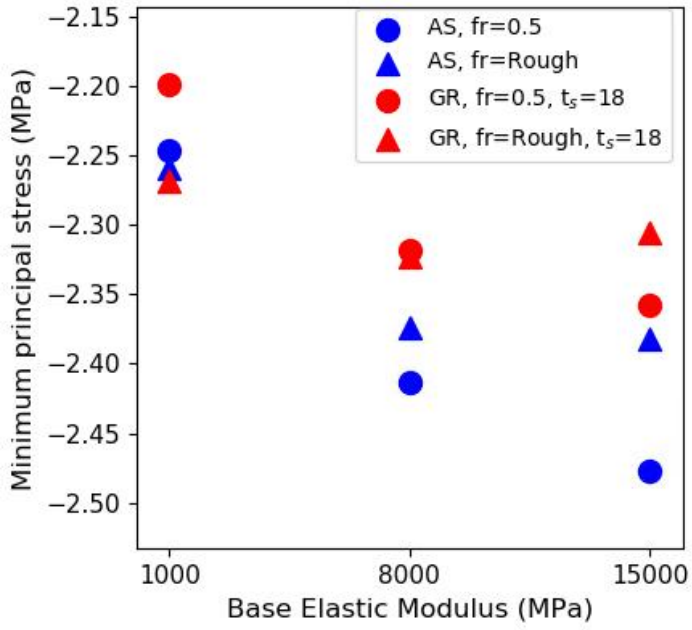

Figure 6-5. Minimum panel stresses under negative temperature gradient, with 4,000 MPa support modulus

For a support modulus of 4,000 MPa, the GR stresses increased as the base modulus increased, which is the expected trend. For a base modulus of 8,000 MPa or greater the GR stresses remained approximately the same regardless of the support modulus. This means that the stresses converged to approximately the same magnitude when the base modulus was stiff, regardless of the support stiffness. However, for a base modulus of 1,000 MPa the support modulus influenced the panel stresses. For high friction, the GR stress was approximately -2.27 MPa when the support modulus was low (4,000 MPa) and the GR stress was approximately -2.52 MPa when the support modulus was higher (12,000 MPa). A stiffer support increased the panel stresses.

The minimum panel stresses for the parametric studies of the support modulus and thickness are shown by Figure 6-6 for a base modulus of 1,000 MPa.

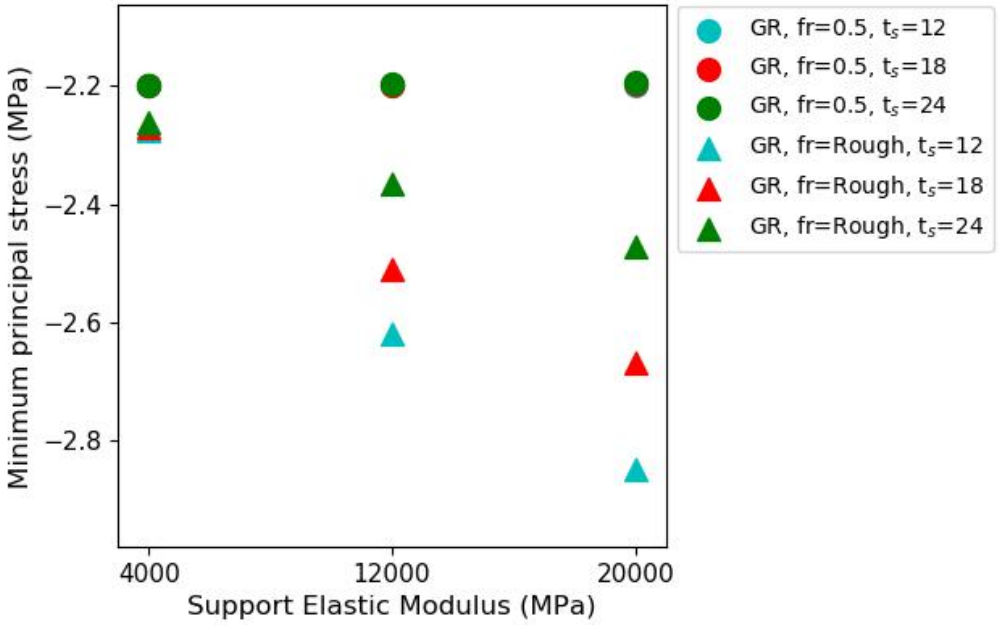

Figure 6-6. Minimum panel stresses under negative temperature gradient with changes in support properties

For larger values of the base modulus (8,000+ MPa), the results are not shown because the support modulus and thickness have minimal effect on the panel stresses.

For low friction, changes in the support thickness and modulus had minimal effect on the panel stresses. For high friction and a higher base modulus, the support modulus and thickness also had minimal impact. For high friction and a low base modulus (1,000 MPa), the stresses increased

significantly with increasing support modulus and decreased with increased support thickness. With a less stiff support the peak stress occurs at the longitudinal edge of the panel, and with a stiffer support the peak stress occurs near the joint. The panel curls more when the support modulus if less stiff because the support layer offers less resistance. When the support is stiffer, the panel curling is more restrained by the interface friction which induces higher stresses in the support and panel. The panel stresses are compared in Figure 6-7 and Figure 6-8 for two different support moduli. When the support thickness increases the panel also curls less, but the support stresses are lower; this in turn reduces the panel stresses at the joint. The panel stresses are compared in Figure 6-8 and Figure 6-9 for two different support thicknesses.

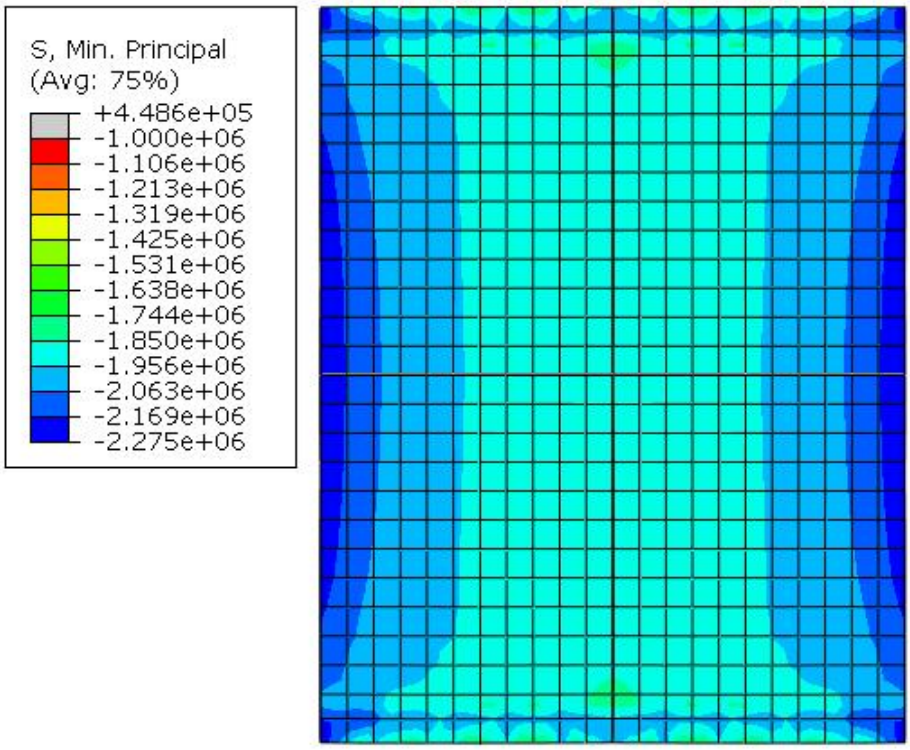

Figure 6-7. Panel stresses for GR model under negative temperature gradient, with low friction, 12 mm support thickness, and 4,000 MPa support modulus

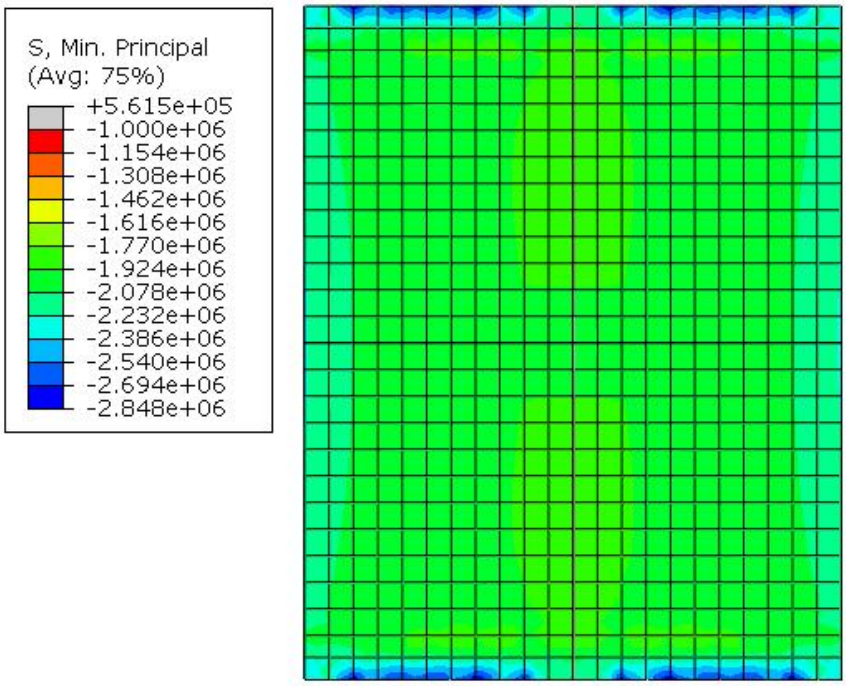

Figure 6-8. Panel stresses for GR model under negative temperature gradient, with low friction, 12 mm support thickness, and 20,000 MPa support modulus

When the support thickness is constant, a higher support modulus results in higher panel stresses.

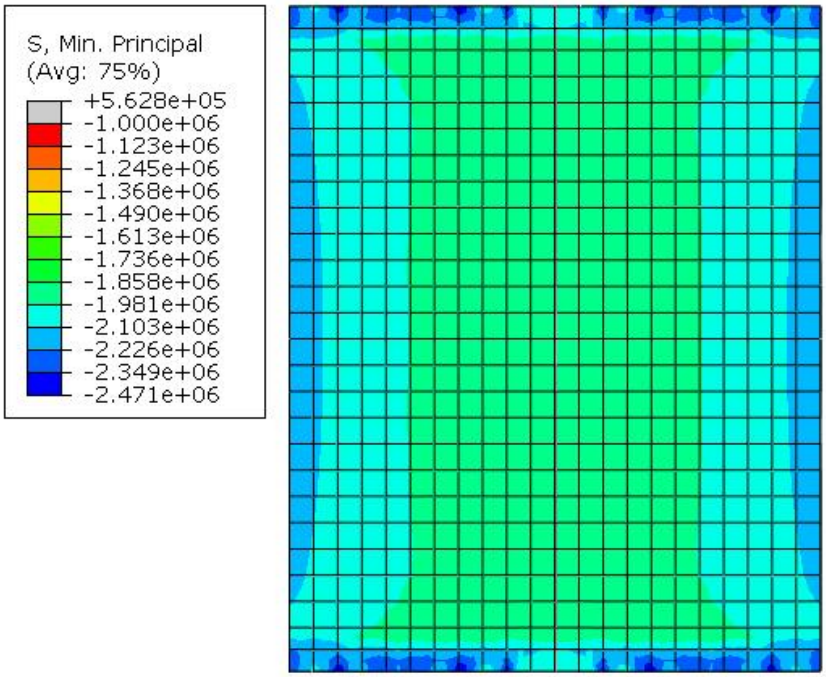

Figure 6-9. Panel stresses for GR model under negative temperature gradient, with low friction, 24 mm support thickness, and 20,000 MPa support modulus

When the support modulus is constant, a thicker support results in lower panel stresses.

6.3.1.3 Positive Temperature Gradient with Axle

The minimum panel stresses under a combination of a positive temperature gradient and axle loading for the first set of parametric studies is shown by Figure 6-10.

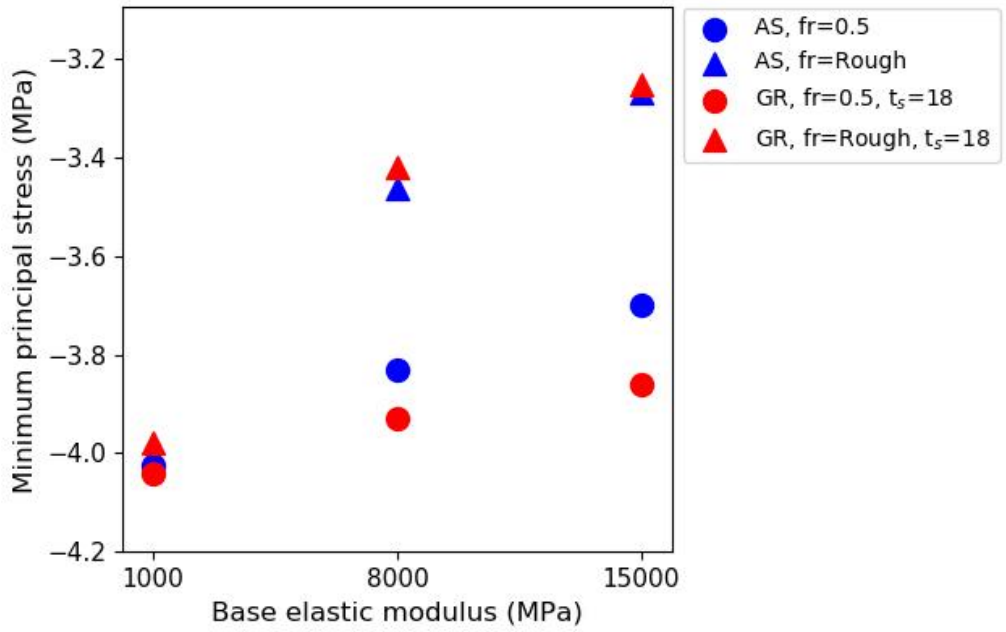

Figure 6-10. Minimum panel stresses under positive temperature gradient and axle loading

The minimum panel stress was located at the longitudinal edge at midpanel, at the top of the panel. This is underneath the outbound wheel of the axle load.

The stresses decreased with increasing friction. For a low base modulus (1,000 MPa), the effect was minimal, but for a higher base modulus there was a significant decrease. It is hypothesized that the stresses were reduced by higher interface friction because the underlying layers provide more distributed support to the panel, reducing the peak stresses that occurred under the wheel loads. For a base modulus of 15,000 MPa the stress contours are compared for low and high friction conditions in Figure 6-11 and Figure 6-12.

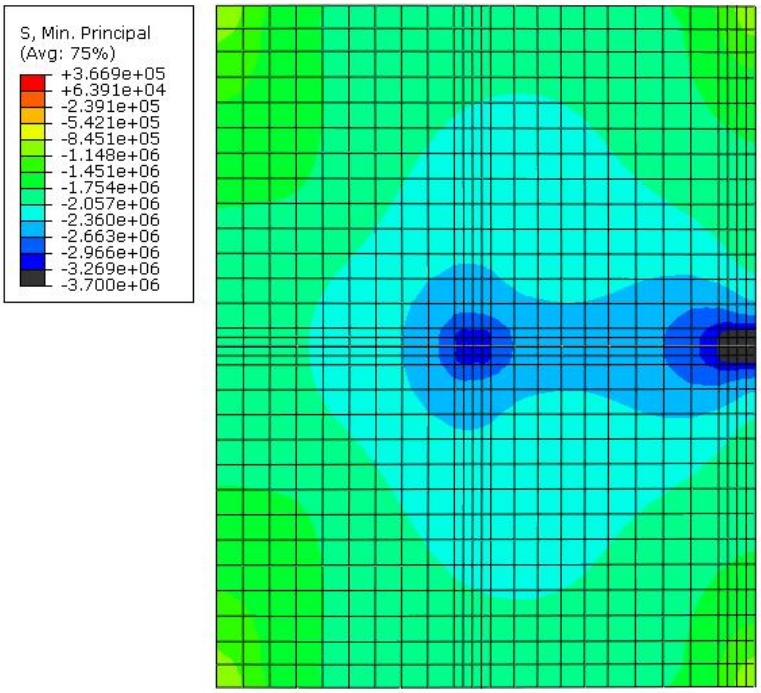

Figure 6-11. Panel stresses for AS model under positive temperature gradient with axle loading, with low friction, and 15,000 MPa base modulus

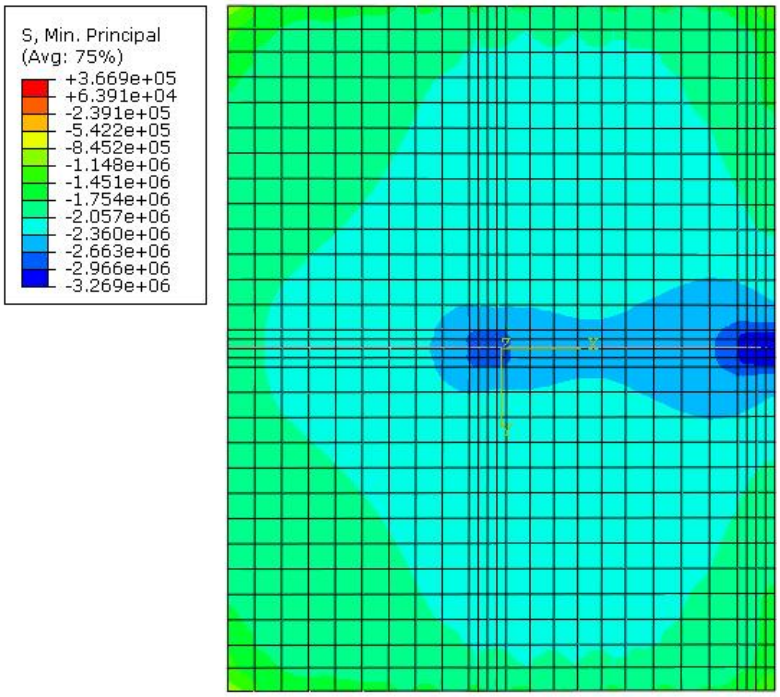

Figure 6-12. Panel stresses for AS model with positive temperature gradient with axle loading, with high friction, and 15,000 MPa base modulus

For visual comparison the same stress range is shown, but for low friction the peak stress is -3.7 MPa which exceeds the peak stress of -3.27 MPa for high friction.

With low friction the AS stresses are lower than the GR stresses, and with high friction the AS and GR stresses are very similar.

For low and high friction, the stresses decreased as the base modulus increased. A stiffer base is expected to increase temperature-induced curling stresses, however under axle loading alone a stiffer base provides more support to the panel which reduces stresses (Davids, 2000). It is hypothesized that under this combination of temperature and axle loading, the net effect is a reduction in stresses. The panel stresses for self-weight and axle loading only (before the positive temperature gradient was applied) are shown in Figure 6-13 and Figure 6-14 for a base modulus of 1,000 MPa and 15,000 MPa, respectively.

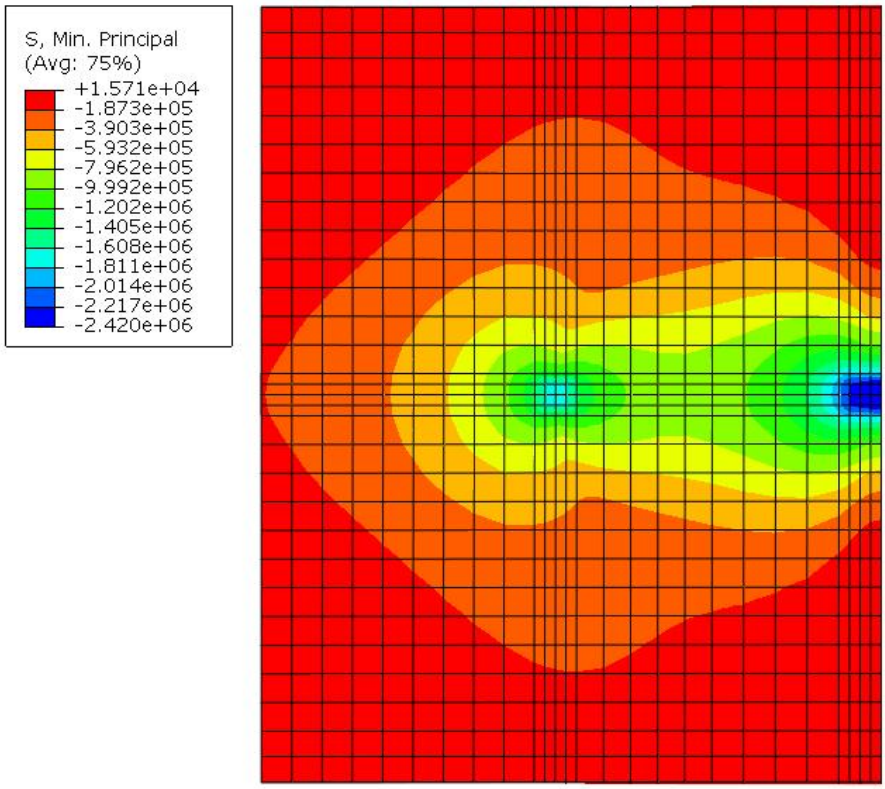

Figure 6-13. Panel stresses for AS model with self-weight and axle loading, with low friction, and 1,000 MPa base modulus

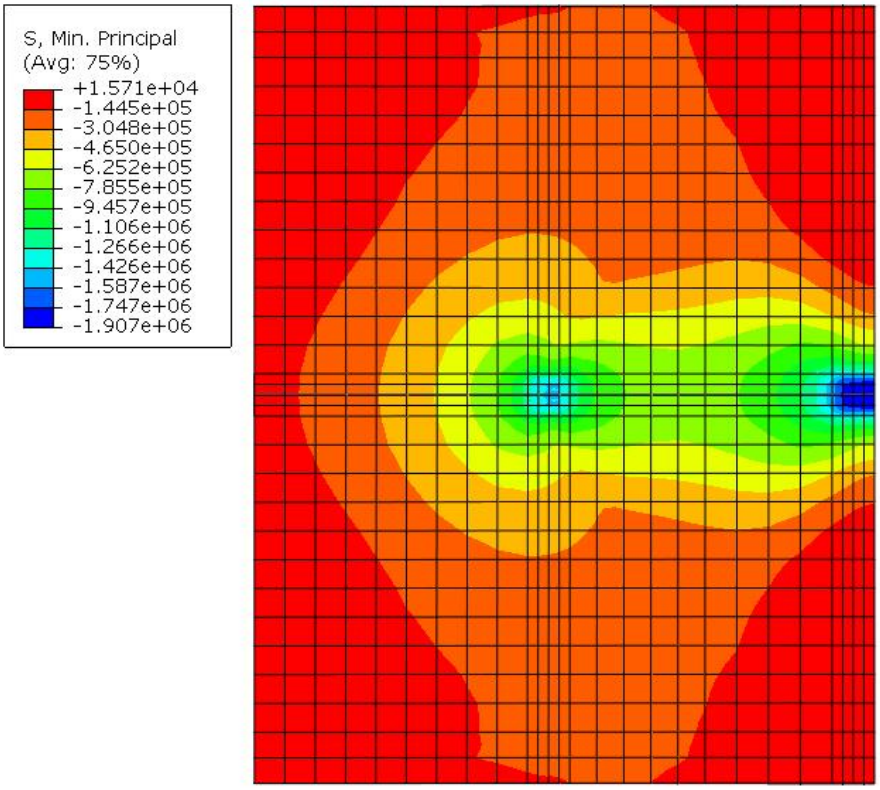

Figure 6-14. Panel stresses for AS model with self-weight and axle loading, with low friction, and 15,000 MPa base modulus

Under axle loading and self-weight only, the peak stresses and panel stresses are reduced by a stiffer base modulus. When the temperature gradient was also applied, the overall effect was still lower stresses with the stiffer base.

The minimum panel stresses for the parametric studies of the support modulus and thickness are shown by Figure 6-15, for a base modulus of 8,000 MPa.

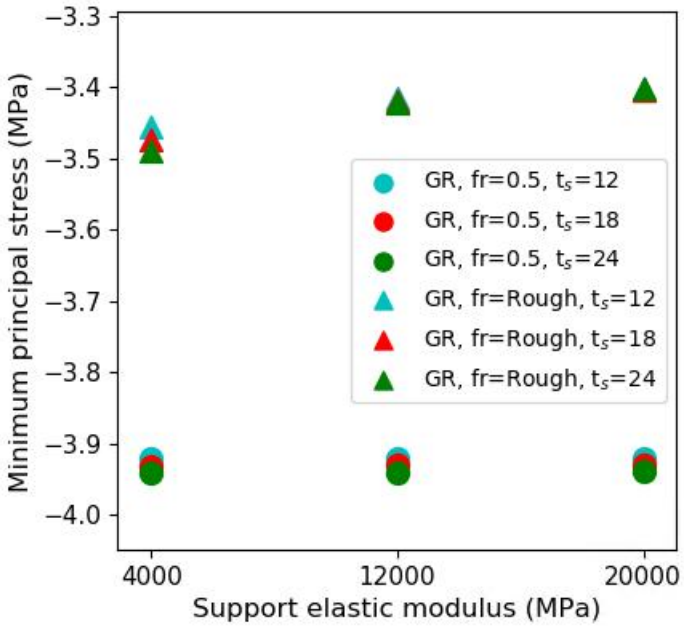

Figure 6-15. Minimum panel stresses under positive temperature gradient and axle loading with changes in support properties

The stresses for other values of the base modulus are not shown since they were fairly similar to the above results.

For low friction, the support modulus and thickness had minimal effect on the panel stresses. For high friction, the effect of the support modulus and thickness was fairly minimal, causing a maximum 3% increase or decrease in the panel stresses over the range of parameters considered.

6.3.1.4 Negative Temperature Gradient with Axle

The minimum panel stresses under a combination of a negative temperature gradient and axle loading for the first set of parametric studies is shown by Figure 6-16.

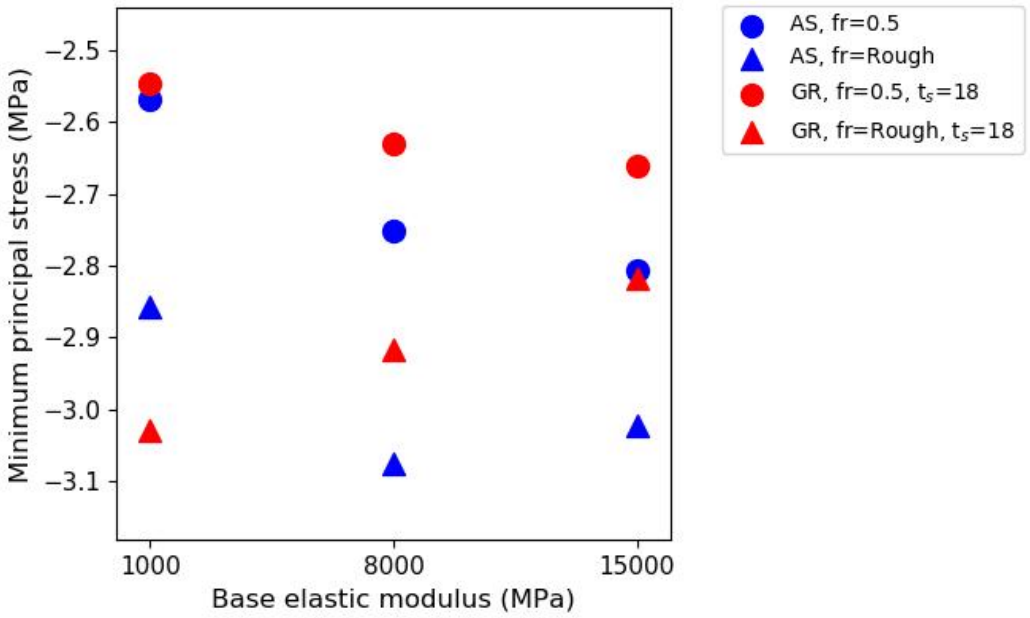

Figure 6-16. Minimum panel stresses under negative temperature gradient and axle loading

The peak stresses occurred at the bottom of the panel. For the AS model with low friction, the peak stresses were located at the longitudinal panel edge offset approximately 1 m from the joint. For the GR model, the peak stresses occurred in the panel corner for a lower base modulus and further from the joint (offset by 1 to 1.3 m from the joint) when the base modulus was higher. For high friction, the peak stresses occurred in the panel corner.

The stresses increased with higher interface friction. This is the expected behaviour which also occurred for the positive gradient loading case.

For low friction, the trend in the comparison of AS and GR stresses was similar to that observed for the loading case of a negative gradient only. For high friction, the GR stresses were larger than the AS stresses when the base modulus was low and smaller than the AS stresses when the base modulus was higher. This is the same trend that was observed for the negative gradient only loading combination. For a base modulus of 1,000 MPa the stress contours are compared for the AS and GR models in Figure 6-17 and Figure 6-18, respectively.

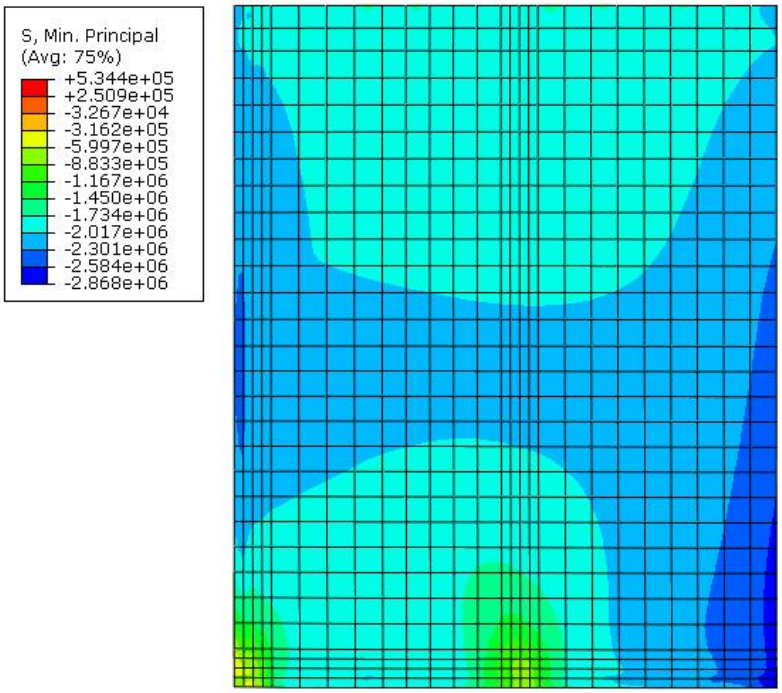

Figure 6-17. Panel stresses for AS model with negative gradient and axle loading, with high friction, and 1,000 MPa base modulus

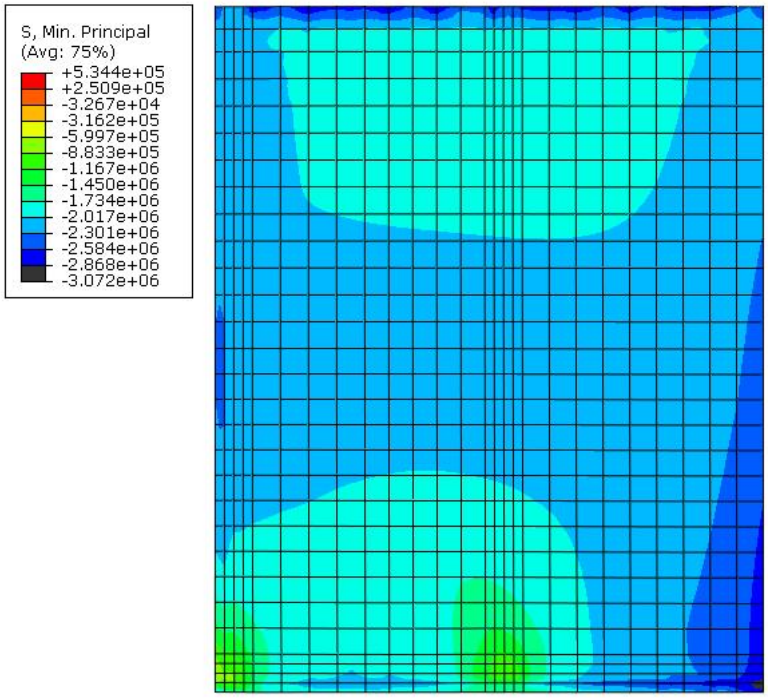

Figure 6-18. Panel stresses for GR model with negative gradient and axle loading, with high friction, and 1,000 MPa base modulus

In the previous figures, the same range of stresses is shown for easy visual comparison. In the GR model, the presence of the support layer caused an increase in stresses throughout the entire panel relative to the AS model. Therefore, with a low base modulus the inclusion of a support layer increased the panel stresses. With a higher base modulus, it is hypothesized that the support and base layers both provided more support to the panels which reduced stresses.

For low friction, the stresses increased as the base modulus increased. This is the same trend that was observed for the negative temperature gradient loading, but the stress increase was smaller when axle loading was applied because a stiffer base is beneficial in reducing stresses under axle loading. For high friction, the GR stresses decreased with an increasing base modulus and the AS stresses changed inconsistently. Under combined loading, it is hypothesized that a stiffer base that is well bonded to the panel would provide more support to the panel, reducing stresses.

The minimum panel stresses for the parametric studies of the support modulus and thickness are shown by Figure 6-19, for a base modulus of 8,000 MPa.

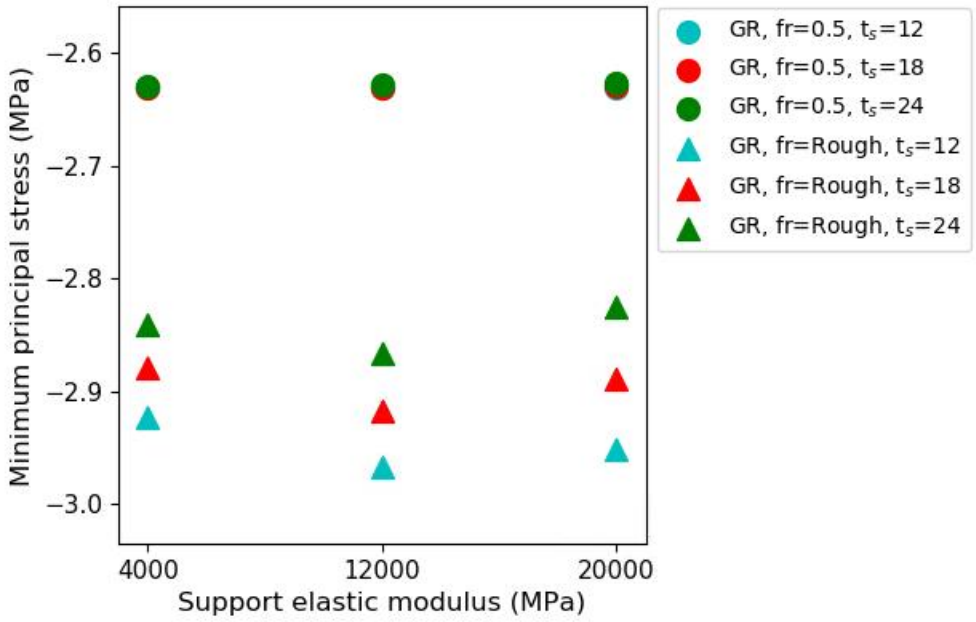

Figure 6-19. Minimum panel stresses under negative temperature gradient and axle loading with changes in support properties

The responses for other values of the base modulus are not shown because the trends were similar.

For low friction, the support modulus and thickness had minimal effect. For high friction, the effect of the support modulus was inconsistent and minimal. Increasing support thickness decreased stresses for high friction, which is the same trend observed for other load combinations.

6.3.1.5 Panel Stresses Summary and Discussion

The trends in the panel stresses observed over the range of parametric studies, for all loading combinations, are summarized in Table 6-3. The trends are discussed with respect to the influence of low versus high friction at the panel to underlying layer, the AS model versus the GR model, the effect of the base modulus, support modulus, and support thickness. Common trends or patterns observed across all four loading combinations are presented.

The maximum panel stresses were produced by the positive temperature gradient and axle loading combination. The smallest panel stresses were produced by the positive temperature gradient only loading.

The effect of interface friction varied depending on the base modulus and the loading combination. It was expected that higher interface bonding would restrain panel movement and increase panel stresses. This trend was observed when the base modulus was low (1,000 MPa); the panel stresses increased or decreased minimally when there was higher interface friction. However, for a higher base modulus (8,000+ MPa) the effect of the bonding condition on stresses depended on the loading combination. With a larger base modulus there is still frictional restraint at the interface, but the stiffer base may offset some of these stresses because it provides more support to the panels. Therefore, greater friction combined with a larger base modulus resulted in either an increase or decrease in stresses, depending on the loading.

Table 6-3. Summary of trends in panel stresses

Property	Secondary Property	Effect under different loading combinations: Positive Gradient	Negative Gradient	Positive Gradient with Axle	Negative Gradient with Axle	Trends
Stress range (MPa)		-2.0 to -2.1	-2.2 to -2.7	-3.2 to -4.1	-2.5 to -3.1	Maximum stresses under positive gradient with axle loading combination.
High friction relative to low friction		Increase	Inconsistent	Decrease or minimal	Increase	For low E_b - stresses generally increased. For high E_b - effect on stresses varied for different loading.
	Low E_b (1,000 MPa)	*+3% for AS +5% for GR*	*Negligible for AS +16% max for GR*	*Minimal for AS -2.5% max for GR*	*+9% for AS +18% max for GR*	
	High E_b (8,000+ MPa)	*+2.5% (all SC)*	*-4% for AS -2.5% for GR*	*-12% for AS -16% max for GR*	*+6% (all SC)*	
Low Friction						
GR relative to AS		Negligible	Decrease	Small increase or negligible	Decrease or negligible	Stresses decreased for loading combinations with a negative gradient. Effect is fairly small when E_b is low.
	Low E_b (1,000 MPa)	*Similar for all*	*-2.5%*	*Negligible*	*Negligible*	
	High E_b (8,000+ MPa)		*-5%*	*+4%*	*-5%*	
Increasing base modulus		Small increase	Increase	Decrease	Increase	Stresses increased for all loading combinations except positive gradient with axle loading.
	AS	*+2.5%*	*+ 9%*	*-8%*	*+7.5%*	
	GR		*+6%*	*-4%*	*+4% max*	
Increasing support modulus		Negligible	Negligible	Negligible	Negligible	Support modulus had a negligible effect.
	Low E_b	*Similar for all*	*Similar for all*	*Similar for all*	*Similar for all*	
	High E_b					
Increasing support thickness		Negligible	Negligible	Negligible	Negligible	Support thickness had a negligible effect.
	Low E_b	*Similar for all*	*Similar for all*	*Similar for all*	*Similar for all*	
	High E_b					

High Friction						
GR relative to AS		Small increase or negligible	Inconsistent	Minimal	Inconsistent	For low E_b - stresses increased up to 14%. For high E_b - stresses generally decreased.
	Low E_b (1,000 MPa)	*+2%*	*+14% max*	*+1% max*	*+9% max*	
	High E_b (8,000+ MPa)	*Negligible*	*-3% max*		*-9% max*	
Increasing base modulus		Small increase or negligible	Inconsistent	Decrease	Inconsistent	For AS - the trend was inconsistent. For GR - the stresses generally decreased up to 20%.
	AS	*+2%*	*+5%*	*-20%*	*Inconsistent increase*	
	GR	*Negligible*	*-10% max*		*-9% max*	
Increasing support modulus		Small increase or negligible	Increase or negligible	Small decrease	Inconsistent (minimal)	For low E_b - the trend was inconsistent. For high E_b - stresses decreased or changed minimally.
	Low E_b (1,000 MPa)	*+2% max*	*+20% max*	*-3% max*	*+4% or -2%*	
	High E_b (8,000+ MPa)	*Negligible*	*Negligible*		*Minimal*	
Increasing support thickness		Negligible	Decrease or negligible	Inconsistent (minimal)	Decrease	For low E_b - stresses generally decreased up to 14%. For high E_b - trend was inconsistent, but the support modulus had relatively minimal effects.
	Low E_b (1,000 MPa)	*Similar for all*	*-14% max*	*-2% max*	*-6% max*	
	High E_b (8,000+ MPa)		*Minimal decrease*	*+2% max*	*-4% max*	

Table Notes

Negligible	Approximately 0% to <1%	AS	AS model (represents asphalt-supported condition)
Minimal	Approximately 1% to 2%	GR	GR model (represents grade-/grout-supported condition)
SC	support condition	E_b	Elastic modulus of base layer

The GR model included a support layer while the AS model did not. For low friction, the presence of the support layer in the GR model had a minimal effect on panel stresses when the base modulus was low (1,000 MPa). It is hypothesized that with low friction and a weak base, a thin support layer provided minimal panel support or resistance so there was little effect on stresses. With low friction and a stiffer base (8,000+ MPa), the inclusion of the support layer had an inconsistent effect; the panel stresses increased for some loading combinations and decreased for others. For high friction, the presence of the support layer increased the panel stresses when the base modulus was low (1,000 MPa) and generally decreased the panel stresses when the base modulus was high (8,000+ MPa). With a lower base modulus, it is hypothesized that the stiff support layer restrained panel movement inducing larger stresses than when the support layer was not present. When the base modulus was higher, the stiffness of the base and support were more similar and the effect of the support was minimal or it reduced panel stresses.

The modulus of the base layer was varied to evaluate its effect on the panel stresses. For low friction, increasing the base modulus increased panel stresses for all loading combinations except the positive gradient with axle loading. It is expected that for temperature gradients alone a stiffer base would increase curling-induced stresses in the panel. Contrarily, for axle loading alone a stiffer base is expected to reduce panel stresses because it provides more support to the panel. Under a combination of a temperature gradient and axle loading these two opposing trends exist. It is hypothesized that an increase in the base modulus caused an increase in stresses when the temperature effect was dominant and reduced stresses when the benefit under axle loading was dominant. The stress increase was larger in the case of the temperature gradients alone compared to the temperature gradients with axle loading. For the positive gradient with axle loading, the stresses were reduced with a stiffer base. For the negative gradient with axle loading, the stresses increased with a stiffer base but less than they did for the negative gradient only loading. For high friction, increasing the base modulus generally reduced the stresses for the GR model. As the base modulus increased, the stiffness of the support and base were more similar which reduced the stresses in the support and panel. For the AS model, increasing the base modulus had inconsistent effects.

The effects of changes to the support modulus and thickness on the minimum panel stresses were negligible for low interface friction and more substantial for high interface friction. With high friction and a low base modulus, stress reduction was generally achieved by a lower support modulus and a thicker support layer. A stiffer support increased panel and support stresses because the support provided more resistance to curling, and a thicker support reduced panel and support stresses. With higher friction and a higher base modulus, the effect of the support modulus and thickness on the stresses was inconsistent but fairly minor. Intuitively, with a stronger interface bond and a stiff base layer, the presence of a thin support layer is minimal and does not substantially influence the pavement behaviour. However, when the base layer is relatively weak, the presence of a well-bonded support layer has a more significant impact.

6.3.2 Base Stresses

6.3.2.1 Positive Temperature Gradient

The minimum base stresses under a positive temperature gradient for the first set of parametric studies is shown by Figure 6-20.

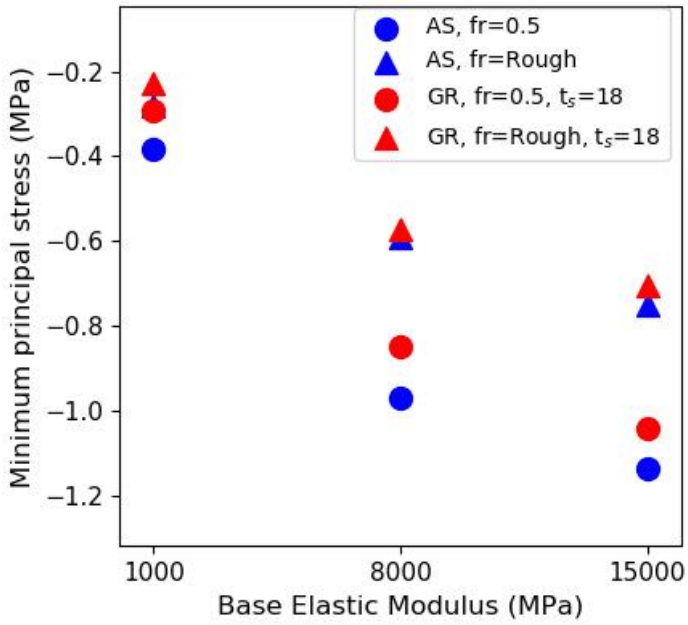

Figure 6-20. Minimum base stresses under positive temperature gradient

The base stresses decreased as friction increased. With low friction the peak stress occurred under the panel corner, and with high friction the peak stresses are more distributed underneath the joint. The stress distributions in the base layer for a base modulus of 8,000 MPa for low and high friction are shown in Figure 6-21 and Figure 6-22, respectively.

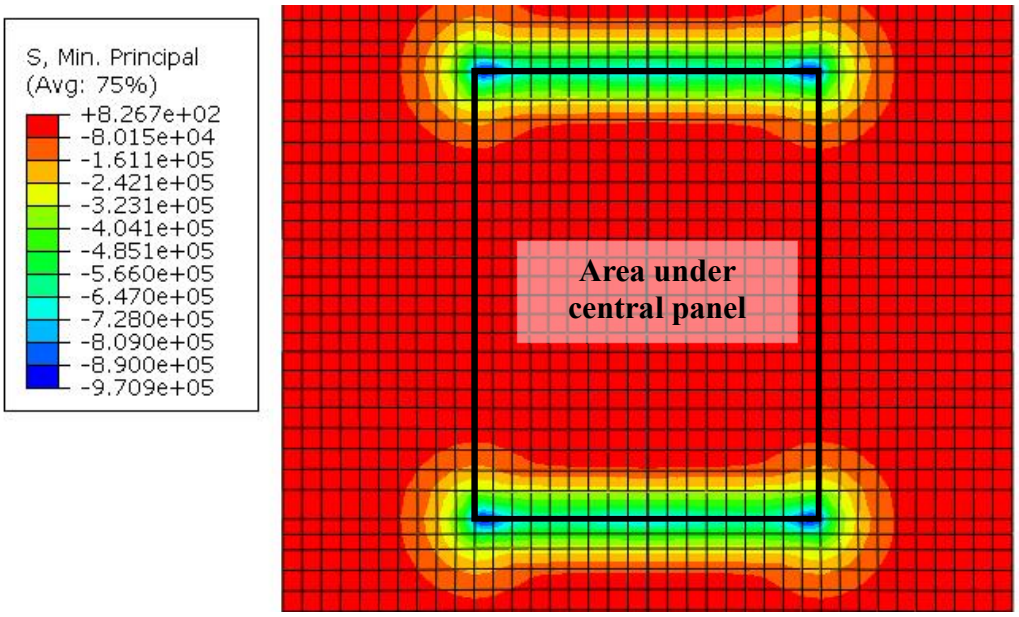

Figure 6-21. Base stresses for AS model under positive temperature gradient with low friction

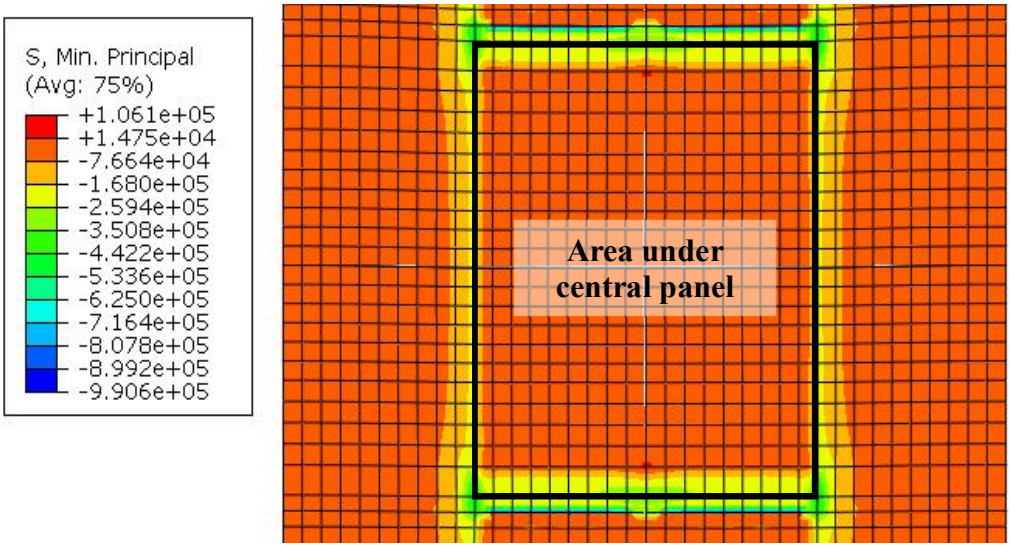

Figure 6-22. Base stresses for AS model under positive temperature gradient with high friction

The area of interest in the study was the base directly underneath the central panel. For this loading case, the stresses directly underneath the central panel were lower with higher friction. However, considering a larger study area beyond the central panel, with high friction the peak stress occurred just beyond the central panel and this stress was higher than with low friction.

The GR stresses are slightly lower than AS stresses for low friction and approximately the same as AS for high friction. Figure 6-23 and Figure 6-24 compare the base stresses for the AS and GR models for low friction, with a base modulus of 1,000 MPa.

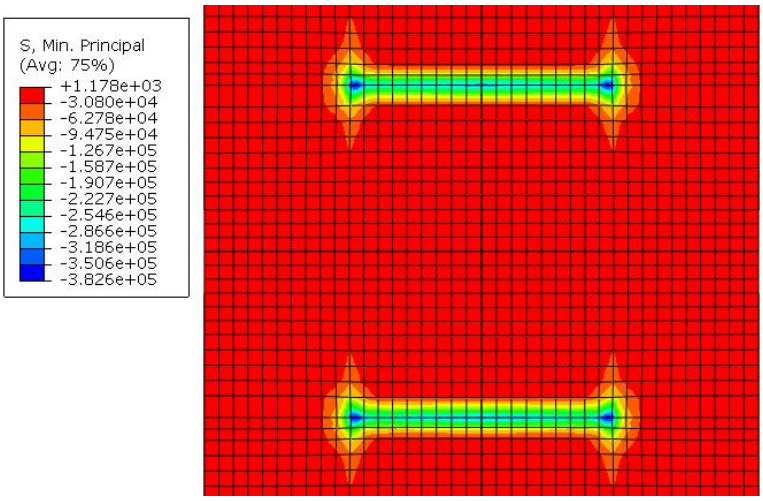

Figure 6-23. Base stresses for AS model with positive temperature gradient, with low friction, and 1,000 MPa base modulus

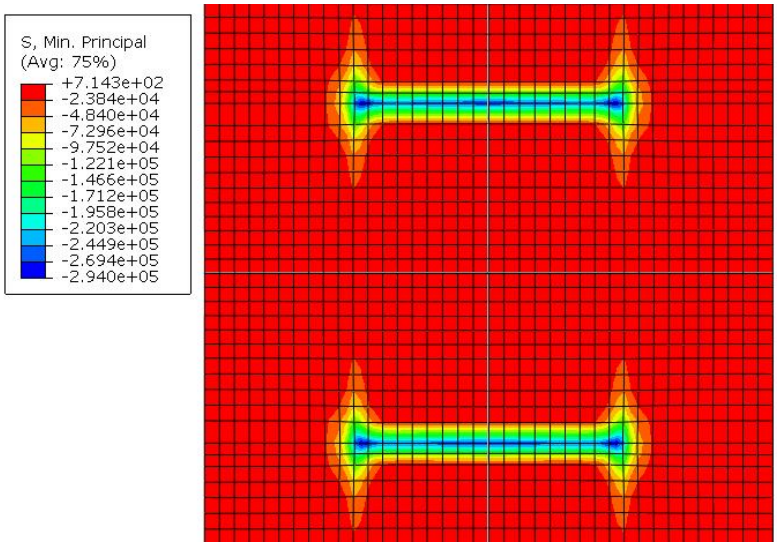

Figure 6-24. Base stresses for GR model with positive temperature gradient and low friction, and 1,000 MPa base modulus

The presence of the support layer in the GR model reduced the peak base stresses. The support layer is likely thin enough that it did not cause a large increase in curling stresses and it dissipated some of the stresses that would otherwise be transferred to the base.

For low and high friction, the base stresses increased as the base modulus increased. This behaviour is expected since a stiffer material will have a greater resistance to load, inducing larger stresses in the material.

The minimum base stresses for the parametric studies of the support modulus and thickness are shown by Figure 6-25 and Figure 6-26, for a base modulus of 1,000 MPa and 8,000 MPa, respectively.

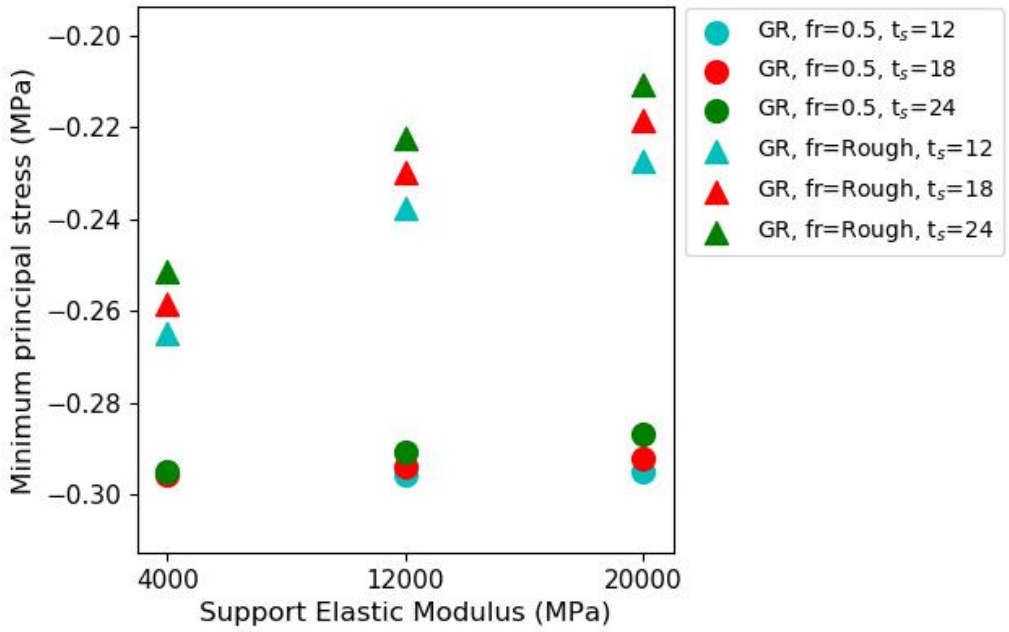

Figure 6-25. Minimum base stresses under positive temperature gradient with changes in support properties for 1,000 MPa base modulus

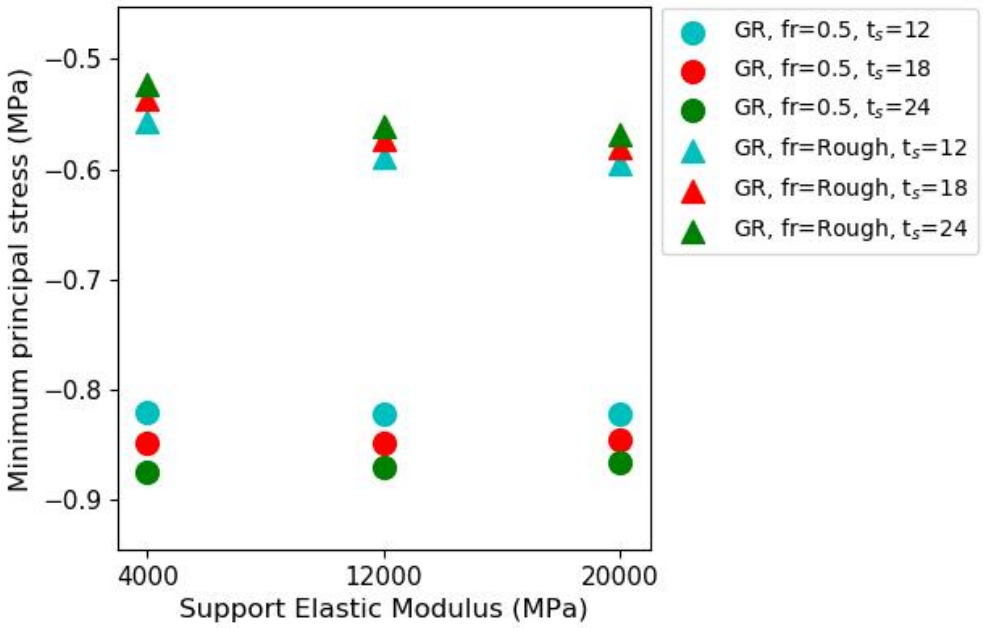

Figure 6-26. Minimum base stresses under positive temperature gradient with changes in support properties for 8,000 MPa base modulus

The responses for a base modulus of 15,000 MPa are similar to those for a modulus of 8,000 MPa.

For low friction the support modulus had a minimal effect on the base stresses, which is consistent for all the loading combinations. For high friction, an increasing support modulus reduced stresses when the base modulus was low (1,000 MPa) and increased stresses when the base modulus was higher (8,000 MPa or greater). When the base modulus was low, the support provided the most stress resistance and reduced the stresses to the base layer. When the base modulus was higher, the stiffness of the base and support were similar and both these layers provide greater resistance; in this case the stresses were higher for both the support and base.

For low friction, the effect of changes in the support thickness depended on the base modulus. For high friction, the stresses decreased with increasing support thickness.

6.3.2.2 Negative Temperature Gradient

The minimum base stresses under a negative temperature gradient for the first set of parametric studies is shown by Figure 6-27.

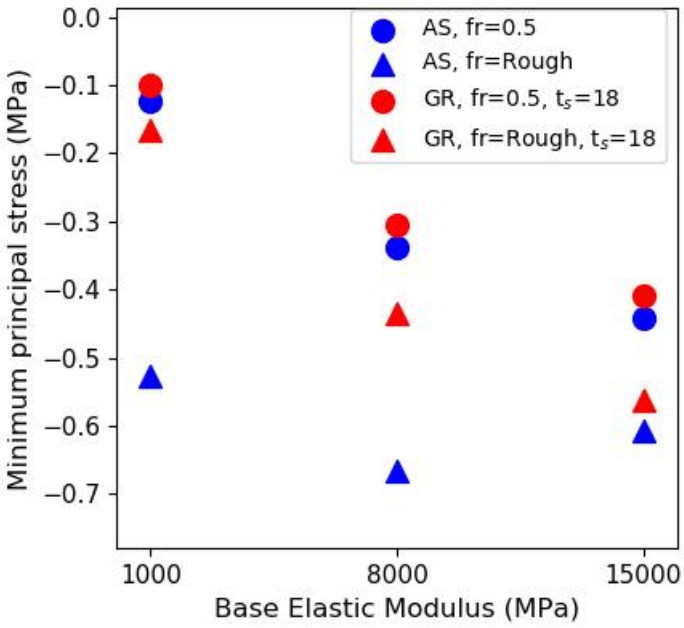

Figure 6-27. Minimum base stresses under negative temperature gradient

With higher friction, the stresses increased. With low friction the peak stress occurred underneath the middle of the central panel, and with high friction the peak stress occurred underneath the joint. With a stronger interface bond, the panel edges were more restrained from curling which caused the increase in stresses. The stress distributions under the central panel for a base modulus of 8,000 MPa are shown for low and high friction in Figure 6-28 and Figure 6-29, respectively.

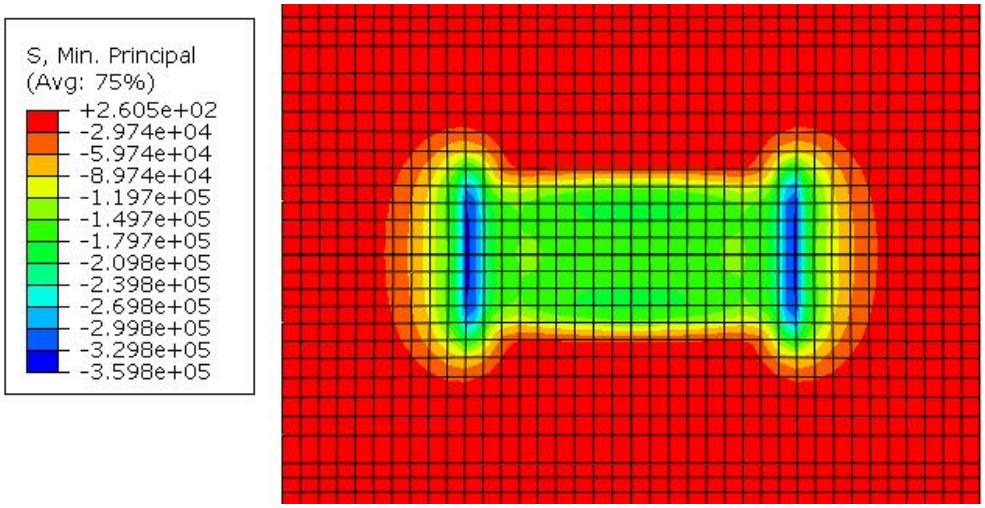

Figure 6-28. Base stresses for AS with negative temperature gradient with low friction

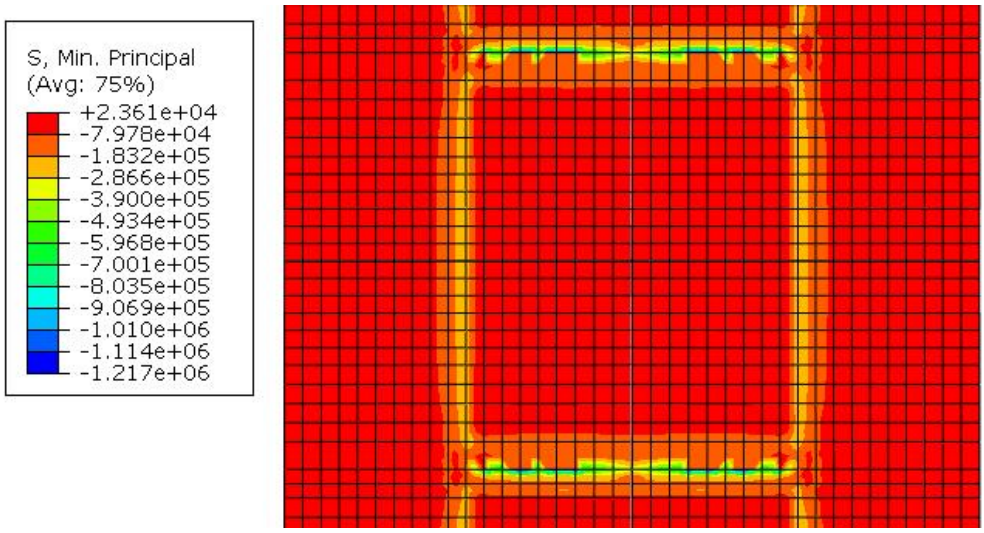

Figure 6-29. Base stresses for AS with negative temperature gradient with high friction

For low and high friction, the base stresses increased as the base modulus increased and the GR stresses were lower than the AS stresses. This is the same behaviour observed for the other loading combinations.

The minimum base stresses for the parametric studies of the support modulus and thickness are shown by Figure 6-30 and Figure 6-31, for a base modulus of 1,000 MPa and 8,000 MPa, respectively.

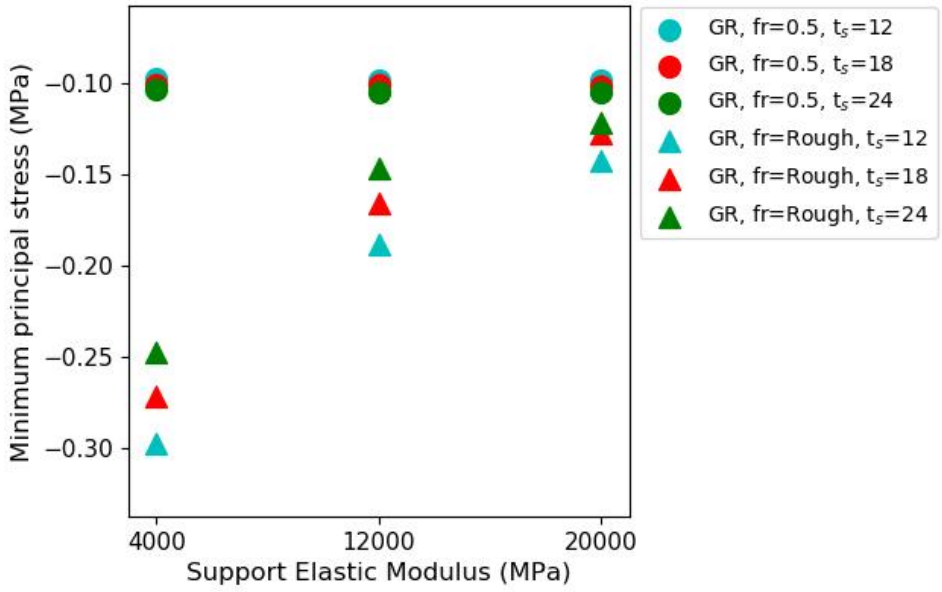

Figure 6-30. Minimum base stresses under positive temperature gradient with changes in support properties for 1,000 MPa base modulus

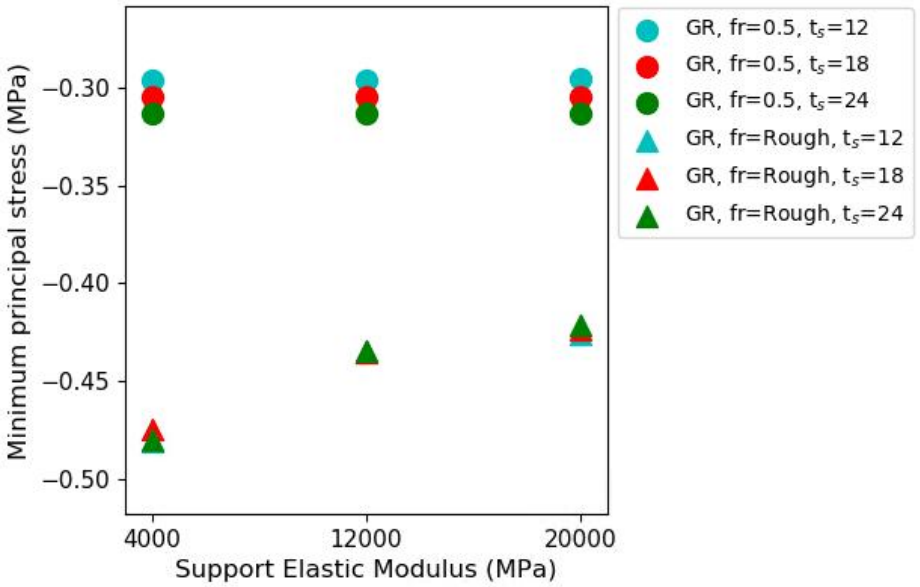

Figure 6-31. Minimum base stresses under positive temperature gradient with changes in support properties for 8,000 MPa base modulus

The responses for a base modulus of 15,000 MPa followed a similar trend to that of 8,000 MPa.

For low friction, the support modulus had minimal effect on the minimum base stresses. For high friction, the base stresses decreased with an increase in the support modulus. For this loading combination, the reduction in base stresses was more significant when the base modulus was low (1,000 MPa). Figure 6-32 and Figure 6-33 compare the base stresses under the central panel for a support modulus of 4,000 MPa and 20,000 MPa, respectively.

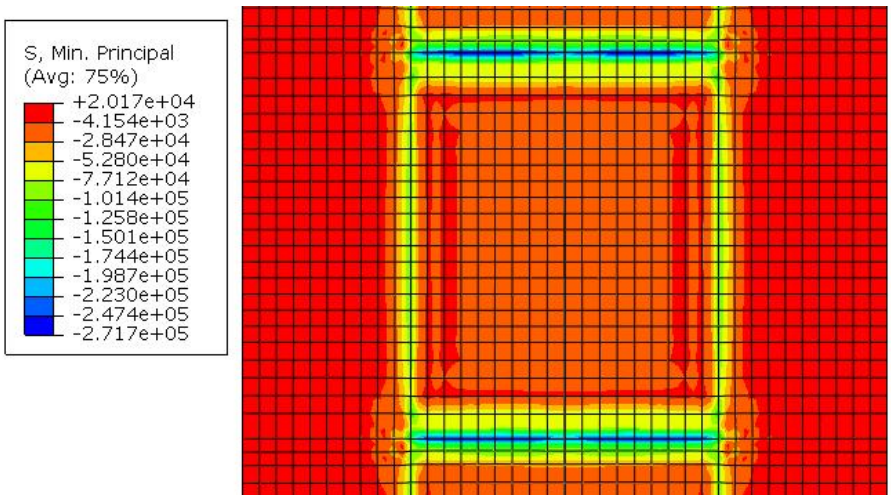

Figure 6-32. Panel stresses for GR model with negative temperature gradient with high friction and a 4,000 MPa base modulus

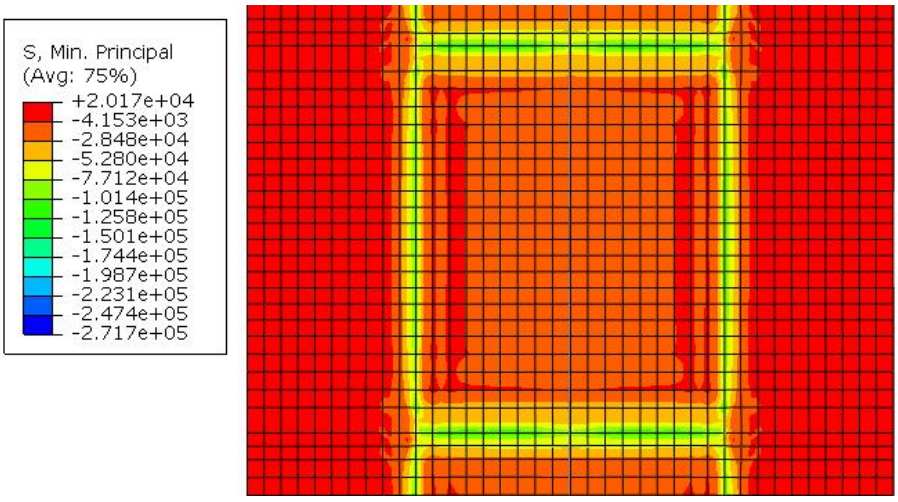

Figure 6-33. Panel stresses for GR model with negative temperature gradient with high friction and a 20,000 MPa base modulus

The same range of stresses is shown for easy visual comparison. As the support modulus increased, the stresses to the base layer were reduced.

For low friction, the stresses increased with increasing support thickness. For high friction, increasing the support thickness had a minimal effect when the base was stiff (8,000+ MPa) and it reduced the stresses when the base stiffness was lower (1,000 MPa). In general, when the base stiffness was low and interface friction was high, increasing the strength and thickness of the support was beneficial in reducing stresses transferred to the base because the support provided more load resistance.

6.3.2.3 Positive Temperature Gradient with Axle

The minimum stresses in the base layer under the positive gradient and axle loading combination are shown in Figure 6-34.

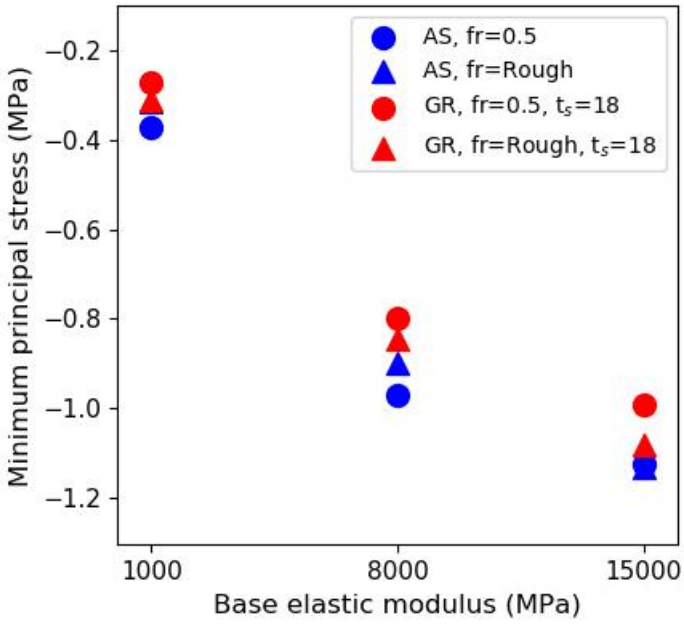

Figure 6-34. Minimum base stresses under positive temperature gradient and axle loading

The minimum base stresses occurred at the top of the base layer. For low friction, the minimum stress occurred under the panel corner, approximately 10 to 20 cm inwards from the longitudinal panel edge. For high friction, the critical stress occurred under the longitudinal panel edge at midpanel.

With higher friction, the base stresses increased slightly for the GR models and decreased slightly or remained approximately constant for the AS models. Similar trends were observed under positive gradient only loading; however, with axle loading, the effect of friction on the stresses is smaller because the axles counteract some of the panel curling caused by the temperature gradient, which in turn reduces the stresses induced by frictional restraint.

For low and high friction, the base stresses increased as the base modulus increased and the GR stresses were lower than the AS stresses. This is the same behaviour observed under the other loading combinations.

The minimum panel stresses for the parametric studies of the support modulus and thickness are shown by Figure 6-35, for a base modulus of 8,000 MPa.

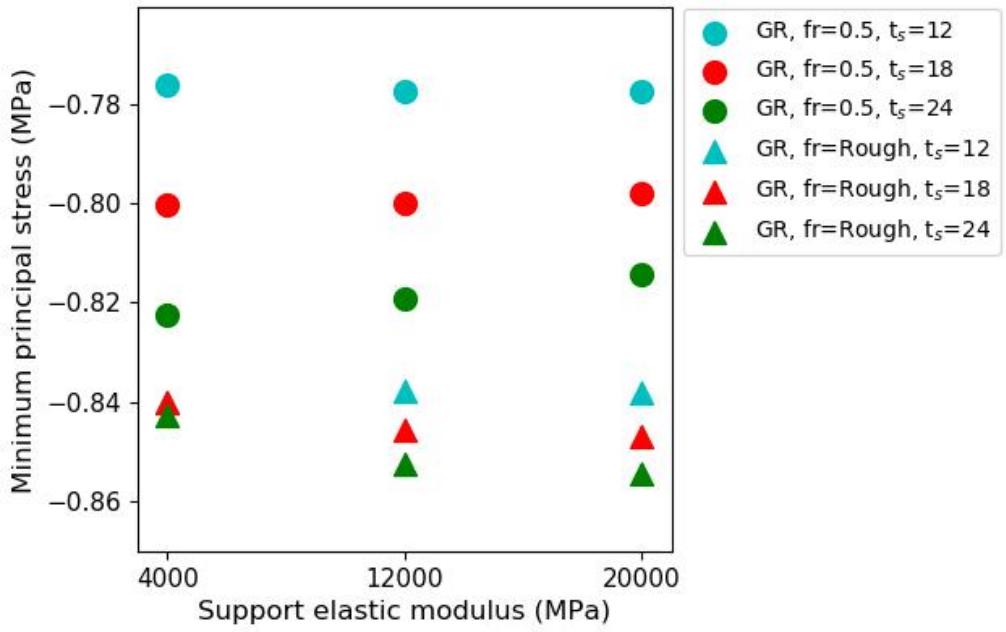

Figure 6-35. Minimum base stresses under positive temperature gradient and axle loading with changes in support properties

The responses for a base modulus of 15,000 MPa are similar to those for a modulus of 8,000 MPa.

Changes in the support modulus had a fairly minimal effect on the base stresses for low and high friction. For a low base modulus (1,000 MPa), changes in the support modulus and thickness had minimal effect on the base stresses. For a high base modulus (8,000 MPa or greater), increasing the support thickness increased the base stresses.

6.3.2.4 Negative Temperature Gradient with Axle

The minimum stresses in the base layer under the negative gradient and axle loading combination are shown in Figure 6-36.

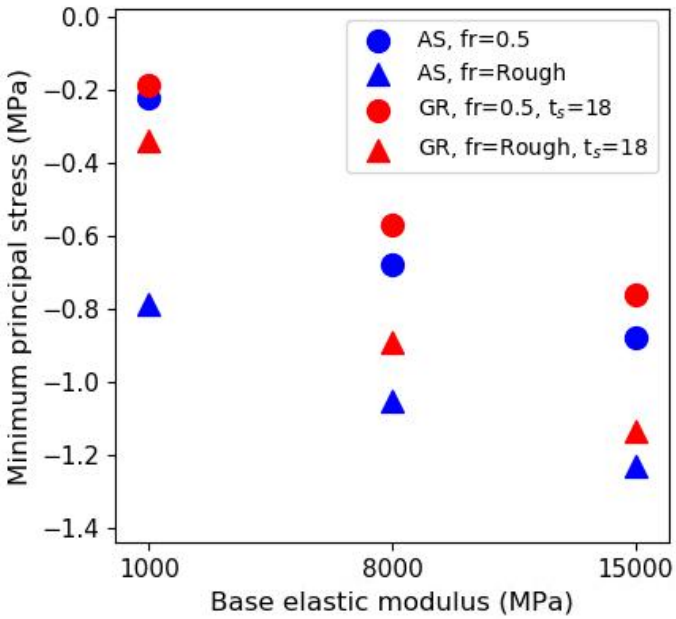

Figure 6-36. Minimum base stresses under negative temperature gradient and axle loading

For low friction, the peak stresses occurred at the top of the base layer, within 15 cm of the longitudinal panel edge and within 30 to 60 cm from the joint. For high friction, the peak stresses also occurred at the top of the base layer under the panel corner.

The base stresses increased with higher friction because larger stresses were induced by the frictional restraint. The behaviour is similar to that observed for the loading case of a negative temperature gradient. However, the addition of axle loading counteracts some of the panel curling so that the stresses caused by frictional restraint are smaller than the case without axle loading.

For low and high friction, the base stresses increased as the base modulus increased, and the GR stresses were lower than the AS stresses. This is the same behaviour observed under the other loading combinations.

The minimum base stresses for the parametric studies of the support modulus and thickness are shown by Figure 6-37, for a base modulus of 8,000 MPa.

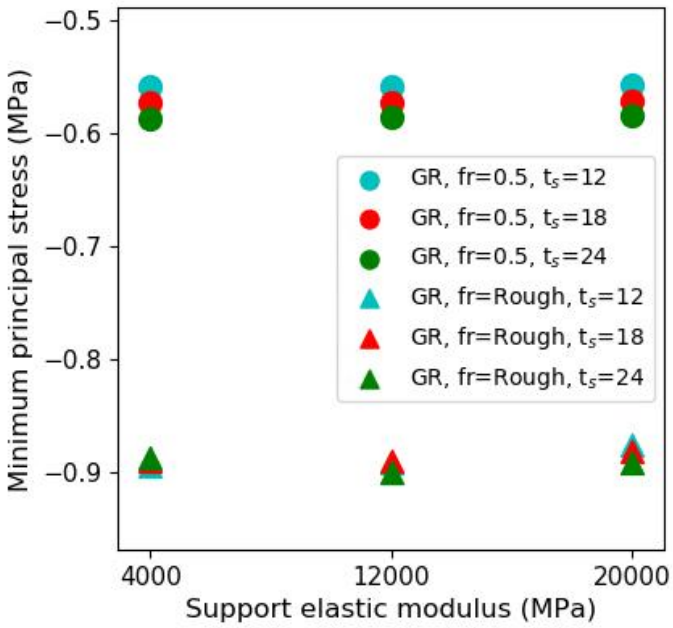

Figure 6-37. Minimum base stresses under negative temperature gradient and axle loading with changes in support properties

Changes in the support modulus had a negligible effect on the base stresses. For low friction, an increasing support thickness increased the base stresses, similarly to other loading combinations. For high friction, an increasing support thickness had minimal effect on the base stresses.

6.3.2.5 Base Stresses Summary and Discussion

Table 6-4 summarizes the trends observed in the minimum base stresses for each of the parametric studies and for each of the loading combinations. The following discusses the trends with respect to the influence of low versus high interface friction, the AS model versus the GR model, the effect of the base modulus, support modulus, and support thickness. Common trends or patterns observed across all four loading combinations are presented.

Table 6-4. Summary of trends in base stresses

Property	Secondary Property	Effect under different loading combinations: Positive Gradient	Negative Gradient	Positive Gradient + Axle	Negative Gradient + Axle	Trends
Stress range (MPa)		-0.2 to -1.2	-0.1 to -0.7	-0.2 to -1.2	-0.2 to -1.3	Minimum stresses under negative gradient only. Other loading combinations are considered for critical stresses.
High friction relative to low friction		Decrease	Increase	Inconsistent	Increase	Stresses generally increased. Stresses decreased for some loading combinations because of the choice of study area (high friction peak stress occurred just beyond study area, and was higher than low friction peak stress).
	Low E_b (1,000 MPa)	*-10% max (all SC)*	*+60% for AS +10% max for GR*	*-7% for AS +3% for GR*	*+45% for AS +10% for GR*	
	High E_b (15,000 MPa)	*-35% max (all SC)*	*+25% max (all SC)*	*Negligible for AS +10% max for GR*	*+35% (all SC)*	
Low Friction						
GR relative to AS		Decrease	Decrease	Decrease	Decrease	Stresses decreased up to 15%.
	Low E_b (1,000 MPa)	*-15% max*	*-4% max*	*-10% max*	*-3% max*	
	High E_b (8,000+ MPa)		*-8% max*	*-15% max*	*-10% max*	
Increasing base modulus		Increase	Increase	Increase	Increase	Stresses increased up to 70%.
	AS	*+70% max*	*+45% max*	*+70% max*	*+50% max*	
	GR					
Increasing support modulus		Small decrease or minimal	Negligible	Negligible	Negligible	Support modulus had fairly minimal effect.
	Low E_b (1,000 MPa)	*-3% max*	*Similar for all*	*Similar for all*	*Similar for all*	
	High E_b (8,000+ MPa)	*Minimal*				

Low Friction (continued)						
Increasing support thickness		Inconsistent	Small increase	Increase or minimal	Small increase or minimal	For low E_b - trend was inconsistent. For high E_b - stresses increased up to 8%.
	Low E_b (1,000 MPa)	*-3% max*	*+5% max*	*Minimal*	*Minimal*	
	High E_b (8,000+ MPa)	*+8% max*		*+7% max*	*+4% max*	
High Friction						
GR relative to AS		Decrease or minimal	Decrease	Decrease or negligible	Decrease	Stresses decreased by up to 60%.
	Low E_b (1,000 MPa)	*-5% max*	*-55% max*	*Negligible*	*-40% max*	
	High E_b (8,000+ MPa)		*-5% max*	*-6% max*	*-10% max*	
Increasing base modulus		Increase	Increase (most cases)	Increase	Increase	Stresses increased up to 75%.
	AS	*+40% max*	*+20%*	*+75% max*	*+35%*	
	GR		*+55% max*		*+65% max*	
Increasing support modulus		Inconsistent	Decrease	Inconsistent	Minimal	For low E_b - stresses decreased up to 50%. For high E_b - trend was inconsistent.
	Low E_b (1,000 MPa)	*-13% max*	*-50% max*	*-2% max*	*Similar for all*	
	High E_b (8,000+ MPa)	*+5% max*	*-12% max*	*+2.5% max*		
Increasing support thickness		Decrease	Inconsistent	Small increase or minimal	Inconsistent and minimal	For low E_b - stresses decreased up to 18%. For high E_b - trend was inconsistent.
	Low E_b (1,000 MPa)	*-5% max*	*-18% max*	*Minimal*	*Minimal*	
	High E_b (8,000+ MPa)		*+3% max*	*+3% max*	*No consistent trend +/- 2% max*	

Table Notes

Negligible	Approximately 0% to <1%	AS	AS model (represents asphalt-supported condition)
Minimal	Approximately 1% to 2%	GR	GR model (represents grade-/grout-supported condition)
SC	support condition	E_b	Elastic modulus of base layer

The smallest panel stresses were produced by the negative temperature gradient only loading. The panel stresses were within the same range for all other loading combinations.

It is expected that the base stresses would increase as interface friction increased because higher restraint from the strong interface bond induces higher stresses. This was generally the case; the stresses increased at the longitudinal panel edges and near the joints where curling was restrained. For the case with a positive temperature gradient, the base stresses with high friction were lower than with low friction within the study area (directly below the central panel). However, the peak stress with high friction was located just outside the study area and was greater than with low friction. In general, the stresses do increase with higher friction.

For all loading combinations and friction conditions, the base stresses increased as the base modulus increased. As the base stiffness increases, its load resistance increases which induces larger stresses in the material. For low friction, the increase in stresses was similar for the AS and GR models and ranged from 50% to 70%. For high friction, the increase in stresses ranged from 20% to 75% for the AS models and 40% to 75% for the GR models.

For low friction and high friction, the stresses were generally reduced by the presence of the support layer in the GR model in comparison to the AS model without the support layer. For low friction the stresses were reduced by up to 15%, and for high friction the stresses were reduced by up to 60%. Therefore, inclusion of the support layer was successful in reducing some of the stresses that are transferred to the base layer underneath.

For low friction, changes in the support modulus generally had a negligible effect on the minimum base stresses. For high friction and a low base modulus (1,000 MPa), increasing the support modulus reduced the base stresses by up to 50%. As the support modulus increased, the support provided greater load resistance and reduced the stresses transferred to the base layer which is relatively weak. The stress reduction was most substantial for the gradient only loading combinations and was minimal for the loading combinations with axle loading. For high friction and a higher base modulus (8,000 MPa or greater), increasing the support modulus either increased or decreased the base stresses depending on the loading combination. In this case, the support and

base have more similar stiffnesses, so further increases to the support modulus are not always beneficial in reducing base stresses.

For low friction and a low base modulus (1,000 MPa), changes in the support thickness had an inconsistent effect on the base stresses. However, the effects were fairly small or minimal for some loading cases. For low friction and a high base modulus (8,000 MPa or greater), increasing the support thickness increased the base stresses. With increasing support thickness, the support stresses generally increased which may result in higher stress transfer to the base layer. For high friction and a low base modulus (1,000 MPa), increasing the thickness of the support layer generally reduced the base stresses by up to 18% or had a minimal effect. These results seem reasonable considering that the presence of the support layer and higher support modulus also reduced base stresses; the general trend shows that a stiffer, thicker support layer helps to reduce base stresses. For high friction and a high base modulus (8,000 MPa or greater), changes in the support thickness had a fairly small but inconsistent effect on the base stresses. For some loading combinations the base stresses increased and for others the stresses decreased. This is similar to the effect of the support modulus, which was also inconsistent when the base modulus was high.

6.3.3 Results Summary and Recommendations

Based on the observed trends in the pavement stresses, recommendations were made for conditions that minimized the panel stresses or the base stresses. The recommendations were then combined to identify the conditions that would improve the performance for the pavement structure, considering both the panel and base stresses. Finally, these recommendations are presented in terms of practical design specifications or construction changes that can be implemented in future PCIP applications.

Two key assumptions were made in developing these recommendations. The first assumption is that the grout-supported condition is more likely to achieve a stronger bond between the panel and underlying layer than the asphalt- or grout-supported conditions. This is based on construction experience; the grout-supported condition makes use of leveling inserts which will likely improve the bond between the support and panel. It was assumed that asphalt- and grade-supported conditions would be equally capable of achieving low bonding states. Second, if the trends observed in the stress responses were inconsistent across the different loading combinations, then

no recommendation was made about this property. The reason being that when the trend was inconsistent, there may be a stress reduction or increase, depending on the loading combination. Since the pavement is exposed to all the loading combinations, no recommendation can be made which will reduce stresses in all cases.

When combining the recommendations across two components, such as the panel and base or low and high base modulus, if the trends were inconsistent for one component and consistent for the other, then a recommendation was made based on the consistent trend. This recommendation would benefit one of the components and would benefit the other component only in certain loading combinations. For example, if including the support layer was beneficial for the base in all loading combinations and was beneficial for the panel only in certain loading combinations, it was recommended to include the support layer. Similarly, if increasing the support thickness reduced the base stresses for a low base modulus (across all loading combinations) and had an inconsistent effect for a high base modulus, then if the base modulus was unknown, it would be recommended to increase the support thickness.

The synthesis of these recommendations is included in Appendix A. The recommendations are also presented as flow charts that can be used as decision-making tools to select the optimal conditions for PCIP performance.

Figure 6-38 is a decision-making aid to select the optimal PCIP support conditions if the stiffness if the existing base is known from field testing. Based on the FEA results, the ideal conditions for PCIP performance include inclusion of the support layer and lower bonding between the panels and underlying layers. The grade-supported condition is recommended because it includes the support layer and it is more likely to achieve low bonding than the grout-supported condition. In the ideal case, the grade-supported condition would be used and the only difference in optimal conditions for the low and high modulus base is the recommendation for the support thickness. For a low base stiffness the results were inconclusive and a recommendation cannot be made, and for a high base stiffness a thinner support is recommended. If low bonding cannot be achieved by any of the support conditions, the alternative conditions for high bonding are presented in Figure 6-38. For high bonding and a low base modulus, a choice must be made between minimizing panel

stresses or base stresses because each leads to different recommendations. For high bonding and a high base modulus, the grout-supported condition is recommended.

In the absence of information about the base modulus or if the type of support condition has already been selected based on other criteria, Figure 6-39 can be used to choose optimal conditions based on the type of support condition. It is possible that the existing base modulus would be unknown if site testing was not performed. Alternatively, the choice of support condition may be preselected based on other criteria such as constructability criteria or equipment needs. If the bonding condition can be controlled by the design and construction choices, then low bonding is again recommended and the grade-supported condition is most optimal. For all the support conditions, the optimal conditions are shown for high and low bonding.

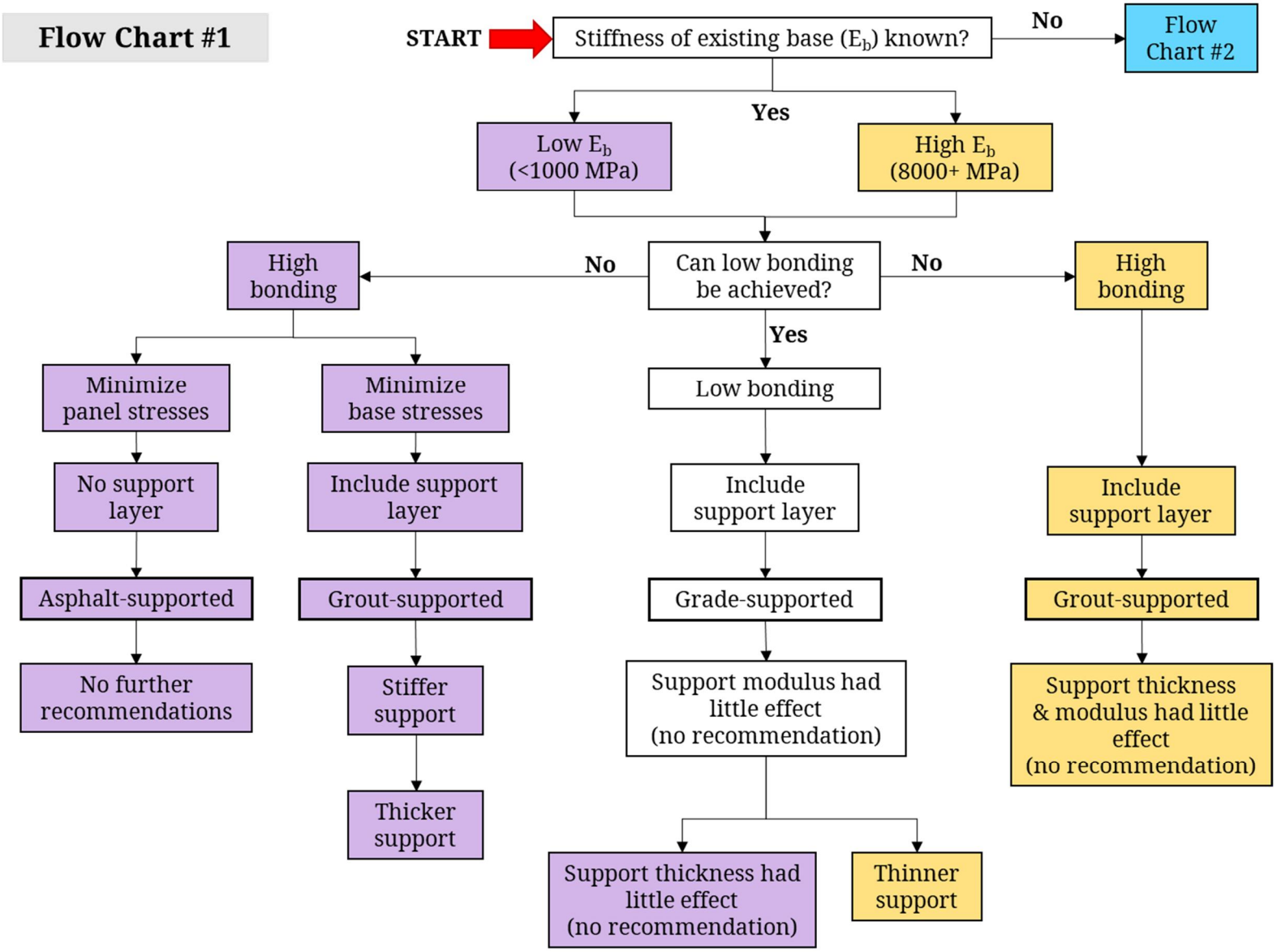

Figure 6-38. Decision-making aid for optimal PCIP conditions if existing base stiffness is known

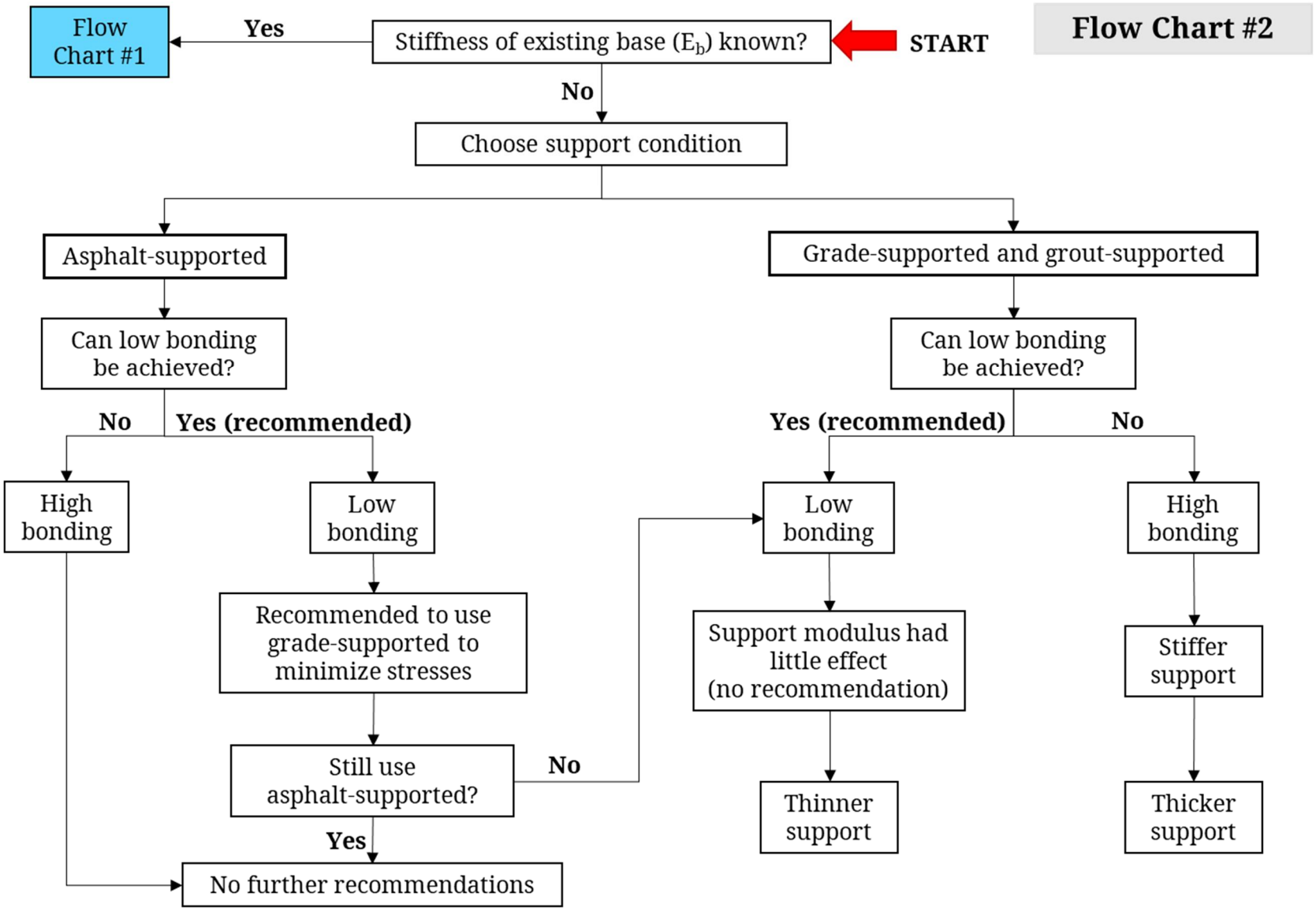

Figure 6-39. Decision-making aid for optimal PCIP conditions based on support condition type

CHAPTER 7 Conclusions and Recommendations

7.1 Conclusions

Proper support for precast concrete inlay panels (PCIPs) is a key component for the successful performance of the pavement. It was hypothesized that changes in the type of support condition, support thickness and modulus, and base modulus would affect the performance of the PCIPs. This hypothesis was evaluated by performing analyses of the field data collected from the PCIP trial installation and by finite element analysis (FEA) of the PCIPs. The main findings of these analyses are presented.

7.1.1 Field Data Analysis Results

The instrumentation installed in the PCIP trial site was Earth Pressure Cells (EPCs) to measure pressure and thermistors to measure temperature at the top of the base layer. The field data analysis revealed some general trends in the pressures and temperatures throughout different seasons. The average pressure and temperature varied between the winter and summer seasons. The magnitudes of the pressures were generally smaller during the summer than winter, and negative. Therefore, in summer the base is subjected to smaller magnitude upwards pressures which may indicate that the panel is curling off the support, and in winter the base is subjected to larger magnitude compressive pressures. The data collected thus far also showed changes over time; from the first to second winter, the magnitude of the mean pressure increased and the average temperature decreased. It is possible that some deterioration occurred which caused an increase in the pressures transferred to the base layer and reduced the insulating properties of the panels; however, the cause of these changes is not conclusive.

Two pairs of EPCs were installed with each type of support condition. The analysis of the pressure data indicated that there were statistically significant differences in the pressures recorded within the same type of support condition; this means that the variations in the pressures cannot be attributed to the type of support condition and may be caused by other factors such as calibration of the EPCs or differences in construction. Therefore, conclusions about the relative performance of the support conditions cannot be drawn at this time from the available data.

7.1.2 Design and Construction Recommendations

Based on the FEA of the PCIPs, the conditions which minimize the stresses in the panel and base layers can be recommended. Recommendations are made regarding the most optimal support condition, and the optimal support layer thickness and stiffness (if applicable). The recommendations are ranked as follows, starting with the most optimal alternative:

1. The grade-supported condition with low bonding is most optimal. If the base modulus is high or unknown, a thinner support layer (12 mm) is recommended.
2. If low bonding cannot be achieved with the grade-supported condition, then the asphalt-supported condition with low bonding is recommended.
3. If low bonding cannot be achieved, then the following alternatives for high bonding are recommended:
    a. If the base modulus is low:
        i. If minimizing panel stresses is a priority: asphalt-supported condition with high bonding;
        ii. If minimizing base stresses is a priority: grout-supported condition with high bonding, a thicker support (24 mm), and high stiffness support.
    b. If the base modulus is high: grout-supported condition with high bonding;
    c. If the base modulus is unknown: grout-supported condition with high bonding, a thicker support (24 mm), and high stiffness support.

The most critical aspect of PCIP design/construction that can be controlled to improve its performance is the bonding at the interface between the panel and underlying layer. Low bonding was beneficial and resulted in lower critical tensile stresses than high bonding. With low bonding, presence of the support layer was also beneficial. Therefore, the grade-supported condition is recommended as the ideal support condition to improve PCIP performance. If low bonding cannot be achieved, then alternatives are provided depending on the other site conditions.

This thesis also contains two flow charts that can be used as decision-making aids to select the most optimal conditions to minimize stresses in the PCIP.

7.2 Future Research

The recommendations for future research relating to performance evaluation of the support conditions for PCIPs are grouped into recommendations for the improvement of field data and the FEA.

7.2.1 Field Data

The collection of field data is critical for developing a model that is calibrated and validated to match the existing site conditions. Therefore, it is recommended to continue further field testing and data collection from the PCIP trial site and for any future PCIP installations. Performing additional Falling Weight Deflectometer (FWD) testing with full deflection basins on a yearly or bi-yearly basis would be beneficial to provide further data for calibration and validation of the model. Continued FWD testing will be useful to evaluate the changes in PCIP performance over time. Site and laboratory testing that can be used to ascertain the material properties of the pavement, such as coring, would also be useful to better calibrate the model to match site conditions.

Continued collection and monitoring of the EPC data would be useful to evaluate general trends in the temperature and pressure over seasons and with service age of the pavement. In future installations of PCIP, it is recommended to install strain gauges or other instrumentation that may be more sensitive in capturing the behaviour of the pavement and for comparison of different conditions. It is also recommended to install thermistors to capture panel surface temperature rather than relying on ambient temperature, which is less accurate.

7.2.2 Finite Element Analysis

The recommendations for improvements to the finite element model (FEM) and FEA generally relate to creating a more realistic representation of the pavement, more realistic loading, expanding the conditions or parameters considered in parametric studies, and improving the prediction of pavement performance. Each of these is discussed in more detail.

The FEM developed thus far makes use of some idealizations and assumptions commonly made in FEA of rigid pavements. The model could be improved to obtain more accurate results and to

more realistically represent the pavement behaviour by adding more complexity to the model. A more complex model is more time-consuming to develop and to run analyses; however, it may be used to obtain more accurate results and more detailed results in areas of interest such as near the dowel bars.

The main assumptions in the model development was the use of linear-elastic, homogenous, isotropic materials and the idealization of static axle loading. These assumptions are invalid if the pavement is distressed, such as with cracked concrete or asphalt or concrete crushing around the dowels, or if unbound granular and subgrade materials behave nonlinearly (Channakeshava et al., 1993; Uddin, Zhang, & Fernandez, 1994). Furthermore, soils are heterogeneous by nature and constructed materials are rarely homogeneous due to construction imperfections. To further this research, it is recommended to consider nonlinearity in the granular materials and in distressed pavement layers. In this rehabilitation strategy, some of the existing asphalt is left in place and has likely experienced some deterioration.

Another idealized condition in the FEM is the assumption of perfectly uniform support under the panels. It is recommended to model gaps or non-uniform support under the panels to consider the effect of non-uniform panel support caused by voids, rutting issues, or other pavement distresses. Previous researchers have considered the effects of cracking distresses (Uddin et al., 1994) and non-uniform support (Brand & Roesler, 2014).

The dowel bars were also idealized as beam elements embedded into the panel with a perfect bond. The dowels could be modelled in more detail, but only if it is of interest to obtain more accurate or detailed responses of the dowels and panel near the joints or to consider distresses such as loss of bond or concrete crushing around the dowels. There is a trade-off between obtaining more accurate and detailed results and the computation time. For more realistic behaviour, it is recommended to model the dowel bars as continuum solid elements inserted into the panel. The dowel slot material that bonds the dowels to the panel could also be modelled with contact properties to define bonding at the dowels-to-dowel slot and dowel slot-to-panel interfaces.

More loading combinations could be evaluated including different axle configurations and axle positions, different magnitudes of the temperature gradients, and the effect of non-linear temperature gradients in comparison to linear gradients. In this research, the axle loading was

positioned in the locations that typically produce critical responses, however other axle positions and loading combinations could be investigated to determine whether there are more critical combinations. Previous studies have shown that non-linear temperature gradients are more realistic than linear gradients (Liang & Niu, 1998; Mohamed & Hansen, 1997). The axle loads were idealized as static loads, however dynamic loading should be considered to more accurately represent traffic loading on the pavement.

For further analysis of the PCIPs, the parametric studies performed in this research can be extended to include other conditions. The scope of this research focused on changes to the panel support conditions through parametric studies of the support and asphalt properties, support condition type, and bonding at the panel-to-support interface. More parametric studies may be performed to consider the impacts of other parameters such as the thickness of the base and granular layers, modulus of the granular layer, and the modulus of subgrade reaction. It is hypothesized that the effect of the granular layer modulus and modulus of subgrade reaction may not be significant, but changes in the base thickness could have a greater impact on the results. Furthermore, three levels of the base modulus were evaluated (1,000, 8,000, and 15,000 MPa); the trends were fairly similar for a higher base modulus of 8,000 MPa or greater, but the trends varied between a modulus of 1,000 MPa and 8,000 MPa. Therefore, it would be recommended to evaluate the responses for base moduli between the range of 1,000 and 8,000 MPa to determine critical changes in the stresses.

To improve the evaluation of PCIP performance it is recommended to consider its long-term performance. Two main suggestions are to evaluate the effects of fatigue loading and the impact of pavement distresses due to materials deteriorated over time.

References

Abaqus Analysis User's Guide (6.14). (2014). Providence, RI: Dassault Systèmes Simulia Corp.

Abdelmohsen, A. Z., & El-Rayes, K. (2016). Optimal Trade-Offs between Construction Cost and Traffic Delay for Highway Work Zones. *Journal of Construction Engineering and Management*, *142*(7). https://doi.org/10.1061/(ASCE)CO.1943-7862

American Concrete Institute. (2005). *ACI 318-05: ACI Manual of Concrete Practice Part 3: Use of Concrete in Buildings - Design, Specifications, and Related Topics*. Detroit, MI: American Concrete Institute.

ARA Inc. (2003). Appendix QQ: Structural Response Models for Rigid Pavements. In *Guide for Mechanistic-Empirical Design of New and Rehabilitated Pavement Structures*. Retrieved from http://onlinepubs.trb.org/onlinepubs/archive/mepdg/2appendices_QQ.pdf

ARA Inc. (2004). Part 3. Design Analysis. In *Guide for Mechanistic-Empirical Design of New and Rehabilitated Pavement Structures*. Retrieved from http://onlinepubs.trb.org/onlinepubs/archive/mepdg/Part3_Chapter4_RigidDesign.pdf

Bing Sii, H. (2014). *Three-Dimensional Finite Element Analysis of Concrete Pavement on Weak Foundation*. Griffith University. Retrieved from https://www120.secure.griffith.edu.au/rch/file/fb16d358-b439-4d91-ad76-494b71d27c06/1/Sii_2015_02Thesis.pdf

Bradbury, R. D. (1938). *Reinforced concrete pavement. Wire Reinforcement Institute, Washington D.C.* Washington, D.C.: Wire Reinforcement Institute.

Brand, A. S., & Roesler, J. R. (2014). Finite element analysis of a concrete slab under various non-uniform support conditions. *International Journal of Pavement Engineering*, *15*(5), 460–470. https://doi.org/10.1080/10298436.2013.837463

Chan, S., & Lane, B. (2005). *Falling Weight Deflectometer (FWD) Testing Guideline*. Downsview, ON: Ontario Ministry of Transportation.

Channakeshava, C., Barzegar, F., & Voyiadjis, G. Z. (1993). Nonlinear FE Analysis of Plain Concrete Pavements with Doweled Joints. *Journal of Transportation Engineering*, *119*(5), 763–781. Retrieved from https://ascelibrary.org/doi/pdf/10.1061/%28ASCE%290733-947X%281993%29119%3A5%28763%29

Cho, Y.-H., McCullough, B. F., & Weissmann, J. (1996). Considerations on Finite-Element Method Application in Pavement Structural Analysis. *Transportation Research Record*, *1539*, 96–101. https://doi.org/10.3141/1539-13

Davids, W. G. (2000). Foundation Modeling for Jointed Concrete Pavements. *Transportation Research Record*, *1730*(1), 34–42. Retrieved from https://journals.sagepub.com/doi/pdf/10.3141/1730-05

Davids, W. G. (2001). 3D Finite Element Study on Load Transfer at Doweled Joints in Flat and Curled Rigid Pavements. *The International Journal of Geomechanics*, *1*(3), 309–323. https://doi.org/10.1061/(ASCE)1532-3641(2001)1:3(309)

Davids, W. G., & Turkiyyah, G. M. (1997). Development of Embedded Bending Member to Model Dowel Action. *Journal of Structural Engineering*, *123*(10), 1312–1320. Retrieved from https://ascelibrary.org/doi/pdf/10.1061/%28ASCE%290733-9445%281997%29123%3A10%281312%29

Davids, W. G., Wang, Z., Turkiyyah, G., Mahoney, J. P., & Bush, D. (2003). Three-Dimensional Finite Element Analysis of Jointed Plain Concrete Pavement with EverFE2.2. *Transportation Research Record*, *1853*, 92–99. https://doi.org/10.3141/1853-11

Delatte, N. (2014). *Concrete Pavement Design, Construction, and Performance* (2nd ed.). New York, NY, FL: CRC Press.

Friberg, B. F. (1940). Design of dowels in transverse joints of concrete pavements. *Transactions of the American Society of Civil Engineers*, *105*(1), 1076–1095.

Hajek, J. J., Smith, K. L., Rao, S. P., & Darter, M. I. (2008). *Adaptation and Verification of AASHTO Pavement Design Guide for Ontario Conditions* (Vol. 61820).

Hammons, M. I. (1998). Advanced Pavement Design: Finite Element Modeling for Rigid Pavement Joints, Report II: Model Development, (March).

Huang, Y. H. (2004). *Pavement Analysis and Design* (2nd Ed). Upper Saddle River, NJ: Pearson Prentice Hall.

Ioannides, A. M. (1984). *Analysis of Slabs-on-grade for a Variety of Loading and Support Conditions*. University of Illinois.

Ioannides, A. M., Khazanovich, L., & Becque, J. L. (1992). Structural Evaluation of Base Layers in Concrete Pavement Systems. *Transportation Research Record*, *1370*, 20–28. Retrieved from http://onlinepubs.trb.org/Onlinepubs/trr/1992/1370/1370-003.pdf

Ioannides, A. M., Thompson, M. R., & Barenberg, E. J. (1985). Westergaard Solutions Reconsidered. *Transportation Research Record*, (1043), 13–23. Retrieved from http://onlinepubs.trb.org/Onlinepubs/trr/1985/1043/1043-003.pdf

Khazanovich, L. (1994). *Structural Analysis of Multi-Layered Concrete Pavement Systems*. University of Illinois. https://doi.org/10.16953/deusbed.74839

Kim, J., & Hjelmstad, K. D. (2003). Three-Dimensional Finite Element Analysis of Doweled Joints for Airport Pavements. *Transportation Research Record*, *1853*, 100–109. Retrieved from https://trrjournalonline.trb.org/doi/pdf/10.3141/1853-12

Kuo, C.-M. (1994). *Three-dimensional finite element analysis of concrete pavement*. University of Illinois at Urbana-Champaign. Retrieved from https://search.proquest.com/docview/304131925

Kuo, C.-M., Hall, K. T., & Darter, M. I. (1995). Three-Dimensional Finite Element Model for Analysis of Concrete Pavement Support. *Transportation Research Record*, *1505*, 119–127. Retrieved from http://onlinepubs.trb.org/Onlinepubs/trr/1995/1505/1505-014.pdf

Liang, R. Y., & Niu, Y.-Z. (1998). Temperature and Curling Stress in Concrete Pavements: Analytical Solutions. *Journal of Transportation Engineering*, *124*(1), 91–100. Retrieved from https://ascelibrary-org.proxy.lib.uwaterloo.ca/doi/pdf/10.1061/%28ASCE%290733-

947X%281998%29124%3A1%2891%29

Maitra, S. R., Reddy, K. S., & Ramachandra, L. S. (2009). Experimental Evaluation of Interface Friction and Study of Its Influence on Concrete Pavement Response. *Journal of Transportation Engineering*, *135*(8), 563–571. https://doi.org/10.1061/ASCE0733-947X2009135:8563

Maitra, Swati Roy, Reddy, K. S., & Ramachandra, L. S. (2009). Load Transfer Characteristics of Dowel Bar System in Jointed Concrete Pavement. *Journal of Transportation Engineering*, *135*(11), 813–821. https://doi.org/10.1061/ASCETE.1943-5436.0000065

Mallela, J., & George, K. P. (1994). Three-Dimensional Dynamic Response Model for Rigid Pavements. *Transportation Research Record*, *1448*, 92–99. Retrieved from http://onlinepubs.trb.org/Onlinepubs/trr/1994/1448/1448-012.pdf

Masad, B. E., Taha, R., & Muhunthan, B. (1996). Finite-Element Analysis of Temperature Effects on Plain-Jointed Concrete Pavements. *Journal of Transportation Engineering*, *122*(5), 388–398. Retrieved from https://ascelibrary-org.proxy.lib.uwaterloo.ca/doi/pdf/10.1061/%28ASCE%290733-947X%281996%29122%3A5%28388%29

Merritt, D. K., McCullough, B. F., Burns, N. H., & Schindler, A. K. (2000). *The Feasibility of Using Precast Concrete Panels to Expedite Highway Pavement Construction*. Austin, TX. Retrieved from http://ctr.utexas.edu/wp-content/uploads/pubs/7_1517_1.pdf

Mohamed, A. R., & Hansen, W. (1997). Effect of Nonlinear Temperature Gradient on Curling Stress in Concrete Pavements. *Transportation Research Record*, *1568*, 65–71. Retrieved from https://journals.sagepub.com/doi/pdf/10.3141/1568-08

Northmore, A. B. (2014). *Canadian Solar Road Panel Design: A Structural and Environmental Analysis*. Retrieved from https://uwspace.uwaterloo.ca/bitstream/handle/10012/8247/Northmore_Andrew.pdf?sequence=3&isAllowed=y

Northmore, A. B., & Tighe, S. (2016). Performance modelling of a solar road panel prototype

using finite element analysis. *International Journal of Pavement Engineering*, *17*(5), 449–457. https://doi.org/10.1080/10298436.2014.993203

Ontario Provincial Highways Traffic Volumes On Demand. (2016). Retrieved January 24, 2018, from http://www.raqsa.mto.gov.on.ca/techpubs/TrafficVolumes.nsf/tvweb?OpenForm&Seq=4

Pavement ME Deign User Group. (2014). Canadian Guide : Default Parameters for AASHTOWare Pavement ME Design.

Pickel, D. (2018). *Precast Concrete Inlay Panels: Rehabilitation Strategy for High-Volume Highways in Ontario*. University of Waterloo, Waterloo, ON. Retrieved from https://uwspace.uwaterloo.ca/bitstream/handle/10012/13540/Pickel_Daniel.pdf?sequence=3&isAllowed=y

Pickel, D., Tighe, S., Lee, W., & Fung, R. (2018). Highway 400 precast concrete inlay panel project: Instrumentation plan, installation, and preliminary results. *Canadian Journal of Civil Engineering*, *45*(10), 889–898. https://doi.org/10.1139/cjce-2018-0044

Priddy, L. P., Doyle, J. D., Flintsch, G. W., Pittman, D. W., & Anderton, G. L. (2015). Three-dimensional modelling of precast concrete pavement repair joints. *Magazine of Concrete Research*, *67*(10), 513–522. https://doi.org/10.1680/macr.14.00278

Saleh, M. F., Steven, B., & Alabaster, D. (2003). Three-Dimensional Nonlinear Finite Element Model for Simulating Pavement Response. *Transportation Research Record*, *1823*, 153–162. https://doi.org/10.3141/1823-17

Tarr, S. M., Okamoto, P. A., Sheehan, M. J., & Packard, R. G. (1999). Bond Interaction Between Concrete Pavement and Lean Concrete Base. *Transportation Research Record*, *1668*, 9–17. Retrieved from https://doi.org/10.3141/1668-02

Tayabji, S., & Brink, W. (2015, October). Precast Concrete Pavement Implementation by U.S. Highway Agencies. *Tech Brief, FHWA-HIF-16-007*. Retrieved from https://www.fhwa.dot.gov/pavement/concrete/pubs/hif16007.pdf

Tayabji, S., Buch, N., & Kohler, E. (2009). Precast Concrete Pavement for Intermittent Concrete Pavement Repair Applications. In *National Conference on Preservation, Repair, and Rehabilitation of Concrete Pavements* (pp. 317–334). St. Louis, MO: FHWA. Retrieved from http://citeseerx.ist.psu.edu/viewdoc/download?doi=10.1.1.543.2959&rep=rep1&type=pdf

Tayabji, S., & Tyson, S. (2017). Precast Concrete Pavement Implementation. *Concrete International*, *39*(4), 41–46. Retrieved from https://global-factiva-com.proxy.lib.uwaterloo.ca/ga/default.aspx

Tayabji, S., Ye, D., & Buch, N. (2012). Joint Load Transfer and Support Considerations for Jointed Precast Concrete Pavements. *Transportation Research Record*. https://doi.org/10.3141/2305-08

Tayabji, S., Ye, D., & Buch, N. (2013a). *Precast Concrete Pavement Technology* (No. SHRP 2 Report S2-R05-RR-1). Washington, D.C.: Transportation Research Board. https://doi.org/10.17226/22710

Tayabji, S., Ye, D., & Buch, N. (2013b). Precast concrete pavements: Technology overview and technical considerations. *PCI Journal*, *58*(1), 112–128. Retrieved from https://www.pci.org/PCI_Docs/Design_Resources/Transportation_Resources/JL-13-Winter-13.pdf

Timoshenko, S., & Lessels, J. M. (1925). *Applied elasticity*. Pittsburg, PA: Westinghouse Technical Night School Press.

Tutumluer, E., Xiao, Y., & Wilde, J. W. (2015). *Cost-Effective Base Type and Thickness for Long-Life Concrete Pavements* (No. MN/RC 2015-42). St. Paul, MN, MN: Minnesota Department of Transportation. Retrieved from http://www.lrrb.org/PDF/201542.pdf

Uddin, W., Hackett, R. M., Joseph, A., Pan, Z., & Crawley, A. B. (1995). Three-Dimensional Finite-Element Analysis of Jointed Concrete Pavement with Discontinuities. *Transportation Research Record*, *1482*, 26–32. Retrieved from http://onlinepubs.trb.org/Onlinepubs/trr/1995/1482/1482-004.pdf

Uddin, W., Zhang, D., & Fernandez, F. (1994). Finite Element Simulation of Pavement Discontinuities and Dynamic Load Response. *Transportation Research Record*, *1448*, 100–106. Retrieved from http://onlinepubs.trb.org/Onlinepubs/trr/1994/1448/1448-013.pdf

Westergaard, H. M. (1926). Stresses in Concrete Pavements Computed by Theoretical Analysis. *Public Roads*, *7*(2), 25–35.

Westergaard, H. M. (1948). New Formulas for Stresses in Concrete Pavements of Airfields. *ASCE Transactions*, *113*, 425–439.

White, T. D., Haddock, J. E., Hand, A. J. T., & Fang, H. (2002). *Contributions of Pavement Structural Layers to Rutting of Hot Mix Asphalt Pavements* (No. Report 468). Washington, D.C.: NCHRP. Retrieved from http://onlinepubs.trb.org/onlinepubs/nchrp/nchrp_rpt_468-a.pdf

Wu, J., Liang, J., & Adhikari, S. (2014). Dynamic response of concrete pavement structure with asphalt isolating layer under moving loads. *Journal of Traffic and Transportation Engineering English Edition*, *1*(6), 439–447. https://doi.org/10.1016/S2095-7564(15)30294-4

Zhang, Y.-C., & Gao, L.-L. (2016). Effect of Base Parameters and Interface Contact Status on the Mechanical Characteristics of the Concrete Pavement Slabs. In *16th COTA International Conference of Transportation Professionals*. Shanghai, China: American Society of Civil Engineers. Retrieved from https://ascelibrary-org.proxy.lib.uwaterloo.ca/doi/pdf/10.1061/9780784479896.055

Appendix A: Summary of Recommendations to improve PCIP performance

Summary of stresses and recommendations				
	Recommendations			
Property	**To minimize panel stresses**	**To minimize base stresses**	**To minimize panel & base stresses**	**Modifications to PCIP design/construction**
High friction relative to low friction	If E_b is low - lower bonding. If E_b is high - no recommendation (effect on stresses varied for different loading combinations).	Lower bonding.	Both low and high E_b - lower bonding.	Adjust design specifications or construction method to achieve desired bond. Asphalt- and grade-supported condition is most likely to achieve low bonding. Grout-supported condition is most likely to achieve high bonding.
Low Friction				
GR relative to AS	If E_b is low - no recommendation (the effect was small). If E_b is high - no recommendation (effect on stresses varied for different loading combinations).	Include support layer.	Include support layer.	Use grade- or grout-supported condition.
Increasing base modulus	No recommendation (effect on stresses varied for different loading combinations).	Lower base modulus is beneficial.	Lower base modulus is beneficial.	Better performance when existing base has a lower modulus.
Increasing support modulus	No recommendation - support modulus had little effect on stresses.	No recommendation - support modulus had little effect on stresses.	No recommendation - support modulus had little effect on stresses.	N/A

Increasing support thickness	No recommendation - support thickness had little effect on stresses.	If E_b is low - no recommendation (effect on stresses varied for different loading combinations). If E_b is high - thinner support layer.	If E_b is low - no recommendation. If E_b is high - thinner support layer.	Test site to establish E_b. If E_b is low - no recommendation for support thickness. If E_b is high - specify thinner support layer.
High Friction				
GR relative to AS	If E_b is low - do not include support layer. If E_b is high - include support layer.	Include support layer.	If E_b is low - depends on which stresses should be minimized. Presence of support layer increased panel stresses up to 14% and decreased base stresses up to 60%. If E_b is high - include support layer.	Test site to establish E_b. If E_b is low - use grade- or grout-supported condition if the priority is to minimize stresses transferred to the base. Use asphalt-supported condition if the priority is to minimize panel stresses. If E_b is high - use grade- or grout-supported condition. If E_b is unknown - use grade- or grout-supported condition.
Increasing base modulus	For AS - no recommendation (effect on stresses varied for different loading combinations). For GR - higher base modulus is beneficial.	Lower base modulus is beneficial.	For AS - lower base modulus is beneficial. For GR - Higher base modulus reduced panel stresses up to 20% and increased base stresses up to 75%.	For asphalt-supported case - better performance when existing base has a lower modulus.

Increasing support modulus	No recommendation (effect on stresses varied for different loading combinations). If E_b is high - no recommendation (the effect of support modulus was small).	If E_b is low - higher support modulus. If E_b is high - no recommendation (effect on stresses varied for different loading combinations).	If E_b is low - higher support modulus. If E_b is high - no recommendation.	Test site to establish E_b. If E_b is low - specify higher support modulus. If E_b is high - no recommendation. If E_b is unknown - specify higher support modulus.
Increasing support thickness	If E_b is low - thicker support layer. If E_b is high - no recommendation (effect on stresses varied for different loading combinations), but the effect of support thickness was small.	If E_b is low - thicker support layer. If E_b is high - no recommendation (effect on stresses varied for different loading combinations).	If E_b is low - thicker support layer. If E_b is high - no recommendation.	Test site to establish E_b. If E_b is low - specify thicker support layer. If E_b is high - no recommendation. If E_b is unknown - specify thicker support layer.

Final Recommendations	
Low Friction	**High friction**
Use grade-supported condition since it is more likely to achieve low bonding, and if E_b is high or unknown specify a thinner support layer (closer to 12 mm). No recommendation for support modulus (has little effect on stresses).	If E_b is low: To minimize panel stresses - asphalt-supported condition (only valid if high friction bond can be achieved). To minimize asphalt stresses - grout-supported condition since it will more likely achieve a stronger bond, with stiffer and thicker support layer. If E_b is high: Use grout-supported condition (more likely to achieve higher bonding). No recommendation for support stiffness or thickness. If E_b is unknown: Use grout-supported condition (more likely to achieve higher bonding), with thicker, stiff support layer.

Appendix B: Detailed Finite Element Analysis Results

Responses under +10°C and -10°C temperature gradient

Notes on the following responses:

[1]E_{base}	elastic modulus of base
[2]$E_{support}$	elastic modulus of support
[3]$t_{support}$	thickness of support
[4]X-coord	Relative to centreline of panels (X-coord = 0 at centreline)
[5]Y-coord	Relative to midpanel of first panel, with three panels total (Y-coord = 0.0 at midpanel of panel 1, Y-coord = 4.585 at midpanel of panel 2, etc.)
[6]Z-coord	Relative to top of panel (Z-coord = 0.0 at top of panel, Z-coord = -0.205 at bottom of panel, etc.)

Responses under +10°C and -10°C temperature gradient

Part	Support Condition	Temp. Gradient (°C)	Friction (panel-to-base) (-)	Friction (panel-to-support) (-)	Friction (support-to-base) (-)	E_{base}[1] (MPa)	$E_{support}$[2] (MPa)	$t_{support}$[3] (MPa)	X-Coord[4] (m)	Y-Coord[5] (m)	Z-Coord[6] (m)	Minimum Principal Stress (Pa)
Asphalt	AS	-10	0.5	none	none	1000	none	none	1.830	4.585	-0.205	-123866
Asphalt	AS	-10	0.5	none	none	8000	none	none	1.830	4.395	-0.205	-338451
Asphalt	AS	-10	0.5	none	none	15000	none	none	1.830	4.395	-0.205	-442763
Asphalt	AS	-10	Rough	none	none	1000	none	none	0.830	2.300	-0.205	-527257
Asphalt	AS	-10	Rough	none	none	8000	none	none	1.230	2.300	-0.205	-666154
Asphalt	AS	-10	Rough	none	none	15000	none	none	0.000	2.300	-0.368	-606257
Asphalt	AS	10	0.5	none	none	1000	none	none	1.730	2.300	-0.205	-382555
Asphalt	AS	10	0.5	none	none	8000	none	none	1.730	2.300	-0.205	-970937
Asphalt	AS	10	0.5	none	none	15000	none	none	1.730	2.300	-0.205	-1136790
Asphalt	AS	10	Rough	none	none	1000	none	none	1.830	2.300	-0.205	-279850
Asphalt	AS	10	Rough	none	none	8000	none	none	1.830	2.300	-0.205	-589904
Asphalt	AS	10	Rough	none	none	15000	none	none	1.830	2.300	-0.205	-751786
Granular	AS	-10	0.5	none	none	1000	none	none	0.000	4.585	-0.968	-25064
Granular	AS	-10	0.5	none	none	8000	none	none	0.000	4.585	-0.968	-24096
Granular	AS	-10	0.5	none	none	15000	none	none	0.000	4.585	-0.968	-23563
Granular	AS	-10	Rough	none	none	1000	none	none	0.000	4.585	-0.968	-22678
Granular	AS	-10	Rough	none	none	8000	none	none	0.000	4.585	-0.968	-21265
Granular	AS	-10	Rough	none	none	15000	none	none	0.000	4.585	-0.968	-21016
Granular	AS	10	0.5	none	none	1000	none	none	1.663	2.300	-0.368	-35575
Granular	AS	10	0.5	none	none	8000	none	none	0.000	2.300	-0.968	-25756
Granular	AS	10	0.5	none	none	15000	none	none	0.000	2.300	-0.968	-24861
Granular	AS	10	Rough	none	none	1000	none	none	0.000	2.300	-0.968	-23460
Granular	AS	10	Rough	none	none	8000	none	none	0.000	2.450	-0.968	-21384
Granular	AS	10	Rough	none	none	15000	none	none	0.000	2.450	-0.968	-21024

Part	Support Condition	Temp. Gradient (°C)	Friction (panel-to-base) (-)	Friction (panel-to-support) (-)	Friction (support-to-base) (-)	E_{base}[1] (MPa)	$E_{support}$[2] (MPa)	$t_{support}$[3] (MPa)	X-Coord[4] (m)	Y-Coord[5] (m)	Z-Coord[6] (m)	Minimum Principal Stress (Pa)
Panel	AS	-10	0.5	none	none	1000	none	none	1.830	4.585	-0.205	-2246540
Panel	AS	-10	0.5	none	none	8000	none	none	1.830	4.585	-0.205	-2413320
Panel	AS	-10	0.5	none	none	15000	none	none	1.830	4.585	-0.205	-2477300
Panel	AS	-10	Rough	none	none	1000	none	none	1.830	4.585	-0.205	-2259180
Panel	AS	-10	Rough	none	none	8000	none	none	1.830	2.375	-0.205	-2373560
Panel	AS	-10	Rough	none	none	15000	none	none	1.830	2.450	-0.205	-2381960
Panel	AS	10	0.5	none	none	1000	none	none	0.000	4.585	0.000	-1970260
Panel	AS	10	0.5	none	none	8000	none	none	0.000	4.314	0.000	-2000360
Panel	AS	10	0.5	none	none	15000	none	none	0.000	4.585	0.000	-2021120
Panel	AS	10	Rough	none	none	1000	none	none	0.000	2.780	0.000	-2028220
Panel	AS	10	Rough	none	none	8000	none	none	0.000	2.780	0.000	-2069730
Panel	AS	10	Rough	none	none	15000	none	none	0.000	2.600	0.000	-2072030
Asphalt	GR	-10	none	0.5	0.5	1000	4000	12	1.830	4.585	-0.217	-97598
Asphalt	GR	-10	none	0.5	0.5	1000	4000	18	1.830	4.585	-0.223	-100230
Asphalt	GR	-10	none	0.5	0.5	1000	4000	24	1.830	4.585	-0.229	-103076
Asphalt	GR	-10	none	0.5	0.5	1000	12000	12	1.830	4.585	-0.217	-97954
Asphalt	GR	-10	none	0.5	0.5	1000	12000	18	1.830	4.585	-0.223	-100979
Asphalt	GR	-10	none	0.5	0.5	1000	12000	24	1.830	4.585	-0.229	-104341
Asphalt	GR	-10	none	0.5	0.5	1000	20000	12	1.830	4.585	-0.217	-98164
Asphalt	GR	-10	none	0.5	0.5	1000	20000	18	1.830	4.585	-0.223	-101445
Asphalt	GR	-10	none	0.5	0.5	1000	20000	24	1.830	4.585	-0.229	-105103
Asphalt	GR	-10	none	0.5	0.5	8000	4000	12	1.730	4.585	-0.217	-295819
Asphalt	GR	-10	none	0.5	0.5	8000	4000	18	1.730	4.585	-0.223	-304627
Asphalt	GR	-10	none	0.5	0.5	8000	4000	24	1.730	4.585	-0.229	-313485
Asphalt	GR	-10	none	0.5	0.5	8000	12000	12	1.730	4.585	-0.217	-295838
Asphalt	GR	-10	none	0.5	0.5	8000	12000	18	1.730	4.585	-0.223	-304526
Asphalt	GR	-10	none	0.5	0.5	8000	12000	24	1.730	4.585	-0.229	-313202

Part	Support Condition	Temp. Gradient (°C)	Friction (panel-to-base) (-)	Friction (panel-to-support) (-)	Friction (support-to-base) (-)	E_{base}[1] (MPa)	$E_{support}$[2] (MPa)	$t_{support}$[3] (MPa)	X-Coord[4] (m)	Y-Coord[5] (m)	Z-Coord[6] (m)	Minimum Principal Stress (Pa)
Asphalt	GR	-10	none	0.5	0.5	8000	20000	12	1.730	4.585	-0.217	-295761
Asphalt	GR	-10	none	0.5	0.5	8000	20000	18	1.730	4.585	-0.223	-304326
Asphalt	GR	-10	none	0.5	0.5	8000	20000	24	1.730	4.585	-0.229	-312868
Asphalt	GR	-10	none	0.5	0.5	15000	4000	12	1.730	4.395	-0.217	-395137
Asphalt	GR	-10	none	0.5	0.5	15000	4000	18	1.730	4.585	-0.223	-409646
Asphalt	GR	-10	none	0.5	0.5	15000	4000	24	1.730	4.585	-0.229	-424729
Asphalt	GR	-10	none	0.5	0.5	15000	12000	12	1.730	4.395	-0.217	-395238
Asphalt	GR	-10	none	0.5	0.5	15000	12000	18	1.730	4.585	-0.223	-409688
Asphalt	GR	-10	none	0.5	0.5	15000	12000	24	1.730	4.585	-0.229	-424646
Asphalt	GR	-10	none	0.5	0.5	15000	20000	12	1.730	4.395	-0.217	-395191
Asphalt	GR	-10	none	0.5	0.5	15000	20000	18	1.730	4.585	-0.223	-409535
Asphalt	GR	-10	none	0.5	0.5	15000	20000	24	1.730	4.585	-0.229	-424378
Asphalt	GR	-10	none	Rough	Rough	1000	4000	12	0.623	2.300	-0.217	-297383
Asphalt	GR	-10	none	Rough	Rough	1000	4000	18	0.623	2.300	-0.223	-271684
Asphalt	GR	-10	none	Rough	Rough	1000	4000	24	0.830	2.300	-0.229	-247040
Asphalt	GR	-10	none	Rough	Rough	1000	12000	12	1.230	2.300	-0.217	-188301
Asphalt	GR	-10	none	Rough	Rough	1000	12000	18	1.230	2.300	-0.223	-165680
Asphalt	GR	-10	none	Rough	Rough	1000	12000	24	1.230	2.300	-0.229	-146688
Asphalt	GR	-10	none	Rough	Rough	1000	20000	12	1.230	2.300	-0.217	-141944
Asphalt	GR	-10	none	Rough	Rough	1000	20000	18	0.000	2.300	-0.380	-126909
Asphalt	GR	-10	none	Rough	Rough	1000	20000	24	0.000	2.300	-0.380	-121836
Asphalt	GR	-10	none	Rough	Rough	8000	4000	12	1.230	2.300	-0.217	-480769
Asphalt	GR	-10	none	Rough	Rough	8000	4000	18	0.000	2.300	-0.380	-474500
Asphalt	GR	-10	none	Rough	Rough	8000	4000	24	0.000	2.300	-0.380	-479830
Asphalt	GR	-10	none	Rough	Rough	8000	12000	12	0.000	2.300	-0.380	-434933
Asphalt	GR	-10	none	Rough	Rough	8000	12000	18	0.000	2.300	-0.380	-434820
Asphalt	GR	-10	none	Rough	Rough	8000	12000	24	0.000	2.300	-0.380	-434678

Part	Support Condition	Temp. Gradient (°C)	Friction (panel-to-base) (-)	Friction (panel-to-support) (-)	Friction (support-to-base) (-)	E_{base}[1] (MPa)	$E_{support}$[2] (MPa)	$t_{support}$[3] (MPa)	X-Coord[4] (m)	Y-Coord[5] (m)	Z-Coord[6] (m)	Minimum Principal Stress (Pa)
Asphalt	GR	-10	none	Rough	Rough	8000	20000	12	0.000	2.300	-0.380	-425575
Asphalt	GR	-10	none	Rough	Rough	8000	20000	18	0.000	2.300	-0.380	-423524
Asphalt	GR	-10	none	Rough	Rough	8000	20000	24	0.000	2.300	-0.380	-421587
Asphalt	GR	-10	none	Rough	Rough	15000	4000	12	0.000	2.300	-0.380	-590485
Asphalt	GR	-10	none	Rough	Rough	15000	4000	18	0.000	2.300	-0.380	-599377
Asphalt	GR	-10	none	Rough	Rough	15000	4000	24	0.000	2.300	-0.380	-606959
Asphalt	GR	-10	none	Rough	Rough	15000	12000	12	0.000	2.300	-0.380	-561627
Asphalt	GR	-10	none	Rough	Rough	15000	12000	18	0.000	2.300	-0.380	-562151
Asphalt	GR	-10	none	Rough	Rough	15000	12000	24	0.000	2.300	-0.380	-563050
Asphalt	GR	-10	none	Rough	Rough	15000	20000	12	0.000	2.300	-0.380	-555654
Asphalt	GR	-10	none	Rough	Rough	15000	20000	18	0.000	2.300	-0.380	-554444
Asphalt	GR	-10	none	Rough	Rough	15000	20000	24	0.000	2.300	-0.380	-553792
Asphalt	GR	10	none	0.5	0.5	1000	4000	12	1.730	2.300	-0.217	-295241
Asphalt	GR	10	none	0.5	0.5	1000	4000	18	1.730	2.300	-0.223	-295615
Asphalt	GR	10	none	0.5	0.5	1000	4000	24	1.730	2.300	-0.229	-294832
Asphalt	GR	10	none	0.5	0.5	1000	12000	12	1.730	2.300	-0.217	-295466
Asphalt	GR	10	none	0.5	0.5	1000	12000	18	1.730	2.300	-0.223	-293997
Asphalt	GR	10	none	0.5	0.5	1000	12000	24	1.730	2.300	-0.229	-290675
Asphalt	GR	10	none	0.5	0.5	1000	20000	12	1.730	2.300	-0.217	-294843
Asphalt	GR	10	none	0.5	0.5	1000	20000	18	1.730	2.300	-0.223	-291957
Asphalt	GR	10	none	0.5	0.5	1000	20000	24	1.730	2.300	-0.229	-286709
Asphalt	GR	10	none	0.5	0.5	8000	4000	12	1.630	2.300	-0.217	-821849
Asphalt	GR	10	none	0.5	0.5	8000	4000	18	1.630	2.300	-0.223	-849571
Asphalt	GR	10	none	0.5	0.5	8000	4000	24	1.630	2.300	-0.229	-875609
Asphalt	GR	10	none	0.5	0.5	8000	12000	12	1.630	2.300	-0.217	-823141
Asphalt	GR	10	none	0.5	0.5	8000	12000	18	1.630	2.300	-0.223	-848901
Asphalt	GR	10	none	0.5	0.5	8000	12000	24	1.630	2.300	-0.229	-871456

Part	Support Condition	Temp. Gradient (°C)	Friction (panel-to-base) (-)	Friction (panel-to-support) (-)	Friction (support-to-base) (-)	E_{base}[1] (MPa)	$E_{support}$[2] (MPa)	$t_{support}$[3] (MPa)	X-Coord[4] (m)	Y-Coord[5] (m)	Z-Coord[6] (m)	Minimum Principal Stress (Pa)
Asphalt	GR	10	none	0.5	0.5	8000	20000	12	1.630	2.300	-0.217	-822840
Asphalt	GR	10	none	0.5	0.5	8000	20000	18	1.630	2.300	-0.223	-846747
Asphalt	GR	10	none	0.5	0.5	8000	20000	24	1.630	2.300	-0.229	-866190
Asphalt	GR	10	none	0.5	0.5	15000	4000	12	1.630	2.300	-0.217	-998165
Asphalt	GR	10	none	0.5	0.5	15000	4000	18	1.630	2.300	-0.223	-1041400
Asphalt	GR	10	none	0.5	0.5	15000	4000	24	1.630	2.300	-0.229	-1085380
Asphalt	GR	10	none	0.5	0.5	15000	12000	12	1.630	2.300	-0.217	-999712
Asphalt	GR	10	none	0.5	0.5	15000	12000	18	1.630	2.300	-0.223	-1041130
Asphalt	GR	10	none	0.5	0.5	15000	12000	24	1.630	2.300	-0.229	-1081920
Asphalt	GR	10	none	0.5	0.5	15000	20000	12	1.630	2.300	-0.217	-999521
Asphalt	GR	10	none	0.5	0.5	15000	20000	18	1.630	2.300	-0.223	-1039210
Asphalt	GR	10	none	0.5	0.5	15000	20000	24	1.630	2.300	-0.229	-1077050
Asphalt	GR	10	none	Rough	Rough	1000	4000	12	1.830	2.300	-0.217	-264936
Asphalt	GR	10	none	Rough	Rough	1000	4000	18	1.830	2.300	-0.223	-258390
Asphalt	GR	10	none	Rough	Rough	1000	4000	24	1.830	2.300	-0.229	-251557
Asphalt	GR	10	none	Rough	Rough	1000	12000	12	1.830	2.300	-0.217	-237656
Asphalt	GR	10	none	Rough	Rough	1000	12000	18	1.830	2.300	-0.223	-229751
Asphalt	GR	10	none	Rough	Rough	1000	12000	24	1.830	2.300	-0.229	-222389
Asphalt	GR	10	none	Rough	Rough	1000	20000	12	1.830	2.300	-0.217	-227196
Asphalt	GR	10	none	Rough	Rough	1000	20000	18	1.830	2.300	-0.223	-218569
Asphalt	GR	10	none	Rough	Rough	1000	20000	24	1.830	2.300	-0.229	-210873
Asphalt	GR	10	none	Rough	Rough	8000	4000	12	1.830	2.300	-0.217	-556336
Asphalt	GR	10	none	Rough	Rough	8000	4000	18	1.830	2.300	-0.223	-535353
Asphalt	GR	10	none	Rough	Rough	8000	4000	24	1.830	2.300	-0.229	-523439
Asphalt	GR	10	none	Rough	Rough	8000	12000	12	1.830	2.300	-0.217	-589104
Asphalt	GR	10	none	Rough	Rough	8000	12000	18	1.830	2.300	-0.223	-572921
Asphalt	GR	10	none	Rough	Rough	8000	12000	24	1.830	2.300	-0.229	-560316

Part	Support Condition	Temp. Gradient (°C)	Friction (panel-to-base) (-)	Friction (panel-to-support) (-)	Friction (support-to-base) (-)	E_{base}[1] (MPa)	$E_{support}$[2] (MPa)	$t_{support}$[3] (MPa)	X-Coord[4] (m)	Y-Coord[5] (m)	Z-Coord[6] (m)	Minimum Principal Stress (Pa)
Asphalt	GR	10	none	Rough	Rough	8000	20000	12	1.830	2.300	-0.217	-594848
Asphalt	GR	10	none	Rough	Rough	8000	20000	18	1.830	2.300	-0.223	-580492
Asphalt	GR	10	none	Rough	Rough	8000	20000	24	1.830	2.300	-0.229	-568575
Asphalt	GR	10	none	Rough	Rough	15000	4000	12	1.830	2.300	-0.217	-662665
Asphalt	GR	10	none	Rough	Rough	15000	4000	18	1.830	2.300	-0.223	-646781
Asphalt	GR	10	none	Rough	Rough	15000	4000	24	1.830	2.300	-0.229	-641887
Asphalt	GR	10	none	Rough	Rough	15000	12000	12	1.830	2.300	-0.217	-723749
Asphalt	GR	10	none	Rough	Rough	15000	12000	18	1.830	2.300	-0.223	-705789
Asphalt	GR	10	none	Rough	Rough	15000	12000	24	1.830	2.300	-0.229	-696366
Asphalt	GR	10	none	Rough	Rough	15000	20000	12	1.830	2.300	-0.217	-745181
Asphalt	GR	10	none	Rough	Rough	15000	20000	18	1.830	2.300	-0.223	-730045
Asphalt	GR	10	none	Rough	Rough	15000	20000	24	1.830	2.300	-0.229	-719908
Granular	GR	-10	none	0.5	0.5	1000	4000	12	0.000	4.585	-0.980	-25365
Granular	GR	-10	none	0.5	0.5	1000	4000	18	0.000	4.585	-0.980	-25369
Granular	GR	-10	none	0.5	0.5	1000	4000	24	0.000	4.585	-0.980	-25372
Granular	GR	-10	none	0.5	0.5	1000	12000	12	0.000	4.585	-0.980	-25364
Granular	GR	-10	none	0.5	0.5	1000	12000	18	0.000	4.585	-0.980	-25366
Granular	GR	-10	none	0.5	0.5	1000	12000	24	0.000	4.585	-0.980	-25367
Granular	GR	-10	none	0.5	0.5	1000	20000	12	0.000	4.585	-0.980	-25363
Granular	GR	-10	none	0.5	0.5	1000	20000	18	0.000	4.585	-0.980	-25364
Granular	GR	-10	none	0.5	0.5	1000	20000	24	0.000	4.585	-0.980	-25363
Granular	GR	-10	none	0.5	0.5	8000	4000	12	0.000	4.585	-0.980	-24446
Granular	GR	-10	none	0.5	0.5	8000	4000	18	0.000	4.585	-0.980	-24502
Granular	GR	-10	none	0.5	0.5	8000	4000	24	0.000	4.585	-0.980	-24557
Granular	GR	-10	none	0.5	0.5	8000	12000	12	0.000	4.585	-0.980	-24445
Granular	GR	-10	none	0.5	0.5	8000	12000	18	0.000	4.585	-0.980	-24500
Granular	GR	-10	none	0.5	0.5	8000	12000	24	0.000	4.585	-0.980	-24553

Part	Support Condition	Temp. Gradient (°C)	Friction (panel-to-base) (-)	Friction (panel-to-support) (-)	Friction (support-to-base) (-)	E_{base}[1] (MPa)	$E_{support}$[2] (MPa)	$t_{support}$[3] (MPa)	X-Coord[4] (m)	Y-Coord[5] (m)	Z-Coord[6] (m)	Minimum Principal Stress (Pa)
Granular	GR	-10	none	0.5	0.5	8000	20000	12	0.000	4.585	-0.980	-24445
Granular	GR	-10	none	0.5	0.5	8000	20000	18	0.000	4.585	-0.980	-24499
Granular	GR	-10	none	0.5	0.5	8000	20000	24	0.000	4.585	-0.980	-24550
Granular	GR	-10	none	0.5	0.5	15000	4000	12	0.000	4.585	-0.980	-23916
Granular	GR	-10	none	0.5	0.5	15000	4000	18	0.000	4.585	-0.980	-23994
Granular	GR	-10	none	0.5	0.5	15000	4000	24	0.000	4.585	-0.980	-24071
Granular	GR	-10	none	0.5	0.5	15000	12000	12	0.000	4.585	-0.980	-23915
Granular	GR	-10	none	0.5	0.5	15000	12000	18	0.000	4.585	-0.980	-23992
Granular	GR	-10	none	0.5	0.5	15000	12000	24	0.000	4.585	-0.980	-24068
Granular	GR	-10	none	0.5	0.5	15000	20000	12	0.000	4.585	-0.980	-23915
Granular	GR	-10	none	0.5	0.5	15000	20000	18	0.000	4.585	-0.980	-23991
Granular	GR	-10	none	0.5	0.5	15000	20000	24	0.000	4.585	-0.980	-24066
Granular	GR	-10	none	Rough	Rough	1000	4000	12	0.000	4.585	-0.980	-22539
Granular	GR	-10	none	Rough	Rough	1000	4000	18	0.000	4.585	-0.980	-22513
Granular	GR	-10	none	Rough	Rough	1000	4000	24	0.000	4.585	-0.980	-22481
Granular	GR	-10	none	Rough	Rough	1000	12000	12	0.000	4.585	-0.980	-22320
Granular	GR	-10	none	Rough	Rough	1000	12000	18	0.000	4.585	-0.980	-22266
Granular	GR	-10	none	Rough	Rough	1000	12000	24	0.000	4.585	-0.980	-22215
Granular	GR	-10	none	Rough	Rough	1000	20000	12	0.000	4.585	-0.980	-22235
Granular	GR	-10	none	Rough	Rough	1000	20000	18	0.000	4.585	-0.980	-22173
Granular	GR	-10	none	Rough	Rough	1000	20000	24	0.000	4.585	-0.980	-22117
Granular	GR	-10	none	Rough	Rough	8000	4000	12	0.000	4.585	-0.980	-21464
Granular	GR	-10	none	Rough	Rough	8000	4000	18	0.000	4.585	-0.980	-21468
Granular	GR	-10	none	Rough	Rough	8000	4000	24	0.000	4.585	-0.980	-21471
Granular	GR	-10	none	Rough	Rough	8000	12000	12	0.000	4.585	-0.980	-21425
Granular	GR	-10	none	Rough	Rough	8000	12000	18	0.000	4.585	-0.980	-21414
Granular	GR	-10	none	Rough	Rough	8000	12000	24	0.000	4.585	-0.980	-21404

Part	Support Condition	Temp. Gradient (°C)	Friction (panel-to-base) (-)	Friction (panel-to-support) (-)	Friction (support-to-base) (-)	E_{base}[1] (MPa)	$E_{support}$[2] (MPa)	$t_{support}$[3] (MPa)	X-Coord[4] (m)	Y-Coord[5] (m)	Z-Coord[6] (m)	Minimum Principal Stress (Pa)
Granular	GR	-10	none	Rough	Rough	8000	20000	12	0.000	4.585	-0.980	-21413
Granular	GR	-10	none	Rough	Rough	8000	20000	18	0.000	4.585	-0.980	-21398
Granular	GR	-10	none	Rough	Rough	8000	20000	24	0.000	4.585	-0.980	-21384
Granular	GR	-10	none	Rough	Rough	15000	4000	12	0.000	4.585	-0.980	-21219
Granular	GR	-10	none	Rough	Rough	15000	4000	18	0.000	4.585	-0.980	-21226
Granular	GR	-10	none	Rough	Rough	15000	4000	24	0.000	4.585	-0.980	-21233
Granular	GR	-10	none	Rough	Rough	15000	12000	12	0.000	4.585	-0.980	-21187
Granular	GR	-10	none	Rough	Rough	15000	12000	18	0.000	4.585	-0.980	-21181
Granular	GR	-10	none	Rough	Rough	15000	12000	24	0.000	4.585	-0.980	-21177
Granular	GR	-10	none	Rough	Rough	15000	20000	12	0.000	4.585	-0.980	-21178
Granular	GR	-10	none	Rough	Rough	15000	20000	18	0.000	4.585	-0.980	-21167
Granular	GR	-10	none	Rough	Rough	15000	20000	24	0.000	4.585	-0.980	-21159
Granular	GR	10	none	0.5	0.5	1000	4000	12	1.663	2.300	-0.380	-33871
Granular	GR	10	none	0.5	0.5	1000	4000	18	1.663	2.300	-0.380	-34610
Granular	GR	10	none	0.5	0.5	1000	4000	24	1.663	2.300	-0.380	-35339
Granular	GR	10	none	0.5	0.5	1000	12000	12	1.663	2.300	-0.380	-33856
Granular	GR	10	none	0.5	0.5	1000	12000	18	1.663	2.300	-0.380	-34536
Granular	GR	10	none	0.5	0.5	1000	12000	24	1.663	2.300	-0.380	-35155
Granular	GR	10	none	0.5	0.5	1000	20000	12	1.663	2.300	-0.380	-33832
Granular	GR	10	none	0.5	0.5	1000	20000	18	1.663	2.300	-0.380	-34457
Granular	GR	10	none	0.5	0.5	1000	20000	24	1.663	2.300	-0.380	-34973
Granular	GR	10	none	0.5	0.5	8000	4000	12	0.000	2.300	-0.980	-26050
Granular	GR	10	none	0.5	0.5	8000	4000	18	0.000	2.300	-0.980	-26170
Granular	GR	10	none	0.5	0.5	8000	4000	24	0.000	2.300	-0.980	-26276
Granular	GR	10	none	0.5	0.5	8000	12000	12	0.000	2.300	-0.980	-26049
Granular	GR	10	none	0.5	0.5	8000	12000	18	0.000	2.300	-0.980	-26167
Granular	GR	10	none	0.5	0.5	8000	12000	24	0.000	2.300	-0.980	-26270

Part	Support Condition	Temp. Gradient (°C)	Friction (panel-to-base) (-)	Friction (panel-to-support) (-)	Friction (support-to-base) (-)	E_{base}[1] (MPa)	$E_{support}$[2] (MPa)	$t_{support}$[3] (MPa)	X-Coord[4] (m)	Y-Coord[5] (m)	Z-Coord[6] (m)	Minimum Principal Stress (Pa)
Granular	GR	10	none	0.5	0.5	8000	20000	12	0.000	2.300	-0.980	-26048
Granular	GR	10	none	0.5	0.5	8000	20000	18	0.000	2.300	-0.980	-26165
Granular	GR	10	none	0.5	0.5	8000	20000	24	0.000	2.300	-0.980	-26267
Granular	GR	10	none	0.5	0.5	15000	4000	12	0.000	2.300	-0.980	-25179
Granular	GR	10	none	0.5	0.5	15000	4000	18	0.000	2.300	-0.980	-25326
Granular	GR	10	none	0.5	0.5	15000	4000	24	0.000	2.300	-0.980	-25474
Granular	GR	10	none	0.5	0.5	15000	12000	12	0.000	2.300	-0.980	-25179
Granular	GR	10	none	0.5	0.5	15000	12000	18	0.000	2.300	-0.980	-25323
Granular	GR	10	none	0.5	0.5	15000	12000	24	0.000	2.300	-0.980	-25471
Granular	GR	10	none	0.5	0.5	15000	20000	12	0.000	2.300	-0.980	-25178
Granular	GR	10	none	0.5	0.5	15000	20000	18	0.000	2.300	-0.980	-25322
Granular	GR	10	none	0.5	0.5	15000	20000	24	0.000	2.300	-0.980	-25469
Granular	GR	10	none	Rough	Rough	1000	4000	12	0.000	2.300	-0.980	-23142
Granular	GR	10	none	Rough	Rough	1000	4000	18	0.000	2.300	-0.980	-23104
Granular	GR	10	none	Rough	Rough	1000	4000	24	0.000	2.300	-0.980	-23059
Granular	GR	10	none	Rough	Rough	1000	12000	12	0.000	2.300	-0.980	-22816
Granular	GR	10	none	Rough	Rough	1000	12000	18	0.000	2.300	-0.980	-22736
Granular	GR	10	none	Rough	Rough	1000	12000	24	0.000	2.300	-0.980	-22658
Granular	GR	10	none	Rough	Rough	1000	20000	12	0.000	2.300	-0.980	-22686
Granular	GR	10	none	Rough	Rough	1000	20000	18	0.000	2.300	-0.980	-22591
Granular	GR	10	none	Rough	Rough	1000	20000	24	0.000	2.300	-0.980	-22503
Granular	GR	10	none	Rough	Rough	8000	4000	12	0.000	2.450	-0.980	-21549
Granular	GR	10	none	Rough	Rough	8000	4000	18	0.000	2.450	-0.980	-21551
Granular	GR	10	none	Rough	Rough	8000	4000	24	0.000	2.450	-0.980	-21552
Granular	GR	10	none	Rough	Rough	8000	12000	12	0.000	2.450	-0.980	-21500
Granular	GR	10	none	Rough	Rough	8000	12000	18	0.000	2.450	-0.980	-21484
Granular	GR	10	none	Rough	Rough	8000	12000	24	0.000	2.450	-0.980	-21468

Part	Support Condition	Temp. Gradient (°C)	Friction (panel-to-base) (-)	Friction (panel-to-support) (-)	Friction (support-to-base) (-)	E_{base}[1] (MPa)	$E_{support}$[2] (MPa)	$t_{support}$[3] (MPa)	X-Coord[4] (m)	Y-Coord[5] (m)	Z-Coord[6] (m)	Minimum Principal Stress (Pa)
Granular	GR	10	none	Rough	Rough	8000	20000	12	0.000	2.450	-0.980	-21487
Granular	GR	10	none	Rough	Rough	8000	20000	18	0.000	2.450	-0.980	-21465
Granular	GR	10	none	Rough	Rough	8000	20000	24	0.000	2.450	-0.980	-21443
Granular	GR	10	none	Rough	Rough	15000	4000	12	0.000	2.450	-0.980	-21188
Granular	GR	10	none	Rough	Rough	15000	4000	18	0.000	2.450	-0.980	-21191
Granular	GR	10	none	Rough	Rough	15000	4000	24	0.000	2.450	-0.980	-21195
Granular	GR	10	none	Rough	Rough	15000	12000	12	0.000	2.450	-0.980	-21154
Granular	GR	10	none	Rough	Rough	15000	12000	18	0.000	2.450	-0.980	-21141
Granular	GR	10	none	Rough	Rough	15000	12000	24	0.000	2.450	-0.980	-21130
Granular	GR	10	none	Rough	Rough	15000	20000	12	0.000	2.450	-0.980	-21146
Granular	GR	10	none	Rough	Rough	15000	20000	18	0.000	2.450	-0.980	-21128
Granular	GR	10	none	Rough	Rough	15000	20000	24	0.000	2.450	-0.980	-21111
Panel	GR	-10	none	0.5	0.5	1000	4000	12	1.830	4.585	-0.205	-2199310
Panel	GR	-10	none	0.5	0.5	1000	4000	18	1.830	4.585	-0.205	-2199190
Panel	GR	-10	none	0.5	0.5	1000	4000	24	1.830	4.585	-0.205	-2198600
Panel	GR	-10	none	0.5	0.5	1000	12000	12	1.830	4.585	-0.205	-2199120
Panel	GR	-10	none	0.5	0.5	1000	12000	18	1.830	4.585	-0.205	-2198350
Panel	GR	-10	none	0.5	0.5	1000	12000	24	1.830	4.585	-0.205	-2196730
Panel	GR	-10	none	0.5	0.5	1000	20000	12	1.830	4.585	-0.205	-2198770
Panel	GR	-10	none	0.5	0.5	1000	20000	18	1.830	4.585	-0.205	-2197400
Panel	GR	-10	none	0.5	0.5	1000	20000	24	1.830	4.585	-0.205	-2194970
Panel	GR	-10	none	0.5	0.5	8000	4000	12	1.830	4.585	-0.205	-2318810
Panel	GR	-10	none	0.5	0.5	8000	4000	18	1.830	4.585	-0.205	-2317750
Panel	GR	-10	none	0.5	0.5	8000	4000	24	1.830	4.585	-0.205	-2315910
Panel	GR	-10	none	0.5	0.5	8000	12000	12	1.830	4.585	-0.205	-2319000
Panel	GR	-10	none	0.5	0.5	8000	12000	18	1.830	4.585	-0.205	-2317590
Panel	GR	-10	none	0.5	0.5	8000	12000	24	1.830	4.585	-0.205	-2315080

Part	Support Condition	Temp. Gradient (°C)	Friction (panel-to-base) (-)	Friction (panel-to-support) (-)	Friction (support-to-base) (-)	E_{base}[1] (MPa)	$E_{support}$[2] (MPa)	$t_{support}$[3] (MPa)	X-Coord[4] (m)	Y-Coord[5] (m)	Z-Coord[6] (m)	Minimum Principal Stress (Pa)
Panel	GR	-10	none	0.5	0.5	8000	20000	12	1.830	4.585	-0.205	-2318830
Panel	GR	-10	none	0.5	0.5	8000	20000	18	1.830	4.585	-0.205	-2317010
Panel	GR	-10	none	0.5	0.5	8000	20000	24	1.830	4.585	-0.205	-2313860
Panel	GR	-10	none	0.5	0.5	15000	4000	12	1.830	4.585	-0.205	-2357250
Panel	GR	-10	none	0.5	0.5	15000	4000	18	1.830	4.585	-0.205	-2357940
Panel	GR	-10	none	0.5	0.5	15000	4000	24	1.830	4.585	-0.205	-2357520
Panel	GR	-10	none	0.5	0.5	15000	12000	12	1.830	4.585	-0.205	-2357570
Panel	GR	-10	none	0.5	0.5	15000	12000	18	1.830	4.585	-0.205	-2358000
Panel	GR	-10	none	0.5	0.5	15000	12000	24	1.830	4.585	-0.205	-2357050
Panel	GR	-10	none	0.5	0.5	15000	20000	12	1.830	4.585	-0.205	-2357450
Panel	GR	-10	none	0.5	0.5	15000	20000	18	1.830	4.585	-0.205	-2357530
Panel	GR	-10	none	0.5	0.5	15000	20000	24	1.830	4.585	-0.205	-2356020
Panel	GR	-10	none	Rough	Rough	1000	4000	12	1.830	4.585	-0.205	-2275090
Panel	GR	-10	none	Rough	Rough	1000	4000	18	1.830	4.585	-0.205	-2268790
Panel	GR	-10	none	Rough	Rough	1000	4000	24	1.830	4.585	-0.205	-2262700
Panel	GR	-10	none	Rough	Rough	1000	12000	12	0.664	2.300	-0.205	-2620200
Panel	GR	-10	none	Rough	Rough	1000	12000	18	0.664	2.300	-0.205	-2511180
Panel	GR	-10	none	Rough	Rough	1000	12000	24	0.664	2.300	-0.205	-2366700
Panel	GR	-10	none	Rough	Rough	1000	20000	12	0.664	2.300	-0.205	-2848310
Panel	GR	-10	none	Rough	Rough	1000	20000	18	0.664	2.300	-0.205	-2669020
Panel	GR	-10	none	Rough	Rough	1000	20000	24	0.664	2.300	-0.205	-2471240
Panel	GR	-10	none	Rough	Rough	8000	4000	12	1.830	4.585	-0.205	-2339530
Panel	GR	-10	none	Rough	Rough	8000	4000	18	1.830	4.585	-0.205	-2322750
Panel	GR	-10	none	Rough	Rough	8000	4000	24	1.830	4.585	-0.205	-2309700
Panel	GR	-10	none	Rough	Rough	8000	12000	12	1.830	4.585	-0.205	-2350750
Panel	GR	-10	none	Rough	Rough	8000	12000	18	1.830	4.585	-0.205	-2329260
Panel	GR	-10	none	Rough	Rough	8000	12000	24	1.830	2.450	-0.205	-2310560

Part	Support Condition	Temp. Gradient (°C)	Friction (panel-to-base) (-)	Friction (panel-to-support) (-)	Friction (support-to-base) (-)	E_{base}[1] (MPa)	$E_{support}$[2] (MPa)	$t_{support}$[3] (MPa)	X-Coord[4] (m)	Y-Coord[5] (m)	Z-Coord[6] (m)	Minimum Principal Stress (Pa)
Panel	GR	-10	none	Rough	Rough	8000	20000	12	1.830	2.450	-0.205	-2343910
Panel	GR	-10	none	Rough	Rough	8000	20000	18	1.830	2.450	-0.205	-2324050
Panel	GR	-10	none	Rough	Rough	8000	20000	24	1.830	2.450	-0.205	-2304930
Panel	GR	-10	none	Rough	Rough	15000	4000	12	1.830	4.585	-0.205	-2323650
Panel	GR	-10	none	Rough	Rough	15000	4000	18	1.830	4.585	-0.205	-2305140
Panel	GR	-10	none	Rough	Rough	15000	4000	24	1.830	4.585	-0.205	-2291610
Panel	GR	-10	none	Rough	Rough	15000	12000	12	1.830	2.450	-0.205	-2347190
Panel	GR	-10	none	Rough	Rough	15000	12000	18	1.830	2.450	-0.205	-2326030
Panel	GR	-10	none	Rough	Rough	15000	12000	24	1.830	2.450	-0.205	-2305770
Panel	GR	-10	none	Rough	Rough	15000	20000	12	1.830	2.450	-0.205	-2348240
Panel	GR	-10	none	Rough	Rough	15000	20000	18	1.830	2.450	-0.205	-2326710
Panel	GR	-10	none	Rough	Rough	15000	20000	24	1.830	2.450	-0.205	-2305450
Panel	GR	10	none	0.5	0.5	1000	4000	12	0.000	4.585	0.000	-1970450
Panel	GR	10	none	0.5	0.5	1000	4000	18	0.000	4.585	0.000	-1971540
Panel	GR	10	none	0.5	0.5	1000	4000	24	0.000	4.585	0.000	-1972640
Panel	GR	10	none	0.5	0.5	1000	12000	12	0.000	4.585	0.000	-1970470
Panel	GR	10	none	0.5	0.5	1000	12000	18	0.000	4.585	0.000	-1971650
Panel	GR	10	none	0.5	0.5	1000	12000	24	0.000	4.585	0.000	-1972900
Panel	GR	10	none	0.5	0.5	1000	20000	12	0.000	4.585	0.000	-1970470
Panel	GR	10	none	0.5	0.5	1000	20000	18	0.000	4.585	0.000	-1971730
Panel	GR	10	none	0.5	0.5	1000	20000	24	0.000	4.585	0.000	-1973110
Panel	GR	10	none	0.5	0.5	8000	4000	12	0.000	4.405	0.000	-2000010
Panel	GR	10	none	0.5	0.5	8000	4000	18	0.000	4.405	0.000	-1998890
Panel	GR	10	none	0.5	0.5	8000	4000	18	0.000	4.314	0.000	-1998890
Panel	GR	10	none	0.5	0.5	8000	4000	24	0.000	4.314	0.000	-1998040
Panel	GR	10	none	0.5	0.5	8000	12000	12	0.000	4.405	0.000	-2000020
Panel	GR	10	none	0.5	0.5	8000	12000	18	0.000	4.405	0.000	-1998910

Part	Support Condition	Temp. Gradient (°C)	Friction (panel-to-base) (-)	Friction (panel-to-support) (-)	Friction (support-to-base) (-)	E_{base}[1] (MPa)	$E_{support}$[2] (MPa)	$t_{support}$[3] (MPa)	X-Coord[4] (m)	Y-Coord[5] (m)	Z-Coord[6] (m)	Minimum Principal Stress (Pa)
Panel	GR	10	none	0.5	0.5	8000	12000	18	0.000	4.314	0.000	-1998910
Panel	GR	10	none	0.5	0.5	8000	12000	24	0.000	4.224	0.000	-1998120
Panel	GR	10	none	0.5	0.5	8000	12000	24	0.000	4.314	0.000	-1998120
Panel	GR	10	none	0.5	0.5	8000	20000	12	0.000	4.405	0.000	-2000000
Panel	GR	10	none	0.5	0.5	8000	20000	18	0.000	4.405	0.000	-1998920
Panel	GR	10	none	0.5	0.5	8000	20000	18	0.000	4.314	0.000	-1998920
Panel	GR	10	none	0.5	0.5	8000	20000	24	0.000	4.314	0.000	-1998180
Panel	GR	10	none	0.5	0.5	15000	4000	12	0.000	4.585	0.000	-2019970
Panel	GR	10	none	0.5	0.5	15000	4000	18	0.000	4.585	0.000	-2021870
Panel	GR	10	none	0.5	0.5	15000	4000	24	0.000	4.585	0.000	-2023740
Panel	GR	10	none	0.5	0.5	15000	12000	12	0.000	4.585	0.000	-2020050
Panel	GR	10	none	0.5	0.5	15000	12000	18	0.000	4.585	0.000	-2022070
Panel	GR	10	none	0.5	0.5	15000	12000	24	0.000	4.585	0.000	-2023950
Panel	GR	10	none	0.5	0.5	15000	20000	12	0.000	4.585	0.000	-2020100
Panel	GR	10	none	0.5	0.5	15000	20000	18	0.000	4.585	0.000	-2022160
Panel	GR	10	none	0.5	0.5	15000	20000	24	0.000	4.585	0.000	-2024060
Panel	GR	10	none	Rough	Rough	1000	4000	12	0.000	2.780	0.000	-2048740
Panel	GR	10	none	Rough	Rough	1000	4000	18	0.000	2.780	0.000	-2050660
Panel	GR	10	none	Rough	Rough	1000	4000	24	0.000	2.780	0.000	-2053160
Panel	GR	10	none	Rough	Rough	1000	12000	12	0.498	2.450	0.000	-2068700
Panel	GR	10	none	Rough	Rough	1000	12000	18	0.498	2.450	0.000	-2070340
Panel	GR	10	none	Rough	Rough	1000	12000	24	0.498	2.450	0.000	-2071440
Panel	GR	10	none	Rough	Rough	1000	20000	12	0.498	2.450	0.000	-2082200
Panel	GR	10	none	Rough	Rough	1000	20000	18	0.498	2.450	0.000	-2083740
Panel	GR	10	none	Rough	Rough	1000	20000	24	0.498	2.450	0.000	-2084150
Panel	GR	10	none	Rough	Rough	8000	4000	12	0.000	2.780	0.000	-2070550
Panel	GR	10	none	Rough	Rough	8000	4000	18	0.000	2.780	0.000	-2070690

Part	Support Condition	Temp. Gradient (°C)	Friction (panel-to-base) (-)	Friction (panel-to-support) (-)	Friction (support-to-base) (-)	E_{base}[1] (MPa)	$E_{support}$[2] (MPa)	$t_{support}$[3] (MPa)	X-Coord[4] (m)	Y-Coord[5] (m)	Z-Coord[6] (m)	Minimum Principal Stress (Pa)
Panel	GR	10	none	Rough	Rough	8000	4000	24	0.000	2.780	0.000	-2070840
Panel	GR	10	none	Rough	Rough	8000	12000	12	0.000	2.780	0.000	-2071120
Panel	GR	10	none	Rough	Rough	8000	12000	18	0.000	2.780	0.000	-2071450
Panel	GR	10	none	Rough	Rough	8000	12000	24	0.000	2.780	0.000	-2071790
Panel	GR	10	none	Rough	Rough	8000	20000	12	0.000	2.780	0.000	-2070560
Panel	GR	10	none	Rough	Rough	8000	20000	18	0.000	2.780	0.000	-2070620
Panel	GR	10	none	Rough	Rough	8000	20000	24	0.000	2.600	0.000	-2071000
Panel	GR	10	none	Rough	Rough	15000	4000	12	0.000	2.780	0.000	-2070740
Panel	GR	10	none	Rough	Rough	15000	4000	18	0.000	2.780	0.000	-2071160
Panel	GR	10	none	Rough	Rough	15000	4000	24	0.000	2.780	0.000	-2071310
Panel	GR	10	none	Rough	Rough	15000	12000	12	0.000	2.600	0.000	-2071160
Panel	GR	10	none	Rough	Rough	15000	12000	18	0.000	2.600	0.000	-2071020
Panel	GR	10	none	Rough	Rough	15000	12000	24	0.000	2.780	0.000	-2071000
Panel	GR	10	none	Rough	Rough	15000	20000	12	0.000	2.600	0.000	-2072260
Panel	GR	10	none	Rough	Rough	15000	20000	18	0.000	2.600	0.000	-2072560
Panel	GR	10	none	Rough	Rough	15000	20000	24	0.000	2.600	0.000	-2072910
Support	GR	-10	none	0.5	0.5	1000	4000	12	1.830	4.585	-0.217	-107055
Support	GR	-10	none	0.5	0.5	1000	4000	18	1.830	4.585	-0.223	-126686
Support	GR	-10	none	0.5	0.5	1000	4000	24	1.830	4.585	-0.229	-138153
Support	GR	-10	none	0.5	0.5	1000	12000	12	1.830	4.585	-0.217	-263725
Support	GR	-10	none	0.5	0.5	1000	12000	18	1.830	4.585	-0.223	-292817
Support	GR	-10	none	0.5	0.5	1000	12000	24	1.830	4.585	-0.229	-305013
Support	GR	-10	none	0.5	0.5	1000	20000	12	1.830	4.585	-0.217	-390960
Support	GR	-10	none	0.5	0.5	1000	20000	18	1.830	4.585	-0.223	-422066
Support	GR	-10	none	0.5	0.5	1000	20000	24	1.830	4.585	-0.229	-430130
Support	GR	-10	none	0.5	0.5	8000	4000	12	1.830	4.395	-0.217	-72013
Support	GR	-10	none	0.5	0.5	8000	4000	18	1.830	4.585	-0.223	-81719

Part	Support Condition	Temp. Gradient (°C)	Friction (panel-to-base) (-)	Friction (panel-to-support) (-)	Friction (support-to-base) (-)	E_{base}[1] (MPa)	$E_{support}$[2] (MPa)	$t_{support}$[3] (MPa)	X-Coord[4] (m)	Y-Coord[5] (m)	Z-Coord[6] (m)	Minimum Principal Stress (Pa)
Support	GR	-10	none	0.5	0.5	8000	4000	24	1.830	4.585	-0.229	-93058
Support	GR	-10	none	0.5	0.5	8000	12000	12	1.830	4.585	-0.217	-167477
Support	GR	-10	none	0.5	0.5	8000	12000	18	1.830	4.585	-0.223	-197686
Support	GR	-10	none	0.5	0.5	8000	12000	24	1.830	4.585	-0.229	-218572
Support	GR	-10	none	0.5	0.5	8000	20000	12	1.830	4.585	-0.217	-253769
Support	GR	-10	none	0.5	0.5	8000	20000	18	1.830	4.585	-0.223	-293170
Support	GR	-10	none	0.5	0.5	8000	20000	24	1.830	4.585	-0.229	-319923
Support	GR	-10	none	0.5	0.5	15000	4000	12	1.830	4.204	-0.217	-70549
Support	GR	-10	none	0.5	0.5	15000	4000	18	1.830	4.347	-0.223	-73197
Support	GR	-10	none	0.5	0.5	15000	4000	24	1.830	4.585	-0.229	-81888
Support	GR	-10	none	0.5	0.5	15000	12000	12	1.830	4.585	-0.217	-144261
Support	GR	-10	none	0.5	0.5	15000	12000	18	1.830	4.585	-0.223	-172944
Support	GR	-10	none	0.5	0.5	15000	12000	24	1.830	4.585	-0.229	-193856
Support	GR	-10	none	0.5	0.5	15000	20000	12	1.830	4.585	-0.217	-219580
Support	GR	-10	none	0.5	0.5	15000	20000	18	1.830	4.585	-0.223	-257886
Support	GR	-10	none	0.5	0.5	15000	20000	24	1.830	4.585	-0.229	-285799
Support	GR	-10	none	Rough	Rough	1000	4000	12	0.925	2.300	-0.205	-3611230
Support	GR	-10	none	Rough	Rough	1000	4000	18	0.925	2.300	-0.205	-3267760
Support	GR	-10	none	Rough	Rough	1000	4000	24	0.925	2.300	-0.205	-2944680
Support	GR	-10	none	Rough	Rough	1000	12000	12	0.973	2.300	-0.205	-6007680
Support	GR	-10	none	Rough	Rough	1000	12000	18	0.973	2.300	-0.205	-5151490
Support	GR	-10	none	Rough	Rough	1000	12000	24	0.973	2.300	-0.205	-4448790
Support	GR	-10	none	Rough	Rough	1000	20000	12	0.973	2.300	-0.205	-7126280
Support	GR	-10	none	Rough	Rough	1000	20000	18	0.973	2.300	-0.205	-5912560
Support	GR	-10	none	Rough	Rough	1000	20000	24	0.973	2.300	-0.205	-4994040
Support	GR	-10	none	Rough	Rough	8000	4000	12	0.925	2.300	-0.205	-1545670
Support	GR	-10	none	Rough	Rough	8000	4000	18	0.925	2.300	-0.205	-1503250

Part	Support Condition	Temp. Gradient (°C)	Friction (panel-to-base) (-)	Friction (panel-to-support) (-)	Friction (support-to-base) (-)	E_{base}[1] (MPa)	$E_{support}$[2] (MPa)	$t_{support}$[3] (MPa)	X-Coord[4] (m)	Y-Coord[5] (m)	Z-Coord[6] (m)	Minimum Principal Stress (Pa)
Support	GR	-10	none	Rough	Rough	8000	4000	24	0.925	2.300	-0.205	-1444700
Support	GR	-10	none	Rough	Rough	8000	12000	12	0.973	2.300	-0.205	-2654900
Support	GR	-10	none	Rough	Rough	8000	12000	18	0.973	2.300	-0.205	-2504850
Support	GR	-10	none	Rough	Rough	8000	12000	24	0.973	2.300	-0.205	-2332980
Support	GR	-10	none	Rough	Rough	8000	20000	12	0.973	2.300	-0.205	-3296210
Support	GR	-10	none	Rough	Rough	8000	20000	18	0.973	2.300	-0.205	-3065560
Support	GR	-10	none	Rough	Rough	8000	20000	24	0.973	2.300	-0.205	-2812170
Support	GR	-10	none	Rough	Rough	15000	4000	12	0.925	2.300	-0.205	-1247850
Support	GR	-10	none	Rough	Rough	15000	4000	18	0.925	2.300	-0.205	-1247400
Support	GR	-10	none	Rough	Rough	15000	4000	24	0.925	2.300	-0.205	-1223880
Support	GR	-10	none	Rough	Rough	15000	12000	12	0.973	2.300	-0.205	-2101310
Support	GR	-10	none	Rough	Rough	15000	12000	18	0.973	2.300	-0.205	-2030380
Support	GR	-10	none	Rough	Rough	15000	12000	24	0.973	2.300	-0.205	-1930570
Support	GR	-10	none	Rough	Rough	15000	20000	12	0.973	2.300	-0.205	-2556880
Support	GR	-10	none	Rough	Rough	15000	20000	18	0.973	2.300	-0.205	-2441520
Support	GR	-10	none	Rough	Rough	15000	20000	24	0.973	2.300	-0.205	-2290210
Support	GR	10	none	0.5	0.5	1000	4000	12	1.830	2.255	-0.205	-284171
Support	GR	10	none	0.5	0.5	1000	4000	18	0.000	2.255	-0.205	-274456
Support	GR	10	none	0.5	0.5	1000	4000	24	0.000	2.255	-0.205	-330008
Support	GR	10	none	0.5	0.5	1000	12000	12	0.000	2.255	-0.205	-564634
Support	GR	10	none	0.5	0.5	1000	12000	18	0.000	2.255	-0.205	-725375
Support	GR	10	none	0.5	0.5	1000	12000	24	0.000	2.300	-0.205	-892447
Support	GR	10	none	0.5	0.5	1000	20000	12	0.000	2.255	-0.205	-878778
Support	GR	10	none	0.5	0.5	1000	20000	18	0.000	2.300	-0.205	-1167370
Support	GR	10	none	0.5	0.5	1000	20000	24	0.000	2.300	-0.205	-1399650
Support	GR	10	none	0.5	0.5	8000	4000	12	1.830	2.350	-0.205	-296085
Support	GR	10	none	0.5	0.5	8000	4000	18	1.830	2.255	-0.205	-277220

Part	Support Condition	Temp. Gradient (°C)	Friction (panel-to-base) (-)	Friction (panel-to-support) (-)	Friction (support-to-base) (-)	E_{base}[1] (MPa)	$E_{support}$[2] (MPa)	$t_{support}$[3] (MPa)	X-Coord[4] (m)	Y-Coord[5] (m)	Z-Coord[6] (m)	Minimum Principal Stress (Pa)
Support	GR	10	none	0.5	0.5	8000	4000	24	1.830	2.255	-0.205	-272828
Support	GR	10	none	0.5	0.5	8000	12000	12	0.000	2.255	-0.205	-452887
Support	GR	10	none	0.5	0.5	8000	12000	18	0.000	2.255	-0.205	-520819
Support	GR	10	none	0.5	0.5	8000	12000	24	0.000	2.255	-0.205	-591768
Support	GR	10	none	0.5	0.5	8000	20000	12	0.000	2.255	-0.205	-669345
Support	GR	10	none	0.5	0.5	8000	20000	18	0.000	2.255	-0.205	-792024
Support	GR	10	none	0.5	0.5	8000	20000	24	0.000	2.300	-0.205	-897641
Support	GR	10	none	0.5	0.5	15000	4000	12	1.830	2.350	-0.205	-283259
Support	GR	10	none	0.5	0.5	15000	4000	18	1.830	2.255	-0.205	-267557
Support	GR	10	none	0.5	0.5	15000	4000	24	1.830	2.255	-0.205	-264713
Support	GR	10	none	0.5	0.5	15000	12000	12	0.000	2.255	-0.205	-434306
Support	GR	10	none	0.5	0.5	15000	12000	18	0.000	2.255	-0.205	-480161
Support	GR	10	none	0.5	0.5	15000	12000	24	0.000	2.255	-0.205	-531695
Support	GR	10	none	0.5	0.5	15000	20000	12	0.000	2.255	-0.205	-633431
Support	GR	10	none	0.5	0.5	15000	20000	18	0.000	2.255	-0.205	-716513
Support	GR	10	none	0.5	0.5	15000	20000	24	0.000	2.300	-0.205	-809781
Support	GR	10	none	Rough	Rough	1000	4000	12	0.586	2.255	-0.205	-1687740
Support	GR	10	none	Rough	Rough	1000	4000	18	0.586	2.255	-0.205	-1466330
Support	GR	10	none	Rough	Rough	1000	4000	24	0.830	2.255	-0.205	-1300530
Support	GR	10	none	Rough	Rough	1000	12000	12	0.830	2.255	-0.205	-2142520
Support	GR	10	none	Rough	Rough	1000	12000	18	0.830	2.255	-0.205	-1860060
Support	GR	10	none	Rough	Rough	1000	12000	24	0.586	2.255	-0.205	-1631280
Support	GR	10	none	Rough	Rough	1000	20000	12	0.830	2.255	-0.205	-2204970
Support	GR	10	none	Rough	Rough	1000	20000	18	0.830	2.255	-0.205	-1914510
Support	GR	10	none	Rough	Rough	1000	20000	24	0.586	2.255	-0.205	-1676990
Support	GR	10	none	Rough	Rough	8000	4000	12	1.830	2.255	-0.205	-1242090
Support	GR	10	none	Rough	Rough	8000	4000	18	1.830	2.255	-0.205	-1110590

Part	Support Condition	Temp. Gradient (°C)	Friction (panel-to-base) (-)	Friction (panel-to-support) (-)	Friction (support-to-base) (-)	E_{base}[1] (MPa)	$E_{support}$[2] (MPa)	$t_{support}$[3] (MPa)	X-Coord[4] (m)	Y-Coord[5] (m)	Z-Coord[6] (m)	Minimum Principal Stress (Pa)
Support	GR	10	none	Rough	Rough	8000	4000	24	1.830	2.255	-0.205	-1011400
Support	GR	10	none	Rough	Rough	8000	12000	12	0.973	2.255	-0.205	-1600780
Support	GR	10	none	Rough	Rough	8000	12000	18	1.830	2.255	-0.205	-1446240
Support	GR	10	none	Rough	Rough	8000	12000	24	1.830	2.255	-0.205	-1327430
Support	GR	10	none	Rough	Rough	8000	20000	12	0.830	2.255	-0.205	-1765710
Support	GR	10	none	Rough	Rough	8000	20000	18	0.830	2.255	-0.205	-1612820
Support	GR	10	none	Rough	Rough	8000	20000	24	1.830	2.255	-0.205	-1474900
Support	GR	10	none	Rough	Rough	15000	4000	12	1.830	2.255	-0.205	-1194150
Support	GR	10	none	Rough	Rough	15000	4000	18	1.830	2.255	-0.205	-1069310
Support	GR	10	none	Rough	Rough	15000	4000	24	1.830	2.255	-0.205	-976220
Support	GR	10	none	Rough	Rough	15000	12000	12	1.830	2.255	-0.205	-1550440
Support	GR	10	none	Rough	Rough	15000	12000	18	1.830	2.255	-0.205	-1413360
Support	GR	10	none	Rough	Rough	15000	12000	24	1.830	2.255	-0.205	-1301430
Support	GR	10	none	Rough	Rough	15000	20000	12	1.830	2.255	-0.205	-1723690
Support	GR	10	none	Rough	Rough	15000	20000	18	1.830	2.255	-0.205	-1586750
Support	GR	10	none	Rough	Rough	15000	20000	24	1.830	2.255	-0.205	-1469740

Responses under +10°C temperature gradient with axle loading

Notes on the following responses:

[1]E_{base}	elastic modulus of base
[2]$E_{support}$	elastic modulus of support
[3]$t_{support}$	thickness of support
[4]X-coord	Relative to centreline of panels (X-coord = 0 at centreline)
[5]Y-coord	Relative to midpanel of first panel, with three panels total (Y-coord = 0.0 at midpanel of panel 1, Y-coord = 4.585 at midpanel of panel 2, etc.)
[6]Z-coord	Relative to top of panel (Z-coord = 0.0 at top of panel, Z-coord = -0.205 at bottom of panel, etc.)

Responses under +10°C temperature gradient with axle loading

Part	Support Condition	Friction (panel-to-base) (-)	Friction (panel-to-support) (-)	Friction (support-to-base) (-)	E_{base}[1] (MPa)	$E_{support}$[2] (MPa)	$t_{support}$[3] (MPa)	X-Coord[4] (m)	Y-Coord[5] (m)	Z-Coord[6] (m)	Minimum Principal Stress (Pa)
Asphalt	AS	0.5	none	none	1000	none	none	1.768	2.300	-0.205	-371134
Asphalt	AS	0.5	none	none	8000	none	none	1.768	2.300	-0.205	-969903
Asphalt	AS	0.5	none	none	15000	none	none	1.705	2.300	-0.205	-1124400
Asphalt	AS	Rough	none	none	1000	none	none	1.830	4.585	-0.205	-315055
Asphalt	AS	Rough	none	none	8000	none	none	1.830	4.585	-0.205	-900109
Asphalt	AS	Rough	none	none	15000	none	none	1.830	4.585	-0.205	-1131840
Granular	AS	0.5	none	none	1000	none	none	1.705	2.300	-0.368	-35036.9
Granular	AS	0.5	none	none	8000	none	none	0.527	2.450	-0.968	-26635.7
Granular	AS	0.5	none	none	15000	none	none	0.527	2.600	-0.968	-25907.2
Granular	AS	Rough	none	none	1000	none	none	1.317	4.585	-0.968	-27536.6
Granular	AS	Rough	none	none	8000	none	none	1.404	4.585	-0.968	-25811.2
Granular	AS	Rough	none	none	15000	none	none	1.317	4.585	-0.968	-24951.9
Panel	AS	0.5	none	none	1000	none	none	1.830	4.585	0.000	-4024690
Panel	AS	0.5	none	none	8000	none	none	1.830	4.585	0.000	-3829560
Panel	AS	0.5	none	none	15000	none	none	1.830	4.585	0.000	-3700050
Panel	AS	Rough	none	none	1000	none	none	1.830	4.585	0.000	-4017080
Panel	AS	Rough	none	none	8000	none	none	1.830	4.585	0.000	-3462720
Panel	AS	Rough	none	none	15000	none	none	1.830	4.585	0.000	-3269500
Asphalt	GR	none	0.5	0.5	1000	4000	12	-1.729	2.300	-0.217	-274462
Asphalt	GR	none	0.5	0.5	1000	4000	18	-1.729	2.300	-0.223	-274910
Asphalt	GR	none	0.5	0.5	1000	4000	24	-1.729	2.300	-0.229	-274283
Asphalt	GR	none	0.5	0.5	1000	12000	12	-1.729	2.300	-0.217	-274648
Asphalt	GR	none	0.5	0.5	1000	12000	18	-1.729	2.300	-0.223	-273486
Asphalt	GR	none	0.5	0.5	1000	12000	24	1.768	2.300	-0.229	-272363

Part	Support Condition	Friction (panel-to-base) (-)	Friction (panel-to-support) (-)	Friction (support-to-base) (-)	E_{base}[1] (MPa)	$E_{support}$[2] (MPa)	$t_{support}$[3] (MPa)	X-Coord[4] (m)	Y-Coord[5] (m)	Z-Coord[6] (m)	Minimum Principal Stress (Pa)
Asphalt	GR	none	0.5	0.5	1000	20000	12	1.768	4.585	-0.217	-216616
Asphalt	GR	none	0.5	0.5	1000	20000	18	-1.729	2.300	-0.223	-271695
Asphalt	GR	none	0.5	0.5	1000	20000	24	1.768	2.300	-0.229	-270390
Asphalt	GR	none	0.5	0.5	8000	4000	12	-1.629	2.300	-0.217	-776372
Asphalt	GR	none	0.5	0.5	8000	4000	18	-1.629	2.300	-0.223	-800333
Asphalt	GR	none	0.5	0.5	8000	4000	24	-1.629	2.300	-0.229	-822420
Asphalt	GR	none	0.5	0.5	8000	12000	12	-1.629	2.300	-0.217	-777663
Asphalt	GR	none	0.5	0.5	8000	12000	18	-1.629	2.300	-0.223	-799963
Asphalt	GR	none	0.5	0.5	8000	12000	24	-1.629	2.300	-0.229	-819179
Asphalt	GR	none	0.5	0.5	8000	20000	12	-1.629	2.300	-0.217	-777431
Asphalt	GR	none	0.5	0.5	8000	20000	18	-1.629	2.300	-0.223	-798112
Asphalt	GR	none	0.5	0.5	8000	20000	24	-1.629	2.300	-0.229	-814519
Asphalt	GR	none	0.5	0.5	15000	4000	12	-1.629	2.300	-0.217	-951434
Asphalt	GR	none	0.5	0.5	15000	4000	18	-1.629	2.300	-0.223	-991719
Asphalt	GR	none	0.5	0.5	15000	4000	24	-1.629	2.300	-0.229	-1032510
Asphalt	GR	none	0.5	0.5	15000	12000	12	-1.629	2.300	-0.217	-952882
Asphalt	GR	none	0.5	0.5	15000	12000	18	-1.629	2.300	-0.223	-991819
Asphalt	GR	none	0.5	0.5	15000	12000	24	-1.629	2.300	-0.229	-1030130
Asphalt	GR	none	0.5	0.5	15000	20000	12	-1.629	2.300	-0.217	-952705
Asphalt	GR	none	0.5	0.5	15000	20000	18	-1.629	2.300	-0.223	-990221
Asphalt	GR	none	0.5	0.5	15000	20000	24	-1.629	2.300	-0.229	-1025860
Asphalt	GR	none	Rough	Rough	1000	4000	12	1.830	4.585	-0.217	-310247
Asphalt	GR	none	Rough	Rough	1000	4000	18	1.830	4.585	-0.223	-311510
Asphalt	GR	none	Rough	Rough	1000	4000	24	1.830	4.585	-0.229	-312937
Asphalt	GR	none	Rough	Rough	1000	12000	12	1.830	4.585	-0.217	-311763
Asphalt	GR	none	Rough	Rough	1000	12000	18	1.830	4.585	-0.223	-312688

Part	Support Condition	Friction (panel-to-base) (-)	Friction (panel-to-support) (-)	Friction (support-to-base) (-)	E_{base}[1] (MPa)	$E_{support}$[2] (MPa)	$t_{support}$[3] (MPa)	X-Coord[4] (m)	Y-Coord[5] (m)	Z-Coord[6] (m)	Minimum Principal Stress (Pa)
Asphalt	GR	none	Rough	Rough	1000	12000	24	1.830	4.585	-0.229	-313475
Asphalt	GR	none	Rough	Rough	1000	20000	12	1.830	4.585	-0.217	-309828
Asphalt	GR	none	Rough	Rough	1000	20000	18	1.830	4.585	-0.223	-309508
Asphalt	GR	none	Rough	Rough	1000	20000	24	1.830	4.585	-0.229	-309048
Asphalt	GR	none	Rough	Rough	8000	4000	12	1.830	4.585	-0.217	-840137
Asphalt	GR	none	Rough	Rough	8000	4000	18	1.830	4.585	-0.223	-840075
Asphalt	GR	none	Rough	Rough	8000	4000	24	1.830	4.585	-0.229	-842611
Asphalt	GR	none	Rough	Rough	8000	12000	12	1.830	4.585	-0.217	-837920
Asphalt	GR	none	Rough	Rough	8000	12000	18	1.830	4.585	-0.223	-845535
Asphalt	GR	none	Rough	Rough	8000	12000	24	1.830	4.585	-0.229	-852522
Asphalt	GR	none	Rough	Rough	8000	20000	12	1.830	4.585	-0.217	-838206
Asphalt	GR	none	Rough	Rough	8000	20000	18	1.830	4.585	-0.223	-846913
Asphalt	GR	none	Rough	Rough	8000	20000	24	1.830	4.585	-0.229	-854459
Asphalt	GR	none	Rough	Rough	15000	4000	12	1.830	4.585	-0.217	-1059650
Asphalt	GR	none	Rough	Rough	15000	4000	18	1.830	4.585	-0.223	-1061440
Asphalt	GR	none	Rough	Rough	15000	4000	24	1.830	4.585	-0.229	-1068320
Asphalt	GR	none	Rough	Rough	15000	12000	12	1.830	4.585	-0.217	-1065370
Asphalt	GR	none	Rough	Rough	15000	12000	18	1.830	4.585	-0.223	-1080070
Asphalt	GR	none	Rough	Rough	15000	12000	24	1.830	4.585	-0.229	-1094210
Asphalt	GR	none	Rough	Rough	15000	20000	12	1.830	4.585	-0.217	-1055760
Asphalt	GR	none	Rough	Rough	15000	20000	18	1.830	4.585	-0.223	-1072730
Asphalt	GR	none	Rough	Rough	15000	20000	24	1.830	4.585	-0.229	-1087990
Granular	GR	none	0.5	0.5	1000	4000	12	1.705	2.300	-0.380	-33412.1
Granular	GR	none	0.5	0.5	1000	4000	18	1.705	2.300	-0.380	-34129.1
Granular	GR	none	0.5	0.5	1000	4000	24	1.705	2.300	-0.380	-34840.6
Granular	GR	none	0.5	0.5	1000	12000	12	1.705	2.300	-0.380	-33401.2

Part	Support Condition	Friction (panel-to-base) (-)	Friction (panel-to-support) (-)	Friction (support-to-base) (-)	E_{base}[1] (MPa)	$E_{support}$[2] (MPa)	$t_{support}$[3] (MPa)	X-Coord[4] (m)	Y-Coord[5] (m)	Z-Coord[6] (m)	Minimum Principal Stress (Pa)
Granular	GR	none	0.5	0.5	1000	12000	18	1.705	2.300	-0.380	-34068.6
Granular	GR	none	0.5	0.5	1000	12000	24	1.705	2.300	-0.380	-34690.2
Granular	GR	none	0.5	0.5	1000	20000	12	1.229	4.585	-0.980	-30177.6
Granular	GR	none	0.5	0.5	1000	20000	18	1.705	2.300	-0.380	-34002
Granular	GR	none	0.5	0.5	1000	20000	24	1.705	2.300	-0.380	-34543.6
Granular	GR	none	0.5	0.5	8000	4000	12	0.527	2.450	-0.980	-26984.4
Granular	GR	none	0.5	0.5	8000	4000	18	0.527	2.450	-0.980	-27066.4
Granular	GR	none	0.5	0.5	8000	4000	24	0.527	2.450	-0.980	-27143.8
Granular	GR	none	0.5	0.5	8000	12000	12	0.527	2.450	-0.980	-26982.2
Granular	GR	none	0.5	0.5	8000	12000	18	0.527	2.450	-0.980	-27061.5
Granular	GR	none	0.5	0.5	8000	12000	24	0.527	2.450	-0.980	-27135.7
Granular	GR	none	0.5	0.5	8000	20000	12	0.527	2.450	-0.980	-26980.9
Granular	GR	none	0.5	0.5	8000	20000	18	0.527	2.450	-0.980	-27058.2
Granular	GR	none	0.5	0.5	8000	20000	24	0.527	2.450	-0.980	-27130.6
Granular	GR	none	0.5	0.5	15000	4000	12	0.527	2.600	-0.980	-26301.5
Granular	GR	none	0.5	0.5	15000	4000	18	0.527	2.600	-0.980	-26402.1
Granular	GR	none	0.5	0.5	15000	4000	24	0.527	2.600	-0.980	-26504.6
Granular	GR	none	0.5	0.5	15000	12000	12	0.527	2.600	-0.980	-26300.2
Granular	GR	none	0.5	0.5	15000	12000	18	0.527	2.600	-0.980	-26398.9
Granular	GR	none	0.5	0.5	15000	12000	24	0.527	2.600	-0.980	-26498.6
Granular	GR	none	0.5	0.5	15000	20000	12	0.527	2.600	-0.980	-26299.5
Granular	GR	none	0.5	0.5	15000	20000	18	0.527	2.600	-0.980	-26396.7
Granular	GR	none	0.5	0.5	15000	20000	24	0.527	2.600	-0.980	-26494.8
Granular	GR	none	Rough	Rough	1000	4000	12	1.317	4.585	-0.980	-27917.8
Granular	GR	none	Rough	Rough	1000	4000	18	1.317	4.585	-0.980	-27918.6
Granular	GR	none	Rough	Rough	1000	4000	24	1.317	4.585	-0.980	-27926.9

Part	Support Condition	Friction (panel-to-base) (-)	Friction (panel-to-support) (-)	Friction (support-to-base) (-)	E_{base}[1] (MPa)	$E_{support}$[2] (MPa)	$t_{support}$[3] (MPa)	X-Coord[4] (m)	Y-Coord[5] (m)	Z-Coord[6] (m)	Minimum Principal Stress (Pa)
Granular	GR	none	Rough	Rough	1000	12000	12	1.317	4.585	-0.980	-28029.5
Granular	GR	none	Rough	Rough	1000	12000	18	1.317	4.585	-0.980	-28017.2
Granular	GR	none	Rough	Rough	1000	12000	24	1.317	4.585	-0.980	-28003.1
Granular	GR	none	Rough	Rough	1000	20000	12	1.317	4.585	-0.980	-28036.4
Granular	GR	none	Rough	Rough	1000	20000	18	1.317	4.585	-0.980	-28000.8
Granular	GR	none	Rough	Rough	1000	20000	24	1.317	4.585	-0.980	-27959.9
Granular	GR	none	Rough	Rough	8000	4000	12	1.317	4.585	-0.980	-25907.8
Granular	GR	none	Rough	Rough	8000	4000	18	1.317	4.585	-0.980	-25947.6
Granular	GR	none	Rough	Rough	8000	4000	24	1.317	4.585	-0.980	-25987
Granular	GR	none	Rough	Rough	8000	12000	12	1.404	4.585	-0.980	-25870.3
Granular	GR	none	Rough	Rough	8000	12000	18	1.317	4.585	-0.980	-25895.3
Granular	GR	none	Rough	Rough	8000	12000	24	1.317	4.585	-0.980	-25920.9
Granular	GR	none	Rough	Rough	8000	20000	12	1.404	4.585	-0.980	-25856.1
Granular	GR	none	Rough	Rough	8000	20000	18	1.404	4.585	-0.980	-25872.7
Granular	GR	none	Rough	Rough	8000	20000	24	1.404	4.585	-0.980	-25889.4
Granular	GR	none	Rough	Rough	15000	4000	12	1.317	4.585	-0.980	-25074.1
Granular	GR	none	Rough	Rough	15000	4000	18	1.317	4.585	-0.980	-25122.1
Granular	GR	none	Rough	Rough	15000	4000	24	1.317	4.585	-0.980	-25169.8
Granular	GR	none	Rough	Rough	15000	12000	12	1.317	4.585	-0.980	-25018.4
Granular	GR	none	Rough	Rough	15000	12000	18	1.317	4.585	-0.980	-25050.4
Granular	GR	none	Rough	Rough	15000	12000	24	1.317	4.585	-0.980	-25083.8
Granular	GR	none	Rough	Rough	15000	20000	12	1.317	4.585	-0.980	-24999.4
Granular	GR	none	Rough	Rough	15000	20000	18	1.317	4.585	-0.980	-25024.4
Granular	GR	none	Rough	Rough	15000	20000	24	1.317	4.585	-0.980	-25051.1
Panel	GR	none	0.5	0.5	1000	4000	12	1.830	4.585	0.000	-4040770
Panel	GR	none	0.5	0.5	1000	4000	18	1.830	4.585	0.000	-4042120

Part	Support Condition	Friction (panel-to-base) (-)	Friction (panel-to-support) (-)	Friction (support-to-base) (-)	E_{base}[1] (MPa)	$E_{support}$[2] (MPa)	$t_{support}$[3] (MPa)	X-Coord[4] (m)	Y-Coord[5] (m)	Z-Coord[6] (m)	Minimum Principal Stress (Pa)
Panel	GR	none	0.5	0.5	1000	4000	24	1.830	4.585	0.000	-4043480
Panel	GR	none	0.5	0.5	1000	12000	12	1.830	4.585	0.000	-4040490
Panel	GR	none	0.5	0.5	1000	12000	18	1.830	4.585	0.000	-4041810
Panel	GR	none	0.5	0.5	1000	12000	24	1.830	4.585	0.000	-4043300
Panel	GR	none	0.5	0.5	1000	20000	12	1.830	4.585	0.000	-2458000
Panel	GR	none	0.5	0.5	1000	20000	18	1.830	4.585	0.000	-4041640
Panel	GR	none	0.5	0.5	1000	20000	24	1.830	4.585	0.000	-4043330
Panel	GR	none	0.5	0.5	8000	4000	12	1.830	4.585	0.000	-3921230
Panel	GR	none	0.5	0.5	8000	4000	18	1.830	4.585	0.000	-3931230
Panel	GR	none	0.5	0.5	8000	4000	24	1.830	4.585	0.000	-3941120
Panel	GR	none	0.5	0.5	8000	12000	12	1.830	4.585	0.000	-3920570
Panel	GR	none	0.5	0.5	8000	12000	18	1.830	4.585	0.000	-3930360
Panel	GR	none	0.5	0.5	8000	12000	24	1.830	4.585	0.000	-3940110
Panel	GR	none	0.5	0.5	8000	20000	12	1.830	4.585	0.000	-3920220
Panel	GR	none	0.5	0.5	8000	20000	18	1.830	4.585	0.000	-3929960
Panel	GR	none	0.5	0.5	8000	20000	24	1.830	4.585	0.000	-3939680
Panel	GR	none	0.5	0.5	15000	4000	12	1.830	4.585	0.000	-3849580
Panel	GR	none	0.5	0.5	15000	4000	18	1.830	4.585	0.000	-3861680
Panel	GR	none	0.5	0.5	15000	4000	24	1.830	4.585	0.000	-3873980
Panel	GR	none	0.5	0.5	15000	12000	12	1.830	4.585	0.000	-3848650
Panel	GR	none	0.5	0.5	15000	12000	18	1.830	4.585	0.000	-3860430
Panel	GR	none	0.5	0.5	15000	12000	24	1.830	4.585	0.000	-3872500
Panel	GR	none	0.5	0.5	15000	20000	12	1.830	4.585	0.000	-3848220
Panel	GR	none	0.5	0.5	15000	20000	18	1.830	4.585	0.000	-3859900
Panel	GR	none	0.5	0.5	15000	20000	24	1.830	4.585	0.000	-3871910
Panel	GR	none	Rough	Rough	1000	4000	12	1.830	4.585	0.000	-4006550

Part	Support Condition	Friction (panel-to-base) (-)	Friction (panel-to-support) (-)	Friction (support-to-base) (-)	E_{base}[1] (MPa)	$E_{support}$[2] (MPa)	$t_{support}$[3] (MPa)	X-Coord[4] (m)	Y-Coord[5] (m)	Z-Coord[6] (m)	Minimum Principal Stress (Pa)
Panel	GR	none	Rough	Rough	1000	4000	18	1.830	4.585	0.000	-4000770
Panel	GR	none	Rough	Rough	1000	4000	24	1.830	4.585	0.000	-3995440
Panel	GR	none	Rough	Rough	1000	12000	12	1.830	4.585	0.000	-3997550
Panel	GR	none	Rough	Rough	1000	12000	18	1.830	4.585	0.000	-3977860
Panel	GR	none	Rough	Rough	1000	12000	24	1.830	4.585	0.000	-3957400
Panel	GR	none	Rough	Rough	1000	20000	12	1.830	4.585	0.000	-3979480
Panel	GR	none	Rough	Rough	1000	20000	18	1.830	4.585	0.000	-3948360
Panel	GR	none	Rough	Rough	1000	20000	24	1.830	4.585	0.000	-3916800
Panel	GR	none	Rough	Rough	8000	4000	12	1.830	4.585	0.000	-3454840
Panel	GR	none	Rough	Rough	8000	4000	18	1.830	4.585	0.000	-3473140
Panel	GR	none	Rough	Rough	8000	4000	24	1.830	4.585	0.000	-3488920
Panel	GR	none	Rough	Rough	8000	12000	12	1.830	4.585	0.000	-3414500
Panel	GR	none	Rough	Rough	8000	12000	18	1.830	4.585	0.000	-3419020
Panel	GR	none	Rough	Rough	8000	12000	24	1.830	4.585	0.000	-3422460
Panel	GR	none	Rough	Rough	8000	20000	12	1.830	4.585	0.000	-3403880
Panel	GR	none	Rough	Rough	8000	20000	18	1.830	4.585	0.000	-3403610
Panel	GR	none	Rough	Rough	8000	20000	24	1.830	4.585	0.000	-3402480
Panel	GR	none	Rough	Rough	15000	4000	12	1.830	4.585	0.000	-3294560
Panel	GR	none	Rough	Rough	15000	4000	18	1.830	4.585	0.000	-3322000
Panel	GR	none	Rough	Rough	15000	4000	24	1.830	4.585	0.000	-3345690
Panel	GR	none	Rough	Rough	15000	12000	12	1.830	4.585	0.000	-3241450
Panel	GR	none	Rough	Rough	15000	12000	18	1.830	4.585	0.000	-3253080
Panel	GR	none	Rough	Rough	15000	12000	24	1.830	4.585	0.000	-3263150
Panel	GR	none	Rough	Rough	15000	20000	12	1.830	4.585	0.000	-3226430
Panel	GR	none	Rough	Rough	15000	20000	18	1.830	4.585	0.000	-3232920
Panel	GR	none	Rough	Rough	15000	20000	24	1.830	4.585	0.000	-3238320

Part	Support Condition	Friction (panel-to-base) (-)	Friction (panel-to-support) (-)	Friction (support-to-base) (-)	E_{base}[1] (MPa)	$E_{support}$[2] (MPa)	$t_{support}$[3] (MPa)	X-Coord[4] (m)	Y-Coord[5] (m)	Z-Coord[6] (m)	Minimum Principal Stress (Pa)
Support	GR	none	0.5	0.5	1000	4000	12	-1.830	2.252	-0.205	-272539
Support	GR	none	0.5	0.5	1000	4000	18	1.830	2.300	-0.223	-273944
Support	GR	none	0.5	0.5	1000	4000	24	-1.735	2.252	-0.205	-277074
Support	GR	none	0.5	0.5	1000	12000	12	1.830	2.300	-0.217	-599767
Support	GR	none	0.5	0.5	1000	12000	18	-1.451	2.300	-0.205	-634352
Support	GR	none	0.5	0.5	1000	12000	24	-0.504	2.300	-0.205	-782338
Support	GR	none	0.5	0.5	1000	20000	12	1.830	4.585	-0.217	-650546
Support	GR	none	0.5	0.5	1000	20000	18	-1.451	2.300	-0.205	-1025850
Support	GR	none	0.5	0.5	1000	20000	24	-0.504	2.300	-0.205	-1229190
Support	GR	none	0.5	0.5	8000	4000	12	-1.830	2.350	-0.205	-288935
Support	GR	none	0.5	0.5	8000	4000	18	-1.830	2.252	-0.205	-267292
Support	GR	none	0.5	0.5	8000	4000	24	-1.830	2.252	-0.205	-261764
Support	GR	none	0.5	0.5	8000	12000	12	-1.759	2.252	-0.205	-442960
Support	GR	none	0.5	0.5	8000	12000	18	-0.178	2.252	-0.205	-436581
Support	GR	none	0.5	0.5	8000	12000	24	-0.178	2.252	-0.205	-495511
Support	GR	none	0.5	0.5	8000	20000	12	-1.735	2.252	-0.205	-607172
Support	GR	none	0.5	0.5	8000	20000	18	-0.178	2.252	-0.205	-658688
Support	GR	none	0.5	0.5	8000	20000	24	-0.504	2.300	-0.205	-787301
Support	GR	none	0.5	0.5	15000	4000	12	-1.830	2.350	-0.205	-280528
Support	GR	none	0.5	0.5	15000	4000	18	-1.830	2.252	-0.205	-260863
Support	GR	none	0.5	0.5	15000	4000	24	-1.830	2.252	-0.205	-256529
Support	GR	none	0.5	0.5	15000	12000	12	-1.759	2.252	-0.205	-427938
Support	GR	none	0.5	0.5	15000	12000	18	-0.178	2.252	-0.205	-400960
Support	GR	none	0.5	0.5	15000	12000	24	-0.178	2.325	-0.205	-443558
Support	GR	none	0.5	0.5	15000	20000	12	-1.735	2.252	-0.205	-576785
Support	GR	none	0.5	0.5	15000	20000	18	-0.178	2.252	-0.205	-595924

Part	Support Condition	Friction (panel-to-base) (-)	Friction (panel-to-support) (-)	Friction (support-to-base) (-)	E_{base}[1] (MPa)	$E_{support}$[2] (MPa)	$t_{support}$[3] (MPa)	X-Coord[4] (m)	Y-Coord[5] (m)	Z-Coord[6] (m)	Minimum Principal Stress (Pa)
Support	GR	none	0.5	0.5	15000	20000	24	-0.504	2.300	-0.205	-704696
Support	GR	none	Rough	Rough	1000	4000	12	-0.694	2.252	-0.205	-1627470
Support	GR	none	Rough	Rough	1000	4000	18	-1.830	2.252	-0.205	-1420180
Support	GR	none	Rough	Rough	1000	4000	24	-1.830	2.252	-0.205	-1266030
Support	GR	none	Rough	Rough	1000	12000	12	-1.214	2.252	-0.205	-2036300
Support	GR	none	Rough	Rough	1000	12000	18	-1.214	2.252	-0.205	-1778620
Support	GR	none	Rough	Rough	1000	12000	24	-1.214	2.252	-0.205	-1573460
Support	GR	none	Rough	Rough	1000	20000	12	-1.214	2.252	-0.205	-2101260
Support	GR	none	Rough	Rough	1000	20000	18	-1.214	2.252	-0.205	-1848290
Support	GR	none	Rough	Rough	1000	20000	24	-1.830	2.252	-0.205	-1651600
Support	GR	none	Rough	Rough	8000	4000	12	1.830	2.252	-0.205	-1330770
Support	GR	none	Rough	Rough	8000	4000	18	-1.830	2.252	-0.205	-1166000
Support	GR	none	Rough	Rough	8000	4000	24	-1.830	2.252	-0.205	-1061730
Support	GR	none	Rough	Rough	8000	12000	12	1.830	2.252	-0.205	-1726220
Support	GR	none	Rough	Rough	8000	12000	18	1.830	2.252	-0.205	-1535970
Support	GR	none	Rough	Rough	8000	12000	24	-1.830	2.252	-0.205	-1407640
Support	GR	none	Rough	Rough	8000	20000	12	1.830	2.252	-0.205	-1852310
Support	GR	none	Rough	Rough	8000	20000	18	-1.830	2.252	-0.205	-1684060
Support	GR	none	Rough	Rough	8000	20000	24	-1.830	2.252	-0.205	-1561940
Support	GR	none	Rough	Rough	15000	4000	12	1.830	2.252	-0.205	-1273320
Support	GR	none	Rough	Rough	15000	4000	18	-1.830	2.252	-0.205	-1134930
Support	GR	none	Rough	Rough	15000	4000	24	-1.830	2.252	-0.205	-1035660
Support	GR	none	Rough	Rough	15000	12000	12	1.830	2.252	-0.205	-1694640
Support	GR	none	Rough	Rough	15000	12000	18	-1.830	2.252	-0.205	-1512400
Support	GR	none	Rough	Rough	15000	12000	24	-1.830	2.252	-0.205	-1393270
Support	GR	none	Rough	Rough	15000	20000	12	1.830	2.252	-0.205	-1886830

Part	Support Condition	Friction (panel-to-base) (-)	Friction (panel-to-support) (-)	Friction (support-to-base) (-)	E_{base}[1] (MPa)	$E_{support}$[2] (MPa)	$t_{support}$[3] (MPa)	X-Coord[4] (m)	Y-Coord[5] (m)	Z-Coord[6] (m)	Minimum Principal Stress (Pa)
Support	GR	none	Rough	Rough	15000	20000	18	-1.830	2.252	-0.205	-1693770
Support	GR	none	Rough	Rough	15000	20000	24	-1.830	2.252	-0.205	-1569430

Responses under -10°C temperature gradient with axle loading

Notes on the following responses:

[1]E_{base}	elastic modulus of base
[2]$E_{support}$	elastic modulus of support
[3]$t_{support}$	thickness of support
[4]X-coord	Relative to centreline of panels (X-coord = 0 at centreline)
[5]Y-coord	Relative to midpanel of first panel, with three panels total (Y-coord = 0.0 at midpanel of panel 1, Y-coord = 4.585 at midpanel of panel 2, etc.)
[6]Z-coord	Relative to top of panel (Z-coord = 0.0 at top of panel, Z-coord = -0.205 at bottom of panel, etc.)

Responses under -10°C temperature gradient with axle loading

Part	Support Condition	Friction (panel-to-base) (-)	Friction (panel-to-support) (-)	Friction (support-to-base) (-)	E_{base}[1] (MPa)	$E_{support}$[2] (MPa)	$t_{support}$[3] (MPa)	X-Coord[4] (m)	Y-Coord[5] (m)	Z-Coord[6] (m)	Minimum Principal Stress (Pa)
Asphalt	AS	0.5	none	none	1000	none	none	1.830	2.697	-0.205	-223360
Asphalt	AS	0.5	none	none	8000	none	none	1.768	2.697	-0.205	-679945
Asphalt	AS	0.5	none	none	15000	none	none	1.768	2.697	-0.205	-878613
Asphalt	AS	Rough	none	none	1000	none	none	0.611	6.885	-0.205	-787521
Asphalt	AS	Rough	none	none	8000	none	none	-0.623	6.885	-0.205	-1053530
Asphalt	AS	Rough	none	none	15000	none	none	1.830	2.331	-0.205	-1231240
Granular	AS	0.5	none	none	1000	none	none	1.236	3.187	-0.968	-28458.9
Granular	AS	0.5	none	none	8000	none	none	1.149	3.187	-0.968	-27291.3
Granular	AS	0.5	none	none	15000	none	none	1.063	3.187	-0.968	-26764.3
Granular	AS	Rough	none	none	1000	none	none	1.322	2.488	-0.968	-27845.5
Granular	AS	Rough	none	none	8000	none	none	1.408	2.363	-0.968	-26125.1
Granular	AS	Rough	none	none	15000	none	none	1.322	2.363	-0.968	-25316.6
Panel	AS	0.5	none	none	1000	none	none	-1.830	3.059	-0.205	-2568170
Panel	AS	0.5	none	none	8000	none	none	-1.830	3.398	-0.205	-2751370
Panel	AS	0.5	none	none	15000	none	none	-1.830	3.398	-0.205	-2807040
Panel	AS	Rough	none	none	1000	none	none	-1.830	2.363	-0.205	-2858070
Panel	AS	Rough	none	none	8000	none	none	-1.830	2.363	-0.205	-3075300
Panel	AS	Rough	none	none	15000	none	none	-1.830	2.363	-0.205	-3021990
Asphalt	GR	none	0.5	0.5	1000	4000	12	1.768	2.697	-0.217	-188119
Asphalt	GR	none	0.5	0.5	1000	4000	18	1.768	2.697	-0.223	-190312
Asphalt	GR	none	0.5	0.5	1000	4000	24	1.768	2.697	-0.229	-192479
Asphalt	GR	none	0.5	0.5	1000	12000	12	1.768	2.697	-0.217	-187963
Asphalt	GR	none	0.5	0.5	1000	12000	18	1.768	2.697	-0.223	-190000
Asphalt	GR	none	0.5	0.5	1000	12000	24	1.768	2.697	-0.229	-192246

Part	Support Condition	Friction (panel-to-base)	Friction (panel-to-support)	Friction (support-to-base)	E_{base}[1]	$E_{support}$[2]	$t_{support}$[3]	X-Coord[4]	Y-Coord[5]	Z-Coord[6]	Minimum Principal Stress
		(-)	(-)	(-)	(MPa)	(MPa)	(MPa)	(m)	(m)	(m)	(Pa)
Asphalt	GR	none	0.5	0.5	1000	20000	12	1.768	2.697	-0.217	-187769
Asphalt	GR	none	0.5	0.5	1000	20000	18	1.768	2.697	-0.223	-189793
Asphalt	GR	none	0.5	0.5	1000	20000	24	1.768	2.697	-0.229	-192212
Asphalt	GR	none	0.5	0.5	8000	4000	12	1.705	2.802	-0.217	-557538
Asphalt	GR	none	0.5	0.5	8000	4000	18	1.705	2.697	-0.223	-572234
Asphalt	GR	none	0.5	0.5	8000	4000	24	1.705	2.697	-0.229	-587140
Asphalt	GR	none	0.5	0.5	8000	12000	12	1.705	2.802	-0.217	-557490
Asphalt	GR	none	0.5	0.5	8000	12000	18	1.705	2.697	-0.223	-571712
Asphalt	GR	none	0.5	0.5	8000	12000	24	1.705	2.697	-0.229	-585770
Asphalt	GR	none	0.5	0.5	8000	20000	12	1.705	2.802	-0.217	-557214
Asphalt	GR	none	0.5	0.5	8000	20000	18	1.705	2.697	-0.223	-570961
Asphalt	GR	none	0.5	0.5	8000	20000	24	1.705	2.697	-0.229	-584402
Asphalt	GR	none	0.5	0.5	15000	12000	12	1.705	2.907	-0.217	-739093
Asphalt	GR	none	0.5	0.5	15000	12000	18	1.705	2.907	-0.223	-763149
Asphalt	GR	none	0.5	0.5	15000	12000	24	1.705	2.907	-0.229	-787132
Asphalt	GR	none	Rough	Rough	1000	4000	12	1.830	2.363	-0.217	-537422
Asphalt	GR	none	Rough	Rough	1000	4000	18	0.611	6.885	-0.223	-353883
Asphalt	GR	none	Rough	Rough	1000	4000	24	1.830	2.363	-0.229	-496716
Asphalt	GR	none	Rough	Rough	1000	12000	12	1.830	2.363	-0.217	-339165
Asphalt	GR	none	Rough	Rough	1000	12000	18	1.830	2.363	-0.223	-338921
Asphalt	GR	none	Rough	Rough	1000	12000	24	1.830	2.363	-0.229	-336574
Asphalt	GR	none	Rough	Rough	1000	20000	12	1.830	2.363	-0.217	-335347
Asphalt	GR	none	Rough	Rough	1000	20000	18	1.830	2.363	-0.223	-332003
Asphalt	GR	none	Rough	Rough	1000	20000	24	1.830	2.363	-0.229	-327827
Asphalt	GR	none	Rough	Rough	8000	4000	12	1.830	2.331	-0.217	-894227

Part	Support Condition	Friction (panel-to-base) (-)	Friction (panel-to-support) (-)	Friction (support-to-base) (-)	E_{base}[1] (MPa)	$E_{support}$[2] (MPa)	$t_{support}$[3] (MPa)	X-Coord[4] (m)	Y-Coord[5] (m)	Z-Coord[6] (m)	Minimum Principal Stress (Pa)
Asphalt	GR	none	Rough	Rough	8000	4000	18	1.830	2.363	-0.223	-889750
Asphalt	GR	none	Rough	Rough	8000	4000	24	1.830	2.363	-0.229	-886779
Asphalt	GR	none	Rough	Rough	8000	12000	12	1.830	2.331	-0.217	-890708
Asphalt	GR	none	Rough	Rough	8000	12000	18	1.830	2.363	-0.223	-890439
Asphalt	GR	none	Rough	Rough	8000	12000	24	1.830	2.363	-0.229	-899860
Asphalt	GR	none	Rough	Rough	8000	20000	12	1.830	2.331	-0.217	-875738
Asphalt	GR	none	Rough	Rough	8000	20000	18	1.830	2.363	-0.223	-880889
Asphalt	GR	none	Rough	Rough	8000	20000	24	1.830	2.363	-0.229	-891742
Asphalt	GR	none	Rough	Rough	15000	12000	12	1.830	2.331	-0.217	-1138980
Asphalt	GR	none	Rough	Rough	15000	12000	18	1.830	2.331	-0.223	-1134060
Asphalt	GR	none	Rough	Rough	15000	12000	24	1.830	2.363	-0.229	-1145410
Granular	GR	none	0.5	0.5	1000	4000	12	1.149	3.361	-0.980	-28824
Granular	GR	none	0.5	0.5	1000	4000	18	1.149	3.361	-0.980	-28834.9
Granular	GR	none	0.5	0.5	1000	4000	24	1.149	3.361	-0.980	-28845.3
Granular	GR	none	0.5	0.5	1000	12000	12	1.149	3.361	-0.980	-28821.9
Granular	GR	none	0.5	0.5	1000	12000	18	1.149	3.361	-0.980	-28830.9
Granular	GR	none	0.5	0.5	1000	12000	24	1.149	3.361	-0.980	-28838.6
Granular	GR	none	0.5	0.5	1000	20000	12	1.149	3.361	-0.980	-28820.7
Granular	GR	none	0.5	0.5	1000	20000	18	1.149	3.361	-0.980	-28828.4
Granular	GR	none	0.5	0.5	1000	20000	24	1.149	3.361	-0.980	-28834.4
Granular	GR	none	0.5	0.5	8000	4000	12	1.063	3.187	-0.980	-27745.7
Granular	GR	none	0.5	0.5	8000	4000	18	1.063	3.187	-0.980	-27794.6
Granular	GR	none	0.5	0.5	8000	4000	24	1.063	3.187	-0.980	-27843.6
Granular	GR	none	0.5	0.5	8000	12000	12	1.063	3.187	-0.980	-27744.1
Granular	GR	none	0.5	0.5	8000	12000	18	1.063	3.187	-0.980	-27791.8
Granular	GR	none	0.5	0.5	8000	12000	24	1.063	3.187	-0.980	-27839.1

Part	Support Condition	Friction (panel-to-base) (-)	Friction (panel-to-support) (-)	Friction (support-to-base) (-)	E_{base}[1] (MPa)	$E_{support}$[2] (MPa)	$t_{support}$[3] (MPa)	X-Coord[4] (m)	Y-Coord[5] (m)	Z-Coord[6] (m)	Minimum Principal Stress (Pa)
Granular	GR	none	0.5	0.5	8000	20000	12	1.063	3.187	-0.980	-27743.5
Granular	GR	none	0.5	0.5	8000	20000	18	1.063	3.187	-0.980	-27790.4
Granular	GR	none	0.5	0.5	8000	20000	24	1.063	3.187	-0.980	-27836.7
Granular	GR	none	0.5	0.5	15000	12000	12	1.063	3.187	-0.980	-27232.6
Granular	GR	none	0.5	0.5	15000	12000	18	1.063	3.187	-0.980	-27298.4
Granular	GR	none	0.5	0.5	15000	12000	24	1.063	3.187	-0.980	-27364.7
Granular	GR	none	Rough	Rough	1000	4000	12	1.830	2.363	-0.380	-32712
Granular	GR	none	Rough	Rough	1000	4000	18	1.322	2.488	-0.980	-28220.4
Granular	GR	none	Rough	Rough	1000	4000	24	1.830	2.363	-0.380	-33340.5
Granular	GR	none	Rough	Rough	1000	12000	12	1.322	2.488	-0.980	-28287.4
Granular	GR	none	Rough	Rough	1000	12000	18	1.322	2.488	-0.980	-28297.6
Granular	GR	none	Rough	Rough	1000	12000	24	1.322	2.363	-0.980	-28299.5
Granular	GR	none	Rough	Rough	1000	20000	12	1.322	2.488	-0.980	-28297.3
Granular	GR	none	Rough	Rough	1000	20000	18	1.322	2.363	-0.980	-28286.8
Granular	GR	none	Rough	Rough	1000	20000	24	1.322	2.363	-0.980	-28267.8
Granular	GR	none	Rough	Rough	8000	4000	12	1.322	2.363	-0.980	-26245.4
Granular	GR	none	Rough	Rough	8000	4000	18	1.322	2.363	-0.980	-26295.1
Granular	GR	none	Rough	Rough	8000	4000	24	1.322	2.363	-0.980	-26343.9
Granular	GR	none	Rough	Rough	8000	12000	12	1.322	2.363	-0.980	-26207.6
Granular	GR	none	Rough	Rough	8000	12000	18	1.322	2.363	-0.980	-26245
Granular	GR	none	Rough	Rough	8000	12000	24	1.322	2.363	-0.980	-26282.6
Granular	GR	none	Rough	Rough	8000	20000	12	1.322	2.363	-0.980	-26193.8
Granular	GR	none	Rough	Rough	8000	20000	18	1.322	2.363	-0.980	-26224.4
Granular	GR	none	Rough	Rough	8000	20000	24	1.322	2.363	-0.980	-26255
Granular	GR	none	Rough	Rough	15000	12000	12	1.322	2.363	-0.980	-25404.8
Granular	GR	none	Rough	Rough	15000	12000	18	1.322	2.363	-0.980	-25449.2
Granular	GR	none	Rough	Rough	15000	12000	24	1.322	2.363	-0.980	-25494.9

Part	Support Condition	Friction (panel-to-base)	Friction (panel-to-support)	Friction (support-to-base)	E_{base}[1]	$E_{support}$[2]	$t_{support}$[3]	X-Coord[4]	Y-Coord[5]	Z-Coord[6]	Minimum Principal Stress
		(-)	(-)	(-)	(MPa)	(MPa)	(MPa)	(m)	(m)	(m)	(Pa)
Panel	GR	none	0.5	0.5	1000	4000	12	-1.830	2.363	-0.205	-2545900
Panel	GR	none	0.5	0.5	1000	4000	18	-1.830	2.363	-0.205	-2548030
Panel	GR	none	0.5	0.5	1000	4000	24	-1.830	2.363	-0.205	-2550040
Panel	GR	none	0.5	0.5	1000	12000	12	-1.830	2.363	-0.205	-2545730
Panel	GR	none	0.5	0.5	1000	12000	18	-1.830	2.363	-0.205	-2547730
Panel	GR	none	0.5	0.5	1000	12000	24	-1.830	2.363	-0.205	-2549570
Panel	GR	none	0.5	0.5	1000	20000	12	-1.830	2.363	-0.205	-2545610
Panel	GR	none	0.5	0.5	1000	20000	18	-1.830	2.363	-0.205	-2547530
Panel	GR	none	0.5	0.5	1000	20000	24	-1.830	2.363	-0.205	-2549220
Panel	GR	none	0.5	0.5	8000	4000	12	-1.830	3.398	-0.205	-2630680
Panel	GR	none	0.5	0.5	8000	4000	18	-1.830	3.398	-0.205	-2630600
Panel	GR	none	0.5	0.5	8000	4000	24	-1.830	3.398	-0.205	-2629590
Panel	GR	none	0.5	0.5	8000	12000	12	-1.830	3.398	-0.205	-2630890
Panel	GR	none	0.5	0.5	8000	12000	18	-1.830	3.398	-0.205	-2630430
Panel	GR	none	0.5	0.5	8000	12000	24	-1.830	3.398	-0.205	-2628680
Panel	GR	none	0.5	0.5	8000	20000	12	-1.830	3.398	-0.205	-2630710
Panel	GR	none	0.5	0.5	8000	20000	18	-1.830	3.398	-0.205	-2629790
Panel	GR	none	0.5	0.5	8000	20000	24	-1.830	3.398	-0.205	-2627330
Panel	GR	none	0.5	0.5	15000	12000	12	-1.830	3.568	-0.205	-2660460
Panel	GR	none	0.5	0.5	15000	12000	18	-1.830	3.568	-0.205	-2661590
Panel	GR	none	0.5	0.5	15000	12000	24	-1.830	3.398	-0.205	-2662640
Panel	GR	none	Rough	Rough	1000	4000	12	1.830	2.300	-0.205	-2358300
Panel	GR	none	Rough	Rough	1000	4000	18	-1.830	2.363	-0.205	-2983040
Panel	GR	none	Rough	Rough	1000	4000	24	1.830	2.300	-0.205	-2044230
Panel	GR	none	Rough	Rough	1000	12000	12	-1.830	2.363	-0.205	-3072110
Panel	GR	none	Rough	Rough	1000	12000	18	-1.830	2.363	-0.205	-3029250
Panel	GR	none	Rough	Rough	1000	12000	24	-1.830	2.363	-0.205	-2979530

Part	Support Condition	Friction (panel-to-base)	Friction (panel-to-support)	Friction (support-to-base)	E_{base}[1]	$E_{support}$[2]	$t_{support}$[3]	X-Coord[4]	Y-Coord[5]	Z-Coord[6]	Minimum Principal Stress
		(-)	(-)	(-)	(MPa)	(MPa)	(MPa)	(m)	(m)	(m)	(Pa)
Panel	GR	none	Rough	Rough	1000	20000	12	-0.033	6.870	-0.205	-3123480
Panel	GR	none	Rough	Rough	1000	20000	18	-1.830	2.363	-0.205	-2989510
Panel	GR	none	Rough	Rough	1000	20000	24	-1.830	2.363	-0.205	-2921500
Panel	GR	none	Rough	Rough	8000	4000	12	-1.830	2.363	-0.205	-2923290
Panel	GR	none	Rough	Rough	8000	4000	18	-1.830	2.363	-0.205	-2879220
Panel	GR	none	Rough	Rough	8000	4000	24	-1.830	2.363	-0.205	-2840680
Panel	GR	none	Rough	Rough	8000	12000	12	-1.830	2.363	-0.205	-2966800
Panel	GR	none	Rough	Rough	8000	12000	18	-1.830	2.363	-0.205	-2916730
Panel	GR	none	Rough	Rough	8000	12000	24	-1.830	2.363	-0.205	-2866260
Panel	GR	none	Rough	Rough	8000	20000	12	-1.830	2.363	-0.205	-2951290
Panel	GR	none	Rough	Rough	8000	20000	18	-1.830	2.363	-0.205	-2888170
Panel	GR	none	Rough	Rough	8000	20000	24	-1.830	2.363	-0.205	-2824910
Panel	GR	none	Rough	Rough	15000	12000	12	-1.830	2.363	-0.205	-2868450
Panel	GR	none	Rough	Rough	15000	12000	18	-1.830	2.363	-0.205	-2817850
Panel	GR	none	Rough	Rough	15000	12000	24	-1.830	2.363	-0.205	-2768840

Appendix C: Abaqus Code for Finite Element Model

Abaqus Code for Finite Element Model

```
# SCRIPTS TO BUILD PCIP FINITE ELEMENT MODELS IN ABAQUS
# Code by: Dahlia Malek

# MODULES
#++++++++++++++++++++++++++++++++++++++++++++++++++++++++++++++++++++++++++++

#============================================================================
# GENERAL
# MODULE NAME: common0
#============================================================================

# GENERAL
    #
.....................................................................

# SECONDARY CALCULATIONS BASED ON INPUTS TO MODEL
def secondaryCalcs(nPanels, instNameSubl, tAll, offsetDist):
    partPanels = []
    instPanels = []
    for i in range(1, nPanels+1):
        partPanels.append('panel'+str(i))
        instPanels.append('panel'+str(i)+'-1')

    instAll = instPanels[:]
    instAll.extend(instNameSubl)

    numSubl = len(instNameSubl)
    tTotal = sum(tAll) - offsetDist*(len(tAll)-1)

    return (partPanels, instPanels, instAll, numSubl, tTotal)


# MATERIALS
    #
.....................................................................

# CREATE ALL MATERIALS
def materials(modelName):
    matName = 'concrete'
    mdb.models[modelName].Material(description='Plain concrete, linear
elastic', name=matName)
    mdb.models[modelName].materials[matName].Density(table=((rho_conc, ),  ))
    mdb.models[modelName].materials[matName].Elastic(table=((E_conc,
nu_conc),  ))
    mdb.models[modelName].materials[matName].Expansion(table=((tc_conc, ), ))

    matName = 'asphalt'
    mdb.models[modelName].Material(description='Asphalt, linear elastic',
name=matName)
    mdb.models[modelName].materials[matName].Density(table=((rho_asph, ),  ))
    mdb.models[modelName].materials[matName].Elastic(table=((E_asph,
nu_asph),  ))
    mdb.models[modelName].materials[matName].Expansion(table=((tc_asph, ), ))
```

```
    matName = 'steel dowel'
    mdb.models[modelName].Material(description='Steel for dowels, linear
elastic', name=matName)
    mdb.models[modelName].materials[matName].Density(table=((rho_stdow, ), ))
    mdb.models[modelName].materials[matName].Elastic(table=((E_stdow,
nu_stdow),  ))
    mdb.models[modelName].materials[matName].Expansion(table=((tc_stdow, ),))

    matName = 'granular'
    mdb.models[modelName].Material(description='Granular material
representing mixed base/subbase', name=matName)
    mdb.models[modelName].materials[matName].Density(table=((rho_gran, ),  ))
    mdb.models[modelName].materials[matName].Elastic(table=((E_gran,
nu_gran),  ))
    mdb.models[modelName].materials[matName].Expansion(table=((tc_gran, ), ))

    matName = 'support'
    mdb.models[modelName].Material(description='Support layer material
(general)', name=matName)
    mdb.models[modelName].materials[matName].Density(table=((rho_supp, ),  ))
    mdb.models[modelName].materials[matName].Elastic(table=((E_supp,
nu_supp),  ))
    mdb.models[modelName].materials[matName].Expansion(table=((tc_supp, ), ))


# STEPS & OUTPUT
    #
.....................................................................

# CREATE FIELD OUTPUT REQUEST
def createFieldOut(modelName, varRequestStr):
# Create field output request & set variables
    mdb.models[modelName].FieldOutputRequest(createStepName='Step-1',
        name='F-Output-1', variables=varRequestStr)


# CREATE STATIC STEP
def staticStep(modelName, stepName, prevStepName, descriptionStr):
    mdb.models[modelName].StaticStep(description=descriptionStr,
name=stepName, previous=prevStepName)


# ============================================================================
# CREATE PARTS
# MODULE NAME: create3Dpart
# ============================================================================

# SUBFUNCTIONS TO CREATE PARTS
    #
.....................................................................

# PART GEOMETRY- SOLID PART BY EXTRUSION
def part3Dgeo(modelName, partName, wDim, lDim, tPlate):
      mdb.models[modelName].ConstrainedSketch(name='__profile__',
sheetSize=20.0)
      mdb.models[modelName].sketches['__profile__'].rectangle(point1=(0.0,
0.0), point2=(wDim, lDim))
```

```
      mdb.models[modelName].Part(dimensionality=THREE_D, name=partName, type=
DEFORMABLE_BODY)
      mdb.models[modelName].parts[partName].BaseSolidExtrude(depth=tPlate,
sketch=mdb.models[modelName].sketches['__profile__'])

# DEFINE AND ASSIGN SECTIONS TO PARTS
def part3Dsections(modelName, partName, matName, sctName):
      mdb.models[modelName].HomogeneousSolidSection(material = matName,
name=sctName, thickness=None)
      mdb.models[modelName].parts[partName].SectionAssignment(offset=0.,
offsetField='',
        offsetType=MIDDLE_SURFACE,
region=mdb.models[modelName].parts[partName].sets['all'],
        sectionName= sctName, thicknessAssignment=FROM_SECTION)

# CREATE DATUM AXES/PLANES
def partFeatures(modelName, partName, lDim, tPlate, axesPts):
    # datum planes

mdb.models[modelName].parts[partName].DatumPlaneByPrincipalPlane(offset=tPlat
e, principalPlane=XYPLANE)
    mdb.models[modelName].parts[partName].features.changeKey(fromName='Datum
plane-1', toName='Datum plane-top')

mdb.models[modelName].parts[partName].DatumPlaneByPrincipalPlane(offset=0.,
principalPlane=XYPLANE)
    mdb.models[modelName].parts[partName].features.changeKey(fromName='Datum
plane-1', toName='Datum plane-bot')

mdb.models[modelName].parts[partName].DatumPlaneByPrincipalPlane(offset=0.,
principalPlane=XZPLANE)
    mdb.models[modelName].parts[partName].features.changeKey(fromName='Datum
plane-1', toName='Datum plane-edges1')

mdb.models[modelName].parts[partName].DatumPlaneByPrincipalPlane(offset=lDim,
principalPlane=XZPLANE)
    mdb.models[modelName].parts[partName].features.changeKey(fromName='Datum
plane-1', toName='Datum plane-edges2')
      # datum z-axis
    plane_bot_id=mdb.models[modelName].parts[partName].features['Datum plane-
bot'].id
    # create datum axis for the part; transversely in the middle &
longitudinally at specified point
    plane_bot_id=mdb.models[modelName].parts[partName].features['Datum plane-
bot'].id

mdb.models[modelName].parts[partName].DatumAxisByNormalToPlane(plane=mdb.mode
ls[modelName].parts[partName].datums[plane_bot_id],
      point=(axesPts[0], axesPts[1], 0.) )
    # create axis along Y-AXIS

mdb.models[modelName].parts[partName].DatumAxisByPrincipalAxis(principalAxis=
YAXIS)

# CREATE SETS FOR PART
def setPart(modelName, partName, wDim, lDim, tPlate):
    partPath = mdb.models[modelName].parts[partName]
```

```
    # Sets
    partPath.Set(cells=partPath.cells.getByBoundingBox(
        -edist, -edist, -edist, wDim+edist, lDim+edist, tPlate+edist),
name='all')
    # Surfaces - top and bottom surfaces of parts
    partPath.Surface(side1Faces=partPath.faces.findAt(((wDim/2, lDim/2,
tPlate),)), name='top')
    partPath.Surface(side1Faces=partPath.faces.findAt(((wDim/2, lDim/2,
0.),)), name='bot')
    partPath.Surface(side1Faces=partPath.faces.getByBoundingBox(-wDim-edist,
-edist, -edist, wDim+edist, edist, tPlate+edist), name='edges1')
    partPath.Surface(side1Faces=partPath.faces.getByBoundingBox(-wDim-edist,
lDim-edist, -edist, wDim+edist, lDim+edist, tPlate+edist), name='edges2')

# SKETCH ON 1 FACE
def sketch1Face(modelName, partName, sketchName, face, upEdge, origin, side):
    partPath = mdb.models[modelName].parts[partName]
    mdb.models[modelName].ConstrainedSketch(gridSpacing=0.2, name=sketchName,
sheetSize=20.,
        transform=partPath.MakeSketchTransform(
        sketchPlane=partPath.faces.findAt((face[0], face[1], face[2]),),
        sketchPlaneSide=side,
        sketchUpEdge=partPath.edges.findAt((upEdge[0], upEdge[1],
upEdge[2]),),
        sketchOrientation=RIGHT, origin=(origin[0], origin[1], origin[2])))
    partPath.projectReferencesOntoSketch(filter=
        COPLANAR_EDGES, sketch=mdb.models[modelName].sketches[sketchName])


# CREATE SKETCH ON TOP FACE OF RECTANGULAR PARTS
def sketchGeoTop(modelName, partName, sketchName, wDim, lDim, tPlate, xpts,
ypts):
    # Set up
    sketch1Face(modelName, partName, sketchName, [wDim/2., lDim/2., tPlate],
[wDim, lDim/7., tPlate], [0., 0., tPlate], SIDE1)
    # Create sketch
    numH = len(ypts)
    numV = len(xpts)
    for i in range(numH):
        lineH = ( (0., ypts[i]), (wDim, ypts[i]) )
        mdb.models[modelName].sketches[sketchName].Spline(points=lineH)
    for i in range(numV):
        lineV = ( (xpts[i], 0.), (xpts[i], lDim) )
        mdb.models[modelName].sketches[sketchName].Spline(points=lineV)


# PARTITIONS
    #
.....................................................................

# PARTITION THROUGH PART BY SKETCH ON FACE
def partitionFaceThru(modelName, partName, sketchName, wDim, lDim, tPlate):
    # partition
    mdb.models[modelName].parts[partName].PartitionFaceBySketchThruAll(
        faces=mdb.models[modelName].parts[partName].faces.getByBoundingBox
        (-40, -40, -20, 40, 40, 20),
sketch=mdb.models[modelName].sketches[sketchName],
```

```
sketchPlane=mdb.models[modelName].parts[partName].faces.findAt((wDim/2.,
lDim/2., tPlate), ),
        sketchPlaneSide=SIDE1,

sketchUpEdge=mdb.models[modelName].parts[partName].edges.findAt((wDim,
lDim/2, tPlate),))

# PARTITION TOP OF PART BY SKETCH ON FACE
def partitionFaceTop(modelName, partName, sketchName, coord, edge):
    mdb.models[modelName].parts[partName].PartitionFaceBySketch(
        faces=mdb.models[modelName].parts[partName].faces.getByBoundingBox(
            coord[0]-edist, coord[1]-edist, coord[2]-edist, coord[3]+edist,
coord[4]+edist, coord[5]+edist),

sketchUpEdge=mdb.models[modelName].parts[partName].edges.findAt((edge[0],
edge[1], edge[2]),),
        sketch=mdb.models[modelName].sketches[sketchName])

# PARTITION PAVEMENT LAYERS
def partitionlayers(nPanels, lPanel, lGap, lExtra):
    ypts = []
    ypts2 = []
    for i in range(0,nPanels):
        yStart = lExtra + i*(lPanel + lGap)
        if i == 0:
            yptsAdd = [lPanel*0.5, lPanel-0.3]
            yptsSubl = [yStart, yStart+0.5*lPanel, yStart+lPanel-0.3]
        else:
            yptsAdd = [lPanel*0.5, lPanel-0.3, lLoad*0.25, lLoad*0.75]
            yptsSubl = [yStart, yStart+0.5*lPanel, yStart+lPanel-0.3,
yStart+lLoad*0.25, yStart+lLoad*0.75]
        ypts.extend([yptsAdd])
        ypts2.extend(yptsSubl)

    return (ypts, ypts2)


# PARTITION PANELS
def partitionLines(nPanels, xpts, ypts, wLoad, lLoad, ldLocTr, ldLocLg, FQH):
    # Longitudinal partitions (xpts)
    for k in ldLocTr:
        xpts.extend([k-wLoad/2, k, k+wLoad/2])
    # Transverse partitions (ypts)
    yptsDict = {0:'ypts1', 1:'ypts2', 2:'ypts3', 3:'ypts4'}
    for i in range(0, nPanels):
        yptsDict[i] = ypts[i][:]

    lenPanel = length
    for i in range(0,len(ldLocLg)):
        ldLocLg_panel = ldLocLg[i]
        for j in ldLocLg_panel:
            loadAdd = j + lLoad/2.
            loadSub = j - lLoad/2.
            loadAddHalf = j + lLoad/4.
            loadSubHalf = j - lLoad/4.
            if j == 0:
```

```
                yptsDict[i].append(loadAddHalf)
                yptsDict[i].append(loadAdd)
            if loadSub == 0:
                yptsDict[i].append(loadSubHalf)
                yptsDict[i].append(j)
                yptsDict[i].append(loadAddHalf)
                yptsDict[i].append(loadAdd)
            elif j == lenPanel:
                yptsDict[i].append(loadSubHalf)
                yptsDict[i].append(loadSub)
            elif loadAdd == lenPanel:
                yptsDict[i].append(loadSubHalf)
                yptsDict[i].append(loadSub)
                yptsDict[i].append(j)
                yptsDict[i].append(loadAddHalf)
            else:
                yptsDict[i].append(loadSub)
                yptsDict[i].append(loadSubHalf)
                yptsDict[i].append(j)
                yptsDict[i].append(loadAddHalf)
                yptsDict[i].append(loadAdd)
    return xpts, yptsDict


# CREATE PARTS
    #
.....................................................................

# CREATE PART - DOWEL BEAMS
def partBeam(modelName, rBeam, lBeam):
    partName = 'dowel'
    sketchName = 'sketchDowel'
    matName = 'steel dowel'
    sctName = 'dowel BEAM'
    profileName = 'dowel beam xscn'
    # sketch
    mdb.models[modelName].ConstrainedSketch(name=sketchName, sheetSize=1.)
    mdb.models[modelName].sketches[sketchName].Line(point1=(0,0), point2=(0,
lBeam/2-0.015/2))
    mdb.models[modelName].sketches[sketchName].Line(point1=(0,lBeam/2-
0.015/2), point2=(0, lBeam/2+0.015/2))

mdb.models[modelName].sketches[sketchName].Line(point1=(0,lBeam/2+0.015/2),
point2=(0, lBeam))
    # create extruded part
    mdb.models[modelName].Part(dimensionality=THREE_D, name=partName, type=
        DEFORMABLE_BODY)
    partPath = mdb.models[modelName].parts[partName]
    partPath.BaseWire(sketch=mdb.models[modelName].sketches[sketchName])
    # create set
    partPath.Set(edges=partPath.edges.getByBoundingBox(-10,-10,-10,10,10,10),
name='all')
    partPath.Set(edges=partPath.edges.findAt(((0, lBeam*0.5, 0),)),
name='centre')
    partPath.Set(edges=partPath.edges.findAt(((0, lBeam*0.25, 0),), ((0,
lBeam*0.75, 0),)), name='ends')
```

```
    partPath.Set(edges=partPath.edges.findAt(((0, lBeam*0.25, 0),)),
name='intf_dp_s1')
    partPath.Set(edges=partPath.edges.findAt(((0, lBeam*0.75, 0),)),
name='intf_dp_s2')
    partPath.Set(vertices=partPath.vertices.getByBoundingBox(-1, lBeam-edist,
-1, 1, lBeam+edist, 1), name='end_node')
    # create & assign section
    mdb.models[modelName].CircularProfile(name=profileName, r=rBeam)
    mdb.models[modelName].BeamSection(consistentMassMatrix=False,
        integration=DURING_ANALYSIS, material=matName, name=sctName,
        poissonRatio=nu_stdow, profile=profileName, temperatureVar=LINEAR)
    partPath.SectionAssignment(offset=0.0, offsetField='',
        offsetType=MIDDLE_SURFACE, region=partPath.sets['all'],
        sectionName=sctName, thicknessAssignment=FROM_SECTION)
    partPath.assignBeamSectionOrientation(method=N1_COSINES,
        n1=(0.0, 0.0, -1.0), region=partPath.sets['all'])

# CREATE PART - RECTANGULAR (PANEL, ASPHALT, GRANULAR)
def partRectangular(modelName, partName, matName, sctName, wDim, lDim,
tPlate, axesPts, xpts, ypts, partition):
    part3Dgeo(modelName, partName, wDim, lDim, tPlate)
    partFeatures(modelName, partName, lDim, tPlate, axesPts)
    setPart(modelName, partName, wDim, lDim, tPlate)
    part3Dsections(modelName, partName, matName, sctName)
    sketchGeoTop(modelName, partName, 'sketch_'+partName, wDim, lDim, tPlate,
xpts, ypts)
    if partition == 'TOP':
        partitionFaceTop(modelName, partName, 'sketch_'+partName, [0, 0,
tPlate, wDim, lDim, tPlate], [wDim, lDim/7, tPlate])
    elif partition == 'THRU':
        partitionFaceThru(modelName, partName, 'sketch_'+partName, wDim,
lDim, tPlate)



# ======================================================================
# MESH
# MODULE NAME: createMesh
# ======================================================================

# ASSIGN ELEMENT TYPE
def assignElem(modelName, partName,elemTypeName):
    partPath = mdb.models[modelName].parts[partName]
    partPath.setElementType(elemTypes=(ElemType(elemCode=elemTypeName,
        elemLibrary=STANDARD),),regions=(partPath.sets['all']  ))

# SEED EDGES - UNIFORM NUMBER BY FINDING EDGES
def seedEdgesUniformNumFind(modelName, partName, seedConstraint, edges,
numEl):
    # running the seeding command for each input provided in edges
    for i in range(0,len(edges)):

mdb.models[modelName].parts[partName].seedEdgeByNumber(constraint=seedConstra
int, edges= mdb.models[modelName].parts[partName].edges.findAt(((
     edges[i][0], edges[i][1], edges[i][2]),),), number=numEl)
```

```
# SEED PART
def seedPart(modelName, partName, seedSize):
    mdb.models[modelName].parts[partName].seedPart(deviationFactor=0.1,
minSizeFactor=0.1, size=seedSize)

# CREATE A UNIFORM MESH THROUGHOUT THE PART (STRUCTURED MESH)
def uniformMesh(modelName, partName, elemTypeName, meshSize):
      partPath = mdb.models[modelName].parts[partName]
      assignElem(modelName, partName, elemTypeName)
      partPath.seedPart(deviationFactor=0.1, minSizeFactor=0.1,
size=meshSize)
      partPath.generateMesh()



# ======================================================================
# CREATE ASSEMBLY
# MODULE NAME: createAssembly
# ======================================================================

# CREATE ASSEMBLY SETS
    #
.....................................................................

# CREATE SET OF MULTIPLE UNIQUE INSTANCES IN THE ASSEMBLY
def aSetInstUnique(modelName, instNames, setName):
    setList = []
    for i in instNames:
        instName = i
        addToSet =
mdb.models[modelName].rootAssembly.allInstances[instName].sets['all']
        setList.append(addToSet)
        setTuple = tuple(setList)
    mdb.models[modelName].rootAssembly.SetByBoolean(name=setName,
sets=setTuple)

# CREATE ASSEMBLY SET OF NODES
def aSetNodes(modelName, instName, coord, setName):
    setList = []
    for i in range(0,len(instName)):
        x1 = coord[i][0]
        y1 = coord[i][1]
        z1 = coord[i][2]
        x2 = coord[i][3]
        y2 = coord[i][4]
        z2 = coord[i][5]
        addToSet =
mdb.models[modelName].rootAssembly.instances[instName[i]].nodes.getByBounding
Box(coord[i][0]-edist, coord[i][1]-edist, coord[i][2]-edist,
    coord[i][3]+edist, coord[i][4]+edist, coord[i][5]+edist)
        setList.append(addToSet)
        setTuple = tuple(setList)
    mdb.models[modelName].rootAssembly.Set(name=setName, nodes=setTuple)


# CREATE SET FOR LOADED AREAS ON PANELS
```

```
def aSetPanelLds(modelName, instNames, lPanel, lGap, wLoad, lLoad, ldLocTr,
ldLocLg, FQH):
    lOffDict = {0: 'lOff1', 1: 'lOff2', 2: 'lOff3', 3: 'lOff4'}
    for i in range(0,len(lOffDict)):
        lOffDict[i] = lPanel*(i-0.5) + lGap*i

    wOff = -width/2.
    ldSetNames = []
    for i in range(0,len(instNames)):
        instName = instNames[i]
        count = 0
        for j in ldLocLg[i]:
            count += 1
            for a in range(0,len(ldLocTr)):
                setName = 'wheel'+'_p'+str(i+1)+'_pos'+str(count)+str(a+1)
                ldSetNames.append(setName)
                ldCentreY = j + lOffDict[i]

mdb.models[modelName].rootAssembly.Surface(side1Faces=mdb.models[modelName].r
ootAssembly.instances[instName].
                    faces.getByBoundingBox(wOff+ldLocTr[a]-wLoad/2.-edist,
ldCentreY-lLoad/2.-edist, 0.-edist,
                    wOff+ldLocTr[a]+wLoad/2.+edist, ldCentreY+lLoad/2.+edist,
0.+edist), name=setName)

    return ldSetNames


# CREATE ASSEMBLY SET OF SETS
def aSetSets(modelName, setNames, newSetName):
    setList = []
    for i in range(0,len(setNames)):
        addToSet = mdb.models[modelName].rootAssembly.sets[setNames[i]]
        setList.append(addToSet)
        setTuple = tuple(setList)
    mdb.models[modelName].rootAssembly.SetByBoolean(name=newSetName,
sets=setTuple)

# CREATE ASSEMBLY SET OF SURFACES (VARIOUS SURFACES FROM VARIOUS INSTANCES)
def aSetSurfacesUnique(modelName, instSurfName, surfSetName):
    setList = []
    for i in range(0,len(instSurfName)):
        addToSet =
mdb.models[modelName].rootAssembly.allSurfaces[instSurfName[i]]
        setList.append(addToSet)
        setTuple = tuple(setList)
    mdb.models[modelName].rootAssembly.SurfaceByBoolean(name=surfSetName,
surfaces=setTuple)


# POSITION PARTS IN ASSEMBLY
    #
.....................................................................

# POSITION CONSTRAINT, EDGE-EDGE (PART TO DATUM)
def posEdgeEdgeDatum(modelName, partName, instName, axisName):
      # get IDs
```

```
      zaxis_id=mdb.models[modelName].parts[partName].features[axisName].id
      # edge-to-edge constraint
      mdb.models[modelName].rootAssembly.EdgeToEdge(fixedAxis=mdb.models[mode
lName].rootAssembly.datums[1].axis3, flip=OFF,

      movableAxis=mdb.models[modelName].rootAssembly.instances[instName].datu
ms[zaxis_id])
      mdb.models[modelName].rootAssembly.regenerate()

# POSITION CONSTRAINT, EDGE-EDGE (PART TO PART)
def posEdgeEdgePart(modelName, partNameFix, instNameFix, axisNameFix,
partNameMove, instNameMove, axisNameMove):
      # get IDs

axisIDFix=mdb.models[modelName].parts[partNameFix].features[axisNameFix].id

axisIDMove=mdb.models[modelName].parts[partNameMove].features[axisNameMove].i
d
    # edge-to-edge constraint

mdb.models[modelName].rootAssembly.EdgeToEdge(fixedAxis=mdb.models[modelName]
.rootAssembly.instances[instNameFix].datums[axisIDFix], flip=OFF,

movableAxis=mdb.models[modelName].rootAssembly.instances[instNameMove].datums
[axisIDMove])
    mdb.models[modelName].rootAssembly.regenerate()

# POSITION CONSTRAINT, FACE-FACE
def posFaceFace(modelName, partNameFix, instNameFix, planeNameFix,
partNameMove, instNameMove, planeNameMove, flipNF, clearDist):
       # get IDs

plane_id1=mdb.models[modelName].parts[partNameFix].features[planeNameFix].id

plane_id2=mdb.models[modelName].parts[partNameMove].features[planeNameMove].i
d
    # face-to-face constraint
    mdb.models[modelName].rootAssembly.FaceToFace(clearance=clearDist,

fixedPlane=mdb.models[modelName].rootAssembly.instances[instNameFix].datums[p
lane_id1], flip=flipNF,

movablePlane=mdb.models[modelName].rootAssembly.instances[instNameMove].datum
s[plane_id2])
    mdb.models[modelName].rootAssembly.regenerate()

# POSITION, ROTATE INSTANCE
def posRotate(modelName, instName, aboutAxis, rotAngle):
    if aboutAxis == 'X':
        mdb.models[modelName].rootAssembly.rotate(angle=rotAngle,
            axisDirection=(1.0, 0.0, 0.0), axisPoint=(0.0, 0.0, 0.0),
instanceList=(
            instName, ))
    elif aboutAxis == 'Y':
        mdb.models[modelName].rootAssembly.rotate(angle=rotAngle,
            axisDirection=(0.0, 1.0, 0.0), axisPoint=(0.0, 0.0, 0.0),
instanceList=(instName, ))
```

```
    elif aboutAxis == 'Z':
        mdb.models[modelName].rootAssembly.rotate(angle=rotAngle,
            axisDirection=(0.0, 0.0, 1.0), axisPoint=(0.0, 0.0, 0.0),
instanceList=(
            instName, ))

# POSITION, TRANSLATE INSTANCE
def posTranslate(modelName, instName, vector):
    mdb.models[modelName].rootAssembly.translate(instanceList=(instName, ),
        vector=(vector[0], vector[1], vector[2]))

# SET TOP OF PANEL AT Z=0 WITHIN ASSEMBLY
def setPanelz(modelName, instName, tPanel):
    mdb.models[modelName].rootAssembly.DatumPlaneByPrincipalPlane(offset=0.,
principalPlane=XYPLANE)
    plane_id = mdb.models[modelName].rootAssembly.features['Datum plane-
1'].id
    plane_id_panel = mdb.models[modelName].rootAssembly.features['Datum
plane-1'].id
    mdb.models[modelName].rootAssembly.FaceToFace(clearance=0., fixedPlane=
        mdb.models[modelName].rootAssembly.datums[plane_id], flip=OFF,
movablePlane=

mdb.models[modelName].rootAssembly.instances[instName].faces.getByBoundingBox
(-1, -1, tPanel-edist, edist, edist, tPanel+edist))
    mdb.models[modelName].rootAssembly.regenerate()


# ADD PARTS TO ASSEMBLY
    #
.....................................................................

# ADD INSTANCES TO THE ASSEMBLY
def addInst(modelName, partName, instName, offset):
      mdb.models[modelName].rootAssembly.DatumCsysByDefault(CARTESIAN)
      mdb.models[modelName].rootAssembly.Instance(dependent=ON,
name=instName, part=mdb.models[modelName].parts[partName])
      mdb.models[modelName].rootAssembly.instances[instName].translate(vector
=(offset[0], offset[1], offset[2]))

# ADD & POSITION DOWELS IN ASSEMBLY
def addDowels(modelName, numDowels, startNum, trLoc, wOff, lOff, rotateNF,
lDowel, yDowel, wPanel, lPanel, tPanel, lGap):
    for i in range(0,numDowels):
        instName = 'dowel-'+str(i+1+startNum)
        # add instance
        addInst(modelName, 'dowel', instName, [0, 0, 0])
        # rotate for solid dowels, don't rotate for beams
        if rotateNF == 'ON':
            posRotate(modelName, instName, 'X', -90)
        # translate instance
        posTranslate(modelName, instName, [wOff+trLoc[i], lOff-lDowel/2, -
tPanel+yDowel])
```

```
# DEFINE INTERACTIONS
    #
.....................................................................

# EMBEDDED REGION CONSTRAINT
def constraintEmbedded(modelName, embedSetName, hostSetName, constraintName):
    mdb.models[modelName].EmbeddedRegion(absoluteTolerance=0.0,
        embeddedRegion=mdb.models[modelName].rootAssembly.sets[embedSetName],
        fractionalTolerance=0.05,
hostRegion=mdb.models[modelName].rootAssembly.sets[hostSetName], name=
        constraintName, toleranceMethod=BOTH, weightFactorTolerance=1e-06)

# DEFINE INTERACTION & ASSIGN INTERACTION PROPERTY
def frictionInt(modelName, intName, intPropName, masterSurfName,
slaveSurfName):
    mdb.models[modelName].SurfaceToSurfaceContactStd(adjustMethod=NONE,
clearanceRegion=None,
        createStepName='Initial', datumAxis=None, initialClearance=OMIT,
        interactionProperty=intPropName,

master=mdb.models[modelName].rootAssembly.allSurfaces[masterSurfName],
        slave=mdb.models[modelName].rootAssembly.allSurfaces[slaveSurfName],
        name=intName, sliding=FINITE, thickness=ON)

# DEFINE INTERACTION PROPERTY - TANGENTIAL BEHAVIOUR
def frictionPropTang(modelName, intPropName, tangentialType, fCoeff):
    if tangentialType == PENALTY:

mdb.models[modelName].interactionProperties[intPropName].TangentialBehavior(
            dependencies=0, directionality=ISOTROPIC,
elasticSlipStiffness=None,
            formulation=tangentialType, fraction=0.005,
maximumElasticSlip=FRACTION,
            pressureDependency=OFF, shearStressLimit=None,
slipRateDependency=OFF,
            table=((fCoeff, ), ), temperatureDependency=OFF)
    elif tangentialType == ROUGH:

mdb.models[modelName].interactionProperties[intPropName].TangentialBehavior(
            formulation=tangentialType)
    elif tangentialType == FRICTIONLESS:

mdb.models[modelName].interactionProperties[intPropName].TangentialBehavior(
            formulation=tangentialType)

# DEFINE INTERACTION PROPERTY WITH LINEAR NORMAL BEAHVIOUR
def frictionPropLin(modelName, intPropName, tangentialType, fCoeff, kStiff):
    mdb.models[modelName].ContactProperty(intPropName)
    # Tangential behaviour
    frictionPropTang(modelName, intPropName, tangentialType, fCoeff)
    # Normal behaviour
        # Just for rough contact, use hard pressure-overclosure instead of
linear because linear causes
        # overconstraint issues
    if tangentialType == ROUGH:

mdb.models[modelName].interactionProperties[intPropName].NormalBehavior(
```

```
            allowSeparation=OFF, constraintEnforcementMethod=DEFAULT,
            pressureOverclosure=HARD)
       # For penalty or frictionless contact, use linear pressure-overclosure
    else:
mdb.models[modelName].interactionProperties[intPropName].NormalBehavior(
            constraintEnforcementMethod=DEFAULT, contactStiffness=kStiff,
            pressureOverclosure=LINEAR)

# ELASTIC FOUNDATION
def Winkler(modelName, applSurfInst, kWinkler):
    mdb.models[modelName].ElasticFoundation(createStepName='Initial', name=
'Winkler_foundation',
        stiffness=kWinkler,
surface=mdb.models[modelName].rootAssembly.allSurfaces[applSurfInst])



# ======================================================================
# BOUNDARY CONDITIONS
# MODULE NAME: commonBC
# ======================================================================

# SET BC FOR A SET OF NODES
def BCnodes(modelName, BCname, stepName, setName, setDOF):
      mdb.models[modelName].DisplacementBC(amplitude=UNSET,
createStepName=stepName, distributionType=UNIFORM,
            fieldName='', localCsys=None, name=BCname,
region=mdb.models[modelName].rootAssembly.sets[setName],
            u1=setDOF[0], u2=setDOF[1], u3=setDOF[2], ur1=setDOF[3],
ur2=setDOF[4], ur3=setDOF[5])


# ======================================================================
# LOADS
# MODULE NAME: commonLoads
# ======================================================================

# LOAD - SELF-WEIGHT
def selfWeight(modelName, ldName, applStep, setNameInst):
      mdb.models[modelName].Gravity(comp3=gConstant, createStepName=applStep,
distributionType=UNIFORM,
            field='', name=ldName,
region=mdb.models[modelName].rootAssembly.allSets[setNameInst])


# LOAD - TEMPERATURE GRADIENT (USER-DEFINED) FOR SOLID ELEMENTS
def tempGradSolid(modelName, exprStr, exprName, magn, stepName, fieldName,
setNameInst):
    mdb.models[modelName].ExpressionField(description=
        'Thermal gradient across thickness of panel',
        expression=exprStr, localCsys=None, name=exprName)
    mdb.models[modelName].Temperature(createStepName=stepName,
        crossSectionDistribution=CONSTANT_THROUGH_THICKNESS,
distributionType=FIELD,
        field=exprName, magnitudes=(magn, ), name=fieldName,
        region=mdb.models[modelName].rootAssembly.allSets[setNameInst])
```

```
# LOAD - SET INITIAL TEMPERATURE OF THE PART
def tempLd(modelName, applStep, setNameInst, initTemp):
    mdb.models[modelName].Temperature(createStepName=applStep,
crossSectionDistribution=CONSTANT_THROUGH_THICKNESS,
        distributionType=UNIFORM, magnitudes=(initTemp, ), name='Temp
initial',
       region=mdb.models[modelName].rootAssembly.allSets[setNameInst])


# LOAD - STATIC UNIFORM PRESSURE
def uniformPressure(modelName, ldName, applStep, surfName, ldPressure):
      mdb.models[modelName].Pressure(amplitude=UNSET,
createStepName=applStep, distributionType=UNIFORM,
            field='', magnitude=ldPressure, name=ldName,
region=mdb.models[modelName].rootAssembly.allSurfaces[surfName])



# ============================================================================
# COMPILING FUNCTIONS TO CREATE MODELS
# MODULE NAME: modelCode
# ============================================================================

# CREATE PARTS & MESH
    #
.....................................................................

# CREATE PART & MESH - DOWEL BEAM
def partsDbeam(modelName, rDowel, lDowel, elemTypeDowel, mSizeDowel):
    create3Dpart.partBeam(modelName, rDowel, lDowel)
    createMesh.uniformMesh(modelName, 'dowel', elemTypeDowel, mSizeDowel)
    mdb.models[modelName].parts['dowel'].generateMesh()


# CREATE PARTS & MESH - ASPHALT, GRANULAR
def partsAG(modelName, tAsph, tGran, nPanels, wPanel, lPanel, lGap, wExtra,
lExtra, xpts2, ypts2,
             elemType, mSizeAsph, mSizeGran, mNumAsphThick, mNumGranThick,
FQH):
    # Calculate dimensions for full panel model
    wAsph = wPanel + wExtra*2
    lAsph = lPanel*nPanels + lGap*(nPanels-1) + lExtra*2
    wGran = wAsph
    lGran = lAsph
    lPartOff = lPanel/2 + lExtra
    axesLoc = [wAsph/2, lPartOff]
    # PARTS
    create3Dpart.partRectangular(modelName, 'asphalt', 'asphalt', 'asphalt
ES', wAsph, lAsph, tAsph, axesLoc, xpts2, ypts2, 'THRU')
    create3Dpart.partRectangular(modelName, 'granular', 'granular', 'granular
ES', wGran, lGran, tGran, axesLoc, xpts2, ypts2, 'THRU')
    # MESH GENERATION
    createMesh.seedEdgesUniformNumFind(modelName, 'asphalt', FIXED,
                [[0,0, tAsph/2.], [wPanel, 0, tAsph/2.]], mNumAsphThick)
    createMesh.seedEdgesUniformNumFind(modelName, 'granular', FIXED,
                [[0,0, tAsph/2.], [wPanel, 0, tAsph/2.]], mNumGranThick)
```

```
    createMesh.uniformMesh(modelName, 'asphalt', elemType, mSizeAsph)
    createMesh.uniformMesh(modelName, 'granular', elemType, mSizeGran)


# CREATE PARTS & MESH - ASPHALT, GRANULAR, SUPPORT
def partsSAG(modelName, wSupp, tSupp, tAsph, tGran, nPanels, wPanel, lPanel,
lGap, wExtra, lExtra, xpts2, ypts2,
             elemType, mSizeSupp, mSizeAsph, mSizeGran, mNumAsphThick,
mNumGranThick, FQH):
    # PARTS - Asphalt, granular
    [wAsph, lAsph, wGran, lGran, lPartOff] = partsAG(modelName, tAsph, tGran,
nPanels, wPanel, lPanel, lGap, wExtra, lExtra, xpts2, ypts2,
            elemType, mSizeAsph, mSizeGran, mNumAsphThick, mNumGranThick,
FQH)
    # PARTS & MESH GENERATION - support
    ypts3 = [dist-lExtra for dist in ypts2]
    lSupp = lPanel*nPanels + lGap*(nPanels-1)
    axesLoc = [wPanel/2, lPanel/2]
    xpts3 = [dist-wExtra for dist in xpts2]
    create3Dpart.partRectangular(modelName, 'support', 'support', 'support
ES', wSupp, lSupp, tSupp, axesLoc, xpts3, ypts3, 'THRU')
    createMesh.uniformMesh(modelName, 'support', elemType, mSizeSupp)


# CREATE PARTS - PANEL
def partsPndns(modelName, partPanels, nPanels, wPanel, lPanel, tPanel,
               xpts, ypts, wLoad, lLoad, ldLocTr, ldLocLg,
               elemType, mSizePanel, mNumPanelThick, FQH):
    # PARTS
    [xpts, yptsPanels] = create3Dpart.partitionLines(nPanels, xpts, ypts,
wLoad, lLoad, ldLocTr, ldLocLg, FQH)
    for i in range(0,nPanels):
        create3Dpart.partRectangular(modelName, partPanels[i], 'concrete',
'concrete ES', wPanel, lPanel, tPanel, [wPanel/2, lPanel/2], xpts,
yptsPanels[i], 'THRU')

    # MESH GENERATION
    for i in range(0,nPanels):
        # seed part first
        createMesh.seedPart(modelName, partPanels[i], mSizePanel)
        createMesh.seedEdgesUniformNumFind(modelName, partPanels[i], FIXED,
                [[0,0, tPanel/2.], [wPanel, 0, tPanel/2.]], mNumPanelThick)
        createMesh.assignElem(modelName, partPanels[i], elemType)
        mdb.models[modelName].parts[partPanels[i]].generateMesh()


# CREATE ASSEMBLY
    #
.....................................................................

# ASSEMBLY - ASPHALT, GRANULAR, NO DOWELS
def assemblAGP(modelName, partPanels, instPanels, nPanels, tPanel,
offsetDist):
    for i in range(0,nPanels):
        createAssembly.addInst(modelName, partPanels[i], instPanels[i], [4*i,
0, -tPanel])
```

```
    createAssembly.addInst(modelName, 'asphalt', 'asphalt-1', [8, 0, 0])
    createAssembly.addInst(modelName, 'granular', 'granular-1', [12, 0, 0])
    createAssembly.setPanelz(modelName, instPanels[0], tPanel)
    createAssembly.posEdgeEdgeDatum(modelName, partPanels[0], instPanels[0],
'Datum axis-1')
    createAssembly.posEdgeEdgeDatum(modelName, 'asphalt', 'asphalt-1', 'Datum
axis-1')
    createAssembly.posEdgeEdgeDatum(modelName, 'granular', 'granular-1',
'Datum axis-1')
    createAssembly.posFaceFace(modelName, partPanels[0], instPanels[0],
'Datum plane-bot', 'asphalt', 'asphalt-1', 'Datum plane-top', OFF,
offsetDist)
    createAssembly.posFaceFace(modelName, 'asphalt', 'asphalt-1', 'Datum
plane-bot', 'granular', 'granular-1', 'Datum plane-top', OFF, offsetDist)


# ASSEMBLY - SUPPORT, ASPHALT, GRANULAR, NO DOWELS (1 panel model)
def assemblSAGP(modelName, partPanels, instPanels, nPanels, tPanel,
offsetDist):
    for i in range(0,nPanels):
        createAssembly.addInst(modelName, partPanels[i], instPanels[i], [4*i,
0, -tPanel])

    createAssembly.addInst(modelName, 'asphalt', 'asphalt-1', [8, 0, 0])
    createAssembly.addInst(modelName, 'granular', 'granular-1', [12, 0, 0])
    createAssembly.addInst(modelName, 'support', 'support-1', [20, 0, 0])
    createAssembly.setPanelz(modelName, instPanels[0], tPanel)
    createAssembly.posEdgeEdgeDatum(modelName, partPanels[0], instPanels[0],
'Datum axis-1')
    createAssembly.posEdgeEdgeDatum(modelName, 'support', 'support-1', 'Datum
axis-1')
    createAssembly.posEdgeEdgeDatum(modelName, 'asphalt', 'asphalt-1', 'Datum
axis-1')
    createAssembly.posEdgeEdgeDatum(modelName, 'granular', 'granular-1',
'Datum axis-1')
    createAssembly.posFaceFace(modelName, partPanels[0], instPanels[0],
'Datum plane-bot', 'support', 'support-1', 'Datum plane-top', OFF,
offsetDist)
    createAssembly.posFaceFace(modelName, 'support', 'support-1', 'Datum
plane-bot', 'asphalt', 'asphalt-1', 'Datum plane-top', OFF, offsetDist)
    createAssembly.posFaceFace(modelName, 'asphalt', 'asphalt-1', 'Datum
plane-bot', 'granular', 'granular-1', 'Datum plane-top', OFF, offsetDist)


# ASSEMBLY - ASPHALT, GRANULAR, PANELS WITH EMBEDDED DOWELS
def assemblAGPDns(modelName, partPanels, instPanels, nPanels, wPanel, lPanel,
tPanel,
                  offsetDist, lGap, nDowels, lDowel, yDowel, trLoc,
rotateDowels, FQH):
    trOffset = -wPanel/2
    # ASSEMBLY
    assemblAGP(modelName, partPanels, instPanels, nPanels, tPanel,
offsetDist)
    for i in range(0,nPanels-1):
        createAssembly.posEdgeEdgePart(modelName, partPanels[i],
instPanels[i], 'Datum axis-2', partPanels[i+1], instPanels[i+1], 'Datum axis-
2')
```

```
        createAssembly.posFaceFace(modelName, partPanels[i], instPanels[i],
'Datum plane-edges2', partPanels[i+1], instPanels[i+1], 'Datum plane-edges1',
OFF, lGap)
        # **Add dowels to the assembly
        createAssembly.addDowels(modelName, nDowels, nDowels*i, trLoc,
trOffset, (2*i+1)*(lPanel+lGap)/2, rotateDowels, lDowel, yDowel, wPanel,
lPanel, tPanel, lGap)


# ASSEMBLY - SUPPORT, ASPHALT, GRANULAR, PANELS WITH EMBEDDED DOWELS
def assemblSAGPDns(modelName, partPanels, instPanels, nPanels, wPanel,
lPanel, tPanel,
                   offsetDist, lGap, nDowels, lDowel, yDowel, trLoc,
rotateDowels, FQH):
    trOffset = -wPanel/2
    # ASSEMBLY
    assemblSAGP(modelName, partPanels, instPanels, nPanels, tPanel,
offsetDist)
    for i in range(0,nPanels-1):
        createAssembly.posEdgeEdgePart(modelName, partPanels[i],
instPanels[i], 'Datum axis-2', partPanels[i+1], instPanels[i+1], 'Datum axis-
2')
        createAssembly.posFaceFace(modelName, partPanels[i], instPanels[i],
'Datum plane-edges2', partPanels[i+1], instPanels[i+1], 'Datum plane-edges1',
OFF, lGap)
        # **Add dowels to the assembly
        createAssembly.addDowels(modelName, nDowels, nDowels*i, trLoc,
trOffset, (2*i+1)*(lPanel+lGap)/2, rotateDowels, lDowel, yDowel, wPanel,
lPanel, tPanel, lGap)


# CREATE ASSEMBLY SETS
    #
.....................................................................

# ASSEMBLY SETS COMMON FOR ALL MODELS
def aSetsCommon(modelName, instPanels):
    createAssembly.aSetSurfacesUnique(modelName, [a+'.bot' for a in
instPanels], 'panels_bot')
    createAssembly.aSetInstUnique(modelName, instPanels, 'panels_all')


# ASSEMBLY SETS FOR PANELS WITH DOWELS
def aSetsPDcommon(modelName, instPanels, nPanels, nDowels):
    dowelStr = 'dowel-'
    for i in range(0,nPanels-1):
        createAssembly.aSetInstUnique(modelName, [instPanels[i],
instPanels[i+1]], 'panels_j'+str(i+1))
        dowelSetS1 = []
        dowelSetS2 = []
        for j in range(1, nDowels+1):
            dowelNum = nDowels*i+j
            dowelSetS1.append(dowelStr+str(dowelNum)+'.intf_dp_s1')
            dowelSetS2.append(dowelStr+str(dowelNum)+'.intf_dp_s2')
        createAssembly.aSetSets(modelName, dowelSetS1,
'intf_dp_j'+str(i+1)+'s1')
```

```
        createAssembly.aSetSets(modelName, dowelSetS2,
'intf_dp_j'+str(i+1)+'s2')
        createAssembly.aSetSets(modelName, ['intf_dp_j'+str(i+1)+'s1',
'intf_dp_j'+str(i+1)+'s2'], 'intf_dp_j'+str(i+1))


# ASSEMBLY SETS FOR PANELS WITH EMBEDDED DOWEL BEAMS
def aSetsPDbeam(modelName, instPanels, nPanels, nDowels):
    aSetsCommon(modelName, instPanels)
    aSetsPDcommon(modelName, instPanels, nPanels, nDowels)
    dowelStr = 'dowel-'
    dowelSetEndNodes = []
    for i in range(0,nPanels-1):
        for j in range(1, nDowels+1):
            dowelSetEndNodes.append(dowelStr+str(nDowels*i+j)+'.end_node')
    createAssembly.aSetSets(modelName, dowelSetEndNodes, 'dowel_end_nodes')


# ASSEMBLY SETS FOR BOUNDARY CONDITIONS WITHOUT SUPPORT
def aSetsBC(modelName, instPanels, instSubl, nPanels, numSubl, wPanel,
lPanel, tPanel, wAsph, lAsph, lPartOff, lGap):
    createAssembly.aSetNodes(modelName, instPanels, [[wPanel/2, -40, -10,
wPanel/2, 40, 0]]*nPanels, 'sides1_panels')
    createAssembly.aSetNodes(modelName, instPanels, [[-wPanel/2, -40, -10, -
wPanel/2, 40, 0]]*nPanels, 'sides2_panels')
    createAssembly.aSetNodes(modelName, instSubl, [[wAsph/2, -40, -10,
wAsph/2, 40, 0]]*numSubl, 'sides1_sublayers')
    createAssembly.aSetNodes(modelName, instSubl, [[-wAsph/2, -40, -10, -
wAsph/2, 40, 0]]*numSubl, 'sides2_sublayers')
    createAssembly.aSetNodes(modelName, instSubl, [[-40, -(lPartOff), -20,
40, -(lPartOff), 0]]*numSubl, 'edges1_sublayers')
    createAssembly.aSetNodes(modelName, instSubl, [[-40, lAsph-lPartOff, -20,
40, lAsph-lPartOff, 0]]*numSubl, 'edges2_sublayers')
    createAssembly.aSetNodes(modelName, [instPanels[0]], [[-10, -lPanel/2, -
10, 10, -lPanel/2, 0]], 'edges1_panels')
    createAssembly.aSetNodes(modelName, [instPanels[-1]],
        [[-10, lPanel*(nPanels+0.5)+lGap*(nPanels-1), -10, 10,
lPanel*(nPanels+0.5)+lGap*(nPanels-1), 0]], 'edges2_panels')


# ASSEMBLY SETS FOR BOUNDARY CONDITIONS WITH SUPPORT
def aSetsBCsupp(modelName, instPanels, instSubl, nPanels, numSubl, wPanel,
lPanel, tPanel, wAsph, lAsph, lPartOff, lGap):
    instPanelsSupp = instPanels[:]
    instPanelsSupp.append('support-1')
    createAssembly.aSetNodes(modelName, instPanelsSupp, [[wPanel/2, -40, -10,
wPanel/2, 40, 0]]*(nPanels+1), 'sides1_panels')
    createAssembly.aSetNodes(modelName, instPanelsSupp, [[-wPanel/2, -40, -
10, -wPanel/2, 40, 0]]*(nPanels+1), 'sides2_panels')
    createAssembly.aSetNodes(modelName, instSubl[1:], [[wAsph/2, -40, -10,
wAsph/2, 40, 0]]*(numSubl-1), 'sides1_sublayers')
    createAssembly.aSetNodes(modelName, instSubl[1:], [[-wAsph/2, -40, -10, -
wAsph/2, 40, 0]]*(numSubl-1), 'sides2_sublayers')
    createAssembly.aSetNodes(modelName, instSubl[1:], [[-40, -(lPartOff), -
20, 40, -(lPartOff), 0]]*(numSubl-1), 'edges1_sublayers')
    createAssembly.aSetNodes(modelName, instSubl[1:], [[-40, lAsph-lPartOff,
-20, 40, lAsph-lPartOff, 0]]*(numSubl-1), 'edges2_sublayers')
```

```
    createAssembly.aSetNodes(modelName, [instPanels[0], 'support-1'], [[-10,
-lPanel/2, -10, 10, -lPanel/2, 0]]*2, 'edges1_panels')
    createAssembly.aSetNodes(modelName, [instPanels[-1], 'support-1'],
        [[-10, lPanel*(nPanels+0.5)+lGap*(nPanels-1), -10, 10,
lPanel*(nPanels+0.5)+lGap*(nPanels-1), 0]]*2, 'edges2_panels')


# CREATE INTERACTIONS
    #
.....................................................................

# INTERFACES - PANEL, ASPHALT, GRANULAR
def intfPAG(modelName):
    createAssembly.frictionInt(modelName, 'fr_panel-asph', 'fC_pa', 'asphalt-
1.top', 'panels_bot')
    createAssembly.frictionInt(modelName, 'fr_asph-gran', 'fC_ag', 'asphalt-
1.bot', 'granular-1.top')


# INTERFACES - PANEL, SUPPORT, ASPHALT, GRANULAR
def intfPSAG(modelName):
    createAssembly.frictionInt(modelName, 'fr_panel-supp', 'fC_ps',
'panels_bot', 'support-1.top')
    createAssembly.frictionInt(modelName, 'fr_supp-asph', 'fC_sa', 'asphalt-
1.top', 'support-1.bot')
    createAssembly.frictionInt(modelName, 'fr_asph-gran', 'fC_ag', 'asphalt-
1.bot', 'granular-1.top')


# INTERFACES - EMBED DOWEL BEAMS IN PANEL
def embedDP(modelName, nPanels):
    for i in range(0,nPanels-1):
        createAssembly.constraintEmbedded(modelName, 'intf_dp_j'+str(i+1),
'panels_j'+str(i+1), 'Embed_dowels_j'+str(i+1))


# CREATE BOUNDARY CONDITIONS
    #
.....................................................................

# BOUNDARY CONDITIONS WITH FREE PANEL EDGES
def bcPefreeSse(modelName):
    commonBC.BCnodes(modelName, 'roller_side1_subl', 'Initial',
'sides1_sublayers', [0., UNSET, UNSET, UNSET, UNSET, UNSET])
    commonBC.BCnodes(modelName, 'roller_side2_subl', 'Initial',
'sides2_sublayers', [0., UNSET, UNSET, UNSET, UNSET, UNSET])
    commonBC.BCnodes(modelName, 'roller_side1_panels', 'Initial',
'sides1_panels', [0, UNSET, UNSET, UNSET, UNSET, UNSET])
    commonBC.BCnodes(modelName, 'roller_side2_panels', 'Initial',
'sides2_panels', [0, UNSET, UNSET, UNSET, UNSET, UNSET])
    commonBC.BCnodes(modelName, 'roller_edge1_subl', 'Initial',
'edges1_sublayers', [UNSET, 0, UNSET, UNSET, UNSET, UNSET])
    commonBC.BCnodes(modelName, 'roller_edge2_subl', 'Initial',
'edges2_sublayers', [UNSET, 0, UNSET, UNSET, UNSET, UNSET])
```

```
# BUILD FINITE ELEMENT MODELS
#
++++++++++++++++++++++++++++++++++++++++++++++++++++++++++++++++++++++++++++++++


# ============================================================================
# MODEL INPUTS
# ============================================================================

FQH = 'F'             # quarter symmetric models

offsetDist = 1e-6

# Geometry
nPanels = 3
wExtra = 2
lExtra = 2
lPanel = length
wPanel = width
wSupp = wPanel
# thicknesses
tPanel = 0.205
tGran = 0.600
tSupp = 0.012
lGap = 0.015           # gap width

# Dowels
nDowels = 11           # number of dowels
lDowel = 0.355         # dowel length
rDowel = 0.038/2       # dowel radius
yDowel = tPanel        # vertical location of dowel
# transverse dowel location (relative to x = 0)  and spacing
dSpacing = 0.3
dowel6Loc = 3.66-0.3*11
trLoc = [0.3]
for i in range(1,6):
    trLoc.append(trLoc[-1] + dSpacing)

trLoc.append(trLoc[-1]+dowel6Loc)
for i in range(1,5):
    trLoc.append(trLoc[-1]+dSpacing)

# Foundation
kWinkler = 29e6

# Stiffness for penalty-overclosure relationships
kpa = 15000E6
kag = 500E6
kps = 5000E6
ksa = kps
fCoeff_pd = 0.5
fCoeff_pa = 0.5
fCoeff_ag = 0.5
fCoeff_ps = 0.5
fCoeff_sa = 0.5
sepNF = ON         # allow separation after layers are in contact at
interface
```

```
fType = PENALTY

# Mesh
mSizeDowel = 0.03
mSizePanel = 0.175
mSizeSupp = 0.048
mSizeAsph = 0.2
mSizeGran = 0.18
mNumPanelThick = 3
mNumAsphThick = 3
mNumGranThick = 2
elemType = C3D20R
elemTypeDowel = B32

# Temp loading
tempTop = 10
tempBot = 0
tempInit = (tempTop+tempBot)*0.5

# Wheel loading
wLoad = 0.25
lLoad = 0.25
ldPressure = 40000/(wLoad*lLoad)
# coordinates relative to panel corner at (0,0)
ldLocTr = [wPanel-wLoad/2.-1.8, wPanel-wLoad/2.]
# each element below corresponds to one panel
ldLocLg = [[], [lLoad/2.], []]

# Partitioning parts
xpts = [ldLocTr[0]-wLoad/4., ldLocTr[0]+wLoad/4.,
        ldLocTr[1]-wLoad/4., ldLocTr[1]+wLoad/4.,
        wPanel-1]
xpts2 = [wExtra, wExtra+wPanel*0.5, wExtra+wPanel,
         wExtra+ldLocTr[0]-wLoad*0.5, wExtra+ldLocTr[0],
wExtra+ldLocTr[0]+wLoad*0.5,
         wExtra+ldLocTr[1]-wLoad*0.5, wExtra+ldLocTr[1]]



# ============================================================================
# SCRIPT TO CREATE GR MODEL (WITH SUPPORT)
# ============================================================================

modelName = 'chooseModelName'

tAsph = 0.175 - tSupp
tAll = [tPanel, tSupp, tAsph, tGran]
instSubl = ['support-1', 'asphalt-1', 'granular-1']

# Partitioning parts
[ypts, ypts2] = partitionlayers(nPanels, lPanel, lGap, lExtra)

# Auto calculations/outputs to return using inputs above
[partPanels, instPanels, instAll, numSubl, tTotal] =
common0.secondaryCalcs(nPanels, instSubl, tAll, offsetDist)
# ------------------------------------
```

```
mdb.Model(modelName)


# **MATERIALS (create all)
materials(modelName)


# CREATE PANEL WITH EMBEDDED DOWELS, WITH SUPPORT LAYER

# **PARTS & MESH
    # Dowels
modelCode.partsDbeam(modelName, rDowel, lDowel, elemTypeDowel, mSizeDowel)
    # Asphalt, granular
[wAsph, lAsph, wGran, lGran, lPartOff] = modelCode.partsSAG(modelName, wSupp,
tSupp, tAsph, tGran,
        nPanels, wPanel, lPanel, lGap, wExtra, lExtra, xpts2, ypts2,
          elemType, mSizeSupp, mSizeAsph, mSizeGran, mNumAsphThick,
mNumGranThick, FQH)
    # Panels
modelCode.partsPndns(modelName, partPanels, nPanels, wPanel, lPanel, tPanel,
               xpts, ypts, wLoad, lLoad, ldLocTr, ldLocLg,
               elemType, mSizePanel, mNumPanelThick, FQH)

# **ASSEMBLY
modelCode.assemblSAGPDns(modelName, partPanels, instPanels, nPanels, wPanel,
lPanel, tPanel,
               offsetDist, lGap, nDowels, lDowel, yDowel, trLoc, 'OFF', FQH)

# **ASSEMBLY SETS
modelCode.aSetsPDbeam(modelName, instPanels, nPanels, nDowels)
modelCode.aSetsBCsupp(modelName, instPanels, instSubl, nPanels, numSubl,
wPanel, lPanel, tPanel, wAsph, lAsph, lPartOff, lGap)
ldSetNames = createAssembly.aSetPanelLds(modelName, instPanels, lPanel, lGap,
wLoad, lLoad, ldLocTr, ldLocLg, FQH)


# **STEPS
common0.staticStep(modelName, 'Step-1', 'Initial', 'Apply self-weight & axle
load')
common0.staticStep(modelName, 'Step-2', 'Step-1', 'Apply temperature
gradients')


# **FIELD OUTPUT
common0.createFieldOut(modelName, ('U', 'S', 'COORD'))


# **LOADS
    # Self-weight
commonLoads.selfWeight(modelName, 'sw-panels', 'Step-1', 'panels_all')
commonLoads.selfWeight(modelName, 'sw-support', 'Step-1', 'support-1.all')
commonLoads.selfWeight(modelName, 'sw-asphalt', 'Step-1', 'asphalt-1.all')
commonLoads.selfWeight(modelName, 'sw-granular', 'Step-1', 'granular-1.all')
    # **Wheel loads
for i in range(0,len(ldSetNames)):
    ldAreaName = ldSetNames[i]
    ldAppl = ldPressure
```

```
    commonLoads.uniformPressure(modelName, ldAreaName, 'Step-1', ldAreaName,
ldAppl)
    # Temperature
gradStr = str(tempTop)+'+Z/'+str(tPanel)+'*'+'('+str(tempTop)+'-
'+str(tempBot)+')'
commonLoads.tempLd(modelName, 'Initial', 'panels_all', tempInit)
commonLoads.tempGradSolid(modelName, gradStr, 'Temp gradient', 1.0, 'Step-2',
'Temp gradient', 'panels_all')


# **FOUNDATION
createAssembly.Winkler(modelName, 'granular-1.bot', kWinkler)


# **INTERFACES
    # Interaction properties
createAssembly.frictionPropLin(modelName, 'fC_ps', fType, fCoeff_ps, kps)
createAssembly.frictionPropLin(modelName, 'fC_sa', fType, fCoeff_sa, ksa)
createAssembly.frictionPropLin(modelName, 'fC_ag', fType, fCoeff_ag, kag)
    # Interactions
modelCode.intfPSAG(modelName)
    # Embedded regions
modelCode.embedDP(modelName, nPanels)


# **BOUNDARY CONDITIONS
modelCode.bcPefreeSse(modelName)
for i in range(0, nPanels-1):
    commonBC.BCnodes(modelName, 'torsion_stop', 'Initial', 'dowel_end_nodes',
[UNSET, UNSET, UNSET, UNSET, 0., UNSET])



# ======================================================================
# SCRIPT TO CREATE AS MODEL (WITHOUT SUPPORT)
# ======================================================================

modelName = 'chooseModelName'

tAsph = 0.175
tAll = [tPanel, tAsph, tGran]
instSubl = ['asphalt-1', 'granular-1']

# Partitioning parts
[ypts, ypts2] = partitionlayers(nPanels, lPanel, lGap, lExtra)

# Auto calculations/outputs to return using inputs above
[partPanels, instPanels, instAll, numSubl, tTotal] =
common0.secondaryCalcs(nPanels, instSubl, tAll, offsetDist)
# ------------------------------------

mdb.Model(modelName)

# **MATERIALS (create all)
materials(modelName)
```

```
# CREATE MODEL WITH EMBEDDED DOWELS, NO SUPPORT LAYER
# **PARTS
    # Dowels
modelCode.partsDbeam(modelName, rDowel, lDowel, elemTypeDowel, mSizeDowel)
    # Asphalt, granular
[wAsph, lAsph, wGran, lGran, lPartOff] = modelCode.partsAG(
        modelName, tAsph, tGran, nPanels, wPanel, lPanel, lGap, wExtra,
lExtra, xpts2, ypts2,
        elemType, mSizeAsph, mSizeGran, mNumAsphThick, mNumGranThick, FQH)
# Panels
modelCode.partsPndns(modelName, partPanels, nPanels, wPanel, lPanel, tPanel,
               xpts, ypts, wLoad, lLoad, ldLocTr, ldLocLg,
               elemType, mSizePanel, mNumPanelThick, FQH)

# **ASSEMBLY
modelCode.assemblAGPDns(modelName, partPanels, instPanels, nPanels, wPanel,
lPanel, tPanel,
                   offsetDist, lGap, nDowels, lDowel, yDowel, trLoc, 'OFF',
FQH)

# **ASSEMBLY SETS
modelCode.aSetsPDbeam(modelName, instPanels, nPanels, nDowels)
modelCode.aSetsBC(modelName, instPanels, instSubl, nPanels, numSubl, wPanel,
lPanel, tPanel, wAsph, lAsph, lPartOff, lGap)
ldSetNames = createAssembly.aSetPanelLds(modelName, instPanels, lPanel, lGap,
wLoad, lLoad, ldLocTr, ldLocLg, FQH)


# **STEPS
common0.staticStep(modelName, 'Step-1', 'Initial', 'Apply self-weight & axle
loads')
common0.staticStep(modelName, 'Step-2', 'Step-1', 'Apply temperature
gradients')


# **FIELD OUTPUT
common0.createFieldOut(modelName, ('U', 'S', 'COORD'))


# **LOADS
    # Self-weight
commonLoads.selfWeight(modelName, 'sw-panels', 'Step-1', 'panels_all')
commonLoads.selfWeight(modelName, 'sw-asphalt', 'Step-1', 'asphalt-1.all')
commonLoads.selfWeight(modelName, 'sw-granular', 'Step-1', 'granular-1.all')
    # **Wheel loads
for i in range(0,len(ldSetNames)):
    ldAreaName = ldSetNames[i]
    ldAppl = ldPressure
    commonLoads.uniformPressure(modelName, ldAreaName, 'Step-1', ldAreaName,
ldAppl)
    # Temperature
gradStr = str(tempTop)+'+Z/'+str(tPanel)+'*'+'('+str(tempTop)+'-
'+str(tempBot)+')'
commonLoads.tempLd(modelName, 'Initial', 'panels_all', tempInit)
commonLoads.tempGradSolid(modelName, gradStr, 'Temp gradient', 1.0, 'Step-2',
'Temp gradient', 'panels_all')
```

```
# **FOUNDATION
createAssembly.Winkler(modelName, 'granular-1.bot', kWinkler)


# **INTERFACES
    # Interaction properties
createAssembly.frictionPropLin(modelName, 'fC_pa', fType, fCoeff_pa, kpa)
createAssembly.frictionPropLin(modelName, 'fC_ag', fType, fCoeff_ag, kag)
    # Interactions
modelCode.intfPAG(modelName)
    # Embedded regions
modelCode.embedDP(modelName, nPanels)


# **BOUNDARY CONDITIONS
modelCode.bcPefreeSse(modelName)
for i in range(0, nPanels-1):
    commonBC.BCnodes(modelName, 'torsion_stop', 'Initial', 'dowel_end_nodes',
[UNSET, UNSET, UNSET, UNSET, 0., UNSET])
```